UNIVERSITA DEGLI STUDI DI PADOVA

DIPARTIMENTO DI INGEGNERIA INDUSTRIALE

Universitá degli Studi di Padova

Dipartimento di Ingegneria Industriale

Novel Methodologies for the Analysis and Management of Low Voltage Active Distribution Networks

Dottorando: Muhammad Usman

Ph.D. Thesis

30th November, 2019

Novel Methodologies for the Analysis and Management of Low Voltage Active Distribution Networks

Scuola di Dottorato di Ricerca in Ingegneria Industriale
Indirizzo in Ingegneria Dell'Energia Elettrica
Ciclo XXXII

Submitted in partial fulfilment of the requirements for the degree of Doctor of Philosophy

Muhammad Usman

Direttore della scuola: Ch.mo Prof. Paolo Colombo
Coordinatore d'indirizzo: Ch.mo Prof. Roberto Turri
Supervisore: Ch.mo Dr. Fabio Bignucolo
Co-Supervisore: Ch.mo Prof. Roberto Turri

To my ever-caring, affectionate and loving late mother
May her soul rest in peace forever

Acknowledgement

First of all, I would like to thank the Almighty Allah (SWT) for giving me this opportunity, guiding me during my work and showering His countless blessings on me throughout my life. Secondly, I would like to thank my supervisor, Dr. Fabio Bignucolo, and co-supervisor, Prof. Roberto Turri, for their support, advice and trust during all these years of my research work.

Many thanks to all my colleagues at the Department of Industrial Engineering especially Prof. Lorenzo Finesso, Dr. Massimiliano Coppo, Andrea Cervi and Marco Vanzetto for the fruitful discussions and good time spent together at the office.

In the end, I cannot find the words to pay gratitude to all my family members especially my father and sisters, who not only supported me during the time of the demise of my mother but also became my source of inspiration and motivation. Finally, special thanks to my best friends back in Germany, particularly Saqib, Usman and Umair, whose continuous motivation and support helped me through the difficult times of my life and I hope that I would also be able to support them for the rest of my life as well.

Declaration

The work in this thesis is based on the research carried out at the Department of Industrial Engineering, University of Padova, Italy to fulfil the requirements for the degree of Doctor of Philosophy under the supervision of Dr. Fabio Bignucolo. No part of this thesis has been submitted elsewhere for any other degree or qualification and it is completely my own work unless referenced to the contrary in the text.

Muhammad Usman

Abstract

The continuous proliferation of renewable Distributed Energy Resources (DERs) in Medium Voltage (MV) and Low Voltage (LV) Distribution Networks (DNs) is playing a prominent role in reducing the carbon footprint of fossil-fuel-based electricity generation plants. However, the rapid integration of these resources has also changed the passive nature of these networks, and consequently, special attention is required to ensure their optimal, secure and reliable operation. Moreover, the installed DERs cannot be simply operated on the basis of a *fit-and-forget* policy due to the emergence of several technical problems caused by their interconnection. Issues such as voltage unbalance, reverse power flow, unintentional islanded operation etc. are frequently occurring in these networks which, in turn, require novel control and management schemes to ensure the continuous supply of electricity to end-users. In this context, several countries and network operators have updated their grid codes which put additional constraints on renewable DERs to participate in the provision of ancillary services in the context of maintaining network stability.

In view of this, multi-phase analysis of MV and, especially, LV networks gains unprecedented attention due to the non-capability of single-phase equivalent representation-based network analysis approach in depicting the true picture of system's operating conditions and state variables. Such a detailed network analysis, in turn, sets the path for innovative solutions to effectively manage these networks. Furthermore, concerning LV DNs, neutral conductor must be treated like phases conductors due to the significant presence of current in it under highly unbalanced network loading scenario. Resultantly, the application of the Kron reduction methodology to these networks must be avoided because of its reliance upon the unrealistic assumption of an equipotential neutral conductor. Since LV active DNs will become a central pillar of a decentralized electrical grid in near-future, it is, therefore, incumbent to analyse and manage them by taking into account each aspect of their structure.

With a special emphasis and focus on LV active DNs, this thesis presents novel analysis and management techniques for such networks by taking into account the explicit representation of both phases and neutral conductors in the context of losses management, which includes both losses minimization and losses allocation concepts in its scope. Regarding the latter notion, a novel multi-phase losses allocation procedure is proposed which avoids allocating neutral losses to phases conductors and, consequently, provides explicit information about phase- and neutral-losses allocation factors. The proposed approach successfully takes into account the impact of unbalanced loading through self- and mutual-variable losses coefficients while allocating losses to end-users. Based on the information

provided by positive neutral losses allocation factors, a novel unbalance reduction strategy is further developed which allows the commutation of loads from heavily loaded phases of a critical node to its lightly loaded phases and, therefore, improves network balancing significantly.

In the framework of losses reduction, a multi-phase Optimal Power Flow (OPF) model based on Semi-Definite Programming (SDP) technique is formulated which successfully incorporates neutral conductors as well as wye- and delta-connected loads in its formulation. Moreover, a novel complex voltage variable-based approach is proposed for the incorporation of a complete ZIP load in the proposed relaxation. However, due to excessively high computational requirements of this relaxation in the case of medium- and large-size DNs, a cheap SDP-based OPF model is additionally proposed and three novel propositions are developed in this context for the modelling of constant current loads. The proposed cheap relaxation can be practically realized due to its low computational requirements and provision of exact solution under a range of ZIP load parameters. However, due to the dominance of multi-phase SDP-based approach over cheap SDP-based relaxation, the latter relaxation is further tightened by imposing additional constraints in the form of convex envelopes. As a result, a tight solution is obtained without making any compromise on the computational benefits of cheap SDP-based OPF relaxation.

Finally, all the proposed strategies are simulated on several test cases to demonstrate their positive potential in the context of LV active DNs management.

Sommario

La continua proliferazione di fonti Distribuite di Energia Rinnovabile (DER) nelle reti di distribuzione in media (MT) e bassa tensione (BT) sta giocando un ruolo di primo piano nella riduzione dell'impronta di carbonio degli impianti di produzione di energia elettrica a base di combustibili fossili. Tuttavia, la rapida integrazione di tali risorse ha modificato anche la natura passiva di queste reti e, di conseguenza, è necessaria una particolare attenzione al fine di garantirne un funzionamento ottimale, sicuro ed affidabile. Inoltre, le DER installate non possono funzionare semplicemente sulla base di una politica di "fit-and-forget" a causa dell'emergere di diversi problemi tecnici causati dalla loro interconnessione. Problemi come lo squilibrio di tensione, il flusso inverso di energia, il funzionamento in isola indesiderata, ecc. si verificano frequentemente in queste reti che, a loro volta, richiedono nuovi sistemi di controllo e di gestione per garantire la fornitura continua di energia agli utenti finali. In questo contesto, diversi paesi hanno aggiornato i propri codici di rete per garantire la partecipazione attiva delle DER alla fornitura di servizi ausiliari.

In questo contesto, l'analisi multi-fase delle reti di MT e, soprattutto, BT acquisisce un'attenzione senza precedenti a causa dell'incapacità della rappresentazione monofase equivalente delle reti nel descrivere il quadro reale delle condizioni operative e delle variabili di stato del sistema. Un'analisi dettagliata della rete, a sua volta, stabilisce il percorso per soluzioni innovative per gestire efficacemente queste reti. Inoltre, per quanto riguarda le reti di BT, il neutro deve essere considerato come un conduttore di fase a causa della significativa presenza di corrente circolante in esso in caso di scenario con carico di rete altamente sbilanciato, dove l'applicazione dell'approccio di riduzione di Kron deve essere evitata in quanto dipendente dall'assunzione irrealistica di avere un conduttore di neutro equipotenziale. Perciò, poiché le reti di distribuzione attive in BT diventeranno, in un prossimo futuro, uno dei pilastri della rete elettrica decentralizzata è necessario che esse vengano analizzate e gestite considerando ogni aspetto della loro struttura.

Con particolare riguardo ed attenzione alle reti di distribuzione attive di BT, questa tesi presenta nuove tecniche di analisi e gestione di tali reti nel contesto della gestione delle perdite, che include sia la minimizzazione delle perdite che il concetto di allocazione delle perdite. In particolare, per quanto riguarda quest'ultimo concetto, viene proposta una nuova procedura di allocazione multi-fase delle perdite che evita di attribuire le perdite sul neutro ai conduttori di fase e, di conseguenza, fornisce informazione esplicite sui fattori di allocazione delle perdite di fase e neutro. L'approccio proposto tiene conto con successo dell'impatto di un carico non bilanciato attraverso auto e mutui coefficienti di perdita, assegnando nel contempo le perdite agli utenti. Sulla base delle informazioni

fornite dai fattori positivi di allocazione delle perdite, è stata sviluppata una nuova strategia di riduzione dello sbilanciamento che consente la commutazione dei carichi connessi alle fasi sovraccariche di un nodo critico a quelle a basso carico, migliorando in modo significativo lo sbilanciamento della rete.

All'interno del contesto di riduzione delle perdite, è stato formulato un modello multifase di Ottimizzazione dei Flussi di Potenza (OPF) basato sulla tecnica di Programmazione Semi Definita (SDP) che incorpora con successo nella sua formulazione sia i conduttori di neutro che i carichi collegati a stella e triangolo. Inoltre, viene preso in considerazione un modello completo di carico ZIP e proposto un nuovo complesso approccio basato su variabili di tensione per la sua integrazione nel rilassamento suggerito. Tuttavia, a causa dei requisiti di calcolo eccessivamente onerosi associati a questo tipo di rilassamento nel caso di reti di distribuzione di medie e grandi dimensioni, viene proposto un ulteriore modello meno oneroso di OPF basato sulla SDP e incentrato su tre diverse nuove proposizioni per la modellizzazione di carichi a corrente costante. Il rilassamento proposto, essendo meno gravoso dal punto di vista computazionale, può essere applicato grazie ai suoi bassi requisiti di calcolo ed alla possibilità di ottenere una soluzione esatta con un intervallo di parametri ZIP dei carichi. Tuttavia, a causa del prevalere dell'approccio SDP multifase su quello a basso impatto computazionale, quest'ultimo è stato ulteriormente rafforzato attraverso l'introduzione di vincoli aggiuntivi sotto forma di inviluppi convessi che racchiudono la regione non convessa delle singole variabili di ottimizzazione e, di conseguenza, fornisce una soluzione precisa senza pregiudicare i benefici computazionali apportati dal rilassamento proposto.

Infine, tutte le strategie proposte sono simulate su diversi casi studio per dimostrare il loro potenziale nel contesto della gestione delle reti di distribuzione attive in BT.

Contents

List of Figures

List of Tables

List of Acronyms

Acronyms

AC	Ant-Colony
ADMM	Alternative Direction Method of Multipliers
ADN	Active Distribution Network
ANM	Active Network Management
ANN	Artificial Neural Network
BBBC	Big-Bang Big-Crunch
BCDLA	Branch Current Decomposition method for Losses Allocation
BESS	Battery Energy Storage System
BFM	Branch Flow Model
BIM	Bus Injection Model
CB	Capacitor Bank
CBSDR	Cheap BIM-based Semi-Definite Relaxation
CCI	Correction Current Injection
CLP	Classical Losses Partitioning
CNCV	Cumulative Normalized Constraint Violation
CT	Computational Time
CVC	Coordinated Voltage Control
CVR	Conservation Voltage Reduction
DER	Distributed Energy Resources
DERC	DER Control
DG	Distributed Generator
DLC	Direct Loss Coefficient
DLF	Deterministic Load Flow
DM	Dynamic Maximum
DMS	Distribution Management System
DN	Distribution Network
DNN	Distribution Network which is equipped a with Neutral conductor
DNR	DN Reconfiguration
DSO	Distribution System Operator
DT	Distribution Transformer
EMS	Energy Management System

ENS	Energy Not Supplied
ERM	Exponential Recovery Model
ESB	Energy Storage Batteries
ESM	Energy Storage Management
ESMLA	Energy Summation Method for Losses Allocation
ESU	Energy Storage Unit
EV	Electric Vehicle
EVR	Eigen Value Ratio
FR	Feasible Region
FR/FC V	*First-Row/First-Column Variable*
GA	Genetic Algorithm
GLP	Geometric Losses Partitioning
GMM	Gaussian Mixture Model
HTA	Higher Than Average
HUN	Highly Unbalanced Node
ICT	Information and Communication Technology
IDSA	Improved Differential Search Algorithm
IPSO	Improved PSO
KR	Kron Reduction
LA	Losses Allocation
LAP	Losses Allocation Procedure
LinP	Linear Programming
LM	Load Model
LP	Losses Partitioning
LsMag	Losses Management
LsMin	Losses Minimization
LTA	Lower Than Average
LV	Low Voltage
MCM	Multi-Conductor Modelling
MG	Micro Grid
MILP	Mixed Integer Linear Programming
MISDP	Mixed Integer Semi-Definite Programming
MISOCP	Mixed Integer Second-Order-Cone Programming
MLC	Marginal Loss Coefficient
MM1	Modified Model 1
MO	Multi-Objective
MOEAD	Multi-Objective Evolutionary Algorithm-based Decomposition
MPG	Multiple Point Grounded
MPLAP	Multi-Phase Losses Allocation Procedure
MPSDP	Multi-Phase Semi-Definite Programming
MV	Medium Voltage
NLAF	Neutral Losses Allocation Factor
NNC	Net Neutral Current

NP	Numerical Problem
NR	Network Reconfiguration
NRPF	Newton-Raphson Power Flow
NSGA	Non-Sorted Genetic Algorithm
OADER	Optimal Allocation of DER
OF	Objective Function
OG	Optimality Gap
OLTC	On-Load Tap Changer
OP	Optimization Problem
OPF	Optimal Power Flow
OV	Optimization Variable
PDF	Probabilistic Distribution Function
PhS	Phase Switching
PhSD	Phase Switching Device
PLAF	Phase Losses Allocation Factor
PLF	Probabilistic Load Flow
PM	Participation Matrix
PS	Proportional Sharing
PSA-1	Phase Switching Algorithm-1
PSA-2	Phase Switching Algorithm-2
PSD	Positive Semi-Definite
PSMLA	Power Summation Method for Losses Allocation
PSO	Particle Swarm Optimization
PST	Power System Transformation
PV	Photo Voltaic
QC	Quadratic Convex
QLP	Quadratic Losses Partitioning
R2	Rank-2
RCLP	Resistive Component-based Losses Partitioning
RCNC	Reduced Cross-section Neutral Conductor
RD	Relative Difference
RDN	Radial Distribution Network
RMSE	Root Mean Square Error
SDP	Semi-Definite Programming
SFLA	Shuffle Frog Leaping Algorithm
SM	Static Maximum
SMLA	Succinct Method for LA
SOC	Second Order Cone
SOCP	Second-Order-Cone Programming
SPG	Single Point Grounded
SSV	Sequential Shapely Value
TAL	Total Allocated Losses
T&D	Transmission and Distribution

TN	Transmission Network
TPQC	Three-Phase Quadratic Convex
TPSDP	Three-Phase Semi-Definite Programming
TS	Tabu Search
VLC	Variable Loss Coefficient
VR	Voltage Regulator
WT	Wind Turbine

List of Symbols and Matrices

The main symbols and matrices used throughout this thesis work are presented below. Other less frequent notations are defined in the text.

Symbol	**Description**
a_r	Real part of a complex variable a
a_{im}	Imaginary part of a complex variable a
a^*	Conjugate of a complex variable a
$\|a\|$	Absolute of a complex variable
L_F	Losses on a feeder
N	Set containing the nodes of a DN
N^+	Set of nodes excluding substation node
N_T	Set of terminal nodes
N_{IL}	Set of nodes containing constant current loads
G	Subset of N containing DGs
E	Set containing total lines of a DN
B	Set containing lines in a feeder of a DN
ϕ_i	Set featuring the phase and neutral of a node i
η_i	Set of phase conductors of a node i
δ_i	Set of neutral conductors of a node i
ϕ_{ij}	Set featuring the phase and neutral of a line $i \sim j$
η_{ij}	Set of phase conductors of a line $i \sim j$
δ_{ij}	Set of neutral conductors of a line $i \sim j$
ψ_i	Set featuring phase-neutral connections at node i
χ_i	Set representing phase-phase connections at node i
V_i^{φ}	Scalar complex phase-ground voltage at phase $\varphi \in \phi_i$ of a node i
V_i^{υ}	Scalar complex phase-neutral voltage for $\upsilon \in \psi_i$ of a node i
V_i^{σ}	Scalar complex phase-phase voltage for $\sigma \in \chi_i$ of a node i
I_i^{φ}	Scalar complex current injection at phase/neutral of a node i for $\varphi \in \phi_i$
I_{ij}^{ρ}	Scalar complex current flowing on phase/neutral of a line $i \sim j$
$Y_{i_{(0)}}^{\upsilon}$	Rated complex admittance of a shunt element connected between phase and neutral of a node i for $\upsilon \in \psi_i$
$Y_{i_{(0)}}^{\sigma}$	Rated complex admittance of a shunt element connected between two phases of a node i for $\sigma \in \chi_i$

$P_{l_i}^{\varphi}/Q_{l_i}^{\varphi}$	Active/reactive power demand corresponding to a load connected between phase and neutral of node i for $\varphi \in \psi_i$
$P_{l_i}^{\upsilon}/Q_{l_i}^{\upsilon}$	Active/reactive power demand corresponding to a load connected between two phases of node i for $\upsilon \in \chi_i$
$P_{g_i}^{\varphi}/Q_{g_i}^{\varphi}$	Active/reactive power generation corresponding to a DG connected between phase and neutral of node i for $\varphi \in \psi_i$
$P_{g_i}^{\upsilon}/Q_{g_i}^{\upsilon}$	Active/reactive power generation corresponding to a DG connected between two phases of node i for $\upsilon \in \chi_i$
$\underline{V}, \overline{V}$	Voltage magnitude limits
$\underline{P}_{g_i}, \overline{P}_{g_i}$	Minimum and maximum active power generation bounds at node i
$\underline{Q}_{g_i}, \overline{Q}_{g_i}$	Minimum and maximum reactive power generation bounds at node i
$k_{Z_{p/q}}$	Coefficient related to active/reactive power absorption (injection) of a constant impedance load
$k_{I_{p/q}}$	Coefficient related to active/reactive power absorption (injection) of a constant current load
$k_{P_{p/q}}$	Coefficient related to active/reactive power absorption (injection) of a constant power load
λ_{pq}^{xy}	Variable loss coefficient linking conductors x and y currents of nodes p and q, respectively
δ	Voltage angle deviation parameter
$\theta_{ij}^{\varphi_i \varphi_j}$	Angle difference between phases of nodes i and j for $\varphi_i, \varphi_j \in \phi_{ij}$
$\otimes$	Component wise multiplication

Matrices	**Description**
$\Re(\mathbf{A})$	Real part of a vector/matrix $\mathbf{A}$
$\Im(\mathbf{A})$	Imaginary part of a vector/matrix $\mathbf{A}$
$\mathrm{Tr}(\mathbf{A})$	Trace of a matrix $\mathbf{A}$
$\mathrm{diag}(\mathbf{A})$	Diagonal of a matrix $\mathbf{A}$
$\mathrm{rank}(\mathbf{A})$	Rank of a matrix $\mathbf{A}$
$\mathbf{A} \succeq 0$	Positive semi definiteness condition on a matrix $\mathbf{A}$
$\mathbf{e}_k^{\varphi}$	Standard canonical basis of $\mathbb{R}^{\lvert \eta_k/\phi_k \rvert \times 1}$
$\mathbf{V}_i$	Complex phase-ground voltage vector of a node i
$\mathbf{I}_{lm}$	Complex current vector related to the flow on line $l \sim m$
$\mathbf{I}_i$	Complex current injection vector at node i
$\mathbf{I}_i^G$	Complex current injection vector at node i corresponding to DGs currents
$\mathbf{I}_i^L$	Complex current injection vector at node i corresponding to loads currents
$\mathbf{I}_i^{Net}$	Complex current injection vector at node i corresponding to net (loads and DGs) currents
$\boldsymbol{\theta}_{ij}$	Phase angle difference vector related to a line $i \sim j$
$\mathbf{R}_{ij}$	Series resistance matrix of a line $i \sim j$
$\mathbf{Z}_{ij}$	Series impedance matrix of a line $i \sim j$
$\mathbf{Y}_{ij}$	Shunt admittance matrix of a line $i \sim j$

$\mathbf{P}_{ij}^{loss}$	Active power losses vector on line $i \sim j$
$\mathbf{S}_{\varrho i}$	Phase-ground apparent power injection vector at node i
$\mathbf{Y}_B$	Bus admittance matrix
$\mathbf{Y}_{k,nw}^{\varphi}$	Bus admittance matrix related to phase $\varphi \in \phi_k$ of a node k
$\mathbf{\Psi}_{k,nw_p}^{\varphi}$	Hermitian matrix related to network admittances as seen by the phase φ of a node k with respect to active power injection
$\mathbf{\Psi}_{k,nw_q}^{\varphi}$	Hermitian matrix related to network admittances as seen by the phase φ of a node k with respect to reactive power injection
$\mathbf{\Psi}_{k,nw_v}^{\varphi}$	Hermitian matrix related to the voltage corresponding to phase φ at node k
$\mathbf{\Lambda}_{Y/\Delta_i}$	Load matrix related to Y/Δ load connected at node i
$\mathbf{\Lambda}_{Y/\Delta_i}^{Z}$	Load matrix formed by multiplying k_Z to the admittance of constant impedance component of a ZIP load at node i
$\mathbf{\Lambda}_{Y/\Delta_i}^{I}$	Load matrix formed by multiplying k_I to the admittance of constant current component of a ZIP load at node i
$\mathbf{\Lambda}_{Y/\Delta_i}^{P}$	Load matrix formed by multiplying k_P to the admittance of constant power component of a ZIP load at node i
$\mathbf{\Lambda}_{Y/\Delta_i}^{I_c/P_c}$	Load matrix independent of k_I/k_P load parameters and contains admittance of constant current/constant power load component only
$\mathbf{Y}_L^Z$	Load matrix containing $\mathbf{\Lambda}_{Y/\Delta}^{Z}$ of all nodes
$\mathbf{Y}_L^I$	Load matrix containing $\mathbf{\Lambda}_{Y/\Delta}^{I}$ of all nodes
$\mathbf{Y}_L^P$	Load matrix containing $\mathbf{\Lambda}_{Y/\Delta}^{P}$ of all nodes
$\mathbf{\Psi}_{k,l_p}^{\varphi:Z\%}$	Hermitian matrix of absorbed/injected active power corresponding to Z component of a ZIP load connected at phase φ of node k
$\mathbf{\Psi}_{k,l_p}^{\varphi:I\%}$	Hermitian matrix of absorbed/injected active power corresponding to I component of a ZIP load connected at phase φ of node k
$\mathbf{\Psi}_{k,l_p}^{\varphi:P\%}$	Hermitian matrix of absorbed/injected active power corresponding to P component of a ZIP load connected at phase φ of node k
$\mathbf{\Psi}_{k,l_q}^{\varphi:Z\%}$	Hermitian matrix of absorbed/injected reactive power corresponding to Z component of a ZIP load connected at phase φ of node k
$\mathbf{\Psi}_{k,l_q}^{\varphi:I\%}$	Hermitian matrix of absorbed/injected reactive power corresponding to I component of a ZIP load connected at phase φ of node k
$\mathbf{\Psi}_{k,l_q}^{\varphi:P\%}$	Hermitian matrix of absorbed/injected reactive power corresponding to P component of a ZIP load connected at phase φ of node k
$\mathbf{\Psi}_{k,gnd_p}^{\varphi}$	Hermitian matrix of absorbed/injected active power corresponding to the ground admittance connected at phase φ of node k
$\mathbf{\Psi}_{k,gnd_q}^{\varphi}$	Hermitian matrix of absorbed/injected reactive power corresponding to the ground admittance connected at phase φ of node k
$\mathbf{\Psi}_{i \longrightarrow j}^{\varphi,nw_p}$	Hermitian matrix related to the line flow (active power) from node i to node j
$\lvert\hat{\lambda}_{p-1}\rvert/\lvert\hat{\lambda}_p\rvert$	Eigen Value Ratio
$\hat{\mathbf{W}}$	Optimization variable of MPSDP-based relaxation

CHAPTER 1

Introduction

Across the globe, power sectors are undergoing significant changes to achieve sustainable, affordable and reliable electricity. The continuous progress in both supply- and demand-side technologies along with increased digitalization and automation of end-users is influencing the planning and operation of power systems, and, as a result, innovative approaches ranging from institutional reforms to technical adaptations are emerging in this regard. In view of this, Power System Transformation (PST) idea has attained significant attention across the globe to ensure the reliable and secure operation of a power system.

PST is an active process of creating policy, market and regulatory environments, as well as establishing operational and planning practices, that accelerate investments, innovation and the use of smart, efficient, resilient and environmentally sound technology options to facilitate and manage requisite changes in the power sector [1]. The interactions of technology, physical electricity infrastructure, and market, policy and regulatory frameworks formulate the key components of this process. Being highly context-specific process, the solutions from one administrative area cannot simply be replicated in another; however, common themes are also emerging which allow implementing a number of transferable principles across several regions and countries.

In this context, this chapter examines recent trends in PST process, with a particular focus on the current structure and pathways for transforming the existing power system, and evolution of local grids which ultimately allow to properly define the goals of this thesis work.

1.1 Current structure and transformation pathways for power system

The existing power sector structures show a large degree of diversity when measured within policy, market and regulatory frameworks. However, all of them are evolved from the common vertically integrated model and as a result, can be broadly classified into five separate models: vertical integration; single-buyer; unbundling; wholesale market

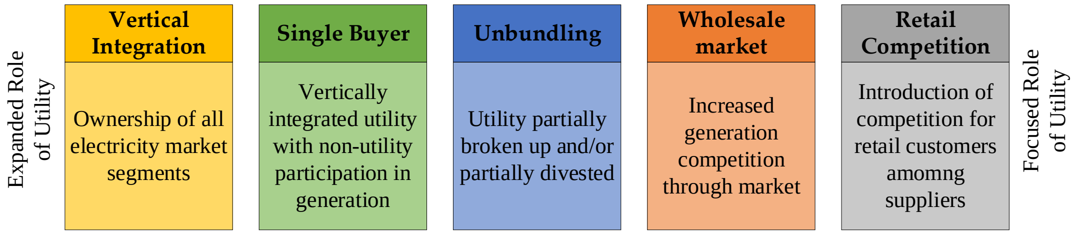

Figure 1.1: Typical models for electricity sector ownership and participation [2].

and retail competition as shown in Fig. 1.1 [2]. Vertically integrated utilities include generation, transmission, distribution and retail sales under one organisational structure and, therefore, considered as a pure monopoly framework having no competition with any other utility organization.

The most basic level of competition involves the incorporation of independent power producers in the vertically integrated model to overcome the associated inefficiencies as well as investment shortages by allowing private investors to build, own and operate power plants and sell their output to the utility. This model is commonly known as a single-buyer model which is followed by an unbundling model which represents a further reform in the market structure. In this model, vertically integrated power structures are replaced by separate distinct companies which own or operate generation sources as well as transmission and distribution grids with related services. The most common form of unbundling is the separation of transmission system operation (and in some cases asset ownership) from the rest of the system. In the next phase, a competitive market is introduced which allows buyers and sellers of wholesale electricity to perform energy transaction in a centralised trading platform. Competitive wholesale markets are a common structure in the United States, the European Union and South America (e.g., Chile, Colombia). Finally, the last step introduces a competitive retail market where end-users (industrial, commercial and/or residential customers) can choose which retail company provides the energy component of their service. New Zealand and Texas are examples of fully restructured electricity markets that have both wholesale and retail competition [3].

From an institutional perspective, PST is taking place across a variety of pathways depending on the initial conditions and the desired end state. In [4], four example scenarios, as shown in Fig. 1.2, are presented which define the relevant end state based on the extent of change and speed required in the initial existing structure. It can be noted that in the adaptation scenario, limited and incremental change reflects efforts which are underway in many regions around the globe. In this context, *Next-generation performance-based regulation* and *Bottom-up coordinated grid expansion* pathways are considered as two leading examples of power system reform. In the former case, vertically integrated utilities still exist but main emphasis is put on the delivery of societal values rather than the simple recovery of capital investment, whereas in the latter pathway, the benefits of innovative technology and business models are utilized to accelerate the end-users access to energy. In evolution pathway, systematic and comprehensive changes over a longer period of time

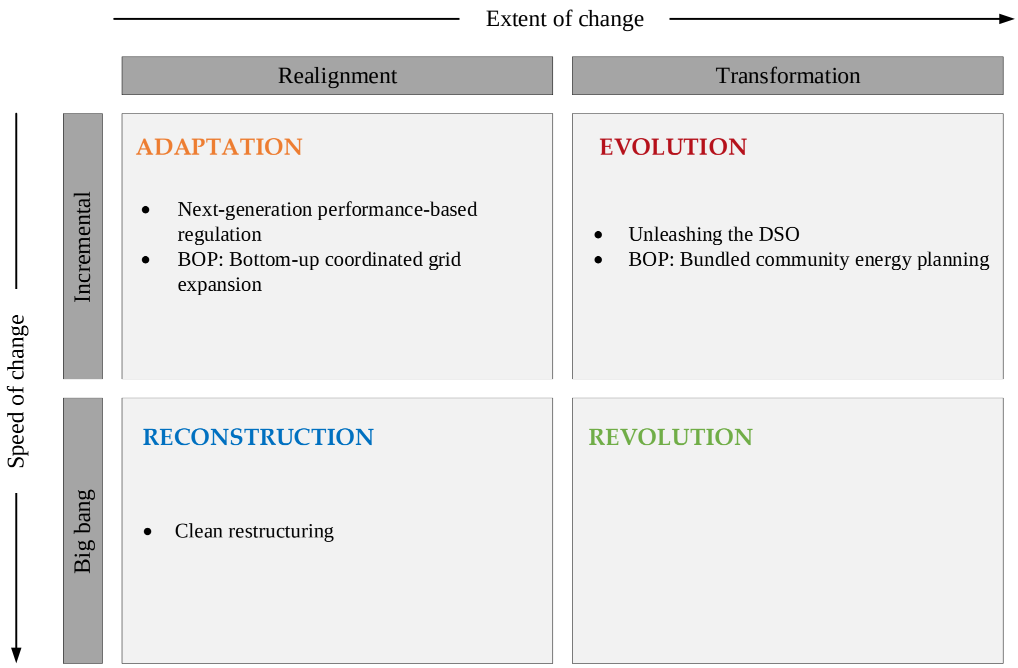

Figure 1.2: Illustrative scenarios for power system transformation [4].

are foreseen to ensure an active participation of demand response and electric vehicle charging station with the objectives of achieving a power system having balanced centralized and distributed generation. In this context, *Unleashing the DSO* is a pathway that champions Distributed Energy Resources (DER) and Low Voltage (LV) market operations. The reconstruction scenario occurs more rapidly but without fundamental changes in technologies or market participants, whereas the most far-reaching scenario, revolution, includes both fundamental and rapid changes which, in turn, lead to a fully competitive market scenario having real-time electricity pricing at the retail level and the emergence of a phenomenon technology, such as highly affordable and widely accessible energy storage that can change the PST from its basic fundamental level.

1.2 Recent trends and developments shaping the existing power sector

The legacies of a power system, as discussed in the previous section, basically shape the landscape of options available for PST. Based on the existing structure of power systems, a range of emerging trends are appearing across the globe which are driving the process of PST. These trends, most notably but not limited to, include successful integration and deployment of renewable DERs, evolution of electricity demand, market dynamics of coal and gas generation, and security of electricity supply. Being more relevant to the context of this work, trends concerning the integration of renewable DERs are briefly discussed in the following sections.

1.2.1 Building on existing knowledge and experience

The effective integration of renewable DERs requires detailed planning and thinking across aspects of generation and transmission infrastructure build-out, system operations techniques, and market and retail rate regulation. Quite recently, there has been healthy international diffusion of ideas and techniques for grid integration, with movement in many jurisdictions from experimentation to more concrete adoption of successful practices, particularly in countries which have higher share of electricity production from renewable DERs such as Denmark, Ireland and Spain. In other words, a growing number of examples of success, failure and good practice are now available from a diverse set of countries which can be considered by other countries and players who are investing heavily in this sector [5].

1.2.2 Evolving actors and interests

The increasing participation of demand side through market, policy and regulatory framework, greater private-sector participation in dynamic electricity markets and innovative support for low-income customers through rooftop solar programmes are identified as the emerging actors which are paving the way for PST.

The demand side presents a substantial opportunity to reduce system costs, promote cost-effective renewable DERs integration, and yield value for both retail and wholesale energy users [2]. Similarly, in dynamic electricity markets, governments are increasingly shifting institutional frameworks to encourage more private-sector investment and reduce energy costs. These transitions, on the one hand, can be incremental in nature, or happen more rapidly depending on local conditions, whereas on the other hand, they may involve only slight changes in existing institutional frameworks, or incite more transformational change. In this regard, Mexico provides a successful case study to achieve a completely deregulated wholesale power market in less than five years from a vertically integrated model by pursuing a relatively accelerated path of market reform [3].

Another emerging trend that has been observed across the globe is the exploration of rooftop solar programmes which are explicitly designed to benefit the poor and low-income customers. The declining solar costs and reforms in utility business models and regulation are driving some utilities and regulators to deploy rooftop solar systems on the premises of such customers by either providing a rooftop rental payment and often free electricity or bill credit to the customers. In this regard, a public-private partnership *Rent-a-Roof* programme has already been established in Gujarat, India, with the aim of providing a rooftop rental payment to private customers, ranging from commercial and industrial to residential consumers [6].

1.2.3 Emerging investment frameworks

In this context, increasingly system friendly procurement of renewable DERs and evolving regulatory frameworks for encouraging investment in DERs are seen as the main drivers pushing the process of PST.

Traditionally, procurement mechanisms for renewable DERs have largely focussed on technical designs and selection sites that, on the one hand, can reduce the Distributed Generators (DGs) costs and, on the other hand, can maximise their output, without consideration of the expected technical or economic impact on the rest of power system. Since the share of these resources are now approaching 20% to 30% in many markets, governments are increasingly creating investment signals which drive site selection to areas that are more *system friendly* and suit the overall electricity grid [7]. Another prevailing mechanism in this regard is the updating of the grid codes which now put additional requirements on wind and solar power plants to provide ancillary services both during the normal and emergency operation of a grid and, therefore, provide economic incentives to the owner of these power plants [8]. Similarly, regulatory incentives are driving Distribution System Operators (DSOs) to weigh traditional upgrades to grid capacity against emerging alternatives such as investing in grid intelligence, energy efficiency, demand response, or various forms of DERs, including decentralised generation and storage. Resultantly, end-users of every type are showing more interest in the uptake of local DERs for the effective management of their production and consumption of energy.

1.2.4 Responses to changing marketing conditions and technology drivers

To cope with the emerging new technologies and changing market conditions, increasing cross-border coordination and power sector integration, with more focus on stand-alone and small-scale power systems for providing rural energy services, are clearly seen as recent evident trends in the process of PST.

The coordination between neighbouring balancing areas within a country or across countries is increasing the power system flexibility in the context of renewable DERs integration as well as optimising the overall system operating cost. A growing number of coordinated and consolidated power system operations are appearing in western United States and northern European countries. The Nordic and Pennsylvania-New Jersey-Maryland balancing markets provide good examples in this scenario. Similarly, an initiative is also currently under way in the Association of Southeast Asian Nations (ASEAN) region to create a regional power grid with integrated system operations [9].

On the other hand, isolated power systems and micro-grids in developing countries are also emerging and the respective governments have started embracing these technologies as a reliable as well as cheap way of providing electricity to un-electrified communities, especially in geographically remote areas. In the near past, the provision of cheap energy, especially, electricity had *often* been perceived as the main responsibility of national utilities, in terms of their infrastructure extension, and deployment of micro-grids was more often left to the non-governmental organisation and donor communities. However, the trend is changing now and in the past several years, an increasing number of governments have begun actively encouraging widespread adoption of micro-grids as a long-term mean of providing rural energy services that can complement rather than compete with the national grid [10].

1.2.5 Evolving public policy and regulatory strategies

In this context, several countries and governments have already stepped up their goals and targets for increasing the incorporation of green energy resources. The continuous declining costs of renewable DERs and increasing experience with their technologies and operations have given enough confidence to countries about their reliability and cost-effectiveness, and resultantly, they are adopting more eco-friendly policies by replacing conventional fossil-fuel-based plant with renewable resources. Furthermore, governments and network system operators across the globe are increasingly using competitive procurement mechanisms to attract competitors and reduce the cost of green DERs. This trend is more visible in markets which have vast diversity from institutional frameworks point of view, including those with wholesale power markets. Although, these mechanisms still offer long-term power purchase contracts, but the ultimate contract price is decided by competition [1].

Another emerging trend among utilities is the adoption of value-based remuneration mechanism for DER customers, which is a significant departure from the traditional compensation mechanisms (net energy metering, feed-in tariffs, net billing etc.), with the aim of closely reflecting the value of DERs energy on a grid [11].

1.3 Evolution of local grid

The trends mentioned in the previous section are a clear indication that local grids, which include both Medium Voltage (MV) and LV networks, are in a transition phase from being passive to becoming active Distribution Networks (DNs). Traditionally considered as passive networks without requiring any or little need of active management, the picture has now begun to change due to substantial penetration of DERs, business model innovation, digitalization and cross-sector coupling between heat, electricity and transportation in these networks. Looking further into the future, it is obvious that these trends may considerably reshape this part of a national power grid, increasing its importance as a critical part of a more cost-effective, reliable and clean energy system. Consequently, a number of questions has arisen such as:

1. Which are the most promising current drivers concerning the transformation of passive DNs?
2. What is the long-term vision for these local grids?
3. How can an optimal and secure operation of these grids be ensured under such drastic transition phase?

1.3.1 Current drivers transforming the grid

The most pivotal and principal drivers currently underpinning evolution in local grids include significant penetration of DERs, smartening of local grids by utilities, which also includes an improvement in the accuracy of pricing signals and revenue collection, and electrification of heating and transport. Since a comprehensive discussion is already carried out for the integration of DERs in the previous section, this section offers a brief yet comprehensive review on the latter drivers in the context of the local grid transformation process.

1.3.1.1 Smartening of local grids

Over recent years, grid companies have tested and adopted a wide range of smart technologies to increase the intelligence and surveillance of local networks. The rapid integration and inclusion of smart meters in many power systems today has made it possible to have a more clear and well-defined track of electricity consumption, and, therefore, a more sophisticated control and operation of these networks is becoming possible with every passing day. Furthermore, utilities have started certain initiatives such as improved situational awareness by the application of Information and Communication Technology (ICT) which, in turn, have increased the reliability, improved the operational efficiencies, and reduced the losses (technical and non-technical) in local grids. For example, in Austria, a pilot project was launched in 2014 to identify several control options for voltage management in local grids which have high share of distributed generation. It was found that by a 20% increase in the hosting capacity of local grids can be achieved by combining the active decentralised network management schemes with smart planning and monitoring approaches [12].

1.3.1.2 Electrification of heating and transport

Currently, demand for low-intensity heat, such as space heating, and individual transport predominantly relies on fossil fuel sources. However, over recent years, a growing number of increasingly cost-competitive and innovative electric supply alternatives have emerged as well to provide these services. The deployment of these technologies is offering a number of benefits. Firstly, the coupling of heat pumps with thermal energy storage units and Electric Vehicles (EVs) is allowing demand shift across time which in turn is reducing the need for expensive peak-time generation and helping integrating more renewable DERs [13]. Secondly, electrification of these services is allowing decarbonisation of an electricity mix. The concept of electric heating, although is not new, and has been fairly common in a number of countries for decades, it has, however, received renewed attention concerning broader decarbonisation of an energy system and integration of renewable DERs.

1.3.2 Long term vision for local grids

Due to continuous transformation of local grids, it is important to envision them as a central component of a clean, reliable and cost-effective energy system in long-terms. Consequently, the following trends are expected, in the near- and far-future, to be appeared in local grids.

- Large scale adoption of DERs and turning them into a central part of electricity supply
- Utilization of ICT for mass enrolment of demand response

- Electrification of heating and transport sector which is largely driven by the decarbonisation and local pollution objectives

Concerning large scale adoption of DERs, their cost-optimal share is, however, subjected to considerable uncertainty particularly in the case of decentralized PV systems. For example, if the cost of EVs keeps declining, the installation of more charging infrastructure could trigger upgrades to a local grid infrastructure and, resultantly, much higher shares of PV systems could be integrated at a very little or no incremental cost.

About the participation of end-users in local grid management, the grid should facilitate the bidirectional flow of both electricity and information data due to the rising intelligence of all network components down to individual smart appliances. Consequently, the emergence of much richer and more complex interactions among devices on a grid, as shown in Fig. 1.3, in the near-future, can pave the way for enhanced grid management within a centralized or decentralized framework.

Finally, due to the combination of technological and cost improvements, as well as with the development of more stricter equipment standards, modern household appliances are becoming more smarter and, resultantly, Energy Management System (EMS) can use real-time data of market prices and grid situation in the near-future to optimise energy flows within a home, a building, at a district or even at city level throughout the day. Furthermore, by automatically making decisions on behalf of end-users, within pre-established boundary conditions, EMS can bring much greater demand response to reality as compared to the situation where each end-user responds to price signals on its own. Such advanced control capabilities subsequently can ensure the efficient uptake of heat pumps, EVs and other end-use technologies such as intelligent thermometers and battery energy storage systems [1].

1.3.3 Secure and optimal operation of local grids

The significant integration of decentralized DERs in local grids raises a natural question regarding the secure and optimal operation of these networks in the presence of uncertainties associated with these DERs and, if possible, how can these resources play a positive role in ensuring the safe supply of electricity? In broader terms, the following queries become extremely relevant in this context:

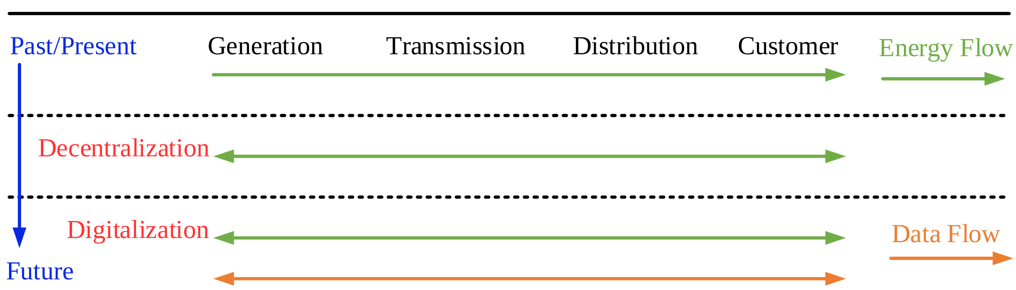

Figure 1.3: Impact of decentralisation and digitalization on local power grids.

- What possible roles DERs, especially rooftop solar PV, can play?
- What are the possible smart grid options in the presence of ICT and supervisory control systems for the effective and secure operation of local grids?
- How can the analysis of local grids be performed by taking into account the DERs models, demand forecasting and end-users profiles?

1.3.3.1 Role of distributed energy resources

With the introduction of DERs, the traditional management approaches about local grids are no longer sufficient. Since DERs are causing more dynamic energy flows, new technical schemes from the operational and management point of view are emerging to tackle the possible impacts, which are shown in Fig. 1.4, of these DERs [14]. On the one hand, distributed solar PVs are making local grid operations more challenging; however, on the other hand, they are also being employed in improving operational network parameters by providing services that support grid stability. Furthermore, using smart inverter-based technology, solar PVs are providing voltage management capabilities and power system support services. The integration of battery storage system with solar PVs is further improving the provision of these services, as shown in Fig. 1.5 [14], and, consequently, enjoys the most important benefit of shifting some or all of the generated power to times of higher system demand. These services not only have value for local grids but are also becoming relevant in ensuring secure electricity supply at high shares of decentralised solar PVs. Nevertheless, accommodating a large number of DERs requires managing their impact at all voltage levels. High levels of DERs, while co-located with loads at a lower

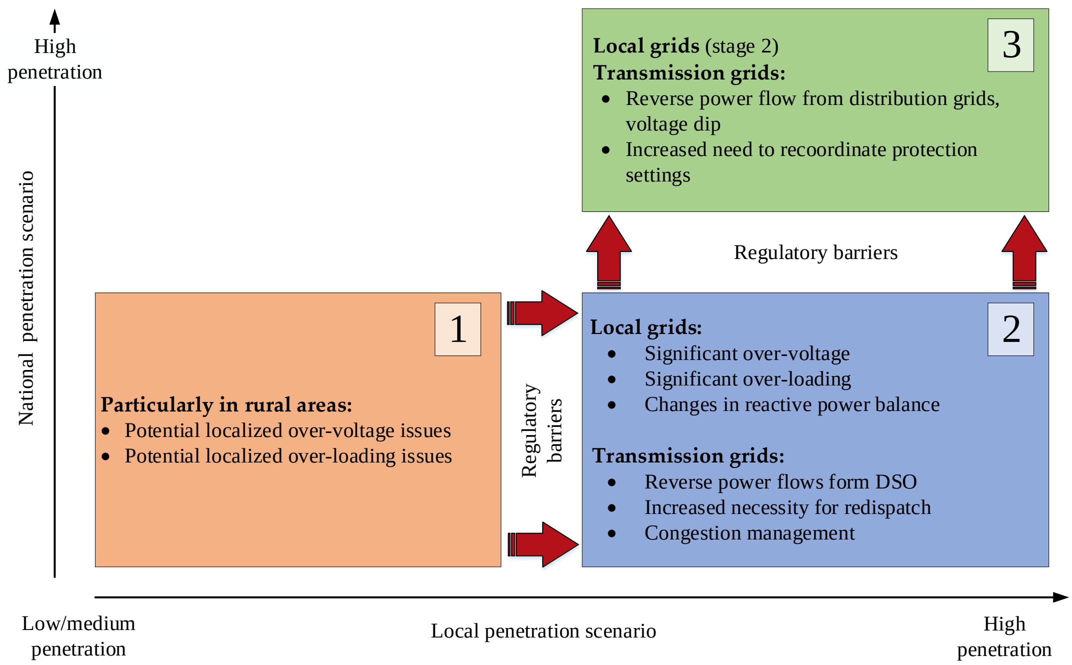

Figure 1.4: Technical impacts of rising deployment of distributed solar PV generation [14].

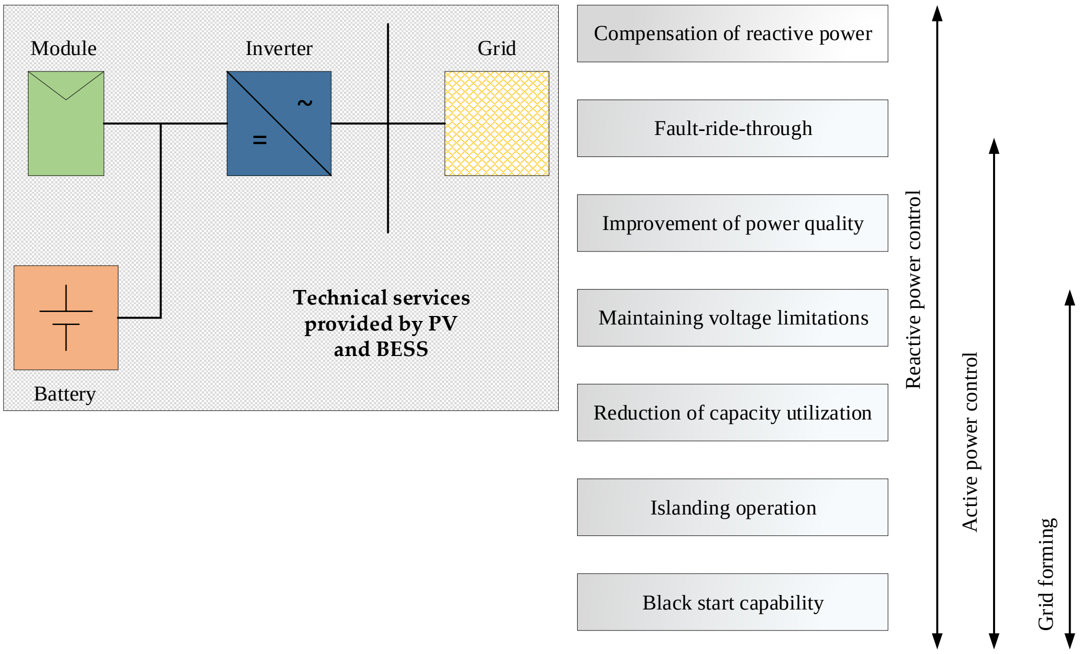

Figure 1.5: Technical services available from solar PV systems [14].

voltage level, still affect dispatch and power flow on a high-voltage network as much as a single-site plant with the same aggregate rating. Consequently, new modelling tools and greater collaboration between planners is critical at all voltage levels for successful technical management of DERs.

1.3.3.2 Smart grid options

ICT and Supervisory Control And Data Acquisition (SCADA) systems have been the most important tools for smartening local grids in recent years [15]. These technologies are increasing the observability of a network by providing the ability to monitor voltages and power flow in distribution feeders as well as allowing better management of bidirectional energy flow. A range of smart grid options are now available for dynamic monitoring and control as mentioned in Table 1.1 which allow the adjustment of DNs in a real-time through specific ways which were previously considered uneconomical or deemed unnecessary.

1.3.4 Advanced modelling capabilities

Historically, the planning of local grid involved a deterministic process aiming at identifying the occurrence and extent of peak load. However, rising levels of DERs have introduced new uncertainties in the form of a more complex supply/demand pattern and events which undermine grid size during peak electricity demand. Consequently, planning standards are being updated using refined network architecture models to include innovative mitigation options such as demand-side response measures or various smart grid techniques as highlighted in the previous sections. In this perspective, system operators and planners of local grids are increasingly relying on modelling tools that can capture

Table 1.1: Overview of different smart grid technology options [11].

DSO Resource	Cost/benefit	Role	Indicative benefit where positive
SCADA system, improved monitoring and forecasting, upstream flow of information	Smart planning and operation	Improves network observability, hosting on nondispatchable generation.	1.1-3.3
Automatic network reconfiguration	Smart planning and operation	Increases hosting capacity of local grids, possible reduction of network losses.	1.1-2.2
On-load tap changer	Smart assets	Allows automated voltage regulation by changing transformer winding ratio, either remotely or autonomously.	1.2-1.8
Boost transformer	Smart assets	Stabilises voltage along heavily loaded branch feeders; typically used in long feeders with dispersed consumers to boost the voltage under heavy load conditions.	1.5-2.1
VAR control	Smart assets	With more DER changing active/reactive power balance, fast-acting power electronic devices, such as static VAR compensators (SVC) can stabilise local grid; mitigates voltage rises and/or compensates reactive power by injection of reactive currents.	1.1-1.9
Conservation voltage reduction	Smart assets	ICT solutions that enable local grid feeders to be operated at the lower end of the voltage range as required for system reliability.	1.1-2.6
Local storage	Storage	At local grid level, storage provides peak shaving, load levelling, power quality services, black-start capability and islanding support	1.1-2.4

the actual behaviour of these networks by taking into account the high-resolution representation of DERs, demand forecasting for both controllable and non-controllable loads, and multiple types of end-users profiles, such as a home with an EV [16].

1.4 Thesis objectives

The discussion in the previous sections has pointed out that the environmental concerns related to the fossil fuel-based power plants have shifted the focus of the world, especially developed nations, from the centralized power generation sources towards the decentralized DERs with a primary focus on renewable energy technologies. However, the rapid proliferation of these resources in local grids, especially LV DNs, has also affected the optimal operation of these networks as evident by the appearance of several technical issues, such as voltage rise, reverse power flow, voltage unbalance, islanding etc. Consequently, the main challenge in ensuring the reliable and secure operation of these DNs involves optimal management of DERs by implementing suitable control mechanisms to regulate both central and local controllers. In this context, as stated earlier, several countries have updated their grid codes which put additional requirements on renewable DERs, particularly those which are interfaced to the grid through static converters. These revised grid codes ensure active participation of DERs in local grid management by providing voltage and frequency control, and even the remote control of these resources.

To ensure the active participation of DERs in the context of grid management, several methodologies have already been presented in the literature. However, the majority of published research work, particularly in the field of LV DNs, assumes single-phase equivalent representation of these networks under the assumption of balanced loading condition which is not the case in real DNs due to the presence of a significant amount of unbalance. Furthermore, few studies which indeed have focused on the multi-phase configuration of a LV DN implicitly take into account the impact of a neutral conductor by applying Kron Reduction (KR) approach under the assumption of the equipotential neutral conductor. However, in the case of Single Point Grounded (SPG) and Multiple Point Grounded (MPG) network configuration, this assumption is not valid any more and, therefore, application of KR approach can lead to poor operational control of such networks. Since local grids are evolving at a fast pace due to the integration of green DERs and, therefore, can be envisioned as a central pillar of electricity supply in a long term, it is, therefore, incumbent to develop such analysis schemes for these grids which take into account the complete model of such networks and, resultantly, provide information about each phase and neutral conductor state variable for optimal control of these systems.

In view of this, the aim of the research is to propose novel analysis and management schemes for LV Active Distribution Networks (ADNs) by taking into account the explicit representation of both phase and neutral conductors of these network in the context of Losses Management (LsMag). LsMag is a broad theme which includes the concept of Losses Minimization (LsMin), Losses Allocation (LA) and other network management schemes, however, the focus in this work is restricted to the first two ideas and in this regard, a multi-phase LA approach and a multi-phase OPF model are proposed for neutral-equipped DNs. These schemes, once developed, can be integrated into a numerical simulation tool which can further be embedded into a centralized and/or decentralized EMS and Distribution Management System (DMS) corresponding to these networks.

1.5 Research gaps and structural overview of the thesis

Based on the research objectives mentioned in the previous section, the thesis is divided into two parts. The first part deals with the development of a multi-phase losses allocation strategy which allows allocating network losses to phases and neutral conductors explicitly and, subsequently, utilize this information for network management. The second part deals with the proposal of convex relaxation-based Optimal Power Flow (OPF) techniques which allow determining the optimal operating points of DERs to optimally reduce network losses.

With respect to the first objective, an extensive literature review on LsMag in LV ADNs is initially carried out. The literature review indicates that the role of LsMin schemes in the management of these DNs has been well researched and many publications are available on this topic. However, a significant research gap still exists in the domain of LAPs. Firstly, these methodologies are predominantly studied and developed for single-phase equivalent representation-based LV DNs and secondly, these approaches are still being considered as passive schemes without paying any attention to the *possible* active role these strategies can play in the context of network management. Furthermore, in the case of solely existed three-phase LAP [17], no explicit consideration has been given to the neutral losses and they are simply allocated to the end-users connected to the phase conductors by ignoring the fact that these losses exist in LV networks due to their inherent unbalance nature. Consequently, it makes little sense to allocate neutral losses to phase conductors. Based on the above-mentioned existing gaps in the domain of LAP, the following research questions are, therefore, set and successfully addressed in this work:

1. ***Can a Multi-Phase Losses Allocation Procedure (MPLAP) be developed for LV ADNs which fairly allocates the losses to each phase and neutral conductor explicitly by taking into account the impact of unbalanced loading? How should the segregation and, subsequently, allocation of the losses be carried out between different phases and neutral conductors? and what might be the possible limitations of the developed approach?***

2. ***Is it possible to utilize MPLAP for real-time management of LV ADNs? What information do losses allocate to a neutral conductor convey? And how can Neutral Losses Allocation Factors (NLAFs) be exploited in improving the inherent unbalance condition of these DNs?***

With respect to the second objective, the extensive literature review on the problem of OPF shows that despite being introduced in 1962, OPF is still an open research topic due to its non-convex and non-deterministic polynomial-time hard nature. Consequently, several deterministic and stochastic algorithms have already been proposed which try to solve the OPF problem while keeping its non-convex structure. However, the application of these algorithms does not guarantee the global optimality and feasibility of the obtained solution due to lack of existence of any sufficient criterion.

More recently, several attempts have been made to transform the non-convex AC-OPF problem into a convex one by employing mathematical tools from the convex optimization theory. These tools either *relax* or *approximate* the non-convex feasible space, which is associated with the power flow equations, into a convex region, and try to find a global solution in the relaxed or approximated Feasible Region (FR). In this context, numerous relaxations based on lift-and-project, convex envelopes, hierarchies of moment/sum-of-square etc. concepts have been developed which ensure the global optimality of a solution, recovered from the relaxed problem, if it satisfies a pre-defined criterion. However, OPF models based on convex relaxation techniques are largely proposed for single-phase equivalent representation of MV and LV ADNs. Few attempts have been made to extend the lift-and-project based schemes to three-phase DNs; however, OPF model for a LV DN which contains neutral conductor and hosts shunt elements between phase-phase and phase-neutral conductors does not exist in the literature. Due to the increasing focus on the active participation of these networks in day-ahead and ancillary services electricity markets, it is, therefore, necessary to develop an OPF model for such DNs. Correspondingly, the following research questions concerning this domain are set and successfully addressed in this work:

1. ***What are the limitations of existing single-phase equivalent and three-phase convex optimization-based OPF relaxations which hinder their direction extension to a Distribution Network which is equipped a with Neutral conductor (DNN)? Can a KR-based three-phase OPF model be substituted for a four-conductor DN? and how can a convexified OPF relaxation be developed for a LV DNN which contains coupled power injections between network conductors because of wye- and delta-connected end-users?***

2. ***How to model a complete ZIP load, instead of considering only constant power end-users, in a multi-phase OPF model? Do the schemes propose for the handling of ZIP loads in a single-phase equivalent network framework sufficient enough to be used in the context of a multi-phase network framework?***

3. ***Is it possible to practically realize a multi-phase OPF model for medium and large size DNs? If not, what are the possible alternatives to ensure the real-time optimal control of these networks? and finally, how can an optimal participation of neutral equipped LV ADNs be assured in day-ahead and ancillary service electricity markets?***

In the context of above-mentioned research gaps and correspondingly proposed methodologies to fill these gaps, the thesis is divided into two parts. With respect to the part I, chapter 2 presents a detailed literature overview on LsMag concept with main focus on the ideas of LsMin and Losses Allocation Procedures (LAPs). The presented review work sets the basis for the development of a novel MPLAP which is presented in chapter 3 and allows explicit allocation of power system losses to each phase and neutral conductor. The explicit allocation of losses to neutral conductors provides an opportunity to exploit this information in the context of LV DN management and, resultantly, a novel NLAFs-based unbalance reduction strategy is proposed in chapter 4 for a DNN.

With regard to the part II, a comprehensive overview on the convex optimization-based OPF relaxations and approximations is carried out in chapter 5. In chapter 6, a novel Multi-Phase Semi-Definite Programming (MPSDP)-based OPF relaxation is developed for neutral-equipped DNs which is capable of taking into account both wye- and delta-connected end-users as well as grounding impedance in its formulation. Furthermore, a new modelling approach is also presented which allows incorporating ZIP loads in the framework of a multi-phase DN. Due to large Computational Time (CT) requirements of the developed MPSDP-based OPF relaxation, a novel cheap conic Semi-Definite Programming (SDP)-based OPF model is further proposed in chapter 7, which, on the one hand, allows practical realization of a multi-phase OPF model for neutral-equipped DNs and, on the other hand, is as tight as MPSDP-based OPF model under a large combination of ZIP Load Models (LMs). To further tighten the cheap conic relaxation, a new methodology is reported in chapter 8 which introduces additional convex envelopes on the non-linear terms of power balance formulations to enclose the associated non-convex region. Finally, the most important achievements and perspectives for future developments are discussed in chapter 9.

The case studies presented in this work utilize several network models (duly detailed in the appendices) to fully demonstrate the applicability of proposed methodologies to systems with different characteristics and peculiarities.

PART I

Losses Management in Low Voltage Active Distribution Networks

CHAPTER 2

Literature Review on Losses Management in Distribution Networks

This chapters presents a detailed literature review on the concept of losses management in active distribution networks. The main methodologies related to network and end-users modelling, losses minimization and losses allocation are discussed in detail and finally, key publications on these topics are summarized in two tables for a quick reference.

As stated in chapter 1, the large proliferation of renewable DERs along with the incorporation of ICT, advanced metering infrastructures, DMS and EMS has changed the passive nature of DNs and put them in a transition phase from passive to active networks. The integration of DERs, although, on the one hand, is reducing the carbon footprint of fossil-fuel-based conventional power plants, but, on the other hand, has also started to obscure the secure and reliable operation of DNs. Since such networks have high R/X ratio, the intermittent nature of DERs can cause a large variation in their operating conditions. Several technical issues such as voltage rise, reverse power flow, unintentional islanding, voltage unbalance etc. have been reported in the published literature as a consequence of the presence of DERs in such networks [18]–[20].

To mitigate the undesirable impacts of DERs on DNs, several developed countries have revised their grid codes which ensure active participation of these resources in the provision of ancillary services in the context of grid management. Since DSO is responsible for the reliable operation of a grid, it will involve DERs in the near-future for the optimal operation of ADNs within the regulatory framework and energy policies of each area. The optimal operation of ADNs is a broad theme which involves management of power system losses and power factor, mitigation of voltage rise and unbalance, ensuring system reliability, load balancing, and optimizing network operating costs. Since each domain of this theme is a huge topic in of itself, it would, therefore, be inefficacious to shed light on each topic in this chapter. Rather, a comprehensive literature review on the topic of LsMag is provided here because of its relevance to the theme of this work.

The LsMag includes the following concepts which are discussed at length in the subsequent sections.

1. Modelling of DNs (both MV and LV) and end-users
2. Classification of Active Network Management (ANM) schemes for LsMin
3. Taxonomy of LAPs in ADNs

2.1 Power losses assessment in active distribution networks

For the analysis and management of power system losses, the first and foremost step involves the comprehensive modelling of a power system along with the connected end-users, followed by its analysis through a suitable numerical tool which can provide in-depth information about all of its state variables. Once information about each state variable is obtained, the subsequent steps involve the application of LsMin strategies and LA procedures. Fig. 2.1 shows a general scheme of power losses assessment in ADNs.

2.1.1 Low voltage distribution network modelling

The accurate modelling of LV ADNs is a critical step in their analysis since the non-uniform distribution of end-users in these networks makes them unbalanced and, therefore, it is essential to model these networks using Multi-Conductor Modelling (MCM) approach [21],

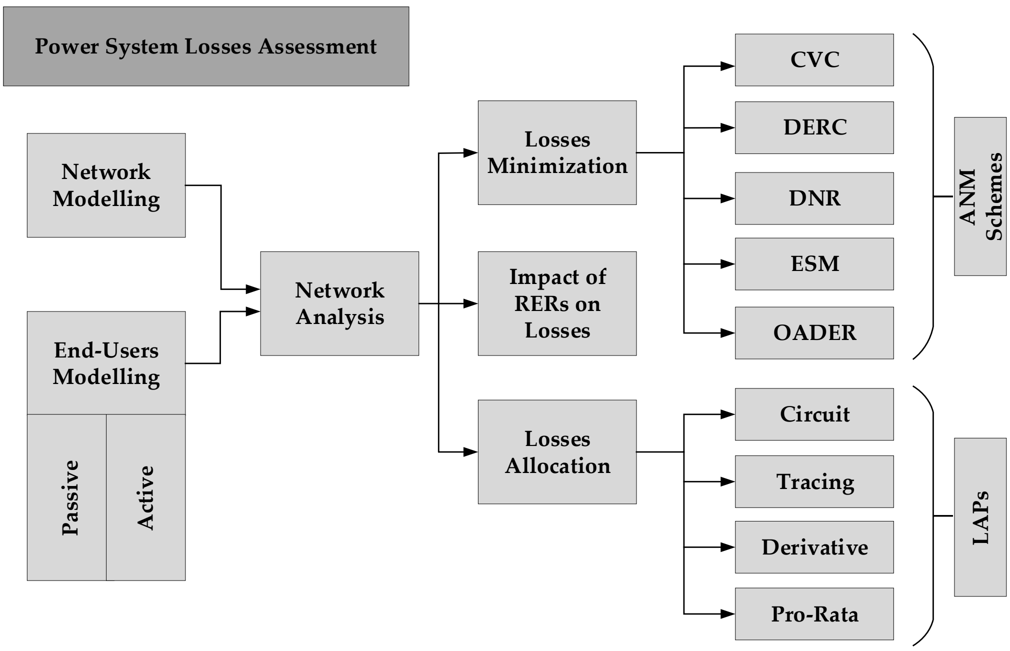

Figure 2.1: Power system losses assessment.

rather than considering their single-phase equivalent representation. The MCM method has the ability to model branch elements including neutral conductor, transformers, Voltage Regulators (VRs) and any shunt-connected element on a phase basis and, resultantly, becomes extremely useful methodology for the modelling of LV ADNs.

The branch elements of a DN, which consists of both overhead lines and underground cables, are modelled using modified Carson's equations-based multiphase pi-model, whereas shunt admittance of an individual phase is determined using Maxwell potential coefficients [21]. A general multi-phase pi-model of a branch element along with its primitive impedance matrix can be seen in Fig. 2.2.

For the modelling of Distribution Transformers (DTs), several models have been presented in the literature which are based on modal analysis [22], linearly decoupled equations [23], phase frame of reference [24], [25], graph theory and nodal admittance building algorithm [26], [27], modified augmented nodal admittance algorithm [28], symmetrical component approach [29], [30], fifth order Park model [31], classical incidence matrix method [32], non-linear leakage reactance [33], primitive [34] and inductance matrix [35] methods. The extension of an open-wye model by adding a grounded mid tap is discussed in [36] and a new model of auto-transformer is reported in [37]. Finally, a detailed discussion on the modelling of transformer's magnetic core can be found in [38]–[43].

2.1.2 End-users modelling

Inappropriate end-users models can lead to simulated responses which may differ significantly from the real ones and, therefore, can affect the network stability. Consequently, it is required to model end-users as accurately as possible. The passive end-users modelling is a well-researched topic and comprehensive information on various LMs in the context of load flow and dynamic power system studies can be found in [44], [45]. Furthermore, a detailed bibliographical list of papers for LMs; developed and implemented for numerous system studies; was published in 1993 by *IEEE Task Force on Load Representation for*

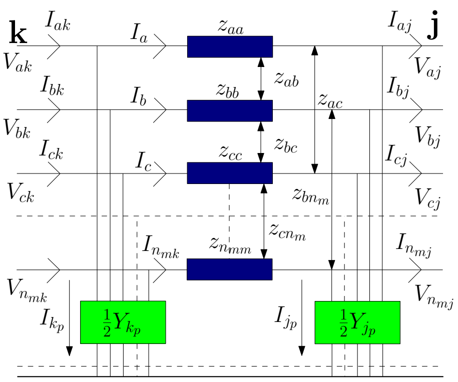

(a)

$$\mathbf{z}_p = \begin{bmatrix} z_{aa} & z_{ab} & z_{ac} & z_{an_1} & z_{an_2} & \cdots & z_{an_m} \\ z_{ba} & z_{bb} & z_{bc} & z_{bn_1} & z_{bn_2} & \cdots & z_{bn_m} \\ z_{ca} & z_{cb} & z_{cc} & z_{cn_1} & z_{cn_2} & \cdots & z_{cn_m} \\ z_{n_1a} & z_{n_1b} & z_{n_1c} & z_{n_1n_1} & z_{n_1n_2} & \cdots & z_{n_1n_m} \\ z_{n_2a} & z_{n_2b} & z_{n_2c} & z_{n_2n_1} & z_{n_2n_2} & \cdots & z_{n_2n_m} \\ \vdots & \cdots & \cdots & \cdots & \cdots & \cdots & \vdots \\ z_{n_ma} & z_{n_mb} & z_{n_mc} & z_{n_mn_1} & z_{n_mn_2} & \cdots & z_{n_mn_m} \end{bmatrix}$$

(b)

Figure 2.2: Distribution network modelling (a) multi-phase branch model (b) primitive impedance matrix.

Dynamic Performance [46].

However, with the appearance of new non-conventional loads types (power electronics-based loads), researchers have turned their attention towards this topic again. In 2010, CIGRE established a working group with the objectives of providing detailed information on the following: (i) overview of existing LMs and their parameters for all types of power system studies, (ii) identification of load classes for which LMs are not present, (iii) overview of currently used modelling methodologies with focus on component- and measurement-based modelling procedures, (iv) providing recommendations for the development and validation of LMs based on previously mentioned methodologies, (v) development of missing LMs for customer classes and (vi) providing recommendation for the development of LMs for ADNs. A detailed report [47] on the above-mentioned points was presented by CIGRE in 2013. Based on this report, several researchers have published milestone works [48], [49] which summarize important sections of this report and also provide a comprehensive review of the modelling approaches being utilized in the published literature. From a modelling point of view, the published literature can be categorized into passive and active end-users modelling groups. In the category of passive end-users representation, the most promising approaches are component- and measurement-based techniques, whereas, in the second category, statistical approaches are widely adopted to take into account the uncertainties related to the active end-users.

In the component-based method, LM is based upon the detailed information of load structure at the aggregated point, characteristics of individual components and composition of the total aggregated demand. This method depicts load characteristics accurately but it requires an extensive load composition data and individual consumer electricity usage patterns which are not readily available. LMs based upon this methodology are reported in [50]–[52]. In the measurement-based method, normally occurring or intentionally made disturbances data is used to derive an aggregated LM downstream the observation site [47], [48]. Based on this approach, composite load model [53], [54], seventh-order quasi state-space model [55], linear-approximation based dynamic Exponential Recovery Model (ERM), real-time generic ERM development [56], dynamic field measurement-based model for voltage stability analysis [57] and least square optimization algorithms-based LM [58] are developed recently. Furthermore, intelligent-based methods such as Artificial Neural Network (ANN) [59], non-linear auto-regressed model with exogenous output [60] and buddying approach [61] are also reported. The advantage of using these intelligence methods lies in their capabilities of identifying a non-linear system from a set of measurement data without referring to a pre-defined LM and developing a load profile for a whole system in the case of limited data availability. Apart from the above-mentioned methods, researchers have also developed LMs using statistical techniques in case of unavailability of end-users or disturbance data. A number of Probabilistic Distribution Functions (PDFs) which include Gaussian [62], Weibull [63], Beta [64], log-normal [65], Gaussian Mixture Model (GMM) [66], chi-square [67] and principle component analysis [68], [69] have been explored in this context.

Active end-users modelling involves representation of Wind Turbines (WTs) and solar Photo Voltaics (PVs) panels. The key issue in the modelling of these end-users involves

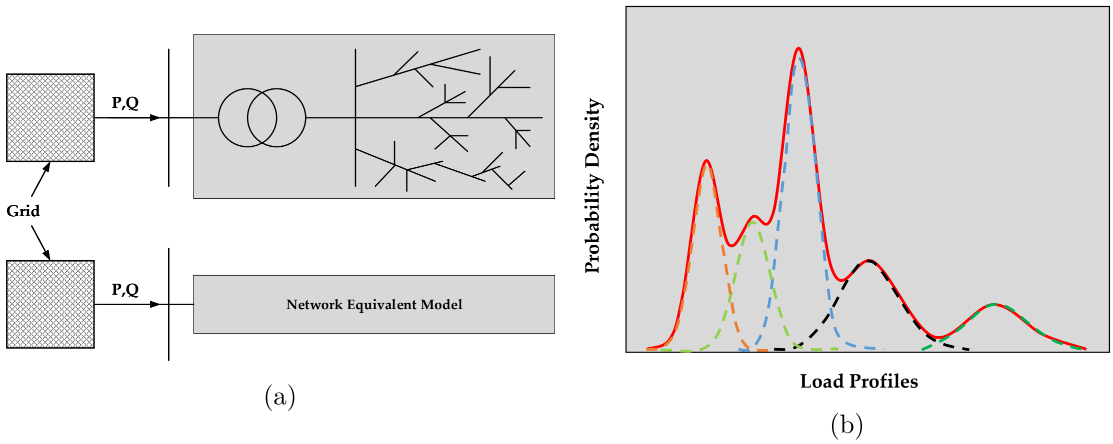

Figure 2.3: Passive end-users modelling (a) measurement-based load modelling technique (b) Gaussian mixture model probability distribution function.

the representation of uncertainties associated with the stochastic nature of solar and wind inputs. Consequently, a lot of effort has been put in the modelling of stochastic wind speed through Weibull PDF [70]–[72], times-series model [73], data mining algorithms [74], clustering approach [75] and Rayleigh PDF [76], [77]. Similarly, the intermittent nature of solar irradiance is modelled through Beta PDF [70], [71], [76], [78], [79], time-series [77] and clearness-index [72] methods. A detailed review on uncertainty handling methods for WTs, PVs and load demands is presented in [71], [77], [78], [80] for interested readers. Finally, a generic measurement-based approach and a GMM curve is shown in Fig. 2.3 for better understanding of these techniques.

2.1.3 Analysis of low voltage active distribution networks

The network analysis is the next step in LsMag after performing network and end-users modelling. For load flow analysis, Deterministic Load Flow (DLF) and Probabilistic Load Flow (PLF) methods are frequently used. The DLF techniques do not take into account the uncertainties associated with load demands and DERs and solve the non-linear power system equations for a deterministic value of load and DER output. Backward/Forward Sweep, Newton-Raphson, Gauss-Seidel and Correction Current Injection [81] methods fall under this category. In PLF methods, the uncertainties of load demand and intermittent nature of DERs are taken into account, and numerical and analytical approaches are used to get a solution to the problem. Examples of PLF methods are Monte-Carlo simulations, Point Estimate (symmetrical and asymmetrical), Cornish-Fisher expansion series, Gram-Charlier series, Latin hypercube sampling techniques etc. An interesting overview of load flow techniques for a DN can be found in [82].

Apart from the above-mentioned load flow methods, one of the most important technical and economical tools for power system studies is OPF approach which allows determining the optimal operating points of network control variables by solving a specified objective function without violating network constraints. Several OPF methods have been proposed in the literature such as static, dynamic, transient stability-constrained, security-constrained, deterministic, stochastic, probabilistic, AC, DC and mixed AC/DC OPF approaches. Since OPF is the topic of part II of this thesis, a detailed discussion is carried out in the latter chapters.

2.2 Active network management schemes for losses minimization

The multi-phase model of a network, accurate representation of end-users and utilization of an analysis tool give detailed information on network operating conditions, and, therefore, provide an opportunity to implement suitable network management schemes to achieve a satisfactory operational state of a network. The schemes can be applied in a centralized, de-centralized or local architecture manner. In the context of ANM schemes for LsMin, the presented schemes have been developed for both MV and LN ADNs. However, the majority of published work, related to some of the ANM schemes, have considered only MV DN as a test case. Please refer to Table 2.1 which reports the test case network (either MV or LV) of the selected published literature. A general classification of ANM schemes along with their possible control architecture is shown in Fig. 2.4 and a brief overview of the existing work for each management scheme is presented in the subsequent sections.

2.2.1 Coordinated voltage control

This control scheme refers to the coordination of conventional regulating devices, On-Load Tap Changer (OLTC) transformers, shunt Capacitor Banks (CBs), and DERs to regulate network voltage by controlling reactive power flow in a system. It has been mostly applied to MV DNs which are by and large equipped with a centralized controller. Nevertheless, there exist some papers which discuss the application of Coordinated Voltage Control (CVC) approach in the context of LV ADNs.

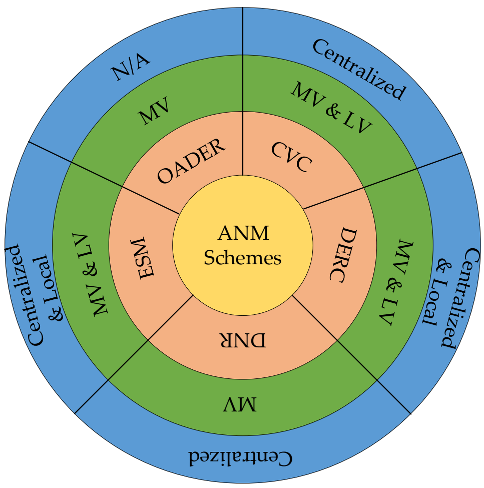

Figure 2.4: Classification of ANM schemes.

The CVC strategy can be categorized based upon the type and combination of devices and algorithms involved in its realization. With respect to the first category, the researchers have proposed CVC scheme involving OLTC transformer and DERs [83], shunt CBs and DERs [84], OLTC transformer, step VRs and Energy Storage Units (ESUs) [85], and VRs along with DGs [72], [86], whereas *rule-based* and *optimization-based* algorithms [87] are proposed in the second category.

In [83], a centralized CVC scheme is reported to minimize the voltage variations and power losses through the optimal exchange of reactive power by implementing a coordinated action between OLTC transformer and DERs controller. In [84], authors have established a coordinated control among multiple capacitors and DERs to reduce the effect of capacitors' discrete switching states by utilizing a continuous reactive power control of DERs. Consequently, over/under reactive power compensation is successfully avoided. In order to ensure the active participation of ESUs during peak generation and load demand, an effective centralized control is developed among OLTC transformer, step VRs and distributed ESUs in [85], which allows achieving load shaving and minimizing active power flow towards the substation [85]. The coordination among multiple VRs and DGs is established by dividing the network into several control zones where each zone has a primary voltage regulation equipment and is further supported by the devices of other zones in case of its equipment saturation [86]. A dynamic area selection approach is proposed in [88] which clusters the network nodes, based upon common power quality objectives, to coordinate the control actions of both MV and LV active end-users and finally, a one-day ahead reactive power dispatch control is proposed in [72] by implementing a coordinating action among DGs and conventional reactive power devices to reduce system losses. The above-mentioned papers have largely utilized the *rule-based* algorithms in determining the optimal coordination between different components. Since CVC approach which is based on *optimization-based* algorithms normally falls under the OPF (AC, DC, security constrained etc.) category, they are discussed in the part II of the thesis. Nevertheless, few papers are mentioned below where both rule- and optimization-based algorithms are combined to achieve maximum benefits.

In [87], authors have proposed a novel strategy which utilizes these algorithms to determine the set point of every regulating equipment in a sequential (rule-based) and simultaneous (optimization-based) manner. Resultantly, *active* voltage control method is implemented, instead of *passive* voltage control approach, to reduce the voltage rise problem. Lastly, in [89], Conservation Voltage Reduction (CVR) method is combined with the installation of DGs to alleviate voltage violations which, in turn, allows DSO to implement more deeper voltage reduction to reduce network losses.

Despite the availability of significant amount of literature on CVC strategy in the domain of MV DNs, it must be noted that the inherent high R/X ratio of LV DNs makes voltage regulation through reactive power less effective in these networks. Therefore, active power regulation, which can play a more significant role in maintaining a secure and stable operation of these system, must be considered.

2.2.2 Distributed energy resource control

This ANM scheme covers the contribution of DERs in the provision of ancillary services to a grid in the light of revised grid codes and it has been developed for both MV and LV DNs since these resources can be connected to both networks. A few local DER Control (DERC) schemes which are reported in [90] and implemented by several researchers are as follows: (i) active power curtailment $P(V)$, (ii) droop-based reactive power as a function of active power $Q(P)$ and (iii) droop-based reactive power as a function of voltage $Q(V)$. Fig. 2.5 shows $Q(P)$ and $Q(V)$ schemes, respectively. During the initial stages of the application of these schemes, researchers put a lot of attention on $Q(V)$ approach due to the economical loss that can be caused by the curtailment of available active power through $P(V)$ scheme. Based on $Q(V)$ approach, the fundamental idea is to maintain the voltage of network critical buses [91], mitigate the local over-voltages [92] and ensure the active participation of all PV inverters, rather than putting more stress on the distant PV systems (with respect to the substation), in the provision of reactive power [93]. Furthermore, in [92], the gain of $Q(V)$ curve is dynamically updated at each iteration as well as further assistance is provided to it by $P(V)$ method to enhance the reactive power capability limit of the inverter. In [94], a new approach is introduced which redesigns the $P(V)$ and $Q(V)$ curves through first order splines by dynamically re-optimizing the control parameters of these curves and, consequently, the objectives of optimal reactive power flow and minimization of active power curtailment are achieved. The same schemes are applied to Australian ADN in [95] and concepts of Static Maximum (SM) and Dynamic Maximum (DM) reference point are introduced for the $P(V)$ scheme. It has been shown that the latter method results in a better voltage regulation as compared to the former scheme. However, it is achieved at the expense of increased curtailed losses.

Quite recently, a new local $cos\phi(P, V)$ strategy is proposed in [96] which generates reactive power from each inverter by implementing a position-dependent variable lower limit of power factor for each inverter. However, this method fails to maintain the bus

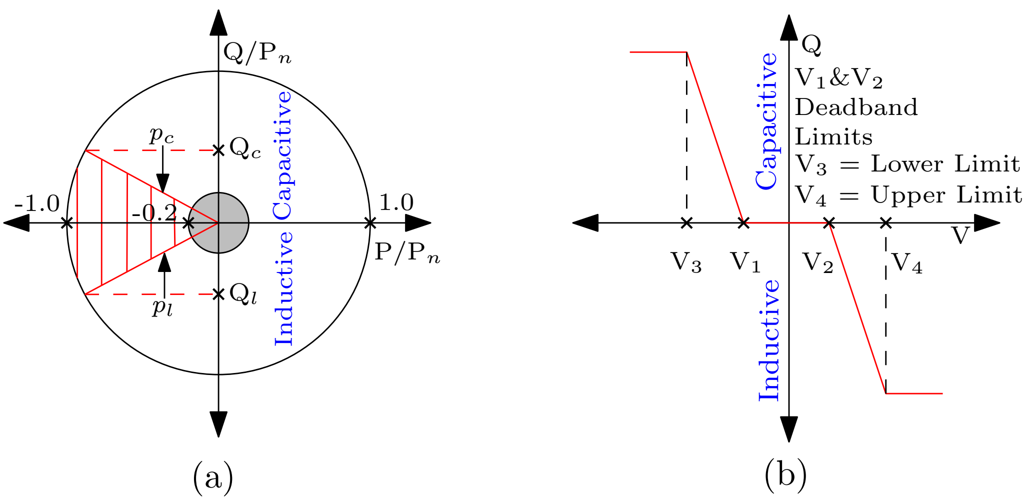

Figure 2.5: Local DERC schemes (a) $Q(P)$ (b) $Q(V)$.

voltage, in case of the saturation of its inverter, due to the lack of participation of the neighbouring inverters. In such cases, a centralized reactive power compensation controller [97] communicates with all the inverters and changes the operating mode of the saturated inverter from $cos\phi(P,V)$ to constant power factor mode to limit the voltage violations. This scheme also forces the neighbouring controllers to participate in the voltage regulation on the basis of their sensitivity with respect to the critical bus. Lastly, both $Q(V)$ and $P(V)$ approaches are combined with $cos\phi(P,V)$ strategy in [98] with the aim of improving voltage regulation and increasing network hosting capacity.

2.2.3 Distribution network reconfiguration

This control scheme deals with the reconfiguration of a network topology (providing alternative path to end-users) by operating remote tie-switches with the objectives of reducing power system losses and alleviating network congestion. In the past, DN Reconfiguration (DNR) strategy is solved alone; however, with the emergence of DERs in MV and LV DNs, a lot of attention has been put recently in determining the solution of a combined DNR and Optimal Allocation of DERs (OADERs) management strategies. This concurrent implementation results in a highly complex combinatorial problem which requires advanced optimization algorithms for computing its solution. Due to the complex nature of this problem, deterministic/analytical methods fail for large-size systems involving a lot of binary decision variables. Resultantly, either heuristic/meta-heuristic algorithms or combined analytical-heuristic methods are used to solve this problem. Quite recently, this problem is reformulated by using tools from the convex optimization theory and optimization models based on Mixed Integer Second-Order-Cone Programming (MISOCP) are proposed [99]–[101]. Apart from the solution algorithms, DNR problem is studied with respect to both single- and Multi-Objectives (MOs) functions ranging from technical (minimizing power losses, voltage sag, active power curtailment) to economical (minimizing financial risk) objectives as well. Finally, due to the lack of presence of remotely-controlled tie-switches in LV Radial Distribution Networks (RDNs), this scheme is mainly studied for MV DNs. A brief overview of the published literature with respect to the Objective Functions (OFs) and algorithms is presented below.

In the case of single OF-based DNR problem, adaptive Ant-Colony (AC) [102], modified Tabu Search (TS) [103], Particle Swarm Optimization (PSO) [104], adaptive Genetic Algorithm (GA) [105], multi-objective honey bee mating optimization [106], combination of adaptive AC with fuzzy variables [107], harmony search [108], hybridized Shuffle Frog Leaping Algorithm (SFLA) with PSO [109], runner-root [110], Prim's PSO [111], modified PSO [112] and many more algorithms are proposed in the literature for reducing power system losses. For MO functions which involve a combination of minimization of losses, reliability improvement, voltage variability reduction, improvement of Total Harmonic Distortion (THD) and/or maximizing annual savings etc., the previously mentioned conventional heuristic algorithms are unable to provide an optimal and feasible solution of this highly non-convex problem. Consequently, these algorithms have been modified and new hybrid algorithms, based on the combination of fuzzy Pareto dominance method and

SFLA [113] and Non-Dominated Sorting PSO [114] algorithms, have been proposed for solving the MOs-based DNR problem. Similarly, a hybrid Big-Bang Big-Crunch (BBBC) algorithm is presented in [115] which improves the BBBC method by incorporating the PSO exploration capabilities to avoid local optimum solutions.

In the case of simultaneous control of DERs and network tie switches, an hourly Network Reconfiguration (NR) is proposed in [116] in the presence of fluctuating load demand and DGs output. The high penetration of DGs and their intermittent output justify the hourly NR for losses reduction. The DNR is combined with the var-optimization approach [117] which leads to significant power losses reduction as compared to the scenario when these schemes are implemented separately. A combined active/reactive power control of DERs and DNR is presented in [118] to minimize system losses and active power curtailment by performing the online network reconfiguration.

The problem of DNR is largely studied and solved from a centralized control point-of-view. However, the trend of solving this problem in a decentralized manner is also emerging. In this context, a multi-agent-based NR scheme for losses minimization is proposed in [119] where each monitoring, data exchange and decision making device acts as an agent and a proper coordination among them provides the optimum reconfiguration to achieve the pre-defined objectives. In [120], the mechanism of multi-agent technology and characteristics of PSO algorithm are combined together to propose a new algorithm for solving the NR problem. The proposed methodology reduces the probability of finding the infeasible solution and have fast convergence towards the global minimum point.

The introduction of reward and penalty scheme for DNs allows DSOs to earn profit through the provision of reliable services. However, uncertainties associated with loads, DGs and economic parameters have also raised financial risks for DSOs due to their limited ability in handling these uncertainties and, consequently, maintaining the system reliability. As a result, NR becomes a natural alternative choice for DSOs to improve the reliability of services provision to end-users . Considering the financial risks to which DSOs are exposed, a risk-based NR strategy is proposed in [121] which allows DSOs to consider financial risks in the reconfiguration problem and, therefore, enables them to optimize the network with an acceptable financial risk. The real-time benefits associated with the reconfiguration strategy in the presence of time-varying loads are difficult to quantify. Consequently, to secure enough confidence on achieving benefits through the real-time implementation of a NR scheme, a network model validation process is proposed in [122] which compares different NR schemes by taking into account the uncertainties associated with time-varying loads and, thus, guarantees the practical application of this scheme.

Lastly, some new concepts such as static and dynamic reconfiguration, and selective automation upgrade of a DN are also emerging in this field. In this regard, a static and dynamic NR scheme is proposed in [123] to increase the hosting capacity of a network. The latter reconfiguration scheme is further reported in [124] where a dynamic analysis method updates the parameters of initial network topology in real-time and restores the network connectivity after electrical interruption or system expansion. Finally, selective automation upgrade of a typical DN is presented in [125] with the objective of identifying those open tie-switches which play a significant role in losses reduction and reliability improvement in the framework of optimal network management.

2.2.4 Energy storage management

The Energy Storage Management (ESM) control scheme refers to the involvement of ESUs in the provision of multiple ancillary services. The commonly used ESUs in DNs are electrochemical Energy Storage Batteriess (ESBs), compressed air energy storage, fuel cells and fly wheel [126]–[128]. However, in this work, the main focus is put on ESBs which are either integrated alone or with PVs for securing the reliable operation of a grid. Nevertheless, various models and working principle of ESUs as well as their selection criteria can be found in [126] and [127], respectively. Similarly, several multi-criteria-based evaluation methodologies for ESUs are discussed in [128]. In terms of implementation, the scheme can be applied to both MV and LV DNs since ESU is another type of DER and, thus, can be connected to either of these networks in a centralized, decentralized or stand-alone manner.

The integration of ESBs in ADNs is largely studied from the *stand-alone management* and *combined allocation and management* perspectives. From the first outlook, batteries are considered solely for the purpose of improving network conditions and mitigating power quality issues [129], whereas from the second perspective, the optimal size and locations of batteries are also determined to ensure their optimal operation[130].

About the first viewpoint, a consensus algorithm-based distributed control of ESBs is suggested in [131] to regulate network voltages by absorbing excessive active power during the period of high production from PVs, whereas dynamic charging/discharging strategy of distributed ESBs is proposed in [132] to achieve the same objectives. The ageing effect of ESBs is considered in [133] which reports a deterministic algorithm-based approach to ensure continuous supply to the loads through the participation of ESBs in case of a power mismatch between load demand and solar PV generation. On the other hand, peak-shaving and day-ahead energy dispatch objectives are achieved in [134] by implementing a prediction-based power management scheme.

A shared ownership of residential ESBs is established between DSO and end-users in [135]. The proposed strategy dynamically changes the shared proportion of ownership and, thus, optimizes the demand response with respect to network loading and wholesale energy price. A rule-based control algorithm for the operation of Battery Energy Storage System (BESS) is proposed in [136] with the aim of smoothing the intermittent output of renewable DERs to use them as dispatchable generators, whereas a self-consumption and storage strategy is reported in [137] to inhibit reverse power flow and voltage rise along DN feeder.

In the context of optimal allocation of ESBs, the optimal size of BESS, based on cost-benefit analysis, is determined in [138] for grid-connected and islanded Micro Grid (MG) configurations, whereas optimum location of the same system is determined in [139] for the provision of voltage control and peak-shaving services. The size and management scheme of a BESS are combined together in [140] to achieve peak-shaving, voltage regulation and network losses reduction objectives. The optimal allocation and power factor of combined

PV-BES units are studied in [141] for energy losses minimization. The resultant problem is formulated as a MO-index-based problem and employed in a self-corrective algorithm to ensure voltage stability and energy losses reduction. Similarly, the optimal allocation of ESBs and power factor of capacitors are determined in [130] by implementing an analytical approach to achieve losses minimization at peak load demand.

Lastly, an approximated convexified AC-OPF model for an unbalanced DN is proposed in [142] for optimal dispatch of active and reactive powers from ESUs. The proposed OPF approach takes into account neutral branch voltages and current which is an inherent feature of such DNs. The significant feature of this methodology is the complete independence between problem convexity and time scheduling of ESUs. Resultantly, the future output values of ESUs can be calculated in a computationally efficient way.

2.2.5 Optimal allocation of distributed energy resources

The OADERs is a strategy that is usually employed in the planning stage of DNs by DSOs to determine the optimal size and location of DERs to achieve maximum gains from their integration. This is a mixed-integer non-linear Optimization Problem (OP) and can be categorized either on the basis of its mathematical formulation or solution algorithms. Furthermore, the scheme is applicable to both MV and LV DNs; however, the majority of available literature discusses its application with respect to MV DNs.

The mathematical formulation of this scheme includes OF, DG variables (number, size, location and technology of DGs), types of load profiles and network constraints. The OF can be a single or MO-based function with commonly implemented objectives are power losses minimization, voltage regulation, reliability improvement and economical benefits maximization. Concerning DG variables, the frequently implemented variables are simultaneous determination of size, number and location of DGs, whereas, the load profiles can be categorized in four categories (i) single-level, (ii) multi-level, (iii) time-varying and (iv) stochastic load profiles.

Lastly, the optimization algorithms can be divided in three groups (i) classical and analytical (ii) meta-heuristic and (iii) hybrid (combination of the previous two methods) algorithms. In the following subsections, these algorithms are reported in detail which solve either a single or MO-based function by involving one of the above-mentioned load profiles and DG variables.

2.2.5.1 Classical and analytical methods

The allocation of a single DG for uniformly, centrally and increasingly distributed load profiles is proposed in [143], whereas an exact loss-based formula is used in [144] to determine the size of a DG. Fuzzy logic and analytical approaches are presented in [145] to determine the DG's location and size, respectively. An equivalent current injection algorithm along with Jacobian matrices is reported in [146], whereas, system reliability and 2/3 absorption rules are implemented in [147] for the allocation purpose. The sizes of multiple DGs and Vanadium redox battery are determined in [148] and [149], respectively. A *sequential* allocation process is reported in [150] whereas *simultaneous* allocation and determination of multiple DGs' power factors are reported in [151], [152] for different kinds of DGs. Lastly, a multi-period AC OPF approach has been reported in [153] for energy losses minimization by taking into account the time variability of load demand and DGs output along with the real time control of OLTC transformer secondary voltage and DGs' power factors in each time horizon. It has also been demonstrated that in the case of single objective focusing on the minimization of energy losses, the true potential associated with the capacity of renewable DERs cannot be fully utilized. Therefore, a trade-off must be found that can maximize the benefit between DGs output and energy losses.

2.2.5.2 Meta-heuristic methods

Since OADER is a non-linear and non-convex problem, analytical methods either might not be able to solve the problem or may provide an infeasible solution. Consequently, a significant effort has been put in solving this problem through heuristic algorithms. In this context, an adaptive GA [154], [155], hybrid Grey-Wolf [156], Non-Sorted Genetic Algorithm (NSGA) [157], GA [76], [158], artificial bee colony [159], [160], TS [161], [162], PSO [163], AC optimization [164], whale optimization [165], ant-lion optimization [166] and Jaya algorithm [167] are reported in the literature. A combine techno-economic OF is considered in [168] and is solved by Improved Differential Search Algorithm (IDSA), whereas simultaneous allocation of multiple DGs is carried out in [169] with the objectives of maximizing annual savings. The problem is solved by an Improved PSO (IPSO) algorithm supported by a guided-search algorithm which narrows down the solution search space. A MO-based OP which focuses on active losses reduction and optimum reactive power flow is solved by a Multi-Objective Evolutionary Algorithm-based Decomposition (MOEAD) in [170].

The allocation of DGs and NR schemes are strongly interlinked in the context of achieving efficient performance of a power system. Therefore, these two approaches should be considered simultaneously. The concurrent operation of NR and OADERs in the presence of a storage system is reported in [171] and is solved using NSGA to reduce Energy Not Supplied (ENS) and power system losses objectives. A convex probabilistic-based planning technique is proposed in [172] for WTs allocation to optimize energy losses reduction and voltage profile improvement. An integrated dispatch model is reported in [173] for the allocation of a CHP-based DG in an urban DN, whereas, the optimal allocation of distributed ESUs to maximize economical benefits is proposed in [174].

Due to the existence of vulnerable nodes in a DN, it is not recommended to install DGs at these sites since power fluctuation of these nodes can severely effect the voltage balance of a system and can lead to a total voltage collapse. To overcome this issue, vulnerable nodes are first identified using small-world network theory in [175] and, subsequently, allocation is performed through GA without taking into consideration these nodes. Finally, to take into account the costs related to system upgrade, variable energy, and time-dependant deterioration, a risk factor-based allocation scheme is proposed in [176] with the objectives of maximizing annual energy savings.

2.2.5.3 Hybrid methods

Recent publications show the implementation of hybrid approaches which combine either two heuristics algorithms or a heuristic algorithm with an analytical method to combine the beneficial properties of both approaches. Hybrid methods based on TS and GA [177], [178], three-phase PLF and binary SFLA [179], Lagrangian method and GA [180], GA and Hereford Ranch [181], combined GA-OPF [182], [183], Fuzzy and GA-OPF [184] and MO GA [185] are reported in literature for system expansion planning and losses minimization. A combination of PSO and Newton-Raphson Power Flow (NRPF) method is also proposed in [186] to solve a MO-based OP, whereas, the allocation of DGs and DNR problem is solved using an artificial intelligent algorithm in [187].

Lastly, to conclude this section, a comprehensive review of the selected published papers concerning ANM schemes is provided in Table 2.1.

Table 2.1: Review of ANM schemes.

ANM Scheme	Brief Description	Load Profile	Control Architecture	Test System	Objective Function	Ref (Year)
CVC	Centralized control of OLTC & DERs	Single-level	Centralized	Fictitious DN (MV)	Optimal management of reactive power flow	[83]-(2008)
	Coordinated control of ESU with OLTC and CBs	24h mix-demand curve of domestic and commercial loads	Centralized	Fictitious DN utilized by General Electric (MV)	Minimize voltage rise, shave peak load and reduce switching operation of a tap-changer	[85]-(2012)
	Voltage control algorithms for OLTC, CBs and DERs	Multi-level (maximum, minimum and in between these two extremes)	Centralized	Real Finish DN (MV)	Minimize network losses and generation curtailment	[87]-(2014)
	Zonal control among OLTC, VRs and DERs	Constant, statistical and increasing load demand	Centralized	Rural Australian DN (LV)	Minimize voltage deviation	[86]-(2015)
	Coordinated control between CBs & DERs	Single-level (Constant Power and Constant Impedance)	Centralized	Utility DN (MV)	Minimize power losses and voltage deviation	[84]-(2016)
	Centralized control of CBs, OLTC and DERs	24h daily load curve	Centralized	Real 54-bus utility DN (MV)	Minimize power losses, switching operation of CBs and voltage deviation	[72]-(2016)
	Improving CVR by installing DGs	Single-level (Constant Power ZIP model)	Centralized	New York DN (LV)	Voltage regulation in a network operated under CVR	[89]-(2016)
	Coordinating control between OLTC & DERs	24h load curve scaled down to few minutes for study purpose	Centralized	Rural 11kV Swedish DN (MV)	Minimize voltage fluctuation	[188]-(2016)
DERC	$Q(V)$	Random load allocation between min and max value	Local	Fictitious RDN (LV)	Minimize losses and voltage deviation	[189]-(2010)
	$cos\phi(P,V)$	24h load curve	Local	Suburban utility network (LV)	Minimize voltage variation and reactive power consumption from the grid	[96]-(2011)
	$Q(V)$	24h load curve	Centralized	European benchmark network (LV)	Optimized reactive power of each PV system to reduce system losses	[93]-(2012)
	Token-Ring control among DERs	Simple R-L series load	Local	Residential MG (LV)	Minimize losses, increase local voltage support and utilization of DERs	[190]-(2012)
	Enhancement of $Q(V)$ by applying $P(V)$	24h load curve	Local	IEEE 34-bus network with PV plant integration	Minimize local node voltage rise	[92]-(2014)
	First order $P(V)$ & $Q(V)$ spline curves	24h load profiles constructed through Markov Model	Combine centralized and local control	Semi-urban RDN in Belgium (LV)	Minimize active power curtailment and network losses by optimum flow of reactive power	[94]-(2014)
	$Q(V)$	24h aggregated residential load profiles	Decentralized	9-bus Italian DN (LV)	Voltage unbalance mitigation	[191]-(2014)
	Sensitivity matrix	Single-level (Constant Power)	Centralized	Rural 20kV German DN (MV)	Minimize voltage variation	[91]-(2015)
	$Q(V)$ & SM/DM based $P(V)$	24h statistical load profiles	Local	Rural Australian Network (MV)	Over-voltage prevention and increasing network hosting capacity	[95]-(2015)
	$cos\phi(P,V)$ & constant power factor	Single-level (Constant Power)	Centralized	Fictitious RDN (LV)	Voltage regulation using a centralized reactive power scheduler	[97]-(2015)
	$Q(V)\&P(V)$ and $cos\phi(P,V)$	24h load profile	Local	Urban RDN (LV)	Minimize voltage deviation and increase the penetration of DGs	[98]-(2016)
DNR	Selective automation upgrade for NR	Stochastic load	N/A	Real 62-bus DN (MV)	Minimize power losses and improve reliability	[125]-(2010)
	Multi-agent based NR	Single-level (Constant Power)	Centralized	Fictitious 16-bus DN (NR)	Minimize power losses	[119]-(2014)
	Static NR	Single-level (Constant Power)	Centralized	Fictitious 19-bus 11kV DN (MV)	Minimize power losses	[115]-(2015)
	Static & Dynamic NR (MP-OPF)	Single-level (Constant Power)	Centralized	34-bus 12.66kV DN (MV)	Maximize network hosting capacity through static and dynamic NR	[123]-(2015)
	Hourly NR (MI-SCP)	24h load curve	Centralized	Baran 33-bus system (MV)	Minimize power losses	[116]-(2015)
	Combine Multi-agent & PSO based NR	Single-level	N/A	IEEE 16,33 and 69-bus test networks	Minimize power losses and voltage deviation	[120]-(2016)

ANM Scheme	Brief Description	Load Profile	Control Architecture	Test System	Objective Function	Ref (Year)
	Combine Pareto dominance & SFLA based NR	Single-level	N/A	IEEE 33-bus test network	Minimize power losses, switching operations and bus voltage deviations	[113]-(2016)
	Non-dominated Sorting PSO	Single-level	N/A	136-bus DN (MV)	Minimize power losses, voltage sag and THD	[114]-(2016)
	Risk-based NR	Time varying load	N/A	Real 95-bus DN (MV)	Optimize financial risk with respect to participation of DGs	[121]-(2016)
	Dynamic NR	Single-level	N/A	IEEE 33-bus test network & 118 Real DN (MV)	Minimize power losses	[124]-(2018)
DNR & DERC	VAR optimization & NR (MI-SCP)	Single-level (Constant Power)	Centralized	Modified IEEE 33 & 123-bus systems	Minimize power losses	[117]-(2016)
	Online NR (MI-NLP)	Load profiles based on clustered yearly load data	Centralized	Modified 34, 70 and 135-bus DN (MV)	Minimization of power losses and active power curtailment	[118]-(2017)
ESM	Optimal control strategy for BESS	N/A	Local	Test battery system connected to the grid (NA)	Smooth the intermittent output of RER by optimal operation of BESS	[136]-(2010)
	DP based EM	Single-level (Constant Power)	Local	Fictitious test system (NA)	Peak shaving and predictive day ahead power dispatch	[134]-(2011)
	MO optimization using BESS & CBs	Single-level (Constant Power)	Local	15 & 69-bus test DN (LV)	Losses minimization by optimum location and size of ESUs	[130]-(2011)
	Optimal sizing of BESS for MG	24h forecasted load curve	N/A	Islanded and grid-connected MG (NR)	Optimal size of BESS to study the economic feasibility of BESS integration into MG	[138]-(2012)
	Consensus algorithm based resource control	Single-level (Constant Power)	De-centralized	Fictitious 6-node RDN (LV)	Minimize active power curtailment and voltage variation	[131]-(2013)
	Shared ownsership of ESB for EM	Half-hour interval yearly load profile	Centralized	Real utility RDN (LV)	Optimization of demand response and wholesale energy price by a shared ownership of ESBs	[135]-(2013)
	Charging/Discharging strategy for ESU	24h aggregated load curve	Local	New South Wales DN with MV and LV feeders	Dynamic charging/discharging strategy of ESBs to store/supply energy during peak generation and demand scenarios	[132]-(2013)
	MO optimization using BESS	Statistical 16 weeks load profiles	N/A	Semi-urban RDN (LV)	Optimum location of a single BESS to mitigate voltage variations, provides peak shaving and defers network upgrade	[139]-(2013)
	MO optimization using BESS	IEEE-RTS load model	N/A	IEEE 33-bus MV DN and Perth City LV DN	Optimal management of BESS to achieve peak shaving, voltage regulation and losses reduction	[140]-(2016)
	Self-consumption/storage	24h typical load curves of summer and winter days	Local	Rural utility DN (LV)	Minimize reverse power flow and voltage rise	[137]-(2016)
OADER	Single DG - Exact loss formula method	Single-level (Constant Power)	N/A	30, 33 and 69-bus test DN (MV)	Minimize power losses	[144]-(2006)
	Single DG - Equivalent current injection method	Single-level (Constant Power)	N/A	12, 34 and 69-bus test DN (MV)	Minimize power losses	[146]-(2009)
	Single DG - Analytical expression based OADER for different types of DGs	Single-level (Constant Power)	N/A	16, 33 and 69-bus test DN (MV)	Minimize power losses	[152]-(2010)
	Single DG - ENS based and 2/3 Absorption methods	Average and peak load demands	N/A	Real utility 15kV RDN (MV)	Minimize power losses	[147]-(2012)
	Multiple DGs - Improved analytical method	Single-level (Constant Power)	N/A	16, 33 and 69-bus test RDN (MV)	Minimize power losses	[150]-(2013)
	Multiple DGs - Analytical method	Single-level	N/A	IEEE 14 and 30-bus test networks	Simultaneous sizing to reduce system losses	[148]-(2014)
	Multiple DGs - combination of small-world network theory and GA	Power disturbance exerted on constant load	N/A	IEEE 30-bus network	Minimize power losses and voltage profile improvement	[175]-(2014)

ANM Scheme	Brief Description	Load Profile	Control Architecture	Test System	Objective Function	Ref (Year)
	Single DG - adaptive GA	Single-level (Constant Power)	N/A	IEEE 33-bus and 11kV 52-node real DN (MV)	Minimize power losses and voltage deviation	[154]-(2015)
	DERs - binary SFLA	Gaussian PDF based load curves	N/A	IEEE 13-bus system	Minimize power losses	[179]-(2015)
	DERs&CBs - TS&GA	Multi-level (Constant Power)	N/A	69-bus RDN (MV)	Minimize investment and operations costs	[178]-(2016)
	Multiple DERs - Lagrangian and GA methods	Single-level (Constant Power)	N/A	33 and 69-bus DN	Minimize power losses by simultaneous consideration of DGs active power and power factor	[180]-(2016)
	Multiple DGs - Grey-Wolf	Single-level (Constant Power)	N/A	IEEE 33, 69, 85-bus DN	Minimize power losses	[156]-(2017)
	Single DG - DP method	24h statistical load curves	Centralized	Real DN in China (MV)	Optimum size calculation of ESU for realizing the maximum consumption of wind and solar PV	[149]-(2017)
	Multiple DGs - Jaya Algorithm	Single-level (Constant Power, Current and Impedance)	N/A	IEEE 123-bus test system	Minimize power losses	[167]-(2017)
	Multiple DGs - IDSA	Single-level (Constant Power)	N/A	33 and 69-bus test DN (MV)	Combination of technical and economical objectives	[168]-(2017)
	Multiple DGs along with NR - IPSO	Multiple-level	N/A	IEEE 33 & 69-bus test networks	Minimize economical benefits (annual savings)	[169]-(2017)
	Multiple DGs - MOEAD	Single-level	N/A	IEEE 33, 69 & 119-bus networks	Minimize real and reactive power losses	[170]-(2017)
	Multiple DGs - Convex Probabilistic technique	Stochastic load & DGs model	N/A	IEEE 33-bus network	Voltage profile improvement and energy losses reduction	[172]-(2017)
	Multiple DGs - GA	Single level	N/A	Real 40 nodes network (MV)	Maximize Annual Profits	[174]-(2017)
	Single DG - combination of PSO and NRPF	Single level	N/A	IEEE 14-bus network	MO OF transformed to a weighted single OF	[186]-(2017)
	Multiple DGs and OLTC - adaptive GA	Single level	N/A	69 bus test and 52-bus real networks (MV)	Minimize power losses and voltage profile improvement	[155]-(2017)

N/A: Not Applicable
NR: Not Reported

2.3 Losses allocation procedures in distribution network

End-users utilize Transmission and Distribution (T&D) networks to consume or sell energy. The network operators, therefore, charge them for the provision of different kinds of services and one of the major allocated costs is related to network losses. Consequently, losses should be allocated in a proper way to end-users without making any discrimination among them. Several LAPs have been proposed for both T&D networks; however, LA methods which are developed for Transmission Networks (TNs) cannot be applied directly to DNs due to the peculiar nature and structure of the latter networks. Therefore, a specific adaptation of the proposed LAPs for TNs is needed to make them applicable for DNs. The LAPs for TNs can be broadly classified into three major categories (i) pro-rata (ii) and derivative-based (iii) Proportional Sharing (PS). Since methods for TNs fall outside the scope of this thesis, they are not reported here. Nevertheless, a detailed comparison among these methods can be found in [192].

The pro-rata and derivative-based LAPs are adopted by researchers for DNs and a variety of new methods which fall under the categories of circuit-based and tracing methods are also proposed for such networks. These LAPs are comprehensively discussed in the following sections. However, before proceeding further, it is extremely important to shed some light on the role of a slack bus in a DN in the context of LA.

2.3.1 Role of slack bus

In TNs, a portion of overall network losses is allocated to slack node due to the fact that there are multiple generating sources which do not prevail each other in a much larger context. However, this is not true for DNs where slack node prevails the other DG connected nodes since a bulk amount of power flows through it. As a result, a huge portion of overall network losses should be allocated to the slack node but, practically, it cannot be done due to the non-existence of any load or DG on this node. Furthermore, it is intuitively wrong to allocate losses to this node since it is the only point of entry of bulk power in a DN. Therefore, it should be treated uniquely because of its peculiar nature and losses allocated to it by any LAP must be reallocated to the other nodes hosting passive and active end-users.

2.3.2 Derivative- and circuit-based methods

In this category, Marginal Loss Coefficients (MLCs)- and Direct Loss Coefficients (DLCs)-based LAPs are reported in [193]. The former methodology allocates *variation* in network losses, due to the change in complex power, to end-users, whereas DLC-based scheme assigns *total* network losses to end-users.

A Z-bus method, developed for TNs, is reported in [194] which incorporates exact network equations and nodal injected currents, and, therefore, naturally segregates the losses among network buses. However, this method in its original developed form cannot be applied to DNs due to the singular nature of bus admittance matrix of these networks. Furthermore, it also allocates losses to the slack bus and does not provide any flexibility in the selection of buses for LA. These shortcomings are addressed in [195] and [196] which reallocate the losses, initially assigned to the slack bus and DGs, to the load buses. A Succinct Method for LA (SMLA) is reported in [197] which establishes a linear relation between the line losses and nodal injected power under the assumption that end-users are responsible for keeping the voltage profile within the prescribed feasible range at each node.

2.3.3 Tracing methods

The tracing methods make use of the radial topology of DNs and sweep the network either in a forward or backward manner to determine the contribution of each end-user in the overall network losses. Among these methods, PS, Branch Current Decomposition method for Losses Allocation (BCDLA) and Power Summation Method for Losses Allocation (PSMLA) are the most promising LA approaches.

In [198], the downstream and upstream versions of PS algorithm are implemented to determine the contribution of passive and active end-users, respectively in the overall branch current, whereas the same algorithm is utilized in [199] to take into account the actual demand and generation of end-users. A BCDLA procedure is reported in [200] which establishes a direct relation between the branch current and net injected complex bus currents. A Resistive Component-based Losses Partitioning (RCLP) scheme is proposed in [201] which distributes each branch losses among its individual phases. Furthermore, BCDLA method is updated by incorporating RCLP scheme in its algorithm to make it applicable for LA process in an unbalanced three-phase RDN.

An exact losses formula-based LAP is reported in [202], [203] which calculates each branch losses on the basis of actual load demand and voltage level at each node downstream of that branch. The same concept is extended in [204] by developing mathematical expressions for several types of DGs. In [205], PSMLA method is proposed which establishes a direct relation between the branch losses and net injected complex nodal power. The losses related to the cross-terms are allocated using quadratic LA factor approach in this methodology. The same LA factor technique is utilized in BCDLA method [206] where each branch current is expressed as a summation of real and imaginary components of the downstream nodal current injections. Apart from the quadratic Losses Partitioning (LP) method, two different LP approaches termed as geometric [207], [208] and multiplicative end-user's power [209] methodologies are utilized for the segregation of cross-terms induced losses, whereas a completely cross-term free mathematical expression is reported in [210], [211] in the context of power summation approach. In [212], the authors of PSMLA approach extended their algorithm and proposed a novel Energy Summation Method for Losses Allocation (ESMLA) which allocates energy losses, instead of power losses, of each branch to the respective end-users. Furthermore, uncertainties associated with the loads and generation curves are also taken into the proposed approach by modelling them through a second-order moment.

A novel methodology is reported in [213] where allocated losses to a particular node depends on the losses assigned to its adjacent power delivering nodes. However, this approach results in an over-recovery of the losses and, consequently, a normalization process is required at the end of this procedure. A Participation Matrix (PM)-based LAP is proposed in [214] where correlation among network branches and nodes is established through a PM and, subsequently, used to determine the share of each bus in overall network losses. The cross-terms are allocated by utilizing the contractual power of each consumer, instead of implementing quadratic or geometric LP methodologies. Lastly, a Sequential Shapely Value (SSV) approach which works in a forward sweep manner is presented in [215] to allocate each branch losses to the downstream branches and nodes using shapely value formula.

A comprehensive comparative analysis among Z-bus, SMLA, MLC and DLC methods is reported in [216], whereas shortcoming of SMLA are clearly reported and eliminated in [217] by replacing impedance of a branch with its resistance in the LA formulae. The problem of unfair LA which can occur due to the open access philosophy is resolved in [218] by reallocating the DGs' induced losses to independent energy consumers and captive end-users and, finally, a reduced-network representation is reported in [201] for LA to voltage-control DG nodes which is not possible through the derivative-based methods.

Lastly, to conclude this section, a detailed review of the most important LAPs is provided in Table 2.2 which summarizes the mathematical formulation, merits and demerits of these methodologies.

2.4 Summary

The increased penetration of mainly renewable DERs in DNs due to the environmental concerns have started obscuring the reliable and safe operation of such networks and, as a result, several developed countries have updated their grid codes which put additional requirements on DERs to actively participate in the provision of ancillary services in the context of grid management. Several network management schemes have been developed in this regard for ensuring the optimal operation of ADNs and in this chapter, a detailed literature overview of the methodologies related to LsMin and LA, which fall under the LsMag concept, is presented.

The LsMag in ADNs depends on the accurate modelling of network and end-users, ANM scheme for losses reduction and fair allocation of losses to end-users. The MCM approach for network modelling is more suitable than the *single-phase equivalent network representation-based* approach since it takes into account the inherent asymmetrical and unbalanced nature of DNs. The passive and active end-users modelling is a complicated task due to the non-availability of end-users data, uncertainty in loads demand and intermittent nature of DERs. The component- and measurement-based modelling techniques are commonly used approaches, whereas in the case of non-availability of end-users and measurement data, probabilistic load models are usually employed.

Concerning ANM schemes for LsMin, CVC and DERC are the most commonly utilized schemes. The high cost of ESBs is still a barrier in their integration in a DN. However, with the reduction in prices and advancements in the technology, ESM and combined DERC-DNR approaches can be envisioned as the emerging ANM methodologies for losses reduction. OADERs approach, on the other hand, can be implemented in the planning phase of a DN to increase its hosting capacity by avoiding congestion.

Fair LA to end-users is a pure economic problem and, therefore, unfair allocation leads to the issue of cross-subsidies. The LAPs which are developed for TNs cannot be directly applied to DNs due to the specific characteristics of the latter network. The branch-oriented-based LAPs for DNs are easy to understand and simple to apply in comparison to the derivative-based approaches. Nevertheless, all LAPs provide some kind of arbitrariness due to the inherent non-linear relation between system losses and network power flow which, in turn, prohibits an exact breakdown of the cross-terms induced losses among end-users.

Published papers

The work presented in this chapter led to the publication of following papers.

- Usman, M., M. Coppo, F. Bignucolo, and R. Turri. "Losses management strategies in active distribution networks: A review." *Electric Power Systems Research* 163 (2018): 116-132.
- Usman, Muhammad, Fabio Bignucolo, Roberto Turri, and Alberto Cerretti. "Power losses management in low voltage active distribution networks." in *52nd International Universities Power Engineering Conference (UPEC)*, pp. 1-6. IEEE, 2017.

Table 2.2: Review of losses allocation procedures.

LA Method	Mathematical Expression	Merits	Demerits	Ref-(Year)
MLC & DLC	**MLC** $L=\sum_{i=1}^{n-1}\rho_{P_i}P_i+\sum_{i=1}^{n-1}\rho_{Q_i}Q_i$ where $\rho_{P_i}=\frac{\partial L}{\partial P_i}$ & $\rho_{Q_i}=\frac{\partial L}{\partial Q_i}$ **DLC** $L=\gamma[\ P \quad Q\ ]^T$ where $\gamma=\frac{1}{2}[\ \Delta\theta \quad \Delta V\ ][H][J]^{-1}$	• Minimise cross-subsidies • Takes into account temporal and spatial variability of end-users • Consistent results for large DNs as compared to substitution method	• Calculation of Jacobian and Hessian matrices • Based on results of Newton-Raphson load flow method which has inherent shortcomings for DNs • Reconciliation for over-recovery of losses in case of MLC method • Second order approximation of Taylor series for DLC method	[193]-(2000)
Z-Bus	$L=\sum_{i=0}^{n}L_i$ where $L_i=\Re[I_i^*\sum_{j=0}^{n}R_{ij}I_j)]$	• Exact network equations utilisation • Segregation of losses among network buses • Put more emphasis on complex currents • Award strategically well-located end-users	• Losses allocation to Slack bus in a DN • Formation of a singular Y_{bus} in case of overhead-based DNs • No flexibility in custom selection of buses	[194]-(2001)
Succinct	$L=\sum_{i=1}^{n}L_i$ where $L_i=\Re[\sum_{b=1}^{B}(\frac{z_{ki}-z_{qi}}{Z^b})(\frac{V_k-V_q}{V_i})^*(P_i-jQ_i))]$	• Spatial consideration of end-users • Consideration of injected apparent power • Linear division of losses among end-users • Flexible selection of buses for LA	• Paradox as reported in [200] where more losses are allocated to users having less reactive power consumption under certain circumstances	[197]-(2002)
Improved Z-Bus	$\mathbf{L_{cn}}=\mathbf{L}_{co}+\mathbf{L}_{gal}$ $\mathbf{L}_{gal}=\frac{\mathbf{P_d}+\mathbf{L_{co}}}{(\sum_{j=1}^{n}P_{gj}/\sum_{j=1}^{n}L_{gj})-1}$	• Avoid negative loss allocation to DG buses by re-distributing the allocated losses to load buses	•No reward for DGs in lowering down the network losses	[195]-(2004)
Modified Y-Bus	$L_x=\boldsymbol{I}_x^{t^*}(\boldsymbol{K}_{bx}^{t^*}\boldsymbol{R}_p\boldsymbol{K}_{bx})\boldsymbol{I}_x$; $\mathbf{K}_{bl}=[\mathbf{A}_{bg}\|\mathbf{A}_{bl}]\begin{bmatrix}-[\mathbf{Y}_{gg}+\mathbf{Y}_G]^{-1}\mathbf{Y}_{gl}\\V_l\end{bmatrix}$ $*[\mathbf{Y}_{ll}-\mathbf{Y}_{lg}(\mathbf{Y}_{gg}+\mathbf{Y}_G)^{-1}\mathbf{Y}_{gl}]^{-1}$ $\mathbf{K}_{bg}=[\mathbf{A}_{bg}\|\mathbf{A}_{bl}]\begin{bmatrix}\mathbf{V}_g\\-[\mathbf{Y}_{ll}+\mathbf{Y}_L]^{-1}\mathbf{Y}_{lg}\end{bmatrix}$ $*[\mathbf{Y}_{gg}-\mathbf{Y}_{gl}(\mathbf{Y}_{ll}+\mathbf{Y}_L)^{-1}\mathbf{Y}_{lg}]^{-1}$	• No reconciliation factor • Less computational effort • Minimize cross-subsidies	• No combined loss allocation to passive and active end-users • Singular Y-bus matrix in case of overhead based DN	[219]-(2005)
BCDLA	$L=\sum_{i=1}^{n}L_i=\Re(W_iI_i)$ where $W_i=\sum_{b\in B_k}(R^{(b)}I^{(b)})$	• Properly allocate losses to consumers of same power having different distances from root node • No approximation and requirement of Jacobian/Hessian matrices • Allocation factors are defined for apparent power at each node	• Less negative loss allocation to DGs • Increases spatial and temporal cross-subsidies as compared to PSMLA	[200]-(2006)

LA Method	Mathematical Expression	Merits	Demerits	Ref-(Year)
Exact Method	$L^{(b)} = \sum_{k=1}^{N} (a_k I_{\alpha k} + jb_k I_{\beta k})$ $(V_i - V_j)^* = a_k + jb_k \ b$	• No approximation as exact loss formula is used • Can easily be extended for unbalanced RDN • Properly takes into account the location of users	• Based on BCDLA concept, therefore allows cross-subsidies among end-users	[203]-(2012)
PSMLA	$L = \sum_{b=1}^{B} L^{(b)}$ where $L^{(b)} = \sum_{j \in \alpha} (P_j + Q_j) + \sum_{\substack{j \in \alpha \\ j \neq b}} (\triangle P_j + j\triangle Q_j)$	• Less temporal and spatial cross-subsidies than MLC & BCDLA • Computationally more efficient than ESMLA in case of availability of metered customer data	• Approximation is introduced by using quadratic allocation of crossed terms • Improper allocation of losses to consumers of same power based on their distance from root node • Complex mathematical expressions as compared to BCDLA	[205]-(2012)
ESMLA	$L = \sum_{b=1}^{B} L^{(b)}$ where $L^{(b)} = \sum_{j \in \alpha} (\bar{P}_j + \bar{Q}_j) + \sum_{\substack{j \in \alpha \\ j \neq b}} (\triangle \bar{P}_j + j\triangle \bar{Q}_j)$ $\bar{P}_j + j\bar{Q}_j = \frac{W_j^P + jW_j^Q}{T}$	• Utilizes statistical representation of daily load curve and daily generation curve • Outperforms PSMLA if limited real time data is available • Successful implementation for planning purpose	• Total allocated losses are not equal to the losses obtained through power flow • Computationally less efficient for large available data set	[212]-(2012)
Sequential Shapely Value	$L = \sum_{b=1}^{B} I^{2(b)} R^{(b)}$ and contribution of each downstream branch and load current is determined through Shapley Formula $\phi_i(v) = \sum_{\substack{S \subseteq N \\ i \in S}} \frac{(\lvert S\rvert-1)!(n-\lvert S\rvert)!}{n!} [v(S) - v(s - \{i\})]$	• Less computational time and memory burden as compared to conventional Shapley formula • No allocation to slack bus and no reconciliation of total losses • No need of power flow solution if metered data is available	• Less negative loss allocation to DGs as it is based on current summation method, thus have inherit drawbacks of BCDLA	[215]-(2017)

LA Method	Mathematical Expression	Merits	Demerits	Ref-(Year)
Participation Matrix	**Type I buses** $L = \sum_{k=1}^{n} L_k$ where $L_{k,1} = \sum_{i=1}^{B_k} M_k(i) Z_i [I_k I_k^* + \sum_{\substack{j=1 \\ j \neq k \\ j \notin S}}^{N_k} N_i(j) port_{k,j} +$ $\sum_{j \in S} N_i(j)(port_{k,load_j} + port_{k,DG_j})]$ **Type II bus** $L_{k,2} = \sum_{i=1}^{B_k} M_k(i) Z_i [(I_k I_k^* + port_{load,DG}) +$ $\sum_{\substack{j=1 \\ j \neq k \\ j \notin S}}^{N_k} N_i(j) port_{x_k,j} + \sum_{j \in S} N_i(j)(port_{x_k,x_j} +$ $port_{x1_k,x2_j})]$ $port_{k,j} = \frac{s_k}{(s_k+s_j)}(I_k I_j^* + I_j I_k^*)$	• Better performance in LA as compared to BCDLA to consumers of same power having different distances from root node • No spatial cross-subsidies • Applicable in prising mechanism of restructured RDN • Recovers total losses	• Approximation is introduced by using contractual power LA factors • Complex mathematical expressions • Use of contractual power rather than actual load demand in LA factors	[214]-(2017)

n: total number of nodes
L: total losses in a network
L_i*: losses allocated to node 'i'*
L^b*: losses allocated to branch 'b'*
B_i*: set of branches from root node to node 'i'*
α*: set of nodes that have branch b on their path to the root node*
N*: total number of nodes beyond a branch*
S: set of type II buses
x: {load (l), gen (g)}

CHAPTER 3

Multi-Phase Losses Allocation Procedure based on Branch Current Decomposition Methodology

This chapter presents a novel multi-phase losses allocation procedure, which allocates losses explicitly to each phase and neutral conductor, and, subsequently, presents the concepts of self and mutual variable loss coefficients, and neutral losses allocation factors in a neutral-equipped distribution network. A detailed derivation related to the bifurcation of cross-terms induced losses, through quadratic and geometric partitioning approaches, among end-users is presented. Finally, a comprehensive analysis of the proposed methodology is carried out on a highly unbalanced test network to validate its effectiveness.

The extensive literature review presented in chapter 2 indicates that a significant research has been conducted, and still in progress, concerning ANM schemes for both MV and LV ADNs. Although novel management schemes are being proposed on a regular basis, there is also a strong need for developing new indicators which can represent the true picture of DNs operating conditions. In this context, LAPs can play a pivotal role since these methodologies allow quantifying the impact of each end-user on the overall network losses. On the one hand, several LAPs, as reported in chapter 2, successfully deal with the interdependence that exists among end-users due to the non-linear relation between network losses and power flows. However, on the other hand, the majority of these methods are developed using *single-phase equivalent representation* of multi-phase DNs by assuming symmetrical network configuration and balanced loading conditions, and, as a result, they are unable to provide critical information about the contribution of each end-user, connected to each phase of these networks, to the network operational state. The solely existing three-phase LAP is reported in [17]; however, this methodology imposes equal weighting factors to the cross-terms of different phases currents. Consequently, a large portion of the cross-terms induced losses can be allocated to a lightly loaded phase(s) due to the flow of high current in a heavily loaded phase(s). Furthermore, this scheme allocates neutral losses to each phase conductor in proportion to its current which makes this methodology unfair since neutral losses are not dependent on the energy consumption of end-users but are related to the degree of unbalance in a DN.

The key questions such as whether neutral losses should be assigned to phases or not, allocation of losses to each end-user on a particular phase of a node, and possible applications of LAPs in the context of LsMag in ADNs have not been addressed in the existing literature yet. Consequently, it is essential to develop a MPLAP which should perform explicit allocation of losses to each phase and neutral conductor, and, subsequently, to each end-user connected to the respective phases. Furthermore, it should be able to clearly point out the possible *active* role of Phase Losses Allocation Factors (PLAFs) and NLAFs, if any, in DN management. In view of this, a novel MPLAP is proposed in this chapter, whereas a management scheme based on the information provided by the proposed MPLAP is presented in the next chapter.

The developed MPLAP introduces appropriate weighting factors for the cross-terms induced losses by taking into account the real-time value of phases and neutral currents, and also proposes a mathematical formulation for the explicit allocation of losses to neutral conductors. Furthermore, the proposed methodology can be successfully applied to any RDN (high, medium or low voltage), equipped with or without neutral conductors. In the absence of a neutral conductor, the scheme would redistribute the phase losses associated with the cross-terms in a fairly manner, whereas in the presence of the neutral conductor, additional information about NLAFs would also be available. From practical point of view, the information obtained from MPLAP results can be utilized by DSOs in planning and management of ADNs by taking specific actions such as identification of highly unbalanced nodes in a network and, consequently, implementation of a suitable unbalance compensation scheme at those nodes. Furthermore, a fair financial policy/plan can be built on the top of MPLAP results to penalize/reward end-users for their negative/positive impact on the overall network losses as well as to charge them for their network usage.

3.1 Three-phase losses allocation procedure based on branch current decomposition

In this section, a detailed analysis of the solely existed three-phase RCLP-BCDLA is carried out with special emphasis being put on its shortcomings which, in turn, sets the basis for the development of a MPLAP. Consider a simple radial DN as shown in Fig. 3.1 where each branch is modelled as a multi-conductor branch as shown in Fig. 2.2a. According to RCLP concept, active power losses in a three-phase branch $m : l \sim m$ can be computed as follows:

$$\mathbf{P}_{lm}^{loss} = \Re\left\{\mathbf{I}_{lm}^{*} \otimes \left(\mathbf{R}_{lm}^{abc} \cdot \mathbf{I}_{lm}\right)\right\} \tag{3.1}$$

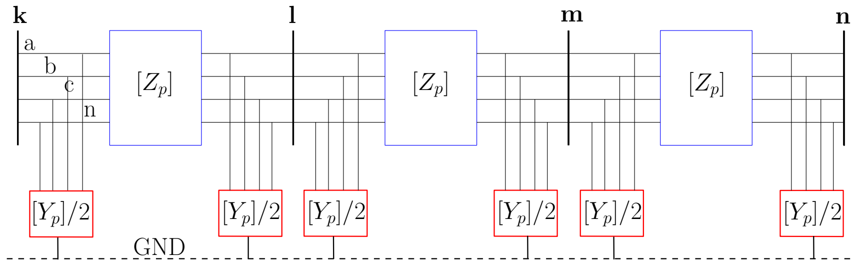

Figure 3.1: Example of a simple DN with series impedance and transversal admittances.

where $\mathbf{P}^{loss}_{lm} = [P^a_{lm}\ P^b_{lm}\ P^c_{lm}]^T$represents branch active power losses, $\mathbf{I}_{lm} = [I^a_{lm}\ I^a_{lm}\ I^c_{lm}]^T$ represents branch complex current, $\mathbf{R}_{abc} = \Re\{\mathbf{Z}^{abc}_{lm}\}$ where $\mathbf{Z}^{abc}_{lm}$ is Kron reduced form of the original multi-conductor impedance matrix $\mathbf{Z}^{p}_{lm}$ and $\otimes$ is component-wise multiplication. The total active power losses in such a branch can then be determined as:

$$P^{loss}_{lm_{tot}} = P^a_{lm} + P^b_{lm} + P^c_{lm} \tag{3.2}$$

Due to the symmetrical nature of $\mathbf{R}^{abc}_{lm}$, (3.2) can be expanded by invoking $R^{xy} = R^{yx} = R^{x/y}$ where $x, y \in \{a, b, c\}$

$$\begin{aligned} P^{loss}_{lm_{tot}} &= \{I^{*a}_{lm} \cdot R^{aa}_{lm} \cdot I^a_{lm}\} + \{I^{*b}_{lm} \cdot R^{bb}_{lm} \cdot I^b_{lm}\} + \{I^{*c}_{lm} \cdot R^{cc}_{lm} \cdot I^c_{lm}\} \\ &\quad + R^{a/b}_{lm}\{I^{*a}_{lm} I^b_{lm} + I^{*b}_{lm} I^a_{lm}\} + R^{b/c}_{lm}\{I^{*b}_{lm} I^c_{lm} + I^{*c}_{lm} I^b_{lm}\} + R^{c/a}_{lm}\{I^{*a}_{lm} I^c_{lm} + I^{*c}_{lm} I^a_{lm}\} \end{aligned} \tag{3.3}$$

which can further be written as:

$$\begin{aligned} P^{loss}_{lm_{tot}} &= \{I^{*a}_{lm} \cdot R^{aa}_{lm} \cdot I^a_{lm}\} + \{I^{*b}_{lm} \cdot R^{bb}_{lm} \cdot I^b_{lm}\} + \{I^{*c}_{lm} \cdot R^{cc}_{lm} \cdot I^c_{lm}\} \\ &\quad + R^{a/b}_{lm}\{2\Re(I^{*a}_{lm} \cdot I^b_{lm})\} + R^{b/c}_{lm}\{2\Re(I^{*b}_{lm} \cdot I^c_{lm})\} + R^{c/a}_{lm}\{2\Re(I^{*c}_{lm} \cdot I^a_{lm})\} \end{aligned} \tag{3.4}$$

Finally, (3.4) can be split into each phase losses components as follows:

$$\begin{aligned} P^{loss}_{lm_{tot}} &= \left\{\{I^{*a}_{lm} \cdot R^{aa}_{lm} \cdot I^a_{lm}\} + R^{ab}_{lm}\{\Re(I^{*a}_{lm} \cdot I^b_{lm})\} + R^{ac}_{lm}\{\Re(I^{*c}_{lm} \cdot I^a_{lm})\}\right\} \\ &\quad + \left\{\{I^{*b}_{lm} \cdot R^{bb}_{lm} \cdot I^b_{lm}\} + R^{ba}_{lm}\{\Re(I^{*a}_{lm} \cdot I^b_{lm})\} + R^{bc}_{lm}\{\Re(I^{*b}_{lm} \cdot I^c_{lm})\}\right\} \\ &\quad + \left\{\{I^{*c}_{lm} \cdot R^{cc}_{lm} \cdot I^c_{lm}\} + R^{ca}_{lm}\{\Re(I^{*c}_{lm} \cdot I^a_{lm})\} + R^{cb}_{lm}\{\Re(I^{*b}_{lm} \cdot I^c_{lm})\}\right\} \end{aligned} \tag{3.5}$$

Since $\Re\{I^{*x}_{lm} \cdot I^y_{lm}\} = \Re\{I^{*y}_{lm} \cdot I^x_{lm}\}$, (3.5) can then be written as:

$$\begin{aligned} P^{loss}_{lm_{tot}} &= \left\{\{I^{*a}_{lm} \cdot R^{aa}_{lm} \cdot I^a_{lm}\} + R^{ab}_{lm}\{\Re(I^{*a}_{lm} \cdot I^b_{lm})\} + R^{ac}_{lm}\{\Re(I^{*a}_{lm} \cdot I^c_{lm})\}\right\} \\ &\quad + \left\{\{I^{*b}_{lm} \cdot R^{bb}_{lm} \cdot I^b_{lm}\} + R^{ba}_{lm}\{\Re(I^{*b}_{lm} \cdot I^a_{lm})\} + R^{bc}_{lm}\{\Re(I^{*b}_{lm} \cdot I^c_{lm})\}\right\} \\ &\quad + \left\{\{I^{*c}_{lm} \cdot R^{cc}_{lm} \cdot I^c_{lm}\} + R^{ca}_{lm}\{\Re(I^{*c}_{lm} \cdot I^a_{lm})\} + R^{cb}_{lm}\{\Re(I^{*c}_{lm} \cdot I^b_{lm})\}\right\} \end{aligned} \tag{3.6}$$

The terms enclosed within big curly brackets represent the losses allocated to each phase of a branch. The first term ($I_{lm}^{*x} \cdot R_{lm}^{xx} \cdot I_{lm}^{x}$) shows the losses in each phase due to its self current, whereas the remaining two entries, defined as cross-terms $\{R_{lm}^{xy} \cdot \Re(I_{lm}^{*x} \cdot I_{lm}^{y})\}$, represent the losses in a particular phase due to the current in other phases. It can be noticed that the cross-terms in (3.4) and (3.5), as initially proposed in [17], are equally divided between the phases which leads to a paradox in case of an unbalanced system where heavily loaded phases induce more losses in lightly loaded phases and, as a result, end-users connected to the latter phases are held accountable for the losses for which they are not responsible. On the other hand, the end-users of heavily loaded phases are penalized less and, therefore, it is not possible to achieve impartial allocation of losses through this approach.

Furthermore, RCLP-BCDLA reduces the original $n \times \tau$ branch impedance matrix ($\mathbf{Z}_{lm}^{p}$) to a 3×3 phase impedance matrix $\mathbf{Z}_{lm}^{abc}$ under the assumption that neutral conductor in each network branch is solidly grounded i.e., earthing resistance $R_{gr} \approx 0$, at both of its ends and, therefore, it can be considered as an equipotential conductor. However, this is generally not the case in real DNs where neutral conductor is grounded at a single or multiple points through a finite earthing resistance ($R_{gr} \approx$ 5-15 Ω) and as a result, voltage profile along a neutral conductor follows a descending (SPG) or U-shaped (MPG) pattern. Under such scenarios, applying KR on $\mathbf{Z}_{lm}^{p}$ would lead to under/over estimation of the values of network state variables. Although, in the case of solidly-grounded MPG systems, the assumption implied in KR technique can be practically realized. But it is still unrealistic to allocate neutral losses to each phase conductor since these losses exist in a system due to the uneven distribution of single-phase end-users which leads to *inherent* unbalancing of a grid. Therefore, explicit information about the losses allocated to neutral conductors is provided in the proposed methodology.

The *equal* segregation of cross-terms induced losses and allocation of neutral losses to phases give rise to cross-subsidies and, ultimately, make RCLP-BCDLA an unfair LA approach. Since fair allocation of losses is a pure economical problem, therefore, in the following section, a novel MPLAP is proposed which treats neutral conductors like other phases and assigns appropriate weighting factors to the cross-terms to avoid equal distribution of losses which ultimately leads to fair allocation of losses among end-users.

3.2 Multi-phase losses allocation procedure for explicit representation of neutral conductor

In order to derive the mathematical formulation of the proposed approach, a generic two-phase (α and β) RDN composed of two branches, as shown in Fig. 3.2, is considered. In the presented methodology, the active power losses of terminal and non-terminal branches are first calculated followed by the allocation of these losses to the respective end-users[1]. Please note that the two-phase branch model is considered to derive the compact derivation

[1] It should be kept in mind that the derived losses formulae should only be used for LA purpose. The standard formulae for the calculation of active power losses in a multi-conductor branch can be found in [21] and must be used when one wants to determine the losses in a system.

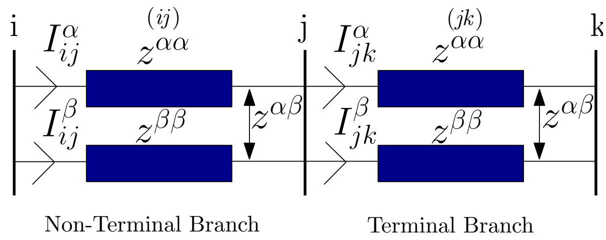

Figure 3.2: Two-phase generic radial DN for calculation of active power losses in terminal and non-terminal branches.

of losses formulation to facilitate the reading process. Nevertheless, the presented approach is easily extendable to any number of conductors and in section 3.2.4, the generalized losses formulae in terminal and non-terminal branches for τ number of conductors are presented which can be employed in the context of multi-node and multi-phase losses allocation process.

3.2.1 Active power losses of a terminal branch

Starting from the terminal branch *jk*, the active power losses in this branch can be computed as follows:

$$\mathbf{P}_{jk}^{loss} = \Re\left\{\mathbf{I}_{jk}^{*} \otimes (\mathbf{R}_{jk}^{\alpha\beta} * \mathbf{I}_{jk})\right\} \tag{3.7}$$

where $\mathbf{P}_{jk}^{loss} = [P_{jk}^{\alpha}\ P_{jk}^{\beta}]^T$ represents branch active power losses and $\mathbf{I}_{jk} = [I_{jk}^{\alpha}\ I_{jk}^{\beta}]^T$ represents branch currents. Since terminal branch complex current is equal to its receiving node k current, (3.7) can be written as:

$$\mathbf{P}_{jk}^{loss} = \begin{bmatrix} P_{jk}^{\alpha} \\ P_{jk}^{\beta} \end{bmatrix} = \Re\left\{ \begin{bmatrix} I_k^{*\alpha} \\ I_k^{*\beta} \end{bmatrix} \otimes \begin{bmatrix} R_{jk}^{\alpha\alpha} & R_{jk}^{\alpha\beta} \\ R_{jk}^{\beta\alpha} & R_{jk}^{\beta\beta} \end{bmatrix} \cdot \begin{bmatrix} I_k^{\alpha} \\ I_k^{\beta} \end{bmatrix} \right\} \tag{3.8}$$

The total active power losses in branch *jk* can then be computed as:

$$P_{jk_{tot}} = P_{jk}^{\alpha} + P_{jk}^{\beta} \tag{3.9}$$

$$P_{jk_{tot}} = \{I_k^{*\alpha} \cdot R_{jk}^{\alpha\alpha} \cdot I_k^{\alpha}\} + \{I_k^{*\alpha} \cdot R_{jk}^{\alpha\beta} \cdot I_k^{\beta}\} + \{I_k^{*\beta} \cdot R_{jk}^{\beta\alpha} \cdot I_k^{\alpha}\} + \{I_k^{*\beta} \cdot R_{jk}^{\beta\beta} \cdot I_k^{\beta}\} \tag{3.10}$$

Due to the symmetrical nature of $\mathbf{R}_{jk}^{\alpha\beta}$, (3.10) can be re-written by substituting $R_{jk}^{\alpha\beta} = R_{jk}^{\beta\alpha} = R_{jk}$

$$P_{jk_{tot}} = \{I_k^{*\alpha} \cdot R_{jk}^{\alpha\alpha} \cdot I_k^{\alpha}\} + \{I_k^{*\beta} \cdot R_{jk}^{\beta\beta} \cdot I_k^{\beta}\} + R_{jk} \cdot \{I_k^{*\alpha} \cdot I_k^{\beta} + I_k^{*\beta} \cdot I_k^{\alpha}\} \tag{3.11}$$

Since

$$\{I_k^{*\alpha} \cdot I_k^{\beta} + I_k^{*\beta} \cdot I_k^{\alpha}\} = \{(I_k^{*\alpha} \cdot I_k^{\beta}) + (I_k^{*\alpha} \cdot I_k^{\beta})^{*}\} = 2\Re\{I_k^{*\alpha} \cdot I_k^{\beta}\} \tag{3.12}$$

(3.11) can be further written as:

$$P_{jk_{tot}} = \{I_k^{*\alpha} \cdot R_{jk}^{\alpha\alpha} \cdot I_k^{\alpha}\} + \{I_k^{*\beta} \cdot R_{jk}^{\beta\beta} \cdot I_k^{\beta}\} + 2R_{jk} \cdot \Re\{I_k^{*\alpha} \cdot I_k^{\beta}\} \tag{3.13}$$

The cross-terms $2\Re\{I_k^{*\alpha} \cdot I_k^{\beta}\}$ can then be split into two components as follows:

$$2\Re\{I_k^{*\alpha} \cdot I_k^{\beta}\} = \lambda_{kk}^{\alpha\beta} \cdot \Re\{I_k^{*\alpha} \cdot I_k^{\beta}\} + \lambda_{kk}^{\beta\alpha} \cdot \Re\{I_k^{*\alpha} \cdot I_k^{\beta}\} \tag{3.14}$$

where $\lambda_{kk}^{\alpha\beta}$ and $\lambda_{kk}^{\beta\alpha}$ are termed as Variable Loss Coefficients (VLCs) for the phases α and β of node k, respectively. It is clear from (3.14) that the distribution of losses related to the cross-terms depends upon the chosen value of VLCs. For $\lambda_{kk}^{\alpha\beta} = \lambda_{kk}^{\beta\alpha} = 1$, losses are distributed equally between phases α and β, which is basically done in [17], whereas for $\lambda_{kk}^{\alpha\beta} \neq \lambda_{kk}^{\beta\alpha} \neq 1$, unequal distribution of losses between phases can be achieved. This indicates that the goal of LA problem is reduced to determine these factors which, in turn, must take into account the loading effect of one phase on another phase to achieve fair segregation of the cross-terms induced losses among end-users. In this work, these coefficients are determined by Quadratic Losses Partitioning (QLP) and Geometric Losses Partitioning (GLP) approaches which are comprehensively explained in section 3.2.5. Once these factors are calculated, the terminal branch active power losses can be written in the following form:

$$\mathbf{P}_{jk}^{loss} = \Re\left\{\begin{bmatrix} I_k^{*\alpha} \\ I_k^{*\beta} \end{bmatrix} \otimes \begin{bmatrix} \lambda_{kk}^{\alpha\alpha} * R_{jk}^{\alpha\alpha} & \lambda_{kk}^{\alpha\beta} * R_{jk}^{\alpha\beta} \\ \lambda_{kk}^{\beta\alpha} * R_{jk}^{\beta\alpha} & \lambda_{kk}^{\beta\beta} * R_{jk}^{\beta\beta} \end{bmatrix} \cdot \begin{bmatrix} I_k^{\alpha} \\ I_k^{\beta} \end{bmatrix}\right\} \tag{3.15}$$

Eq. (3.15) is used for the allocation of losses in the terminal branch to the phases of its downstream node.

3.2.2 Active power losses of a non-terminal branch

The branch current of a non-terminal branch, in general, can be written as a sum of net injected nodal currents downstream of that branch.

$$\mathbf{I}_{(b)} = \sum_{q \in Q} \mathbf{I}_q \tag{3.16}$$

where $\mathbf{I}_q$ is the nodal current of a generic node $q \in Q$ and Q is a set of downstream nodes being supplied by an upstream non-terminal branch (b). Consequently, the active power losses of the non-terminal branch ij in Fig. 3.2 can be computed by substituting (3.17) in (3.7),

$$\mathbf{I}_{ij} = \begin{bmatrix} I_{ij}^{\alpha} \\ I_{ij}^{\beta} \end{bmatrix} = \begin{bmatrix} I_j^{\alpha} + I_k^{\alpha} \\ I_j^{\beta} + I_k^{\beta} \end{bmatrix} \tag{3.17}$$

which leads to

$$\mathbf{P}_{ij}^{loss} = \Re\left\{\begin{bmatrix} I_j^{*\alpha} + I_k^{*\alpha} \\ I_j^{*\beta} + I_k^{*\beta} \end{bmatrix} \otimes \begin{bmatrix} R_{ij}^{\alpha\alpha} & R_{ij}^{\alpha\beta} \\ R_{ij}^{\beta\alpha} & R_{ij}^{\beta\beta} \end{bmatrix} * \begin{bmatrix} I_j^{\alpha} + I_k^{\alpha} \\ I_j^{\beta} + I_k^{\beta} \end{bmatrix}\right\} \tag{3.18}$$

Based on (3.12) and (3.14), (3.18) can be expanded as shown in (3.19) which can further be written in a compact form as shown in (3.20).

$$\begin{aligned}\mathbf{P}_{ij}^{loss} = \Re\left\{\begin{bmatrix} I_j^{*\alpha} \\ I_j^{*\beta}\end{bmatrix} \otimes \begin{bmatrix} R_{ij}^{\alpha\alpha} & R_{ij}^{\alpha\beta} \\ R_{ij}^{\beta\alpha} & R_{ij}^{\beta\beta}\end{bmatrix} \otimes \begin{bmatrix} (\lambda_{jj}^{\alpha\alpha} * I_j^{\alpha} + \lambda_{jk}^{\alpha\alpha} * I_k^{\alpha}) & (\lambda_{jj}^{\alpha\beta} * I_j^{\beta} + \lambda_{jk}^{\alpha\beta} * I_k^{\beta}) \\ (\lambda_{jj}^{\beta\alpha} * I_j^{\alpha} + \lambda_{jk}^{\beta\alpha} * I_k^{\alpha}) & (\lambda_{jj}^{\beta\beta} * I_j^{\beta} + \lambda_{jk}^{\beta\beta} * I_k^{\beta})\end{bmatrix}\right\} \\ + \Re\left\{\begin{bmatrix} I_k^{*\alpha} \\ I_k^{*\beta}\end{bmatrix} \otimes \begin{bmatrix} R_{ij}^{\alpha\alpha} & R_{ij}^{\alpha\beta} \\ R_{ij}^{\beta\alpha} & R_{ij}^{\beta\beta}\end{bmatrix} \otimes \begin{bmatrix} (\lambda_{kk}^{\alpha\alpha} * I_k^{\alpha} + \lambda_{kj}^{\alpha\alpha} * I_j^{\alpha}) & (\lambda_{kk}^{\alpha\beta} * I_k^{\beta} + \lambda_{kj}^{\alpha\beta} * I_j^{\beta}) \\ (\lambda_{kk}^{\beta\alpha} * I_k^{\alpha} + \lambda_{kj}^{\beta\alpha} * I_j^{\alpha}) & (\lambda_{kk}^{\beta\beta} * I_k^{\beta} + \lambda_{kj}^{\beta\beta} * I_j^{\beta})\end{bmatrix}\right\}\end{aligned} \tag{3.19}$$

$$\mathbf{P}_{ij}^{loss} = \Re\sum_{w\in Q}\left\{\begin{bmatrix} I_w^{*\alpha} \\ I_w^{*\beta}\end{bmatrix} \otimes \textstyle\sum_{(1:m)C}\left\{\begin{bmatrix} R_{ij}^{\alpha\alpha} & R_{ij}^{\alpha\beta} \\ R_{ij}^{\beta\alpha} & R_{ij}^{\beta\beta}\end{bmatrix} \otimes \textstyle\sum_{q\in Q}\begin{bmatrix} \lambda_{wq}^{\alpha\alpha} * I_q^{\alpha} & \lambda_{wq}^{\alpha\beta} * I_q^{\beta} \\ \lambda_{wq}^{\beta\alpha} * I_q^{\alpha} & \lambda_{wq}^{\beta\beta} * I_q^{\beta}\end{bmatrix}\right\}\right\} \tag{3.20}$$

Eq. (3.19) contains a lot of information in its formulation. As stated earlier in this section that current in each phase of a non-terminal branch is equal to the summation of downstream net nodal currents being fed by that branch; this indicates that apart from taking into consideration the impact of currents of mutually coupled phases of the non-terminal branch ij, the impact of currents of the downstream terminal and non-terminal branches being fed the branch ij must be taken into consideration while allocating losses of this branch to the downstream nodes. This takes the complexity of the proposed LAP to a whole new level since for non-terminal branches, two types of VLCs are now needed to fully take into account the impact of currents of self- and mutually coupled branches. In this regard, the following two types of VLCs are introduced for a non-terminal branch:

- VLCs representing the segregation of losses between phases currents of different nodes being fed by the *same* phase of an upstream branch. These VLCs are termed as self-VLCs.
- VLCs representing the segregation of losses between phases currents of different nodes being fed by the *mutually* coupled phases of an upstream branch. These VLCs are termed as mutual-VLCs.

It can be seen in (3.19) that $\lambda_{jk}^{\alpha\alpha}, \lambda_{jk}^{\beta\beta}, \lambda_{kj}^{\alpha\alpha}, \lambda_{kj}^{\beta\beta}$ are the self-VLCs, whereas $\lambda_{jj}^{\beta\alpha}, \lambda_{jk}^{\beta\alpha}, \lambda_{jj}^{\alpha\beta}, \lambda_{jk}^{\alpha\beta}$, $\lambda_{kk}^{\beta\alpha}, \lambda_{kj}^{\beta\alpha}, \lambda_{kk}^{\alpha\beta}, \lambda_{kj}^{\alpha\beta}$ are the mutual-VLCs for the non-terminal branch ij. Eqs. (3.15) and (3.20) represent the active power losses in terminal and non-terminal branches, respectively of the two-phase network and involve self- and mutual-VLCs to achieve fair segregation and, subsequently, allocation of the cross-terms induced losses among respective end-users.

3.2.3 Bifurcation of power losses between passive and active end-users

In the previous section, net injected nodal current is considered in (3.15) and (3.20) for terminal and non-terminal branches, respectively. However, in any LA procedure, it is mandatory to allocate losses to loads and DGs separately to penalize/reward them properly. Consequently, in this section, a detailed derivation is carried out which shows how losses can be allocated explicitly to loads and DGs of a specific node. The mathematical formulation is presented for both terminal and non-terminal branches by considering only one load and DG at each phase of a node to effectively define VLCs between different end-users being connected to a same/different phase of a same/different node. Once the formulation is developed for a single load and DG case, it can simply be extended using the below-mentioned procedure for any number of passive and active end-users.

For the terminal branch jk, $\mathbf{I}_{jk}$ in (3.7) can be defined as:

$$\mathbf{I}_{jk} = \begin{bmatrix} I_k^{\alpha} \\ I_k^{\beta} \end{bmatrix} = \begin{bmatrix} I_k^{\alpha:L} + I_k^{\alpha:G} \\ I_k^{\beta:L} + I_k^{\beta:G} \end{bmatrix} \tag{3.21}$$

where superscripts L and G represent load and DG, respectively. By substituting (3.21) in (3.7), the active power losses in terminal branch jk becomes:

$$\begin{aligned} \mathbf{P}_{jk}^{loss} &= (I_k^{*\alpha:L} + I_k^{*\alpha:G}) \cdot \{R_{jk}^{\alpha\alpha} \cdot (I_k^{\alpha:L} + I_k^{\alpha:G}) + R_{jk}^{\alpha\beta} \cdot (I_k^{\beta:L} + I_k^{\beta:G})\} \\ &+ (I_k^{*\alpha:L} + I_k^{*\alpha:G}) \cdot \{R_{jk}^{\beta\alpha} \cdot (I_k^{\alpha:L} + I_k^{\alpha:G}) + R_{jk}^{\beta\beta} \cdot (I_k^{\beta:L} + I_k^{\beta:G})\} \end{aligned} \tag{3.22}$$

which can be separated between the loads and DGs connected at each phase of the node k as follows:

$$\begin{aligned} \mathbf{P}_{jk}^{loss} &= \{I_k^{*\alpha:L} \cdot R_{jk}^{\alpha\alpha} \cdot (I_k^{\alpha:L} + I_k^{\alpha:G})\} + \{I_k^{*\alpha:L} \cdot R_{jk}^{\alpha\beta} \cdot (I_k^{\beta:L} + I_k^{\beta:G})\} \\ &+ \{I_k^{*\alpha:G} \cdot R_{jk}^{\alpha\alpha} \cdot (I_k^{\alpha:L} + I_k^{\alpha:G})\} + \{I_k^{*\alpha:G} \cdot R_{jk}^{\alpha\beta} \cdot (I_k^{\beta:L} + I_k^{\beta:G})\} \\ &+ \{I_k^{*\beta:L} \cdot R_{jk}^{\beta\alpha} \cdot (I_k^{\alpha:L} + I_k^{\alpha:G})\} + \{I_k^{*\beta:L} \cdot R_{jk}^{\beta\beta} \cdot (I_k^{\beta:L} + I_k^{\beta:G})\} \\ &+ \{I_k^{*\beta:G} \cdot R_{jk}^{\beta\alpha} \cdot (I_k^{\alpha:L} + I_k^{\alpha:G})\} + \{I_k^{*\beta:G} \cdot R_{jk}^{\beta\beta} \cdot (I_k^{\beta:L} + I_k^{\beta:G})\} \end{aligned} \tag{3.23}$$

Each line of (3.23) represents the losses caused either by a load or DG in its own phase and mutually coupled phase of the branch jk. This indicates that VLCs has to be defined not only between the currents of same end-users type but also between the currents of different end-users type. By introducing proper VLCs between each end-user type, (3.23) can be written in a compact form for both load and DG explicitly as shown in (3.24) and (3.25), respectively.

$$\mathbf{P}_k^L = \begin{bmatrix} I_k^{\alpha:L} \\ I_k^{\beta:L} \end{bmatrix}^* \otimes \sum_{(1:m)C} \left\{ \begin{bmatrix} R_{jk}^{\alpha\alpha} & R_{jk}^{\alpha\beta} \\ R_{jk}^{\beta\alpha} & R_{jk}^{\beta\beta} \end{bmatrix} \otimes \left\{ \begin{bmatrix} \lambda_{kk}^{\alpha\alpha^{LL}} I_k^{\alpha:L} & \lambda_{kk}^{\alpha\beta^{LL}} I_k^{\beta:L} \\ \lambda_{kk}^{\beta\alpha^{LL}} I_k^{\alpha:L} & \lambda_{kk}^{\beta\beta^{LL}} I_k^{\beta:L} \end{bmatrix} + \begin{bmatrix} \lambda_{kk}^{\alpha\alpha^{LG}} I_k^{\alpha:G} & \lambda_{kk}^{\alpha\beta^{LG}} I_k^{\beta:G} \\ \lambda_{kk}^{\beta\alpha^{LG}} I_k^{\alpha:G} & \lambda_{kk}^{\beta\beta^{LG}} I_k^{\beta:G} \end{bmatrix} \right\} \right\} \tag{3.24}$$

where $(1:m)C$ denotes the column-wise summation of resultant matrix.

$$\mathbf{P}_k^G = \begin{bmatrix} I_k^{\alpha:G} \\ I_k^{\beta:G} \end{bmatrix}^* \otimes \sum_{(1:m)C} \left\{ \begin{bmatrix} R_{jk}^{\alpha\alpha} & R_{jk}^{\alpha\beta} \\ R_{jk}^{\beta\alpha} & R_{jk}^{\beta\beta} \end{bmatrix} \otimes \left\{ \begin{bmatrix} \lambda_{kk}^{\alpha\alpha^{GG}} I_k^{\alpha:G} & \lambda_{kk}^{\alpha\beta^{GG}} I_k^{\beta:G} \\ \lambda_{kk}^{\beta\alpha^{GG}} I_k^{\alpha:G} & \lambda_{kk}^{\beta\beta^{GG}} I_k^{\beta:G} \end{bmatrix} + \begin{bmatrix} \lambda_{kk}^{\alpha\alpha^{GL}} I_k^{\alpha:L} & \lambda_{kk}^{\alpha\beta^{GL}} I_k^{\beta:L} \\ \lambda_{kk}^{\beta\alpha^{GL}} I_k^{\alpha:L} & \lambda_{kk}^{\beta\beta^{GL}} I_k^{\beta:L} \end{bmatrix} \right\} \right\} \tag{3.25}$$

For the non-terminal branch ij, $\mathbf{I}_{ij}$ in (3.17) can be defined as:

$$\mathbf{I}_{ij} = \begin{bmatrix} I_j^{\alpha} + I_k^{\alpha} \\ I_j^{\beta} + I_k^{\beta} \end{bmatrix} = \begin{bmatrix} (I_j^{\alpha:L} + I_j^{\alpha:G}) + (I_k^{\alpha:L} + I_k^{\alpha:G}) \\ (I_j^{\beta:L} + I_j^{\beta:G}) + (I_k^{\beta:L} + I_k^{\beta:G}) \end{bmatrix} \tag{3.26}$$

By substituting (3.26) in (3.7), the power losses in non-terminal branch ij becomes:

$$\mathbf{P}_{ij}^{loss} =$$
$$(I_j^{*\alpha:L} + I_j^{*\alpha:G})\Big\{R_{ij}^{\alpha\alpha}\{(I_j^{\alpha:L} + I_j^{\alpha:G}) + (I_k^{\alpha:L} + I_k^{\alpha:G})\} + R_{ij}^{\alpha\beta}\{(I_j^{\beta:L} + I_j^{\beta:G}) + (I_k^{\beta:L} + I_k^{\beta:G})\}\Big\} +$$
$$(I_k^{*\alpha:L} + I_k^{*\alpha:G})\Big\{R_{ij}^{\alpha\alpha}\{(I_j^{\alpha:L} + I_j^{\alpha:G}) + (I_k^{\alpha:L} + I_k^{\alpha:G})\} + R_{ij}^{\alpha\beta}\{(I_j^{\beta:L} + I_j^{\beta:G}) + (I_k^{\beta:L} + I_k^{\beta:G})\}\Big\} +$$
$$(I_j^{*\beta:L} + I_j^{*\beta:G})\Big\{R_{ij}^{\alpha\alpha}\{(I_j^{\alpha:L} + I_j^{\alpha:G}) + (I_k^{\alpha:L} + I_k^{\alpha:G})\} + R_{ij}^{\alpha\beta}\{(I_j^{\beta:L} + I_j^{\beta:G}) + (I_k^{\beta:L} + I_k^{\beta:G})\}\Big\} +$$
$$(I_k^{*\beta:L} + I_k^{*\beta:G})\Big\{R_{ij}^{\alpha\alpha}\{(I_j^{\alpha:L} + I_j^{\alpha:G}) + (I_k^{\alpha:L} + I_k^{\alpha:G})\} + R_{ij}^{\alpha\beta}\{(I_j^{\beta:L} + I_j^{\beta:G}) + (I_k^{\beta:L} + I_k^{\beta:G})\}\Big\} \tag{3.27}$$

Based on (3.27), the contribution of each end-user, connected at nodes j and k, in the active power losses of branch ij can be defined explicitly as shown below. The total losses caused by the load connected at node j in the non-terminal branch ij are defined as:

$$\mathbf{P}_j^L = \begin{bmatrix} I_j^{\alpha:L} \\ I_j^{\beta:L} \end{bmatrix}^* \otimes \sum_{(1:m)C} \Bigg\{ \begin{bmatrix} R_{ij}^{\alpha\alpha} & R_{ij}^{\alpha\beta} \\ R_{ij}^{\beta\alpha} & R_{ij}^{\beta\beta} \end{bmatrix} \otimes \Bigg\{ \begin{bmatrix} \lambda_{jj}^{\alpha\alpha^{LL}} I_j^{\alpha:L} & \lambda_{jj}^{\alpha\beta^{LL}} I_j^{\beta:L} \\ \lambda_{jj}^{\beta\alpha^{LL}} I_j^{\alpha:L} & \lambda_{jj}^{\beta\beta^{LL}} I_j^{\beta:L} \end{bmatrix} + \begin{bmatrix} \lambda_{kk}^{\alpha\alpha^{LL}} I_k^{\alpha:L} & \lambda_{kk}^{\alpha\beta^{LL}} I_k^{\beta:L} \\ \lambda_{kk}^{\beta\alpha^{LL}} I_k^{\alpha:L} & \lambda_{kk}^{\beta\beta^{LL}} I_k^{\beta:L} \end{bmatrix}$$
$$+ \begin{bmatrix} \lambda_{jj}^{\alpha\alpha^{LG}} I_j^{\alpha:G} & \lambda_{jj}^{\alpha\beta^{LG}} I_j^{\beta:G} \\ \lambda_{jj}^{\beta\alpha^{LG}} I_j^{\alpha:G} & \lambda_{jj}^{\beta\beta^{LG}} I_j^{\beta:G} \end{bmatrix} + \begin{bmatrix} \lambda_{kk}^{\alpha\alpha^{LG}} I_k^{\alpha:G} & \lambda_{kk}^{\alpha\beta^{LG}} I_k^{\beta:G} \\ \lambda_{kk}^{\beta\alpha^{LG}} I_k^{\alpha:G} & \lambda_{kk}^{\beta\beta^{LG}} I_k^{\beta:G} \end{bmatrix} \Bigg\}\Bigg\} \tag{3.28}$$

The total losses caused by the DG connected at node j in the non-terminal branch ij are defined as:

$$\mathbf{P}_j^G = \begin{bmatrix} I_j^{\alpha:G} \\ I_j^{\beta:G} \end{bmatrix}^* \otimes \sum_{(1:m)C} \Bigg\{ \begin{bmatrix} R_{ij}^{\alpha\alpha} & R_{ij}^{\alpha\beta} \\ R_{ij}^{\beta\alpha} & R_{ij}^{\beta\beta} \end{bmatrix} \otimes \Bigg\{ \begin{bmatrix} \lambda_{jj}^{\alpha\alpha^{GG}} I_j^{\alpha:G} & \lambda_{jj}^{\alpha\beta^{GG}} I_j^{\beta:G} \\ \lambda_{jj}^{\beta\alpha^{GG}} I_j^{\alpha:G} & \lambda_{jj}^{\beta\beta^{GG}} I_j^{\beta:G} \end{bmatrix} + \begin{bmatrix} \lambda_{kk}^{\alpha\alpha^{GG}} I_k^{\alpha:G} & \lambda_{kk}^{\alpha\beta^{GG}} I_k^{\beta:G} \\ \lambda_{kk}^{\beta\alpha^{GG}} I_k^{\alpha:G} & \lambda_{kk}^{\beta\beta^{GG}} I_k^{\beta:G} \end{bmatrix}$$
$$+ \begin{bmatrix} \lambda_{jj}^{\alpha\alpha^{GL}} I_j^{\alpha:L} & \lambda_{jj}^{\alpha\beta^{GL}} I_j^{\beta:L} \\ \lambda_{jj}^{\beta\alpha^{GL}} I_j^{\alpha:L} & \lambda_{jj}^{\beta\beta^{GL}} I_j^{\beta:L} \end{bmatrix} + \begin{bmatrix} \lambda_{kk}^{\alpha\alpha^{GL}} I_k^{\alpha:L} & \lambda_{kk}^{\alpha\beta^{GL}} I_k^{\beta:L} \\ \lambda_{kk}^{\beta\alpha^{GL}} I_k^{\alpha:L} & \lambda_{kk}^{\beta\beta^{GL}} I_k^{\beta:L} \end{bmatrix} \Bigg\}\Bigg\} \tag{3.29}$$

The total losses caused by the load connected at node k in the non-terminal branch ij are defined as:

$$\mathbf{P}_k^L = \begin{bmatrix} I_k^{\alpha:L} \\ I_k^{\beta:L} \end{bmatrix}^* \otimes \sum_{(1:m)C} \Bigg\{ \begin{bmatrix} R_{ij}^{\alpha\alpha} & R_{ij}^{\alpha\beta} \\ R_{ij}^{\beta\alpha} & R_{ij}^{\beta\beta} \end{bmatrix} \otimes \Bigg\{ \begin{bmatrix} \lambda_{kk}^{\alpha\alpha^{LL}} I_k^{\alpha:L} & \lambda_{kk}^{\alpha\beta^{LL}} I_k^{\beta:L} \\ \lambda_{kk}^{\beta\alpha^{LL}} I_k^{\alpha:L} & \lambda_{kk}^{\beta\beta^{LL}} I_k^{\beta:L} \end{bmatrix} + \begin{bmatrix} \lambda_{jj}^{\alpha\alpha^{LL}} I_j^{\alpha:L} & \lambda_{jj}^{\alpha\beta^{LL}} I_j^{\beta:L} \\ \lambda_{jj}^{\beta\alpha^{LL}} I_j^{\alpha:L} & \lambda_{jj}^{\beta\beta^{LL}} I_j^{\beta:L} \end{bmatrix}$$
$$+ \begin{bmatrix} \lambda_{kk}^{\alpha\alpha^{LG}} I_k^{\alpha:G} & \lambda_{kk}^{\alpha\beta^{LG}} I_k^{\beta:G} \\ \lambda_{kk}^{\beta\alpha^{LG}} I_k^{\alpha:G} & \lambda_{kk}^{\beta\beta^{LG}} I_k^{\beta:G} \end{bmatrix} + \begin{bmatrix} \lambda_{jj}^{\alpha\alpha^{LG}} I_j^{\alpha:G} & \lambda_{jj}^{\alpha\beta^{LG}} I_j^{\beta:G} \\ \lambda_{jj}^{\beta\alpha^{LG}} I_j^{\alpha:G} & \lambda_{jj}^{\beta\beta^{LG}} I_j^{\beta:G} \end{bmatrix} \Bigg\}\Bigg\} \tag{3.30}$$

and finally, the total losses caused by the DG connected at node k in the non-terminal branch ij are defined as:

$$\mathbf{P}_k^G = \begin{bmatrix} I_k^{\alpha:G} \\ I_k^{\beta:G} \end{bmatrix}^* \otimes \sum_{(1:m)C} \left\{ \begin{bmatrix} R_{ij}^{\alpha\alpha} & R_{ij}^{\alpha\beta} \\ R_{ij}^{\beta\alpha} & R_{ij}^{\beta\beta} \end{bmatrix} \otimes \left\{ \begin{bmatrix} \lambda_{kk}^{\alpha\alpha^{GG}} I_k^{\alpha:G} & \lambda_{kk}^{\alpha\beta^{GG}} I_k^{\beta:G} \\ \lambda_{kk}^{\beta\alpha^{GG}} I_k^{\alpha:G} & \lambda_{kk}^{\beta\beta^{GG}} I_k^{\beta:G} \end{bmatrix} + \begin{bmatrix} \lambda_{jj}^{\alpha\alpha^{GG}} I_j^{\alpha:G} & \lambda_{jj}^{\alpha\beta^{GG}} I_j^{\beta:G} \\ \lambda_{jj}^{\beta\alpha^{GG}} I_j^{\alpha:G} & \lambda_{jj}^{\beta\beta^{GG}} I_j^{\beta:G} \end{bmatrix} \right.\right.$$
$$\left.\left. + \begin{bmatrix} \lambda_{kk}^{\alpha\alpha^{GL}} I_k^{\alpha:L} & \lambda_{kk}^{\alpha\beta^{GL}} I_k^{\beta:L} \\ \lambda_{kk}^{\beta\alpha^{GL}} I_k^{\alpha:L} & \lambda_{kk}^{\beta\beta^{GL}} I_k^{\beta:L} \end{bmatrix} + \begin{bmatrix} \lambda_{jj}^{\alpha\alpha^{GL}} I_j^{\alpha:L} & \lambda_{jj}^{\alpha\beta^{GL}} I_j^{\beta:L} \\ \lambda_{jj}^{\beta\alpha^{GL}} I_j^{\alpha:L} & \lambda_{jj}^{\beta\beta^{GL}} I_j^{\beta:L} \end{bmatrix} \right\}\right\} \tag{3.31}$$

Eqs. (3.24)-(3.25) for the terminal branch and eqs. (3.28)-(3.31) for the non-terminal branch indicate that

- To allocate losses to a specific end-user (load or DG) being connected to a particular phase of a terminal node, VLCs have to be defined between the current of that component and the currents of components connected to the same and mutually coupled phases of that node.
- To allocate losses to a specific end-user (load or DG) being connected to a particular phase of a non-terminal node, apart from defining the VLCs which represent the relation between the same node quantities, these coefficients also have to be defined between the current of that component and the currents of components connected to the same and mutually-coupled phases of the downstream non-terminal and terminal nodes.

3.2.4 Generalization of active power losses formulae

The general formulation of active power losses is presented in this section for both net-injected and, segregated loads and DGs current. For a generic multi-phase branch having three phases (a, b, c) and m neutral conductors, the active power losses in a terminal branch in the case of net-injected current and, explicit loads and DGs current can be expressed as shown in (3.32) and (3.33), respectively.

$$\mathbf{P}_{Tr}^{Net:loss} = \Re\{\mathbf{I}_p^{Net*} \otimes \check{\mathbf{R}}_{Tr}^{NetNet} * \mathbf{I}_p^{Net}\} \tag{3.32}$$

$$\mathbf{P}_{Tr}^{L:loss} = \Re\{\mathbf{I}_p^{L*} \otimes \check{\mathbf{R}}_{Tr}^{LL} * \mathbf{I}_p^{L}\} + \Re\{\mathbf{I}_p^{L*} \otimes \check{\mathbf{R}}_{Tr}^{LG} * \mathbf{I}_p^{G}\} \tag{3.33}$$

where Tr stands for a terminal branch, $\mathbf{I}_p = [I_p^a, I_p^b, I_p^c, I_p^{n_1}, \cdots, I_p^{n_m}]^T$ is a nodal current vector at node p and $\check{\mathbf{R}}_{Tr}^{\rho\rho}$ for $\rho = \{Net, L, G\}$ is defined as:

$$\check{\mathbf{R}}_{Tr}^{\rho\rho} = \begin{bmatrix} \lambda_{pp}^{aa^{\rho\rho}} * R_{Tr}^{aa} & \cdots & \lambda_{pp}^{an_m^{\rho\rho}} * R_{Tr}^{an_m} \\ \vdots & \ddots & \vdots \\ \lambda_{pp}^{n_m a^{\rho\rho}} * R_{Tr}^{n_m a} & \cdots & \lambda_{pp}^{n_m n_m^{\rho\rho}} * R_{Tr}^{n_m n_m} \end{bmatrix}$$

For a non-terminal branch, the generalized active power losses formula based on net-injected and, explicit loads and DGs current can be defined as shown in (3.34) and (3.35).

$$\mathbf{P}_{nTr}^{Net:Loss} = \Re\Big\{\sum_{w\in Q}\{\mathbf{I}_{w}^{Net*} \otimes \sum_{(1:m)C}(\mathbf{R}_{nTr} \otimes \sum_{q\in Q}\check{\mathbf{I}}_{wq}^{Net})\}\Big\} \tag{3.34}$$

$$\mathbf{P}_{nTr}^{L:loss} = \Re\Big\{\sum_{w\in Q}\{\mathbf{I}_{w}^{L*} \otimes \sum_{1:m(C)}(\mathbf{R}_{nTr} \otimes \sum_{q\in Q}\check{\mathbf{I}}_{wq}^{LL})\}\Big\} + \Re\Big\{\sum_{w\in Q}\{\mathbf{I}_{w}^{L*} \otimes \sum_{1:m(C)}(\mathbf{R}_{nTr} \otimes \sum_{q\in Q}\check{\mathbf{I}}_{wq}^{LG})\}\Big\} \tag{3.35}$$

where nTr represents a non-terminal branch and $\check{\mathbf{I}}_{wq}^{\rho}\rho$ for $\rho = \{Net, L, G\}$ is defined as:

$$\check{\mathbf{I}}_{wq}^{\rho\rho} = \begin{bmatrix} \lambda_{wq}^{aa^{\rho\rho}} * I_q^a & \cdots & \lambda_{wq}^{an_m{}^{\rho\rho}} * I_q^{n_m} \\ \vdots & \ddots & \vdots \\ \lambda_{wq}^{n_m a^{\rho\rho}} * I_q^a & \cdots & \lambda_{wq}^{n_m n_m{}^{\rho\rho}} * I_q^{n_m} \end{bmatrix}$$

It can be noticed in (3.32)-(3.33) and (3.34)-(3.35) that the resistance matrix contains the resistance of all phases and neutral conductors. Furthermore, cross-terms are redistributed between the phases on the basis of their currents and, as a result, end-users connected to these phases are penalized/rewarded fairly. It must be noted that usually from a load flow algorithm, net load and DG currents are available at each node. Consequently, losses allocated to each node are the combined allocation to all loads and DGs connected at that node. To further divide the allocated losses among each load and DG, one possible way would be to obtain the current of each end-user and then calculate the corresponding VLCs. But this would lead to an extremely large number of VLCs which can easily make the proposed LAP intractable. Consequently, there is a strong need to develop a technique which, on the one hand, can easily provide the information about the contribution of each end-user in the overall network losses and, on the other hand, remains tractable for large-size systems and any number of passive and active end-users.

3.2.5 Calculation of variable loss coefficients

The segregation of cross-terms induced losses strongly depends upon the approach chosen for Losses Partitioning (LP). However, there will always be a degree of arbitrariness in the process of LA, no matter which LP scheme is chosen, due to the non-linear relation between power system losses and line flow. Consequently, two LP approaches, namely QLP and GLP schemes, are adopted in this work to represent how division of the cross-term related losses is influenced by the choice of an LP scheme.

3.2.5.1 Quadratic losses partitioning approach

Since power losses and phases currents in a branch have quadratic relation between them, the following constraint is imposed to determine the self- and mutual-VLCs λ_{pq}^{xy} and λ_{qp}^{yx}.

$$\frac{\lambda_{pq}^{xy}}{I_p^{x^2}} = \frac{\lambda_{qp}^{yx}}{I_q^{y^2}} \tag{3.36}$$

Furthermore, the following constraint can be obtained from (3.14)

$$\lambda_{pq}^{xy} + \lambda_{qp}^{yx} = 2 \tag{3.37}$$

Combining (3.36) and (3.37) results in

$$\lambda_{pq}^{xy} = \frac{2 * I_p^{x^2}}{I_p^{x^2} + I_q^{y^2}}; \quad \lambda_{yx}^{qp} = \frac{2 * I_q^{y^2}}{I_q^{y^2} + I_p^{x^2}} \tag{3.38}$$

3.2.5.2 Geometric losses partitioning approach

Since cross-term is a product of two phases currents, geometric mean can also be used to determine VLCs by imposing the following constraint:

$$\lambda_{pq}^{xy} - logI_p^x = \lambda_{qp}^{yx} - logI_q^y \tag{3.39}$$

Combining (3.37) with (3.39), the coefficients λ_{pq}^{xy} and λ_{qp}^{yx} can be calculated as:

$$\lambda_{pq}^{xy} = 1 + \frac{1}{2} log \frac{I_p^x}{I_q^y}; \quad \lambda_{qp}^{yx} = 1 + \frac{1}{2} log \frac{I_q^y}{I_p^x} \tag{3.40}$$

In both schemes, the sets $\{x, y\}$ and $\{p, q\}$ contain generic phases/neutral conductors and generic nodes of a system, respectively. For a generic two-phase system of Fig. 3.2, $\{x, y\}$ and $\{p, q\}$ become $\{\alpha, \beta\}$ and $\{j, k\}$, respectively. It has to be kept in mind that no losses would be assigned to node g because it is considered as a slack node and as comprehensively explained in chapter 2, it is intuitively wrong to allocate losses to this bus type. The relation between QLP and GLP is shown in Fig. 3.3. It can be noticed that QLP approach is more sensitive to the ratio I^x/I^y when it lies in the range [0.1-10] as compared to the GLP scheme. A slight increase or decrease in the value of I^x with respect to I^y leads to a significant increment or decrement of the losses allocated to I^x. On the other hand, when the ratio lies in between the [0.01-0.1] and [10-100] ranges, the QLP allocates almost the whole share of losses to I^y and I^x, respectively, whereas the GLP

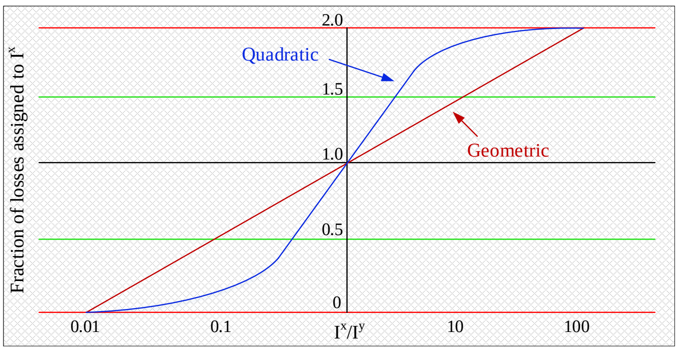

Figure 3.3: Fraction of losses allocated to I^x through quadratic and geometric losses partitioning approaches.

scheme still allocates a considerable portion of losses to I^x and I^y, respectively in these ranges. Consequently, the QLP approach can be considered more accurate in the context of LA as compared to the GLP approach due to the existence of a correlation between system losses and former LP scheme (both are quadratic function of the line currents). Finally, it must be noted that to determine VLCs involving currents of different phases, the current of one phase has to be rotated in the direction of other phase current. In this work, for a multi-phase system, phase a current vector position is chosen as a reference; however, in the absence of load connected to phase a, phase b current vector position becomes the reference.

3.2.6 Multi-phase losses allocation procedure

Once active power losses in terminal and non-terminal branches are determined through (3.32)/(3.33) and (3.34)/(3.35), respectively, the next step is to allocate these losses to the respective nodes by tracing their path towards the root node through these branches.

In the case of terminal branches, the calculated losses are allocated to the three-phases and m neutral conductors of their terminal node, whereas for a non-terminal branch b, the allocated losses are determined by first expanding (3.34) as follows:

$$\mathbf{P}^{loss}_{(b)} = \Re\Big\{(\mathbf{I}^*_1 \otimes \sum_{(1:m)C} \{\mathbf{R} \otimes \sum_{q\in Q} \check{\mathbf{I}}_{1q}\}) + ... + (\mathbf{I}^*_s \otimes \sum_{(1:m)C} \{\mathbf{R} \otimes \sum_{q\in Q} \check{\mathbf{I}}_{sq}\})\Big\} \tag{3.41}$$

where s is the last node in set Q.

Eq. (3.41) shows the contribution of each node in the overall branch b losses. Let $\boldsymbol{\beta}^{(b)}_f$ denotes the losses caused by a generic node f in this branch which allows to express (3.41) as follows:

$$\mathbf{P}^{loss}_{(b)} = \Re\{\sum_{f\in Q_{(b)}} \boldsymbol{\beta}^{(b)}_f\} \tag{3.42}$$

where

$$\boldsymbol{\beta}^{(b)}_f = \begin{cases} \mathbf{I}^*_f \otimes (\mathbf{R} * \sum_{q\in Q} \check{\mathbf{I}}_{fq}) & f \in Q^{(b)} \\ \mathbf{0} & f \notin Q^{(b)} \end{cases} \tag{3.43}$$

Eq. (3.43) represents the losses that has to be allocated to node f due to the flow of current $\mathbf{I}_f$ in branch b. In this way, by sweeping a network either in a backward or forward manner, the losses of all non-terminal branches are allocated to the respective nodes as shown in (3.44).

$$\boldsymbol{\beta}_f = \sum_{b=1}^{B} \boldsymbol{\beta}^{(b)}_f \tag{3.44}$$

where B is the set of branches which connect node f to the root node.

It can now be noticed that (3.43) and (3.44) are the generic mathematical formulae of losses allocated to each node through the proposed MPLAP and these expressions, in turn, are based on the modified active power losses expressions developed for terminal (3.32)/(3.33) and non-terminal branches (3.34)/(3.35), respectively.

3.2.7 MPLAP algorithm

In the following, the proposed MPLAP algorithm is presented which represents the chronological steps involved in its implementation. Two key observations, as mentioned in the

Algorithm 1: Multi-Phase LAP

1 **Input** : Node Voltages ($\mathbf{V}_{node}$) and Nodal Currents ($\mathbf{I}_{node}$) from a Load Flow
2 **Output** : Allocated losses to each phase and neutral conductor
3 Transformer matrix calculation using pseudo-inverse method
4 Formation of a Branch-Node matrix
5 $i \leftarrow 1$
6 **while** $i \leq Max.No.of Branches$ **do**
7   **if** *Terminal Branch* **then**
8   Calculation of mutual-VLCs e.g., $(\lambda_{jk}^{\alpha\alpha}, \lambda_{jk}^{\alpha\beta}, \lambda_{kj}^{\alpha\alpha}, \lambda_{kj}^{\alpha\beta})$
9   Allocation of terminal branch losses (3.32) or (3.33) to terminal nodes through (3.43)
10   **else**
11   Calculation of self- and mutual-VLCs for non-terminal branch e.g., $(\lambda_{jj}^{\beta\alpha}, \lambda_{jk}^{\beta\alpha}, \lambda_{jj}^{\alpha\beta}, \lambda_{jk}^{\alpha\beta}, \lambda_{kk}^{\beta\alpha}, \lambda_{kj}^{\beta\alpha}, \lambda_{kk}^{\alpha\beta}, \lambda_{kj}^{\alpha\beta})$
12   Allocation of losses of a non-terminal branch (3.34) or (3.35) to its downstream nodes through (3.43)
13   **end**
14 **end**

steps 3 and 4, can be made. The first point is the calculation of transformer admittance matrix through a pseudo-inverse approach due to the possible singularity in its impedance matrix which prohibits its inversion. This issue is handled through a singular-value-decomposition based pseudo-inverse method. The second observation is the formation of a branch-node matrix which stores the information of all downstream nodes being fed by both terminal and non-terminal branches, so that proper allocation of losses can be made to these nodes.

3.3 Case study

This section reports a case study focusing on the validation of the proposed MPLAP by comparing its results with the standard three-phase RCLP-BCDLA procedure. For this purpose, a standard MV IEEE-13 node network is chosen which represents a high degree of unbalance and consists of both two-phase and three-phase lines. The standard IEEE-13 bus network consists of 13 nodes but a slight modification has been made in the network. The distributed load connected between the nodes 632 and 671 is replaced by two lumped loads by connecting 2/3 of the total load at the newly introduced node 670 and 1/3 of the total load at node 671. Furthermore, to show the applicability of the proposed methodology for ADNs, a single-phase DG is added at node 646 (100kW, 50kVar), whereas a three-phase DG of type Y-PQ (200kW, 100kVar) is connected at node 680. Both DGs are considered as negative loads. The voltage at three-phase voltage regulator

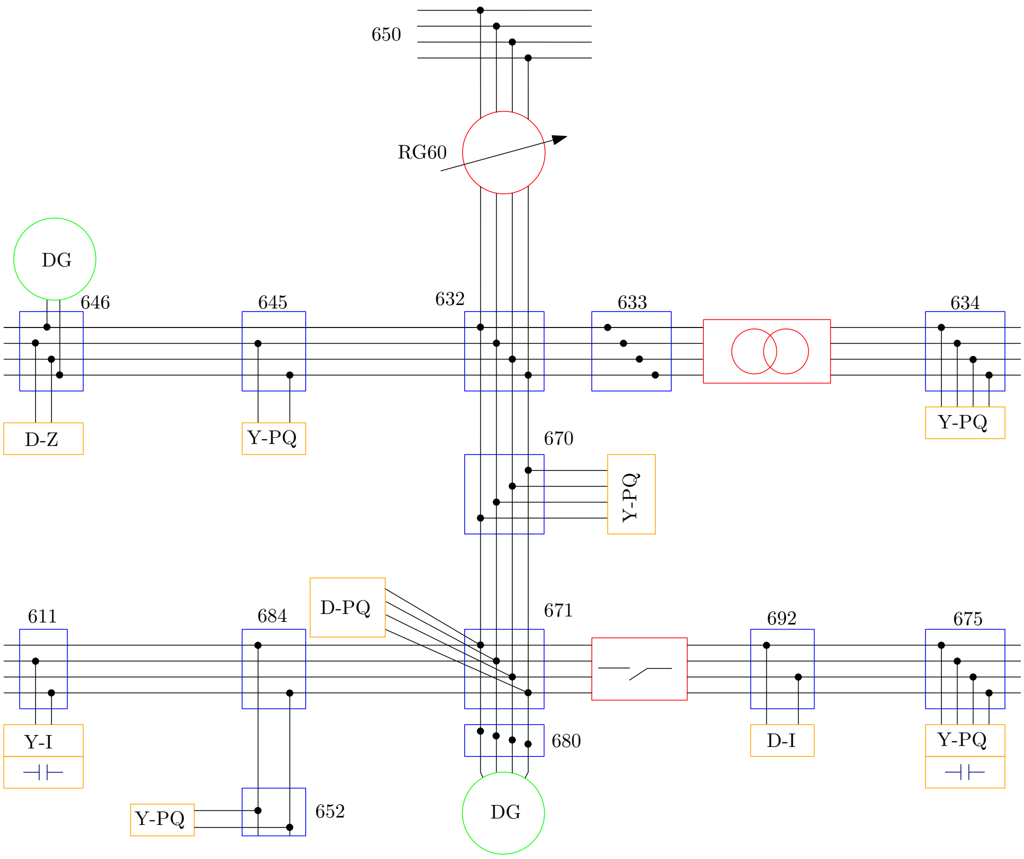

Figure 3.4: Modified IEEE-13 node test system with distributed generators connected at node 646 and 680.

(RG60), which is modelled as a tap-changing transformer, is imposed to 1.05pu. Moreover, SPG configuration is considered for this network with secondary side of RG60 bus is solidly grounded. The network contains both wye- and delta-connected loads of constant impedance, constant current and constant power type. Lastly, load flow simulations are carried out through a multi-phase Correction Current Injection (CCI) methodology-based load flow tool [81]. The multi-wire configuration of the modified network is shown in Fig. 3.4 whereas, its complete data can be found in appendix D.

3.3.1 Comparison of the proposed MPLAP with Z-Bus approach

Before discussing the main results of MPLAP, a comparison has been made between the results of proposed scheme and Z-bus approach [194] to demonstrate the reasons for abandoning the latter scheme in the context of the evaluation of the developed approach. Fig. 3.5 shows the TAL through MPLAP and Z-bus scheme and it can be noticed that the latter methodology either over-allocates or under-allocates the total system losses during [10-14] and [23-24] hours time window. Consequently, a reconciliation factor is required to redistribute the losses among end-users in order to make the TAL equal to the total system losses. Furthermore, it has been comprehensively stated in chapter 2 that Z-bus method allocates a significant portion of the overall network losses to its slack bus which

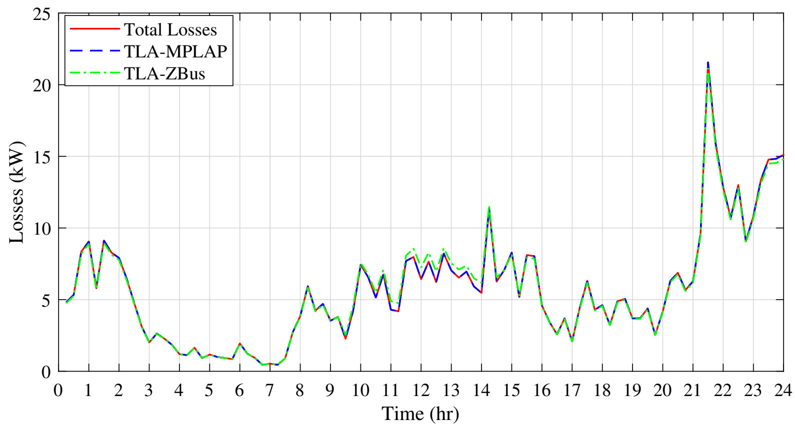

Figure 3.5: Total allocated losses over each time instant for a real low voltage IT-37 bus DN.

is conceptually wrong and, therefore, it becomes a must requirement to reallocate those losses to the network load and generator buses. Because of these inherent shortcomings of the Z-bus LA approach, a detailed comparison between the results of MPLAP and Z-bus methodology is not carried out in this work.

The evaluation of MPLAP is performed by comparing its results with the outcomes of Classical Losses Partitioning (CLP) and BCDLA methodologies in the context of following perspectives:

1. Partitioning of each branch losses among its phases which is shown in Table 3.1

2. Total allocated losses to each phase and neutral conductor of network nodes which are depicted in Table 3.2

3. Impact of LP approaches on the segregation of cross-terms induced losses which is represented in Table 3.3

3.3.2 Branch losses partitioning through CLP, RCLP-based BCDLA and MPLAPs

With respect to the first perspective, it can be observed in Table 3.1 that all LA methodologies calculate the same *total* active power losses for each network branch. However, the partitioning of individual branch losses, among its phases and neutral conductors, exhibits a significant difference. The division of branch losses through CLP-based approach is quite different from the segregation of losses obtained from the other two methodologies due to the dependence of the former scheme on the impedance of a branch. On the other hand, both RCLP-BCDLA and MPLAP utilize resistance of a branch in their mathematical models. Furthermore, the CLP-based LAP calculates negative losses for the lightly loaded phase b of branches 670 and 671 which is counter-intuitive since branch losses, in general, cannot be negative. The comparison between RCLP-BCDLA and MPLAP reveals that albeit the partitioning of branch losses exhibits differences; the obtained results are still

Table 3.1: Branch losses in the modified IEEE-13 node network based upon CLP, RCLP-based BCDLA and MPLAP.

Branches	**Branch Losses [kW]**												**Total Losses**
	CLP[220]				**RCLP-BCDLA**[17]				**MPLAP**				
	a	b	c	n	a	b	c	n	a	b	c	n	
632	16.40	0.99	19.30	2.28	12.82	7.11	16.49	2.55	13.06	6.87	16.25	2.80	38.98
633	0.34	0.18	0.27	0.02	0.37	0.20	0.22	0.02	0.34	0.21	0.23	0.02	0.81
634	2.39	1.49	1.58	0.03	2.39	1.46	1.58	0.03	2.39	1.46	1.58	0.03	5.46
645	0.22	2.01	0.51	1.54	0.21	2.15	0.44	1.48	0.22	2.11	0.43	1.50	4.28
646	0.12	0.23	0.30	0.13	0.13	0.26	0.26	0.13	0.11	0.28	0.28	0.11	0.78
670	3.12	-0.25	2.79	2.37	2.75	0.29	2.53	2.46	2.80	0.25	2.49	2.49	8.03
671	9.00	-0.73	6.85	7.41	8.04	0.67	6.18	7.64	8.12	0.63	6.20	7.60	22.53
692	0	0	0	0	0	0	0	0	0	0	0	0	0
675	1.80	0.16	0.59	4.51	1.68	0.21	0.63	4.54	1.65	0.18	0.64	4.59	7.06
684	0.25	0	0.31	0.03	0.24	0	0.32	0.03	0.24	0	0.32	0.03	0.59
611	0	0	0.32	0.32	0	0	0.32	0.32	0	0	0.32	0.32	0.64
680	0.401	0.09	0.39	0.002	0.31	0.25	0.32	0.003	0.33	0.21	0.34	0.003	0.883
652	0.57	0	0	0.57	0.57	0	0	0.57	0.57	0	0	0.57	1.14
Total Losses	34.61	4.17	33.21	19.212	29.51	12.60	29.29	19.77	29.83	12.2	29.08	20.06	91.183

quite close to each other. The underlying reasons of this behaviour lie in the two basic facts associated with these approaches. Firstly, both methods are branch-oriented-based approaches and utilize branch resistance, as explained above, in their formulations. Secondly, the value of self- and mutual-VLCs i.e., the segregation of cross-terms induced losses through QLP/GLP approaches, is close to 1 in the case of balanced or lightly unbalanced branches. Nevertheless, even though the partitioning of losses among branch phases appears quite close to each other in absolute term, a maximum %Relative Difference (RD) of 3.14% can be observed in the phase b followed by a difference of 1% in the phase a of test network. Despite the fact that the chosen case study system is a small-size DN, the difference of 3.14% clearly indicates that for large-size highly unbalanced DNs, a high %RD with respect to the segregation of branch losses should be expected.

3.3.3 Variable loss coefficients-based bifurcation of cross terms

Table 3.2 shows the losses allocated to each node of the test network by the above-mentioned methodologies. The shortcomings of the CLP-based approach are again evident as, on the one hand, it allocates negative losses to the passive end-users connected at nodes 645 and 680 and, on the other hand, it allocates positive losses to the shunt capacitances connected at nodes 611 and 675 despite the fact that they are reducing the overall network losses. The impact of QLP approach on the segregation of cross-terms induced losses is quite evident from the results as allocated losses to each phase of every node are completely different from one another under MPLAP and RCLP-BCDLA procedure. The former approach results in a higher allocation of losses to the passive and active end-users as compared to the latter methodology. The TAL with RCLP-BCDLA are 111.02 kW and -19.83 kW for the passive and active end-users, respectively, whereas these values become 96.31 kW and -6.01 kW in the case of MPLAP. These results show

Table 3.2: Allocated losses to the nodes of modified IEEE-13 node network based upon CLP, RCLP-based BCDLA and MPLAP.

Nodes	Allocated Losses [kW]														
	CLP[220]					**RCLP-BCDLA**[17]					**MPLAP**				
	a	*b*	*c*	*n*	*TAL*	*a*	*b*	*c*	*n*	*TAL*	*a*	*b*	*c*	*n*	*TAL*
634	4.68	0.81	2.42	-0.13	7.78	5.18	2.94	3.87	0.31	12.3	3.33	2.68	2.92	0.08	9.01
645	–	-0.35	–	-0.24	-0.59	–	3.03	–	-1.02	2.01	–	3.08	–	1.55	4.63
646	–	2.83	-1.00	–	1.83	–	2.63	2.48	–	5.11	–	2.13	1.54	–	3.67
646 (DG)	-1.30	–	–	0.88	-0.42	-1.02	–	–	0.07	-0.95	0.27	–	–	0.69	0.96
670	0.19	-0.26	1.03	1.06	2.02	0.20	0.48	1.51	0.07	2.26	0.003	0.12	0.41	0.017	0.55
671	9.39	-5.33	5.98	0.00	10.04	11.0	5.42	11.25	0.00	27.67	9.53	6.81	14.55	0.00	30.89
692	-3.69	–	4.35	–	0.66	2.12	–	3.18	–	5.3	0.34	–	1.42	–	1.76
675	16.22	-1.63	2.37	14.62	31.58	14.52	0.87	9.19	17.40	41.98	14.34	0.47	9.63	16.17	40.62
675 (SC)	10.16	7.83	11.11	0.09	29.19	-1.72	-0.23	-1.55	1.00	-2.50	-0.31	-0.47	0.25	0.07	-0.46
611	–	–	3.88	7.43	11.31	–	–	5.14	2.22	7.36	–	–	3.26	0.72	3.98
611 (SC)	–	–	5.70	-2.93	2.77	–	–	-0.69	-2.87	-3.56	–	–	0.29	0.04	0.33
680 (DG)	-4.84	2.10	-3.61	-0.20	-6.55	-5.10	-2.26	-5.18	-0.28	-12.82	-1.41	-1.71	-3.73	0.007	-6.84
652	2.99	–	–	-1.42	1.57	4.35	–	–	2.68	7.03	1.39	–	–	0.706	2.096
TAL	33.8	6.00	32.23	19.16	91.19	29.53	12.88	29.2	19.58	91.183	27.483	13.11	30.54	20.05	91.183

that although the TAL by both approaches are equal, the former methodology results in a higher penalization and reward of passive and active end-users, respectively. The reason of this behaviour lies in the fundamental basis of RCLP-BCDLA approach which states that passive end-users are the major cause of losses in a system and active end-users, whenever and wherever connected, reduces the overall grid losses. However, it has been shown later in section 3.3.6 that this is not always the case and active end-users can also lead to an increase in the overall system losses. Consequently, it can be perceived that the proposed MPLAP allows a more fair distribution of the losses which, resultantly, leads to a more fair penalization and reward of the end-users as shown in Fig. 3.6.

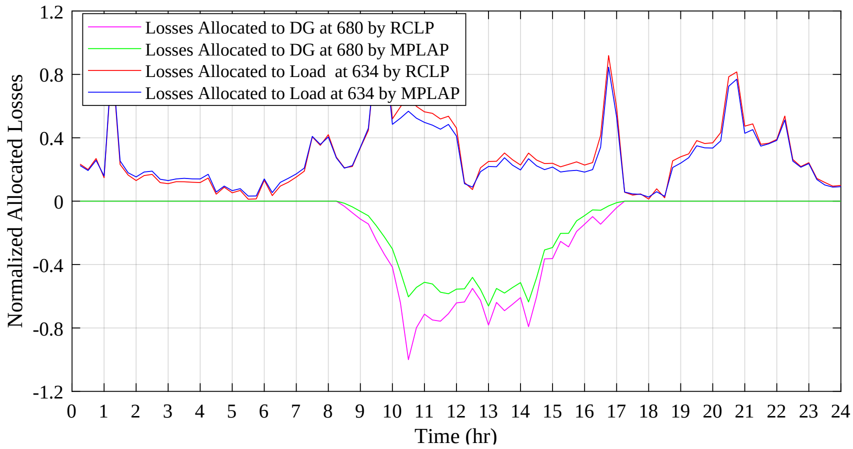

Figure 3.6: Impact of redistribution of losses related to cross-terms by RCLP-based BCDLA and MPLAPs.

3.3.4 Impact of cross term redistribution schemes on losses partitioning

The partitioning of losses among the phases of same and different nodes strongly depends upon the scheme chosen for the segregation of cross-terms. Table 3.3 shows the allocated losses to each phase and neutral conductor of all network nodes through the GLP and QLP schemes and it is quite evident from the results that TAL to each node as well as LP among its phases and neutral conductors vary significantly under both LP approaches.

The comparison between the results of Table 3.2 and Table 3.3 reveals that the behaviour of GLP-based MPLAP, in terms of TAL to each node and LP among its conductors, closely resembles the performance of RCLP-BCDLA methodology, whereas, on the other hand, QLP-based MPLAP shows quite distinctive results in comparison to the standard RCLP-BCDLA approach. The reason of this behaviour can be understood by referring to Fig. 3.3 which shows the division of cross-terms related losses. As stated earlier in section 3.2.5 that if the ratio between I^x/I^y is close to 1, the segregation of losses between conductors (phases and neutral) does not vary significantly when accomplished through the GLP-based MPLAP. Since cross-terms are equally divided between the phases irrespective of their loading in RCLP-BCDLA approach, it becomes evident that the LA pattern of GLP-based MPLAP is much closer to the LA pattern of RCLP-BCDLA approach when the ratio between phases currents is less diversified i.e., system is balanced or lightly unbalanced to a large extent.

3.3.5 Impact of neutral-ground configuration

In [17], neutral losses are implicitly allocated to the respective phases of each node under the assumption that voltage at both ends of a neutral conductor is equal and, as a result,

Table 3.3: Allocated losses to the nodes of modified IEEE-13 node network based on geometric and quadratic losses partitioning approaches.

Nodes	Allocated Losses [kW]									
	Geometric Losses Partitioning					Quadratic Losses Partitioning				
	a	*b*	*c*	*n*	*TAL*	*a*	*b*	*c*	*n*	*TAL*
634	4.66	2.85	3.59	0.13	11.23	3.33	2.68	2.92	0.08	9.01
645	–	3.04	–	-0.37	2.67	–	3.08	–	1.55	4.63
646	–	2.48	2.20	–	4.68	–	2.13	1.54	–	3.67
646 (DG)	-0.55	–	–	0.34	-0.21	0.27	–	–	0.69	0.96
670	0.04	0.32	1.13	0.09	1.58	0.003	0.12	0.41	0.017	0.55
671	10.74	6.10	12.24	–	29.08	9.53	6.81	14.55	0.00	30.89
692	1.49	–	2.64	–	4.13	0.34	–	1.42	–	1.76
675	14.45	0.67	9.40	17.11	41.63	14.34	0.47	9.63	16.17	40.62
675 (SC)	-1.31	-0.33	-1.1	0.45	-2.29	-0.31	-0.47	0.25	0.07	-0.46
611	–	–	4.64	1.80	6.44	–	–	3.26	0.72	3.98
611 (SC)	–	–	-0.34	-1.8	-2.14	–	–	0.29	0.04	0.33
680 (DG)	-4.12	-2.14	-4.83	-0.03	-11.12	-1.41	-1.71	-3.73	0.007	-6.84
652	3.40	–	–	2.1	5.5	1.39	–	–	0.706	2.096
TAL	28.8	12.99	29.57	19.82	91.183	27.483	13.11	30.54	20.05	91.183

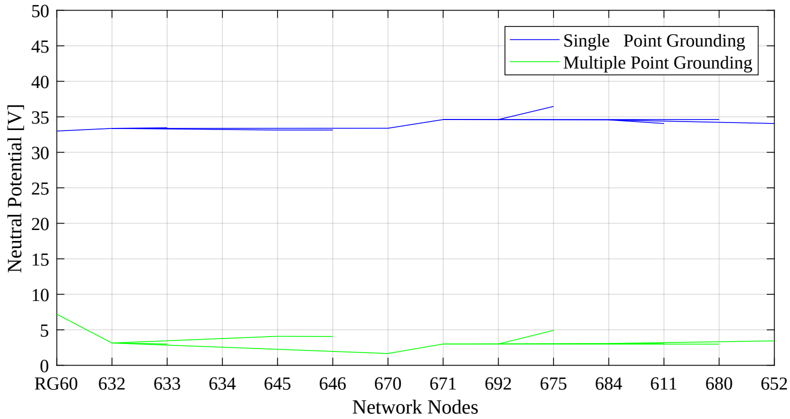

Figure 3.7: Neutral voltage for single- and multiple-point grounding configuration.

KR approach can be applied to each network branch. However, this hypothesis is only applicable in the unrealistic case of solidly grounded neutral across the whole network and as evident from Fig. 3.7, this assumption is no longer valid in realistic scenarios where a neutral conductor is grounded either at single or multiple points through a finite grounding impedance. The figure shows that it is very unlikely to have equal voltage at both ends of the neutral conductor of the test DN. Furthermore, it can also be noted in Table 3.4 that TAL to end-users in the case of solidly grounded neutral case are lower than the TAL in the case of MPG and SPG neutral by 15.0% and 16.3%, respectively, which suggests that the losses allocated under solidly grounded neutral hypothesis do not reflect the true system losses. Moreover, the allocation of neutral losses to each phase connected end-user is conceptually wrong as explained in detail in chapter 4. These results clearly justify the development of a MPLAP in which neutral conductors can be treated like phases conductors of a network.

Table 3.4: Total allocated losses for different neutral-ground configurations.

Total Allocated Losses [kW]		
Solidly-Grounded (Kron Reduced)	**Multiple-Point Grounded**	**Single-Point Grounded**
76.24	89.70	91.183

3.3.6 Discussion on losses allocated to DG units

In the analysed network, RCLP-BCDLA method allocates negative losses to the DGs connected at nodes 680 and 646, whereas the proposed MPLAP allocates positive losses to the DG connected at node 646 as shown in Table 3.2. The idea of allocating negative losses to DGs stems from the fact that local provision of energy from the DGs to fulfil local demand reduces the upstream branch(es) current and ultimately lowers down the overall network losses. This is true in the case of DG connected at node 680 since it supplies active and reactive power to the loads connected in its vicinity and, resultantly,

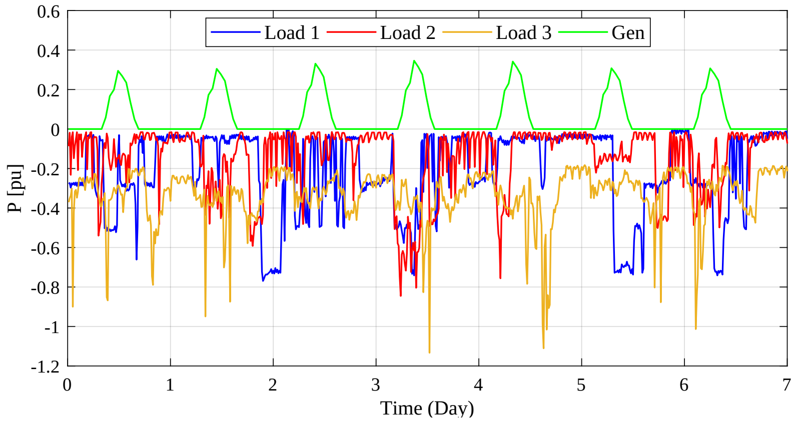

Figure 3.8: Active power profiles of DG and three of the end-users.

reduces the overall losses from 129.9 kW (no DG case) to 86.9 kW. Consequently, negative losses are allocated to this DG. However, the DG connected at the phase a of node 646 causes a reverse power flow since no load is connected to the phase a of nodes 645 and 646, eventually causing an increase in the system losses with respect to the passive case (no DG at 646). Moreover, the installation of this DG also causes additional losses in other phases and neutral conductors of the network branches connected between these nodes due to mutual coupling among them. Consequently, the total network losses in this case increase from 86.9 kW (DG at node 680 is connected only) to 91.183 kW (both DGs are present). Therefore, it is rightly justified to allocate positive losses to this node.

The shortcomings of RCLP-BCDLA approach can be further observed by referring to Fig. 3.9, which shows the losses allocated to the DG connected at node 646 by both methodologies in the presence of time-varying loads profiles which are shown in Fig. 3.8. A careful observation reveals that during the first half of time interval [12-13], the losses allocated to node 646 by both LAPs have opposite signs. During this interval, the total

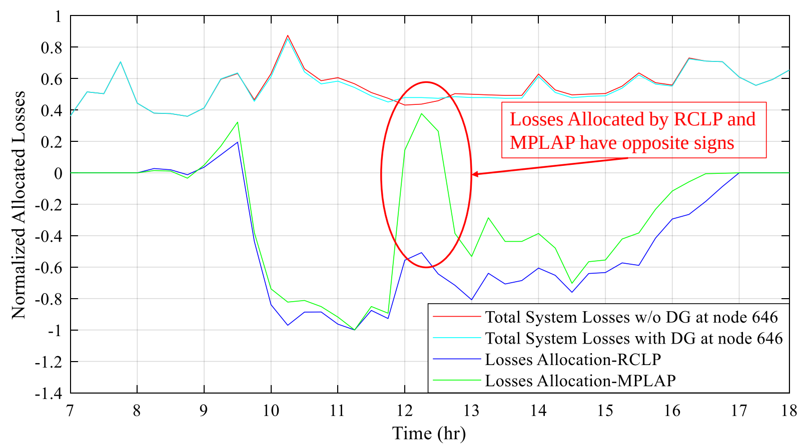

Figure 3.9: Total system losses before and after connection of DG at node 646 and corresponding losses allocated to it.

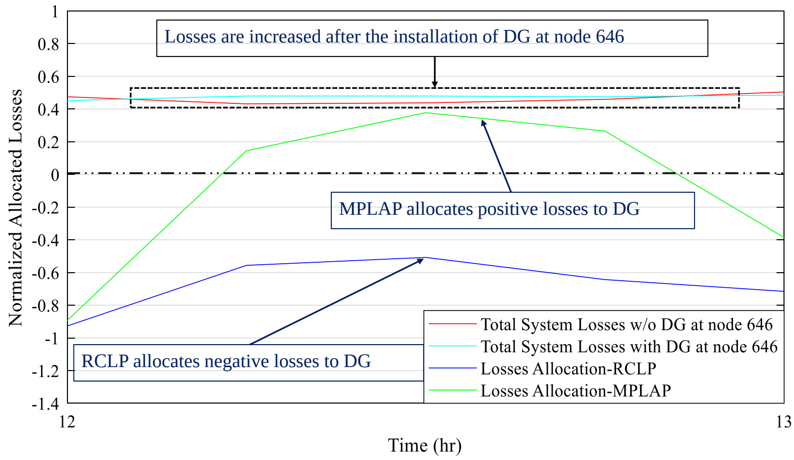

Figure 3.10: Total allocated losses to DG at node 646 during time interval 12-13.

system losses are increased by a small amount in the presence of connected DG. Consequently, it is required to allocate positive losses to the DG containing node during this interval. However, due to the inappropriate division of cross-terms among the phases of same and different nodes by RCLP-BCDLA method, it allocates negative losses to this DG during this time interval as can be clearly observed in Fig. 3.10. Therefore, it can be deduced that since cross-terms induced losses are equally divided among the phases by this LA approach, the beneficial/detrimental effect of any DG/load, on the overall system losses, can be masked due to the over/under estimation of positive/negative contribution of the connected end-users which, ultimately, results in an unfair allocation of positive/negative losses to the connected end-users.

Apart from negative LA to the DG at 646, RCLP-BCDLA methodology wrongly allocates negative losses to the passive loads during few time instants as shown in Fig. 3.11, even though these loads are not controllable, and are the main cause of network losses. On the other hand, the proposed MPLAP avoids such negative losses allocation to the passive end-users. These findings clearly shows the superior performance of the proposed scheme over the existing RCLP-based LAP.

3.3.7 Computational performance

The comparison between the computational performance of RCLP-BCDLA and MPLAP for the test case and several real LV DNs is shown in Table 3.5. The simulations, carried out on MATLAB 2017b using DELL 64-bit OS, core i7 with a processor speed of 2.80 GHz and 16 GB RAM, show that the proposed methodology takes slightly more time in comparison to the existing three-phase RCLP-based LA methodology. This is due to the fact that VLCs are calculated for each branch in an iterative loop and sequential way during a backward feeder sweep. Since the calculation of the coefficients of one branch is completely independent of the calculation of the factors of other branches, a possible reduction in the CT of MPLAP can be achieved by determining these parameters in parallel through the application of parallel computational techniques. Furthermore, the

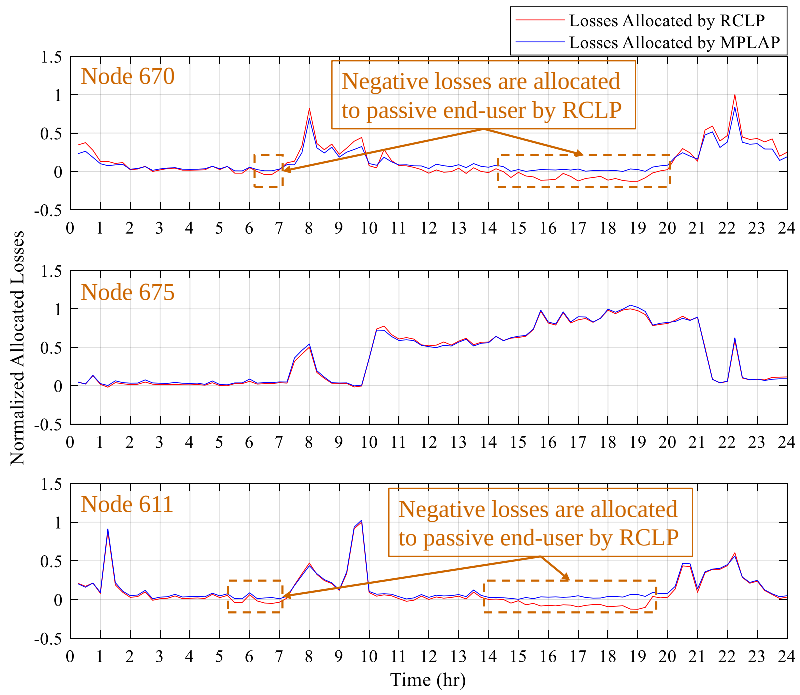

Figure 3.11: Losses allocated to passive nodes by RCLP-BCDLA and MPLAPs.

calculation of these coefficients in a vectorized way can further reduce the CT as compared to the iterative loop technique.

Table 3.5: Comparison between computational performance of RCLP-based BCDLA and MPLAP.

Computational Time [s]				
Test System	**RCLP**		**MPLAP**	
	LF	LA	LF	LA
IEEE-13 Bus	0.17	0.04	0.17	0.11
IT-37 Bus	0.18	0.05	0.18	0.16
IT-111 Bus	0.31	0.15	0.31	2.8

LF: Load Flow

3.4 Summary

In this chapter, a novel MPLAP is proposed which addresses the shortcomings of the solely available three-phase RCLP-BCDLA methodology through the redistribution of cross-terms induced losses among the respective end-users connected to the same and/or different phases of network nodes. Neutral losses are not assigned to the respective phases due to the fact that these losses are part of a system because of its inherent unbalanced nature and, therefore, it is unrealistic to penalize end-users for these network losses. The results indicate that losses are allocated to end-users in a more fairly manner when partitioning of losses is achieved through the proposed MPLAP as compared to the RCLP-based LAP. Additionally, it has been shown that the segregation of cross-terms induced losses is strongly influenced by the selection of LP approach as clearly indicated by the presented results.

It has also been demonstrated that voltage along a neutral conductor follows a unique profile on the basis of its grounding topology which, in turn, has a direct influence on TAL. Consequently, the assumption of equal potential at all points along a neutral conductor, which is the basis of KR approach, cannot be justified in the case of SPG and MPG DNs. Under this hypothesis, the TAL are relatively lower as compared to the case when neutral conductor is not solidly grounded and, therefore, it is impractical as well as unrealistic to apply KR technique on a $n \times \tau$ original branch impedance matrix.

Published paper

The research work presented in this chapter led to the publication of following paper.

1. Usman, Muhammad, Massimilano Coppo, Fabio Bignucolo, Roberto Turri, and Alberto Cerretti. "Multi-Phase Losses Allocation Method for Active Distribution Networks based on Branch Current Decomposition." *IEEE Transactions on Power Systems* (2019).

CHAPTER 4

Neutral Losses Allocation Factors based Network Management Scheme

This chapter initially presents a useful discussion on the significance of phase- and neutral-losses allocation factors, followed by the development of a management scheme which effectively utilizes these factors in its formulation to improve the inherent unbalancing of a distribution network through the phase commutation of end-users. In this regard, two phase switching algorithms are developed which allow shifting an individual and combined load from one phase to another phase. Lastly, the application of the proposed approach on a real distribution network shows a significant reduction in network unbalance and power losses.

The MPLAP presented in chapter 3, on the one hand, provides extremely useful information about the losses allocated to neutral conductors, but, on the other hand, it also raises a lot of serious questions such as what is the meaning of NLAFs? Do they convey the same information as PLAFs? What does a negative sign of NLAF mean? and more importantly, can NLAFs play an active role in the management of ADNs? Resultantly, an informative discussion, which seems indispensable in this regard, is carried out in this chapter to make a clear distinction between the meanings of these factors which, ultimately, sets the foundation of the development of a novel NLAF-based network unbalance management scheme.

4.1 Discussion of phase and neutral losses allocation factors

The losses allocated to each phase of a particular node represent the losses caused by the net power generation/absorption of end-users connected to these phases, which would not

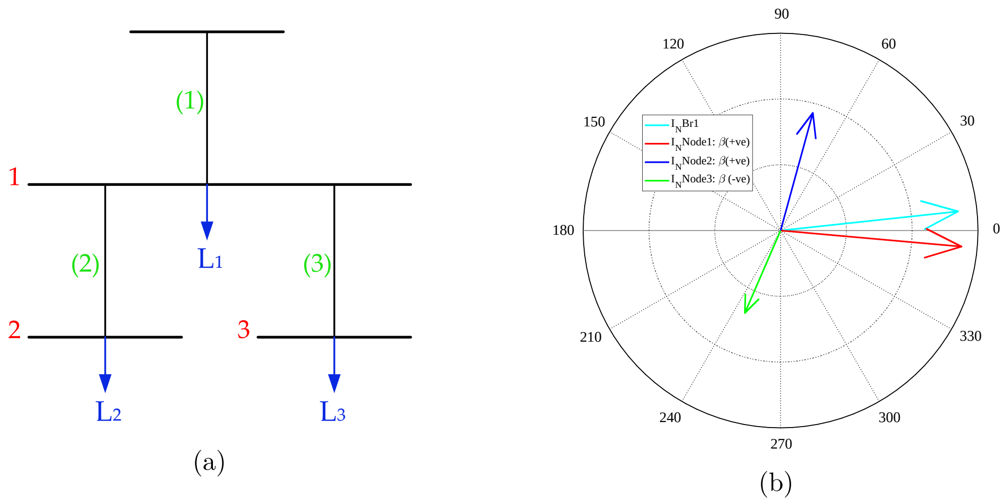

Figure 4.1: Correlation between branch neutral current and associated nodes NLAFs (a) example of a simple DN (b) NLAFs of respective nodes.

occur, otherwise, in a system in the absence of these users. On the other hand, losses in a neutral conductor strictly depend upon the degree of unbalance in a network and are not influenced by the energy consumption of end-users. For a perfectly balanced system, there would be no current in a neutral conductor and, consequently, no losses would be assigned to it. Since LV DNs are unbalanced by nature due to the presence of non-uniformly distributed single-phase end-users, it would be inappropriate to allocate different shares of neutral losses to each phase connected end-users since they are not responsible for the contingent unbalancing of a grid.

Both PLAFs and NLAFs can be positive or negative; however, factors with the same signs have no correlation between them. The positive PLAFs are assigned to passive end-users due to their energy absorption from a network which ultimately leads to an increase in the system losses. PLAFs assigned to active end-users can be either positive (in the case of significant over-production which leads to reverse power flow in a branch) or negative (by partially/completely fulfilling the local demand and, therefore, reducing branch currents). Contrary to the positive PLAFs, the positive NLAFs are allocated to those nodes which are responsible for making a system more unbalanced by increasing the Net Neutral Current (NNC), whereas the opposite statement applies to the negative NLAFs i.e., negative factors are assigned to those nodes which reduces the NNC.

For better understanding of this concept, an elementary DN and neutral current at its nodes are shown in Figs. 4.1a and 4.1b, respectively. Since neutral current in branch 1 is the vector sum of the neutral currents of its downstream nodes, the losses of this branch are allocated to these nodes by taking into consideration their impact on the branch losses. Therefore, negative NLAF is assigned to node 3 due to its positive contribution in reducing the branch NNC. On the other hand, positive NLAFs are allocated to the nodes 1 and 2 since they are responsible for increasing the NNC in this branch. To this extent, the meaning of PLAFs and NLAFs is well explained. The next question which arises naturally

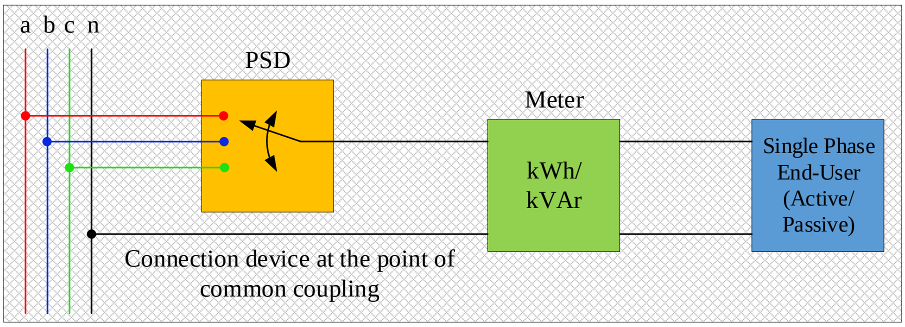

Figure 4.2: Phase switching of a single-phase end-user based upon neutral losses allocation factors.

is how can one make an effective utilization, if possible, of these factors in improving a DN operating conditions?

Since NLAFs are an indication of the severity of unbalance in a network, they can be effectively used by DSOs to take respective corrective measures in the context of grid management. One of the possible applications of utilizing the valuable results of MPLAP is the installation of Phase Switching Devices (PhSDs) which can perform switching of single-phase loads across the phases of critical nodes to reduce network unbalancing. This concept has been introduced in the subsequent sections where positive NLAFs are used to identify Highly Unbalanced Nodes (HUNs) which can then serve as possible potential locations for the installation of PhSDs to dynamically shift the loads across the phases of these nodes over each time horizon. The PhSDs can be installed either on every consumer premises, provided each single-phase end-user has a three-phase connection as depicted in Fig. 4.2, or at selective nodes where combined load connected to each phase of a node, considered as one load unit, can be commutated to other phases.

4.2 Utilization of neutral losses allocation factors in the management of distribution networks

The real-time management of an ADN by utilizing NLAFs depends upon the identification of HUNs, switching algorithm for the phase commutation of loads and selection of an appropriate OF. The complete DN management strategy based on NLAFs is shown in Fig. 4.3.

4.2.1 Identification of potential nodes

The prospective nodes, which can participate in the Phase Switching (PhS) process, are determined by introducing a degree of unbalance factor k_{DUB_v}. This factor, as reported in (4.1), represents the share of energy losses allocated to a neutral of each node with respect to the overall energy losses in the neutral of a feeder, and is used to make a ranked list of

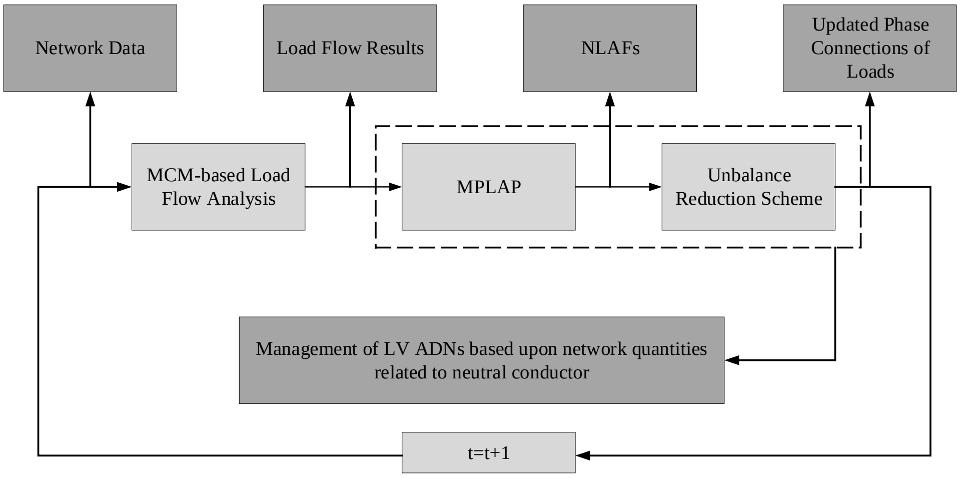

Figure 4.3: Management of a low voltage distribution network based upon neutral losses allocation factors.

the potential nodes.

$$k_{DUB_v} = \begin{cases} \frac{\beta_v^n \times \Delta t}{L_F^n \times \Delta t} & v \in K \\ 0 & v \notin K \end{cases} \tag{4.1}$$

where β_v^n represents the allocated power losses to the neutral of node v, L_F^n represents the overall neutral power losses of a feeder F, Δt is a time step between two real-time data measurements and K is a set of all nodes present in a feeder.

After computing k_{DUB_v} for all network nodes, they are arranged in ascending order with respect to this factor. The nodes with a positive factor are then chosen as critical nodes in the PhS algorithm, whereas nodes with a negative factor are removed from the list since loads connected to these nodes are already improving the network balancing by reducing the NNC in their upstream branches. Furthermore, nodes which contain just three-phase loads are also excluded from the list due to the non-capability of these loads in reducing the network unbalance and, consequently, power system losses even after their phase commutation.

4.2.2 Phase switching algorithms

With the formation of the ranked list of potential nodes, the next step is to perform the PhS of loads connected to such nodes. To achieve this objective, two PhS algorithms are developed and tested, named as Phase Switching Algorithm-1 (PSA-1) and Phase Switching Algorithm-2 (PSA-2). These algorithms differ from each other concerning the load (individual or combined) they can commutate across phases. However, both algorithms compute the average of the overall connected load at a particular node, which, subsequently, allows to determine those phases where connected load is above or below the average. These phases are then termed as Higher Than Average (HTA) and Lower Than Average (LTA) phases.

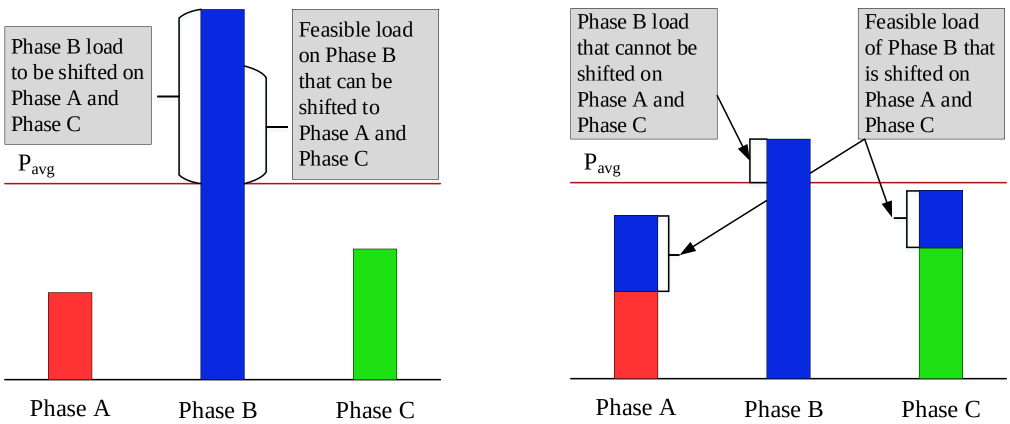

Figure 4.4: Conceptual illustration of phase commutation of a load (a) load on a generic node before switching (b) load on a generic node after switching.

4.2.2.1 Phase switching algorithm-1

In PSA-1, it has been assumed that PhSD is available at every consumer connection point (every house-hold) as depicted in Fig. 4.2 and, as a result, each single-phase load can be switched from one phase to another over each time horizon. Each node in this switching strategy acts as a local controller and has complete information about the real-time energy consumption of all loads connected to each of its phases. The proposal is to find such a suitable combination of the loads which when shifted from the HTA phases to the LTA phases balances the node ideally and makes the load on all phases equal to the average load as pictorially depicted in Fig. 4.4. This is an ideal scenario which requires a three-phase connection for every single-phase end-user. Normally, this is not the case in the present practice and, consequently, it becomes unrealistic to switch each individual end-user from one phase to another. Therefore, a more realistic approach is presented in the next section which can be practically realized without expending too much in the procurement and installation of new infrastructure. The complete flow chart of PSA-1 is shown in Fig. 4.5. It must be noted that the variables $L_{F_{AS}}$ (losses after PhS) and $L_{F_{BS}}$ (losses before PhS) represent the OF (losses in a feeder) which is explained in detail in section 4.2.3.

4.2.2.2 Phase switching algorithm-2

For effective utilization of NLAFs in a more realistic scenario, the total load connected to each phase of a node is considered as one load unit with a presumption that PhSDs are installed only at a node level i.e., one device at each node rather than one device at each household, which forms the basis of PSA-2 as depicted in Fig. 4.6. Resultantly, it is possible only to shift the combined load of a phase to another phase and, therefore, a coordinated control among multiple PhSDs becomes a requirement in this strategy. A single PhSD cannot participate alone in reducing the network unbalance and losses. In the context of PSA-2, each node connected downstream of a non-terminal branch sends its

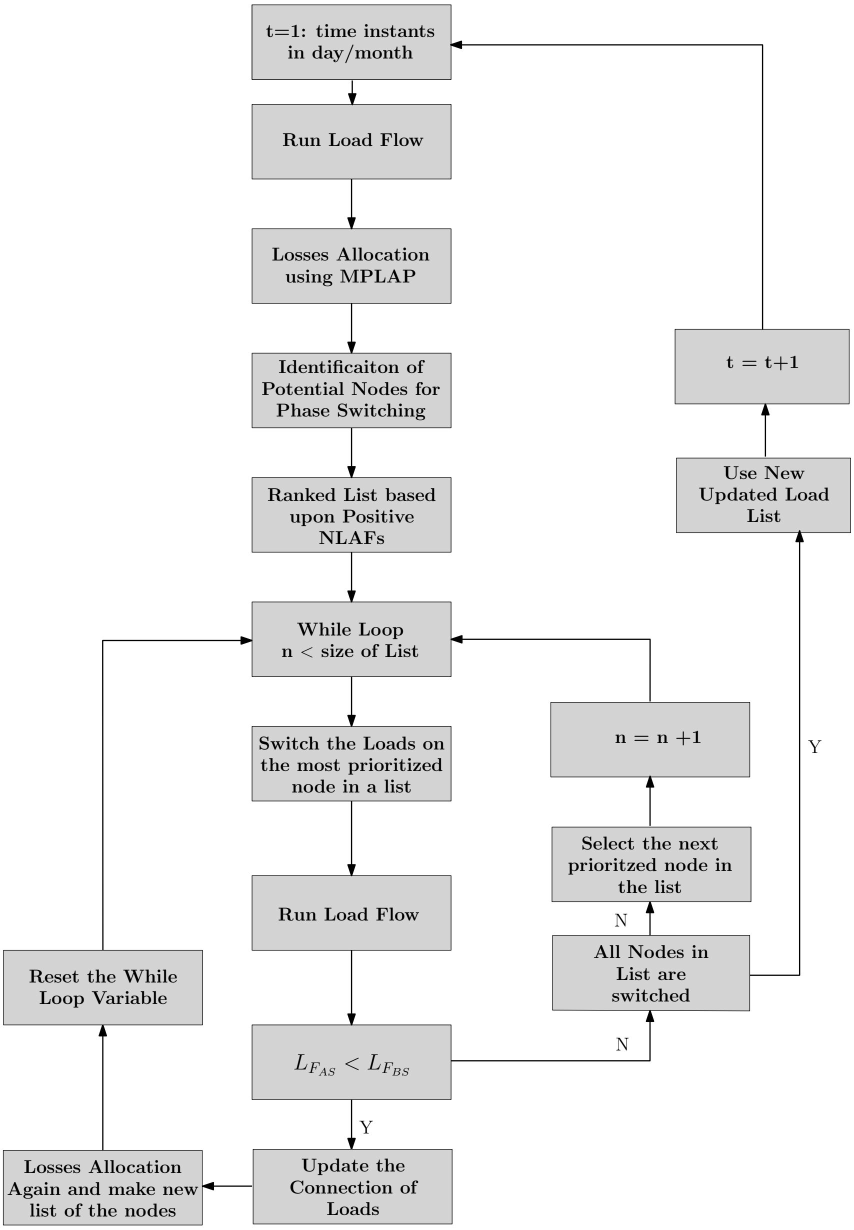

Figure 4.5: Methodology of phase switching algorithm-1.

phase configuration information to the upstream node of that branch, which, in turn, utilizes this information to determine the new phase connections, provided switching criterion (4.2) is satisfied, of the loads attached to the downstream nodes.

To have a combined control of multiple PhSDs, the backward feeder sweep technique is implemented in PSA-2. For better understanding of this methodology, consider the RDN shown in Fig. 4.7 with an assumption that PhSDs are available at all such nodes which are assigned positive NLAFs. This technique first identifies all such non-terminal branches which contain more than one PhSD connected downstream of them. Once all such branches are identified, the last non-terminal branch is selected first (in this case: 3) and the average of the load connected to this branch is calculated, which provides the

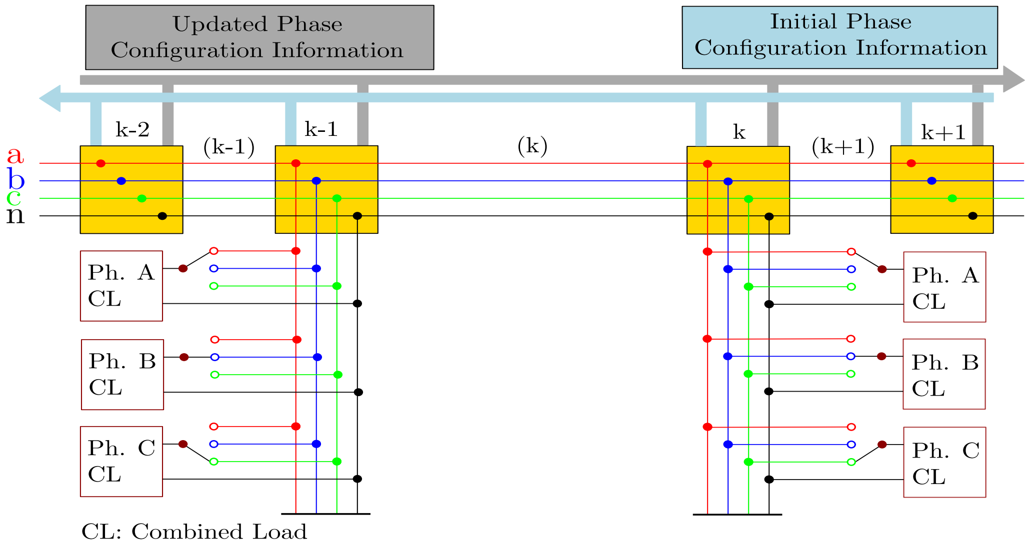

Figure 4.6: Phase switching of the combined load based upon phase switching algorithm-2.

information about the HTA and LTA phases of this branch and, consequently, the HTA and LTA phases of the downstream nodes. As underlying idea in this approach is to balance each non-terminal branch, the HTA phases of the downstream nodes (3 and 5) are selected and such a best possible combination of the combined load on these phases is determined which when shifted to the LTA phases of the respective nodes makes the load distribution more uniform when looking from the perspective of the non-terminal branch 3.

After performing the PhS of loads being served by the branch 3, the upstream non-terminal branch (in this case: 2) is selected. To redistribute the connected-loads on its downstream nodes, two possible scenarios are taken into consideration. The first scenario takes into account the initial phase connection of all the downstream loads connected to the branch 2 to determine its HTA and LTA phases. In other words, the updated phase connection of the loads, which are determined during the processing of branch 3 are not taken into consideration. The second case, on the other hand, calculates the average of the loads connected to the nodes 3 and 5 by taking into consideration their updated phase connections. These scenarios are termed as Case A and Case B, respectively. The new

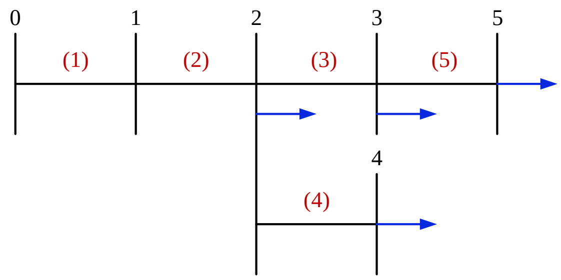

Figure 4.7: Example of a simple DN

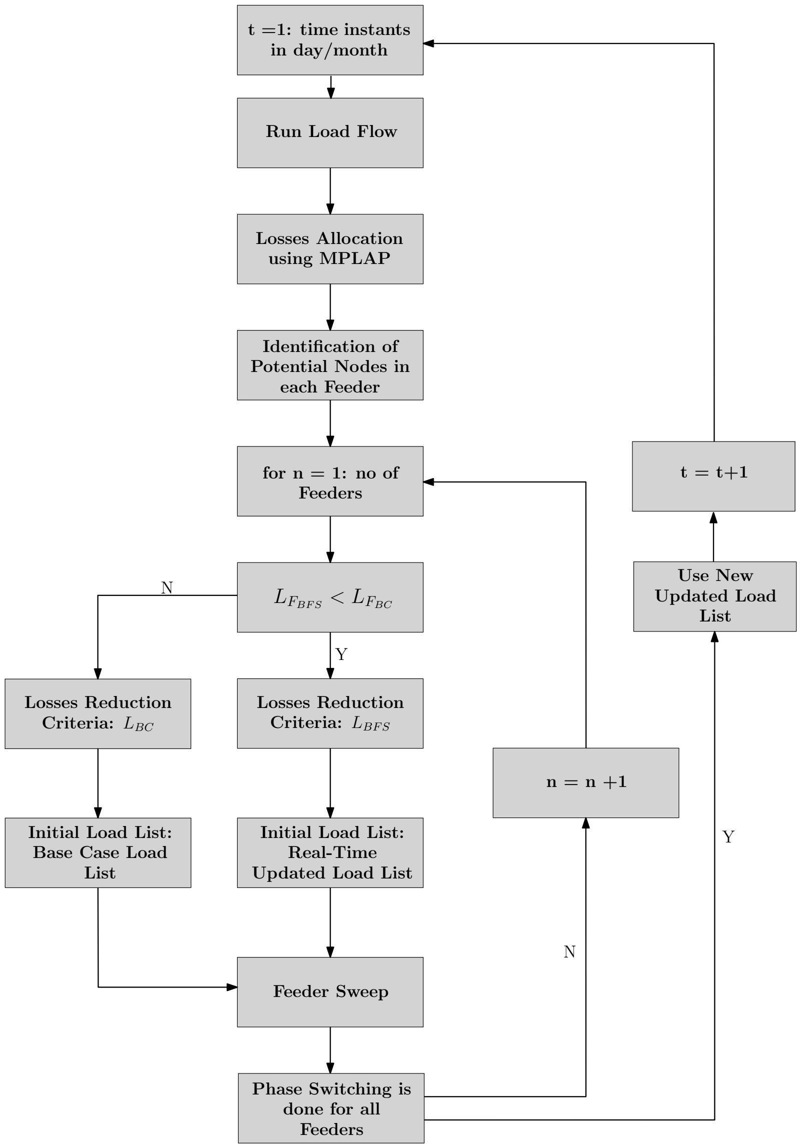

Figure 4.8: Main flow chart of phase switching algorithm-2.

phase connections of the downstream loads are determined for both cases and the most suitable combination of the combined load determined either from Case A or Case B is shifted to the LTA phases of branch 2. Once balancing of the branch 2 is completed, branch 1 is selected and the same procedure, as reported for the branch 2, is iteratively repeated for this branch. This process continues until every non-terminal branch in the direction towards the root node is processed.

In both algorithms, the appropriate combination of the loads is found by satisfying the following criterion.

$$-P_{rs} <= P_{cmb_x} - P_{rs} <= P_{rs} \tag{4.2}$$

where x represents the HTA phase(s) of a node (in case of PSA-1)/downstream nodes (in case of PSA-2), P_{rs} is the power which is required to be shifted from the HTA phase(s)

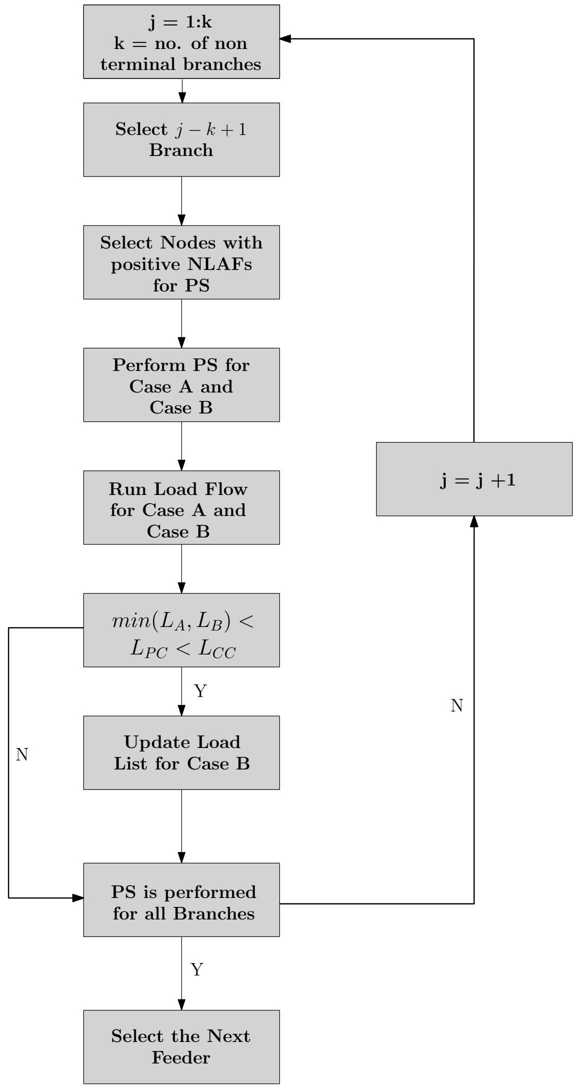

Figure 4.9: Backward feeder sweep methodology.

to the LTA phase(s) and P_{cmb_x} is the power of individual/suitable combination of x. The complete flow-chart of PSA-2 is shown in Figs. 4.8 and 4.9.

4.2.3 Objective functions

Two different OFs which serve as the criteria of keeping the updating phase connections are selected for the proposed PhS algorithms. The OF for PSA-1 is mentioned in (4.3) which compares the losses in a feeder after PhS of the loads ($L_{F_{AS}}$) with losses before PhS of the loads ($L_{F_{BS}}$).

$$L_{F_{AS}} < L_{F_{BS}} \tag{4.3}$$

The OF for PSA-2, as shown in (4.4), is relatively complex with respect to the OF of PSA-1 and requires an explanation.

$$\{min(L_{F_{CA}}, L_{F_{CB}}) < L_{F_{IPC}}\}_{AS} < L_{F_{BS}} \tag{4.4}$$

The subscripts CA, CB and IPC represent *Case A*, *Case B* and *Initial Phase Connection*, respectively.

As can be observed in (4.4), the minimum of the losses determined from CA and CB are compared with the losses calculated for *IPC* scenario. In order to understand the latter scenario (IPC), consider again the DN shown in Fig. 4.7. For the first non-terminal branch (in this case: 3), $L_{F_{IPC}}$ represents the feeder losses for the initial phase connections of loads (no PhS of loads is done) and are equal to the losses of Before Switching (BS) case, whereas for all the lower-indexed non-terminal branches (in this case: 1 and 2) $L_{F_{IPC}}$ represents the losses before performing the PhS of loads through Case A and Case B which, in turn, are calculated using the updated phase connections of the loads determined in the processing of the higher-indexed non-terminal branch(es) (in this case: 3).

In both (4.3) and (4.4), L_F are computed as follows

$$L_F = \sum_{b=1}^{P} \sum_{p=1}^{\tau} L_p^{(b)} \tag{4.5}$$

where τ is the number of branch conductors and P is the total number of branches in a feeder.

Although in this work, it has been assumed that each node which is involved in PSA-2 and has been assigned a positive NLAF contains a PhSD. However, a more realistic scenario can be envisioned by installing a fewer number of PhSDs at suitably identified strategic nodes in a network.

4.3 Case study

The case study network selected for the validation of proposed scheme is an Italian real LV DN consisting of five feeders departing from the MV/LV transformer, as shown in Fig. 4.10. All branches are composed of three phases plus a neutral conductor and 19 different line configurations in terms of phases cross-section and neutral cross-section are used varying from 16 mm^2 to 125 mm^2. Feeder 5 is the longest feeder with a length of 492 m, hosting 76 of the total 174 end-users. The transformer has a 20/0.415 kV ratio and rated power of 250 kVA. Its short circuit impedance is defined by the short circuit voltage $v_{cc} = 4\%$ and short circuit copper losses $p_{cc} = 1.47\%$. The magnetization leakage and iron core losses are $i_0 = 0.841\%$ and $p_0 = 0.32\%$, respectively. The complete data of the network along with the real-time load and generation profiles values can be found in the appendices E and G, respectively. The measured active power profiles, as partially depicted in Fig. 3.8, of end-users (passive and active) are utilized in this study. All power profiles are represented in pu. The DG profile is measured on a real photovoltaic plant since this is the most diffused generation technology in LV systems. The same profile is then assigned to all DGs. The passive power profiles are stochastic in nature, show extremely distinct absorption pattern from one another and are distributed randomly among all the end-users. Lastly, please note that the feeders 3-5 are considered for the evaluation of the proposed approach due to the availability of a large number of single-phase end-users in

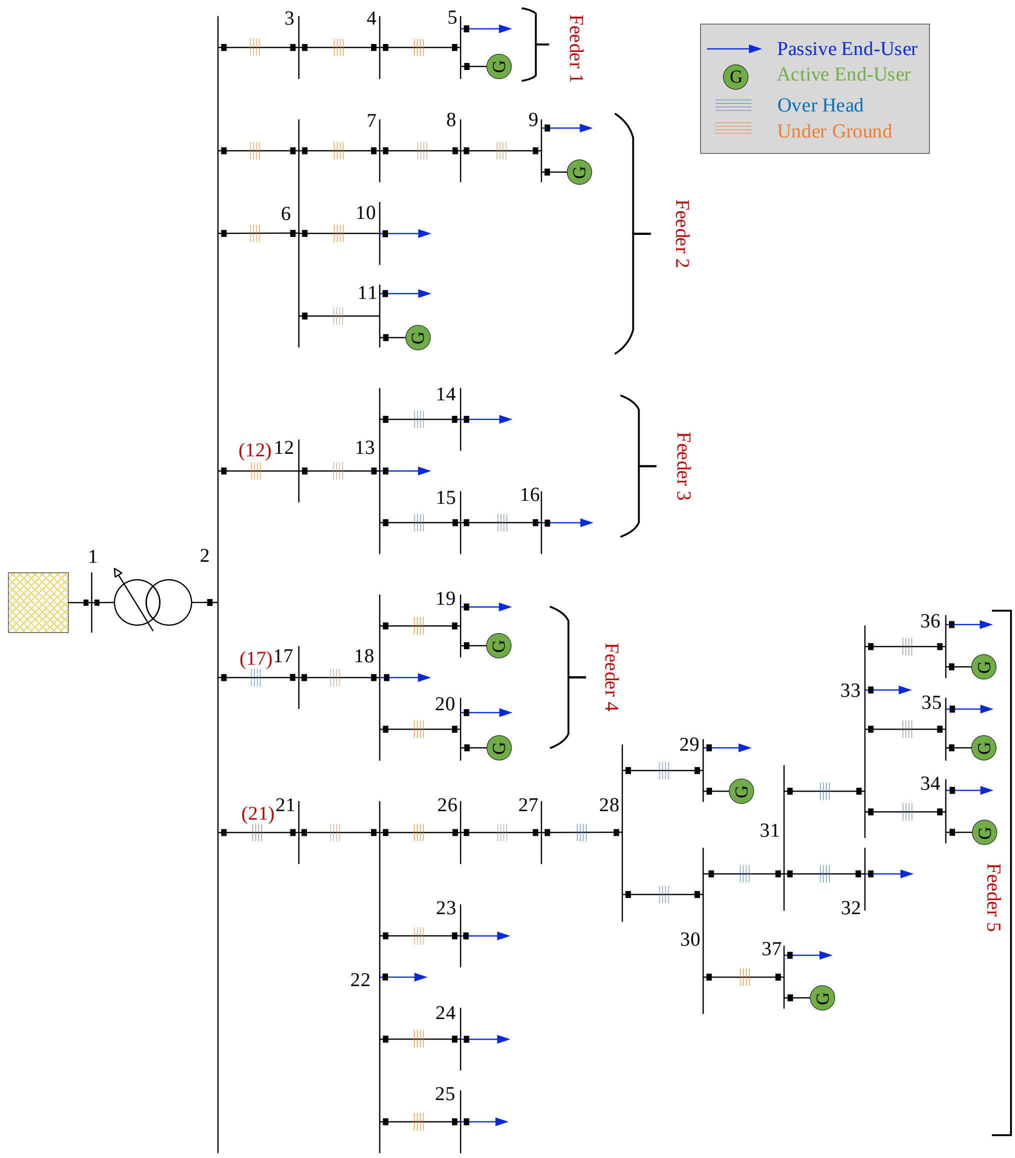

Figure 4.10: Single line diagram of a real low voltage IT-37 node distribution network.

these feeders.

4.3.1 Simulation scenarios

Two simulation scenarios are considered to show the promising impact of the phase commutation of loads connected to the nodes which are assigned positive NLAFs.

S1: Passive network

S2: Active network having random distribution of DGs in the network

In addition to these scenarios, the impact of neutral conductor sizing on neutral losses allocation is also investigated for the following three cases:

Case-0: Real network containing a mixture of two types of neutral conductors with respect to the cross-sectional area which is either equal to or half of the cross-sectional area of phases conductors (45% and 55% of the total network length respectively);

Case-1: Neutral conductor cross-section is equal to the phases conductor cross-section in each branch;

Case-2: Neutral conductor cross-section is reduced to the half of phases conductor cross-section in each branch, with a minimum size of 16 mm^2.

4.3.2 Evaluation of the proposed NLAFs-based management approach

The analysis of the proposed scheme is done from the following perspectives.

- Unbalance reduction and improvement in network power quality
- Impact of DGs installation
- Phase commutation of end-users
- Influence of neutral conductor size

4.3.3 Improvement in network balancing

Results are shown for the branches 12, 17 and 21 since these starting branches of feeders 3-5 act as the last branches in the path of neutral current which flows towards the neutral point on the secondary side of MV/LV transformer. A reduced neutral current in these branches indicates a more balanced network downstream of them as compared to the case when the phase commutation of downstream loads is not carried out. The passive end-users are distributed in such a way as to make feeders 3, 4 and 5 lightly, moderately and highly unbalanced, respectively. For example, in feeder 5, the total energy consumption is 5.6, 4.5 and 1.4 MWh for phases a, b and c, respectively over the simulated 10 days period. Please note that in the presented results, BC represents the base case scenario when no PhSD is present in the network, whereas APS-1 and APS-2 stand for *After Phase Switching* through algorithm 1 and 2, respectively.

Fig. 4.11 represents the current in the above-mentioned branches for scenario S2. It can be seen that the PhS of loads across the phases of HUNs in respective feeders provides a significant reduction in the neutral current and, consequently, the phases current in these branches have come closer to each other in terms of magnitude. Furthermore, it can be noticed that in the case of feeders 3 and 4 which have limited number of non-terminal branches and, resultantly, lower number of installed PhSDs, PSA-1 exhibits a much superior performance than PSA-2 in reducing the network unbalance. However, in the case of feeder 5, where PSA-1 still outperforms PSA-2, a significant improvement in the performance of PSA-2 can be observed as compared to its performance in the case of feeders 3 and 4 due to the availability of higher number of PhSDs which, in turn, is the consequence of the presence of single-phase loads at a large number of nodes in this feeder.

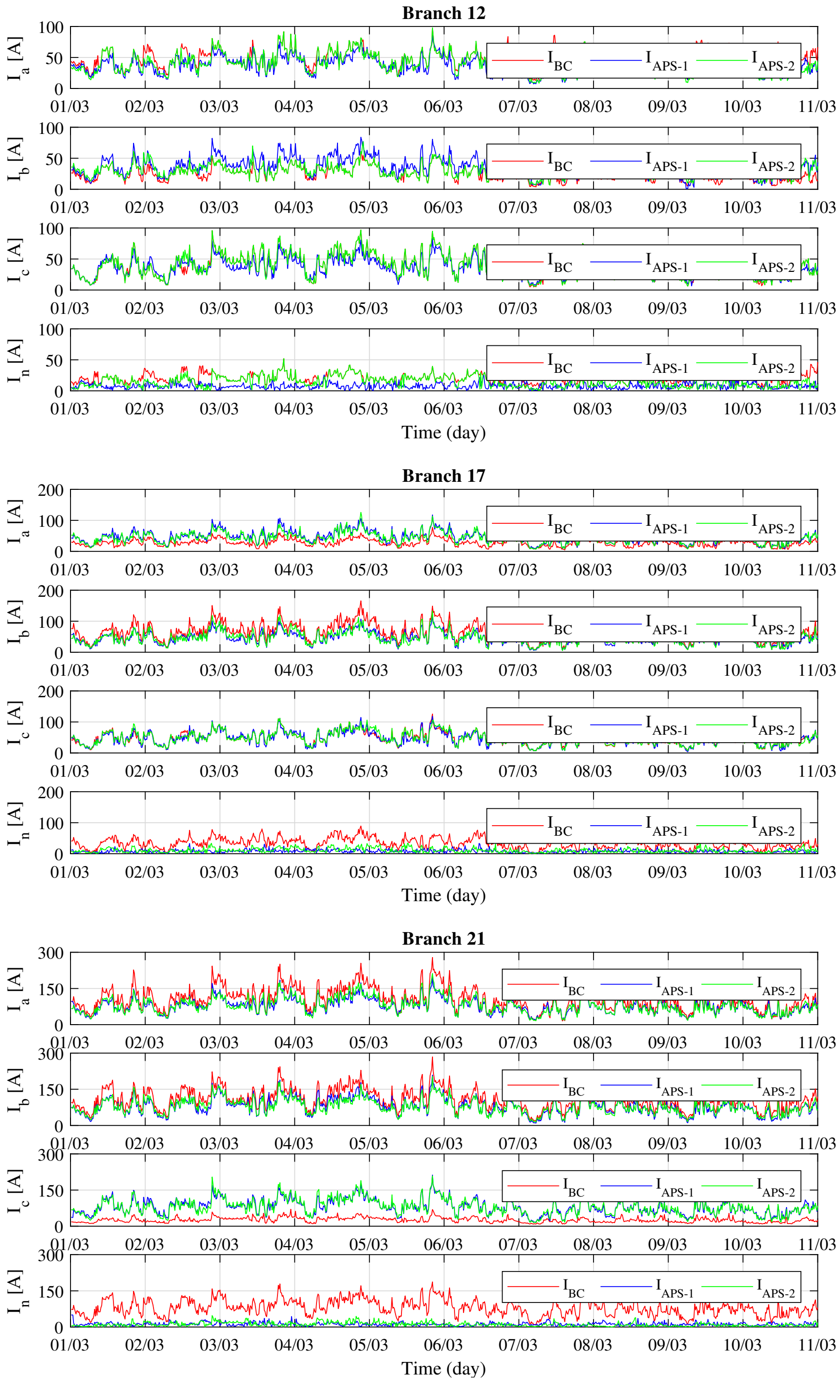

Figure 4.11: Current in branches 12, 17 and 21 before and after phase switching of loads through PSA-1 and PSA-2 for S2 scenario.

Table 4.1 reports the losses in the tested feeders before and after the PhS of loads for case 0. It can be noticed that for both S1 and S2 scenarios, a relatively small reduction in the losses is achieved in feeders 3 and 4 when PSA-2 is implemented as compared to the case when PhS of the loads is performed using PSA-1. The reason is the presence of a limited number of PhSDs and lightly/moderately unbalanced loading of these feeders

Table 4.1: Feeder energy losses for 10 days before and after phase switching of the loads under both phase switching algorithms.

Feeder	**Losses for Passive Network (Scenario S1) [kWh]**			**Losses for Active Network (Scenario S2) [kWh]**		
	BC	**PSA-1**	**PSA-2**	**BC**	**PSA-1**	**PSA-2**
Feeder 3	38.3	30.7 (-19.8%)	37.0 (-3.4%)	38.3	30.7 (-19.8%)	37.0 (-3.4%)
Feeder 4	73.2	53.2 (-27.5%)	65.0 (-11.2%)	71.1	49.7 (-30.1%)	61.1 (-14.1%)
Feeder 5	493.6	278.1 (-43.6%)	339.1 (-31.3%)	487.0	266.5 (-45.3%)	332.0 (-31.8%)
Network	605.1	362.0 (-40.2%)	441.1 (-27.1%)	596.4	346.9 (-41.8%)	430.1 (-27.8%)

BC: Base Case

which is not the case for feeder 5 and, as a result, a comparatively higher reduction in the losses is obtained for this feeder.

4.3.4 Impact of distributed generators installation

It can be observed in Table 4.1 that the phase commutation of loads in the active network also contributes positively to reducing network losses and improving system balancing if the integration of DGs increases unbalance in a specific feeder. Since DGs fulfil the demand locally, their installation on lightly loaded phases can further worsen the network balancing during the hours of peak local generation. In such a case, the PhS of loads from the HTA to LTA phases will result in a relatively higher losses reduction as compared to the passive network case. In order to show this phenomenon, DGs are connected on the lightly loaded phase a of feeder 4 and heavily loaded phase a of feeder 5. In the former case, the PhS of loads provides a notable relative losses reduction (27.5% $\rightarrow$ 30.1%) for PSA-1 and (11.2% $\rightarrow$ 14.1%) for PSA-2. On the other hand, the installation of few DGs on the heavily loaded phase a of feeder 5 does not cause a significant variation in the network unbalance and, as a result, a small increase in the losses reduction (43.6% $\rightarrow$ 45.3%) in the case of PSA-1 is achieved whereas losses are almost identical (31.3% $\rightarrow$ 31.8%) under PSA-2.

4.3.5 Phase commutation of end-users

Fig. 4.12 represents the total number of phase commutations over the simulated 10 days period for each load under both algorithms. Each bar shows the number of phase commutation of each load connected to the respective node (e.g., 10 end-users are connected to the node 13 in feeder 3). However, it should not be confused with the number of switching operation of each PhSD. For PSA-1, the number of switching operations of each PhSD is equal to the total number of phase commutation of an individual load which is being connected to a respective phase through that PhSD (height of one green bar represents the total switching operations of each PhSD), whereas in the case of PSA-2, where each PhSD shifts a combined load from one phase to another, the number of its switching

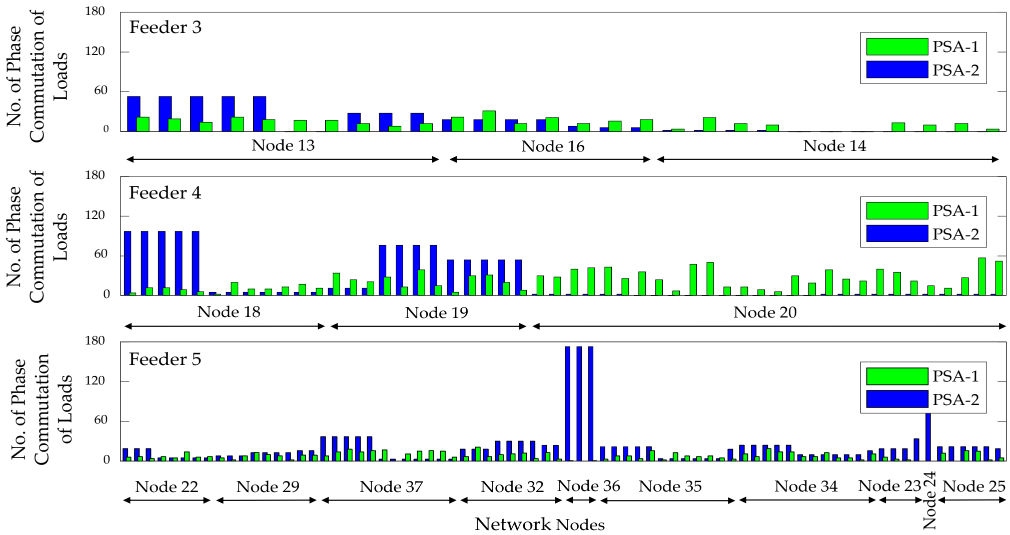

Figure 4.12: Switching pattern of loads in all tested feeders. Each bar represents one load connected to a particular node in a feeder.

operations is equal to the number of phase commutation of a single load in a set of combined load (height of one blue bar among first five bars in node 13 represents the total switching operations of PhSD which connects these five loads to a particular phase). It can be noticed that both PhS algorithms show distinct switching patterns. For PSA-1, the phase commutation profile of each load is random due to the fact that every load has a freedom to switch from one phase to another, whereas in the case of PSA-2, only combined load, which acts as a one load unit, on a phase can be switched, and as a result, all loads connected to a particular phase show the same switching pattern. Furthermore, it is also evident that some nodes (in this case: 23, 24 for PSA-1 and 14, 20 for PSA-2) do not participate in the PhS process due to the violation of criterion reported in (4.2). The node 36 shows a large number of phase commutation in the case of PSA-2 due to the fact that it contains only three light loads which are connected to the heavily loaded phase

Table 4.2: Comparative analysis between phase switching algorithms with respect to the phase switching devices.

Algorithm	**Feeder**	**No. of PhSDs**	**Rated Power of PhSDs [kW]**		**No. of Switching Events**			
			Min	Max	Min	Max	Total	Avg.
PSA-1	3	28	2	3	4	31	379	14
	4	50	1	3	2	57	1202	24
	5	75	1	3	1	21	623	8
PSA-2	3	9	6	13	2	53	115	13
	4	8	8	16	2	97	247	31
	5	23	2	19	3	173	674	29

Avg. = total number of switching events/no. of PhSDs *a* of feeder 5 and, as a result, these loads play a prominent part in determining the best possible combination of the switching loads. Table 4.2 provides the information about the number of installed PhSDs, their rated power and the number of switching operations related to both algorithms for the analysed case. The average value of each switching operation is rounded off to the next higher integer value.

4.3.6 Impact of neutral conductor size

Fig. 4.13 depicts the impact of sizing of neutral conductor cross-section on feeder losses and Table 4.3 reports the losses in each tested feeder for case 1 (equal cross-section for phases and neutral conductors) and case 2 (reduced cross-section of neutral conductor). It can be observed that feeder losses do not differ too much from each other in both cases after carrying out the phase commutation of loads. Therefore, DSOs are justified in installing Reduced Cross-section Neutral Conductors (RCNCs). However, this assumption is true only if a system is balanced to a large extent. Under a highly unbalanced scenario, as shown in Fig. 4.11, the neutral current can even become higher than the phase current and, therefore, such scenario might lead to the system congestion and failure if RCNCs are installed in the system. Furthermore, it is also evident from Table 4.3 that feeder losses increase significantly (e.g., for feeder 5, 427.8→519.8 kWh) in the case of RCNCs as compared to the case of equal cross-section neutral conductors under a large degree of unbalance in a feeder. Therefore, the installation of RCNCs requires the redistribution of loads across the phases of HUNs to avoid any contingency caused by the congestion of a neutral conductor under a highly unbalanced loading scenario.

4.3.7 Feasibility of the proposed management scheme

The presented results confirm that the proposed methodology can lead to a significant reduction in voltage unbalance and power system losses, therefore, it is important to shed

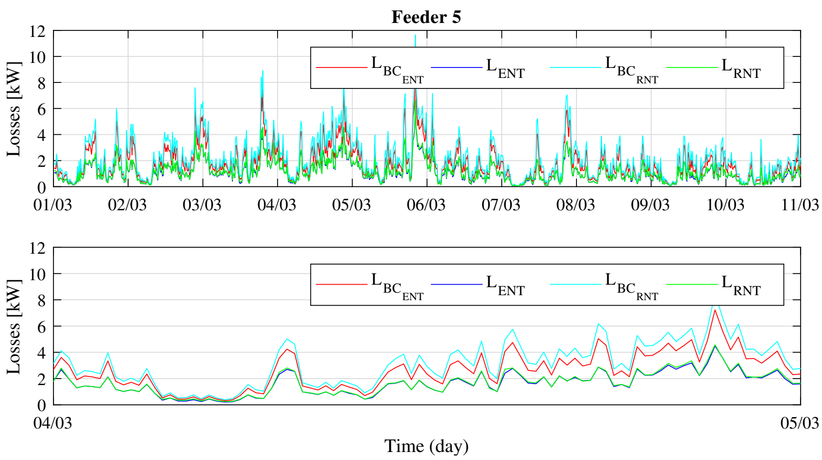

Figure 4.13: Effect of neutral conductor cross-section on feeder losses. ENT: Case-1 RNT: Case-2

Table 4.3: Feeder energy losses for 10 days based on PSA-1 under equal and reduced (half) neutral conductor cross-sectional area.

Feeder	**Case 1 Losses [kWh]**		**Case 2 Losses [kWh]**	
	BC	**APS**	**BC**	**APS**
Feeder 3	37.0	30.5 (-17.6%)	42.0	32.0 (-23.8%)
Feeder 4	66.8	49.2 (-26.3%)	77.8	50.0 (-35.7%)
Feeder 5	427.8	264.5 (-38.2%)	519.8	272.5 (-47.6%)
Network	531.6	344.2 (-35.2%)	639.6	354.5 (-44.6%)

BC: Base Case APS: After Phase Switching

some light on its practical feasibility. In particular, for the real-time implementation of proposed methodology, two important aspects have to be considered: the capital cost of PhSDs (both the device and its installation) and the impact of their actions on the power quality of a network.

The presented scheme can be easily realized practically since the required technologies for its implementation, which include smart meters, centralized and local controllers, communication system and power electronics-based static switches for modifying phase connections of end-users, already exist in a modern DN. At present, DSOs are transforming their networks into intelligent grids by installing centralized DMSs and advanced smart metering and communication infrastructure [221]. In this regard, the only additional investment for the implementation of developed control scheme would be the installation of local controllers along with PhSDs. Due to the recent developments in power electronics sector, switching devices have become less and less expensive, and, as a result, the overall cost of a single PhSD along with its controller would be comparable, or lower, than the cost of a smart meter [222]. This indicates that the overall initial investment is expected to be easily paid off within a short period by the savings associated with a higher network efficiency.

With respect to the impact of PhSDs on the network power quality, the commutation of end-users from one phase to another could originate voltage transients at their point of delivery. However, the dynamic analysis reported in [222] shows that the voltage variations caused by the PhSDs actions strongly depend on the time instant at which these phase commutations take place, i.e., a PhSD could be controlled appropriately to minimize these voltage disturbances. Applying this criterion, the RMS voltage variations can be limited to a few percentage and can last only for few milliseconds, i.e. they become comparable with the typical transients in the case of traditional loads switch-on. Furthermore, the phase commutations of end-users are limited to a 15 minutes time interval in the developed scheme, it is, therefore, expected that the impact of PhSDs on a grid, in terms of transients and power quality, would be minimal.

4.4 Summary

In this chapter, a novel unbalance reduction strategy is proposed which is mainly based on the information provided by the MPLAP. The NLAFs, which represent the degree of unbalance at each node in a system, are used to identify the highly unbalanced nodes of a network, which can then serve as potential locations for the installation of PhSDs. These devices can participate in the real-time management of DNs by switching either individual or combined load across the phases of these critical nodes to reduce unbalance and, consequently, power system losses. To achieve this, two phase switching algorithms, PSA-1 and PSA-2, are developed and tested. The former algorithm can shift any individual load across the phases of HUNs whereas the latter algorithm can shift only combined load from one phase to another phase. The results indicate that PSA-1 exhibits a much superior performance than PSA-2 in reducing network unbalance. However, it is not practically realizable in the present practice since it needs a PhSD at every consumer point of connection. For long and highly unbalanced feeders, PSA-2 can be implemented practically in the place of PSA-1 since the performance of the former algorithm is significantly improved for such feeders as compared to its performance in short and lightly/moderately unbalanced feeders.

Published papers

The research work presented in this chapter led to the publication of following papers.

1. Usman, M., M. Coppo, F. Bignucolo, R. Turri, and A. Cerretti. "A novel methodology for the management of distribution network based on neutral losses allocation factors." *International Journal of Electrical Power & Energy Systems* 110 (2019): 613-622.

2. Usman, Muhammad, Marco Vanzetto, Massimiliano Coppo, Fabio Bignucolo, and Roberto Turri. "Losses allocation methods in planning and management of low voltage active distribution networks." in *53rd International Universities Power Engineering Conference (UPEC)*, pp. 1-6. IEEE, 2018.

PART II

Convex Optimization based Optimal Power Flow in Low Voltage Active Distribution Networks

CHAPTER 5

Optimal Power Flow: A Theoretical Overview

This chapter presents a brief literature review on convex OPF models which are based on semi-definite, second-order-cone and linear programming relaxations. A generalized OPF model is initially presented, followed by the two commonly used approaches for the representation of power injections in such a model. Three case studies are also shown to represent the non-convexity and NP-hardness of an OPF problem, and finally, few studies which have proposed three-phase relaxed OPF models are reported which ultimately sets the basis of the work carried out in the latter chapters.

The deregulation of electricity market has caused a rapid transformation in the existing power system, as discussed in detail in chapter 1, which, on the one hand, has unlocked several opportunities for new market players but, on the other hand, has also introduced several challenges in maintaining a reliable, cost-efficient and secure power system operation. The increasing penetration of non-dispatchable and intermittent renewable DERs, more flexible demand and active participation of local end-users have reduced the predictability of foreseen supply and demand. Consequently, the secure dispatch and provision of electricity to end-users is becoming a major challenge with every passing day. Furthermore, with the liberalization of the electricity market and large cross-border energy flows, the grid is becoming more prone to the deviation of power injections from their planned schedule, and as a result, network system operators have to intervene regularly to maintain the power balance and system integrity. Apart from maintaining the reliability of the power grid, the network operators also have to optimize the system operating costs and provide electricity to end-users at the lowest possible rate. Resultantly, all these factors are pushing the operators to make use of a some kind of an optimization tool which, on the one hand, should be customizable to handle new devices and emerging scenarios, and, on the other hand, must be fast enough to solve large-size power systems, comprising of thousands of buses, in a reasonable amount of time. To this end, AC-OPF is a widely used optimization tool which has been adopted by the power industry across the globe to optimize system costs or minimize losses. AC-OPF is a problem of minimizing a function of voltage, power and current with respect to the power flow and service quality constraints [223]. Since its introduction in 1962 [224], a voluminous amount of literature has been published in the field of deterministic and heuristics algorithms for solving this problem. However, due to its non-convex, non-linear and NP-hard nature [225], AC-OPF is still an open research problem. The deterministic algorithms such as Newton-based methods [226], [227], linear and quadratic programming [228], non-linear and polynomial programming [229], interior point methods [230] and heuristic optimization techniques such as GA, PSO, TS, evolutionary algorithms, ant-colony, harmony search, bacterial foraging etc. [231], [232] have been proposed to solve a single-phase AC-OPF problem. Although, the above-mentioned deterministic algorithms have been proved in the literature to converge to a minimum value and can also be scaled for large-size power networks, the meta-heuristic algorithms have no substantiated proof of optimality and scalability [223]. On the other hand, the global optimality and feasibility of the obtained solution through deterministic algorithms cannot be guaranteed due to lack of any sufficient criterion.

Quite recently, researchers have started leveraging tools from the convex-optimization theory to transform the non-convex OPF problem into a convex one because of the existing problems in classical and meta-heuristic algorithms. These tools either *relax* or *approximate* the non-convex FR, which is associated with the power flow equations, into a convex region, and try to find a global solution in the relaxed or approximated domain. More specifically, *relaxations* enclose the non-convex FR through an enlarged convex FR and, therefore, provides a lower (minimization problem) or upper (maximization problem) bound on the optimal objective value. Furthermore, the relaxation techniques also provide sufficient conditions to certify the infeasibility of AC-OPF problem. *Approximations*, on the other hand, use certain assumptions on the power quantities and try to replicate the non-convex FR by an approximated convex region which closely represents the original non-convex FR under *typical* operating conditions. However, the approximation techniques do not provide any theoretical guarantee for the global optimality of obtained solution which is typically provided by the relaxation techniques [233]. For better understanding of these concepts, Fig. 5.1 shows the relaxed and approximated FRs of a non-convex region.

Concerning relaxation techniques, several methodologies based on the lift-and-project, convex envelopes, hierarchies of moment/sum-of-square etc. concepts have been proposed which ensure the global optimality of recovered solution if it satisfies a pre-defined criterion. Since approximations are out of the scope of this thesis work, they are not presented in this chapter. Nevertheless, a detailed overview on the relaxation and approximation approaches is presented in [233] which can be consulted for better understanding. Since convex optimization-based OPF models for LV active DNs, which are equipped with neutral conductors, have been proposed in this thesis, it is, therefore, incumbent to provide a useful discussion on a general OPF model and specific SDP and Second-Order-Cone Programming (SOCP)-based OPF models in this chapter so that a better understanding of the following chapters can be developed.

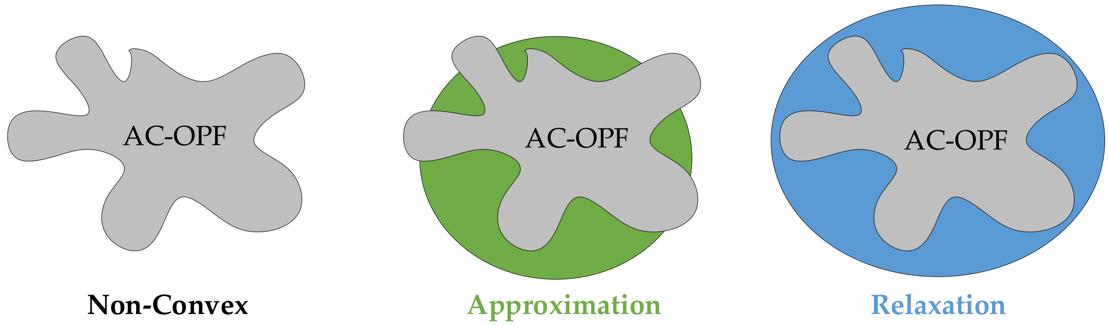

Figure 5.1: From left to right: Illustration of a non-convex and associated approximated and relaxed feasible regions.

5.1 Generalized OPF model

A generic OP can be defined as:

$$\begin{aligned} \underset{x}{\text{minimize}} \quad & f(x) \\ \text{subject to} \quad & g_i(x) \leq 0, \ i = 1, \ldots, m \\ & h_i(x) = b, \ i = 1, \ldots, p \end{aligned}$$

where $f(x)$ is an OF, $\mathbf{g}(x) := \{g_i(x) \leq 0, \ i = 1, \ldots, m\}$ represents the set of inequality constraints and $\mathbf{h}(x) := \{h_i(x) = b, \ i = 1, \ldots, p\}$ represents the set of equality constraints. In terms of an OPF problem, the OF usually chosen is either minimization of network operating costs or reduction in power system losses. The set $\mathbf{g}(x)$ contains the upper and lower bounds on power system control and state variables such as the limits on active and reactive power generation, voltage magnitude and angles, line power flows etc., and is usually defined as:

$$\mathbf{g}(x) = \begin{cases} \mathbf{P}_{g_i}^{min} \leq \mathbf{P}_{g_i} \leq \mathbf{P}_{g_i}^{max} \\ \mathbf{Q}_{g_i}^{min} \leq \mathbf{Q}_{g_i} \leq \mathbf{Q}_{g_i}^{max} \\ |\mathbf{V}_k|^{min} \leq |\mathbf{V}_k| \leq |\mathbf{V}_k|^{max} \\ \theta_{(k,l)}^{min} \leq \theta_{(k,l)} \leq \theta_{(k,l)}^{max} \\ |\mathbf{S}|_{(k,l)} \leq |\mathbf{S}|_{(k,l)}^{max} \end{cases} \tag{5.1}$$

$\forall k \in N$, $(k,l) \in E$ and $i \in G$ where N is a set consisting of all network nodes, E is a set containing all network branches and G is a set of all system buses equipped with a controllable active and reactive power source. It can be noticed that active and reactive power limits, and bounds on the angle difference between two buses are linear inequalities and, consequently, constitute a convex region. The voltage magnitude constraint, on the other hand, is a non-convex constraint mainly due to the enforcement of lower bound as can be seen in Fig. 5.2 .

The equality constraint set $\mathbf{h}(x)$ comprises of active and reactive power balance equa-

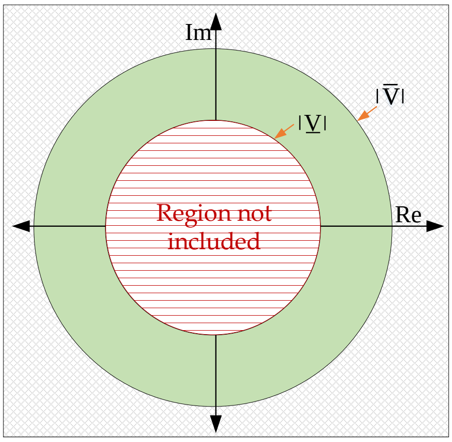

Figure 5.2: Non-convexity caused by the lower bound on voltage magnitude constraint.

tions in addition to other optional constraints such as the reference bus angle value etc. In literature, several representations of power flow equations exist ranging from the traditional Bus Injection Model (BIM) [234] and Branch Flow Model (BFM) [235] to the more recent elliptical [236] and power divider models [237]. In the context of this work, the traditional BIM- and BFM-based power balance equations are presented below to show the inherent non-convexity of AC-OPF model caused by these inevitable equalities. Consequently, the convexification approaches (relaxations and approximations) revolve around the transformation of voltage magnitude and power balance constraints into convex equations by shifting the source of non-convexity to new constraints, which can subsequently be relaxed (dropped) to obtain a convex OPF model.

5.1.1 Bus injection model

In BIM, the electrical quantities at each bus k (net power injection P_k/Q_k and node voltage V_k) are linked in power flow equations. For a single-phase equivalent representation of an electrical network, the complex voltage $V_k \in \mathbb{C}$ at each bus can be represented either in a polar form $V_k = |V_k|e^{j\theta_k}$ or in a rectangular form $V_k = V_{d_k} + jV_{q_k}$, which leads to two different representations of power balance equalities as mentioned below.

- Polar form representation

$$P_k = |V_k| \sum_{i=1}^{n} |V_i| \{\mathbf{G}_{ki} cos(\theta_k - \theta_i) + \mathbf{B}_{ki} sin(\theta_k - \theta_i)\} \qquad \forall k \in N \tag{5.2}$$

$$Q_k = |V_k| \sum_{i=1}^{n} |V_i| \{\mathbf{G}_{ki} sin(\theta_k - \theta_i) - \mathbf{B}_{ki} cos(\theta_k - \theta_i)\} \qquad \forall k \in N \tag{5.3}$$

- Rectangular form representation

$$P_k = \sum_{i=1}^{n} V_{d_k}(\mathbf{G}_{ki}V_{d_i} - \mathbf{B}_{ki}V_{q_i}) + V_{q_k}(\mathbf{B}_{ki}V_{d_i} + \mathbf{G}_{ki}V_{q_i}) \qquad \forall k \in N \tag{5.4}$$

$$Q_k = \sum_{i=1}^{n} V_{d_k}(-\mathbf{B}_{ki}V_{d_i} - \mathbf{G}_{ki}V_{q_i}) + V_{q_k}(\mathbf{G}_{ki}V_{d_i} - \mathbf{B}_{ki}V_{q_i}) \quad \forall k \in N \tag{5.5}$$

$$|V_k|^2 = V_{d_k}^2 + V_{q_k}^2 \tag{5.6}$$

It can be noticed in (5.2)-(5.3) that non-convexity appears due to the presence of trigonometric functions, whereas in (5.4)-(5.5), non-convexity is caused by the quadratic voltage variable which makes these power balance constraints equal to quadratic equality constraints which by nature constitute a non-convex region. Furthermore, the appearance of another quadratic equality constraint (5.6) in the rectangular form representation introduces another source of non-convexity in AC-OPF problem.

5.1.2 Branch flow model

The BFM was initially introduced in [235] under the name *DistFlow equations* in the context of network reconfiguration problem. For almost twenty years, the model did not catch the attention of power system researchers until in 2005, [238] formulated a conic relaxation model by utilizing the power flow equations based on this model. The BFM is based on network branch quantities as shown in Fig. 5.3 and can be expressed as follows:

$$P_{ki} = R_{ki}l_{ki} - P_i + \sum_{m:i\to m} P_{im} \quad \forall (k,i) \in L \tag{5.7}$$

$$Q_{ki} = X_{ki}l_{ki} - Q_i + \sum_{m:i\to m} Q_{im} \quad \forall (k,i) \in L \tag{5.8}$$

$$|V_i|^2 = |V_k|^2 - 2(R_{ki}P_{ki} + X_{ki}Q_{ki}) + (R_{ki}^2 + X_{ki}^2)l_{ki} \quad \forall (k,i) \in N \tag{5.9}$$

$$l_{ki}|V_k|^2 = P_{ki}^2 + Q_{ki}^2 \quad \forall (k,i) \in L \tag{5.10}$$

where P_{ki} and Q_{ki} are the active and reactive power flows from node k to node i with node i being considered as the downstream node (farther from substation), l_{ki} is the squared magnitude of the current flowing on the branch from node k to node i having impedance equal to $Z_{ki} = R_{ki} + jX_{ki}$, o denotes the downstream branches connected to node i, P_i and Q_i denote the active and reactive power injections at node i, and finally $|V_k|$ and $|V_i|$ represent the voltage magnitude at nodes k and i, respectively.

By introducing a new variable $v_k = |V_k|^2$ and substituting it in (5.7)-(5.9), these

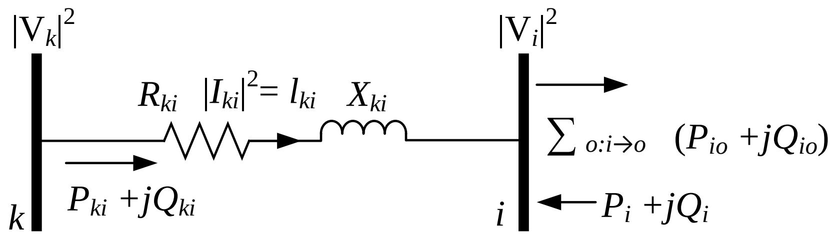

Figure 5.3: Explanations of variables appearing in a branch flow model.

equations become linear equalities in terms of the variable v_k and, consequently, constitute a convex region. The non-convexity of BFM is then restricted to (5.10) which is a quadratic equality ($l_{ki}v_k = P_{ki}^2 + Q_{ki}^2$) and, therefore, represents a non-convex region.

5.2 Illustration of power flow feasible spaces

In this section, few case studies taken from [239]–[242] are reported to better clarify the nature of FRs that can be encountered in AC-OPF problem. The values of line impedance, voltage magnitude set-points and active/reactive power injections for test cases are mentioned on their single-line diagram.

5.2.1 Case study I: Feasible space is connected but non-convex

This case study is taken from [239] and is shown in Fig. 5.4. The voltage at all buses is fixed to 1.05pu, whereas the active and reactive power injection at each bus is unconstrained. The FR, constructed using the continuation approach [239], is cut into half to reveal the inner fold. It can be noticed that although the FR is connected but has a hole in it when projected to the $P_{G2} - Q_{G2}$ plane which makes it a non-convex FR.

5.2.2 Case study II: Feasible space is connected but non-convex

This case study is taken from [240], [241] and is shown in Fig. 5.5. The voltages at nodes 1 and 2 is fixed to 1.0pu whereas the voltage at node 3 is unconstrained. The active and reactive power injections are unconstrained as well at all nodes except at node 3 where reactive power is fixed to 0. The FR is constructed again using the continuation approach [239] and it can be noticed that although the FR is connected but is non-convex due to the hole appearing in the space of active powers (P_{G_1}, P_{G_2} and P_{G_3}) projections.

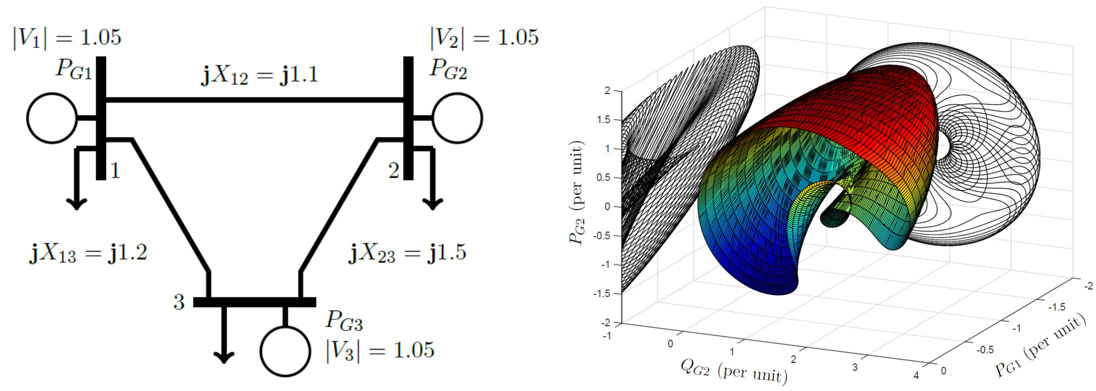

Figure 5.4: Feasible region is connected but non-convex due to the hole seen in the space of $P_{G2} - Q_{G2}$ plane [239].

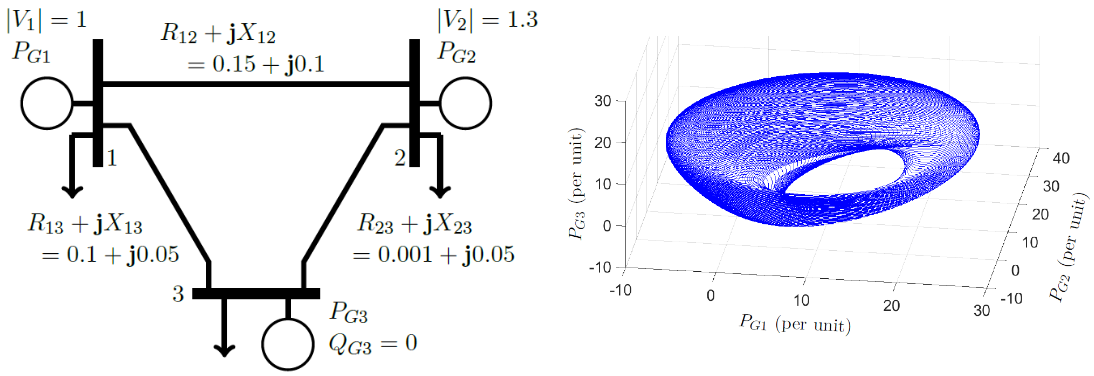

Figure 5.5: Feasible region is connected but non-convex due to the hole seen in the space of P_{G1}, P_{G2} and P_{G3} plane [240], [241].

5.2.3 Case study III: Feasible space is disconnected with multiple minima

This case study is taken from [242] and is shown in Fig. 5.6. The FR is constructed using the algorithm reported in [243]. It can be noticed that the introduction of lower reactive power limit at bus 5 ($Q_{G_5} \geq -0.30$ pu) splits the FR into two disconnected regions which are above the grey plane. One region contains the global solution as indicated by the green star, whereas the other region contains a local minimum as shown by the blue triangle. This example clearly shows that the FR of AC-OPF problem may not only be non-convex (e.g., FR without grey plane) but can also be disconnected (e.g., FR with grey plane).

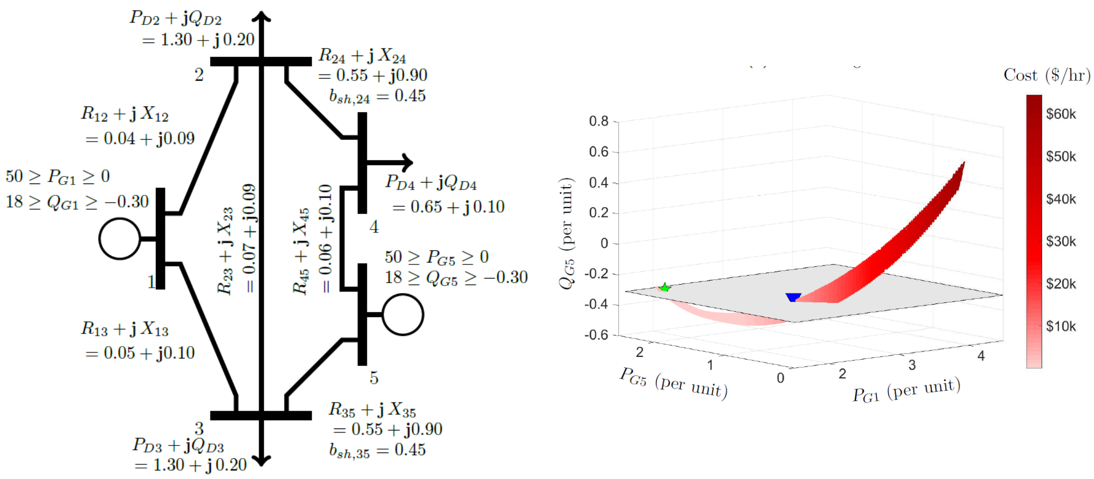

Figure 5.6: Feasible region is non-convex as well as disconnected with multiple minima [242].

5.3 Convex optimization-based OPF model

The non-convexity associated with AC power flow equations and challenges related to the robustness of existing algorithms, for the solution of a non-convex AC-OPF problem, become a strong proponent for the transformation of this problem into a convex one. In this context, as reported earlier, several convex relaxations and approximations have been proposed in the literature which can be classified on the basis of optimization solvers utilized for their solution such as SDP-, SOCP- and Linear Programming (LinP)-based methodologies etc. In the following, a general mathematical formulation of SDP-, SOCP- and LP-based OPs is briefly presented along with the overview of published literature belonging to these relaxation approaches.

5.3.1 Semidefinite programming-based AC-OPF relaxation

SDP is a conic problem in which a generalized inequality is defined over the cone of either symmetric (real) or Hermitian (complex) Positive Semi-Definite (PSD) matrices. The standard SDP-based OP can be expressed as follows:

$$\begin{aligned} \underset{\mathbf{X}}{\text{minimize}} \quad & \mathrm{Tr}(\mathbf{CX}) \\ \text{subject to} \quad & \mathrm{Tr}(\mathbf{A}_i\mathbf{X}) = b_i \qquad \forall\, i = (1, \cdots, n) \in N \\ & \mathbf{X} \succeq 0 \end{aligned}$$

where $\mathbf{A}$ and $\mathbf{C}$ are constant matrices containing problem data, whereas OP decision variable(s) takes the form of a symmetric/Hermitian matrix $\mathbf{X}$ which is subjected to a positive semi-definiteness condition.

In terms of an AC-OPF problem, power flow equalities and control/state variables inequalities are expressed in terms of a rank-1 matrix $\mathbf{X}$, which is subsequently relaxed by imposing a PSD constraint over it to transform the whole problem into a convex one. With regard to this optimization scheme, a brief recap of the published papers is presented below. Please note that the reported articles refer to the development of convexified OPF models for single-phase equivalent representation of DNs unless mentioned otherwise.

The SDP technique is first utilized in [244]; however, the seminal work based on this approach is proposed in [245] which handles the AC-OPF problem by solving its dual version and ensures the global optimality of objective value and decision variables by providing certain sufficient conditions. Following this work, a lot of literature has been published in this domain regarding determining the exactness (and lack thereof) and improving the computational efficiency of SDP-based OPF models.

In terms of exactness, apart from [245] which proved it for IEEE test bench cases, [246], [247] exhibit the exactness for European electric grid. Similarly, the convexified geometrical region and associated sufficient conditions for radial and meshed DNs are derived in [248], [249], and [250], respectively. The exactness of SDP-based relaxation strongly depends upon the nature of chosen OF and it has been shown that relaxed models involving increasing OF with respect to the active power injections have greater tendency to provide an exact solution. However, this is not always the case and as shown in [251], [252], a completely different OF (which is independent of power injections) in the case of large-size power systems provides a completely meaningless solution. Furthermore, the problem constraints such as active/apparent power line flows and maximum power flow limits can also cause the relaxation to become inexact [253], [254]. A detailed overview on the sufficient conditions related to the exactness of this methodology in radial and weakly meshed DNs can be found in [255].

The major hurdle in the real-time implementation of SDP-based OPF model is its large CT. To overcome this difficulty, the *chordal sparsity* of power networks is exploited in [256] and [257] for balanced and unbalanced DNs, respectively. In [246], the maximal cliques of a chordal super graph are merged together which further improves the computational efficiency, whereas in [258], a tight-and-cheap conic relaxation is established by combining the SDP-based OPF relaxation with the reformulation-linearisation technique. The chordal sparsity-based relaxation is further relaxed in [259] which enforces the PSD constraint on those sub-matrices which correspond to the cycle basis of a network graph and, as a result, a further reduction in the CT of SDP-based model is achieved. To be noted that the above-mentioned techniques solve the SDP-based relaxation in a centralized control architecture way. In contrast to these approaches, the decentralized approaches which are largely based on Alternative Direction Method of Multipliers (ADMM) algorithm are also utilized for single-phase equivalently represented [260]–[262] and balanced three-phase networks [263], [264]. These techniques significantly reduce the CT of this relaxation and, consequently, open the window to realize its practical implementation for large size power networks.

Although the SDP-based OPF relaxation has proven to be exact in many power system related OPs, the generalization of this relaxation, which is based on *Lasserre hierarchy for polynomial optimization* [265], [266], is adopted as well in [267]–[273] to get a solution in those cases where it has failed to provide a meaningful solution. However, the moment-based OPF model is extremely expensive from the computational point of view even for a single-phase network and, as per author's knowledge, it has not been studied yet concerning reduction in its CT. Consequently, its application on a multi-phase DN cannot be recommended. The above-mentioned moment-based approaches are based on real voltage variables. Quite recently, a complex voltage variable-based moment/sum-of-squares hierarchy is also proposed in [247] which has computational advantages to some extent over the real variable-based moment relaxation.

5.3.2 Second-order-cone programming-based AC-OPF relaxation

SOCP is a conic problem where a generalized inequality is defined over a second-order-cone constraint. The standard SOCP-based problem can be expressed as follows:

$$\begin{aligned} \underset{x}{\text{minimize}} \quad & c^T x \\ \text{subject to} \quad & \mathbf{A}x = b \\ & ||\mathbf{E}_i x + b||_2 \leq g_i^T x + d_i \qquad \forall\, i = (1, \cdots, r) \end{aligned} \tag{5.11}$$

where $\mathbf{A}$ and $\mathbf{E}$ are specified matrices, g and b are specified vectors, x is a decision variable vector and d is a scalar. It can be noticed that SOCP bears this name because of the presence of a second-order-cone constraint $||\mathbf{E}_i x + b||_2 \leq g_i^T x + d_i$ in its formulation.

For single-phase networks, both BIM- and BFM-based SOCP relaxations are proposed. However, it has been shown in [274], [275] that the BFM-based relaxation has better numerical convergence characteristics than the BIM-based model since it avoids the subtraction of voltage variables in its formulation. Concerning BIM-based relaxation, it is initially proposed in [238] which utilizes the rectangular form of power balance equalities. Later, the authors in [276] introduce the polar form representation-based SOCP relaxation and termed it as Quadratic Convex (QC) relaxation which further strengthens the rectangular form-based SOCP relaxation by introducing additional convex envelopes on the bilinear, trigonometric and square of voltage magnitude terms. It has been shown that the SOCP-based relaxation which is inherently weaker than the SDP-based relaxation surpasses the latter methodology after the introduction of convex envelopes in few instances and provides a much closer solution to the SDP-based relaxation in all other instances. The QC relaxation is further tightened through valid inequalities (lifted nonlinear cuts) in [277], [278] and bound tightening approaches in [279]. Similarly, in [280], [281], additional linear constraints are put on the original SOCP-based relaxation [238] to further tighten it. These constraints are formed by relaxing certain cycle constraints, employing envelopes which are derived from matrix minors and constructing arctangent envelopes which, ultimately, led to the 'Strong SOCP' relaxation [280], [281].

Concerning BFM-based relaxation, [274], [275] proposes this relaxation which surpasses the BIM-based relaxation in terms of numerical convergence. In [282], [283], additional BFM-based SOCP constraints such as Δ *inequalities*, *loss inequalities* and *circle inequalities* are proposed; however, the resultant relaxation has not been compared with other relaxations to evaluate its tightness and computational efficiency. Finally, the equivalence between the BIM- and BFM-based relaxations for radial networks is established in [284], [285].

With regard to the exactness of SOCP-based relaxation, *a priori* sufficient conditions are proposed in [238] and [275] for the BIM- and BFM-based relaxations, respectively. Normally, these conditions involve the presence of sufficient phase-shifting transformers in a mesh network along with the load over-satisfaction condition [286], no reverse power flow or only active or reactive reverse power flow [287] and purely resistive mesh network with either load over-satisfaction condition or other specific conditions on the voltage and power injection limits [288], [289].

5.3.3 Linear programming-based relaxation of AC-OPF model

This technique models the OF and constraints in a linear form and is the least general of all the above-mentioned optimization techniques. The general form of this relaxation is expressed below:

$$\begin{aligned} \underset{x}{\text{minimize}} \quad & c^T x \\ \text{subject to} \quad & \mathbf{A}x = b \\ & x \geq 0 \end{aligned} \tag{5.12}$$

where $\mathbf{A}$ is a specified matrix, c is a specified vector and x is a decision variable vector.

The LP-based models are the weakest relaxations among SDP- and SOCP-based approaches but they enjoy the theoretical and computational advantages over other schemes. In this context, several models such as network flow [290], copper plate [290], Taylor-Hoover [291], McCormick relaxations [292]–[294] and Bienstock-Munoz relaxations [295] are proposed. In the network flow relaxation, Kirchoff and Ohm's laws based power balance equalities are relaxed and line flow is arbitrary distributed as long as the active and reactive flows remain non-negative, whereas in the copper plate method, the power balance equalities are dropped completely, leading to the simplest power balance constraint relating all power injections in a network. Both network flow and copper plate relaxations are proven to be exact for networks having non-negative resistance and reactance of all branches. In Taylor-Hoover model, the linear combination of non-linear power relaxation is developed by considering the squared of voltage magnitude $|V|^2$ terms as a variable. Finally, in McCormick relaxation, the linearisation is achieved by putting convex envelopes on the bilinear terms of power flow equations. Since these envelopes depend on the bounds of Optimization Variables (OVs), putting loose bounds can make this relaxation weaker as compared to the other LinP-based relaxations. Consequently, bound tightening methods [279], [281], [296] must be utilized to strengthen the McCormick-based relaxation.

A complete flow chart of the previously reported relaxations is shown in Fig. 5.7 which represents the relationship between different relaxations and power flow formulations, along with the loss of property in each relaxation.

5.4 Optimization tools for SDP-, SOCP- and LP-based relaxations

The next question which arises after the formulation of above-mentioned relaxations is *how to solve them and get a solution of the respective variables involved in these OPs*? Since LinP is the most mature technique among all optimization strategies, it benefits itself from the existence of sophisticated optimization tools which are available commercially such as CPLEX, Gurobi [298] and MOSEK [299]. These tools are also able to handle discrete variables in a LinP-based OPF relaxation and, as a result, the resultant Mixed Integer Linear Programming (MILP)-based relaxation can be optimally solved with a higher level of confidence. For SOCP-based relaxation, the same above-mentioned solvers can be used for continuous decision variables. Although these solvers are also able to solve an SOCP-based relaxation augmented with discrete variables, the MISOCP problems, as of now, are significantly less tractable as compared to the MILP-based relaxations having same number of discrete variables.

SDP solvers are less mature as compared to the LinP and SOCP solvers, and MOSEK

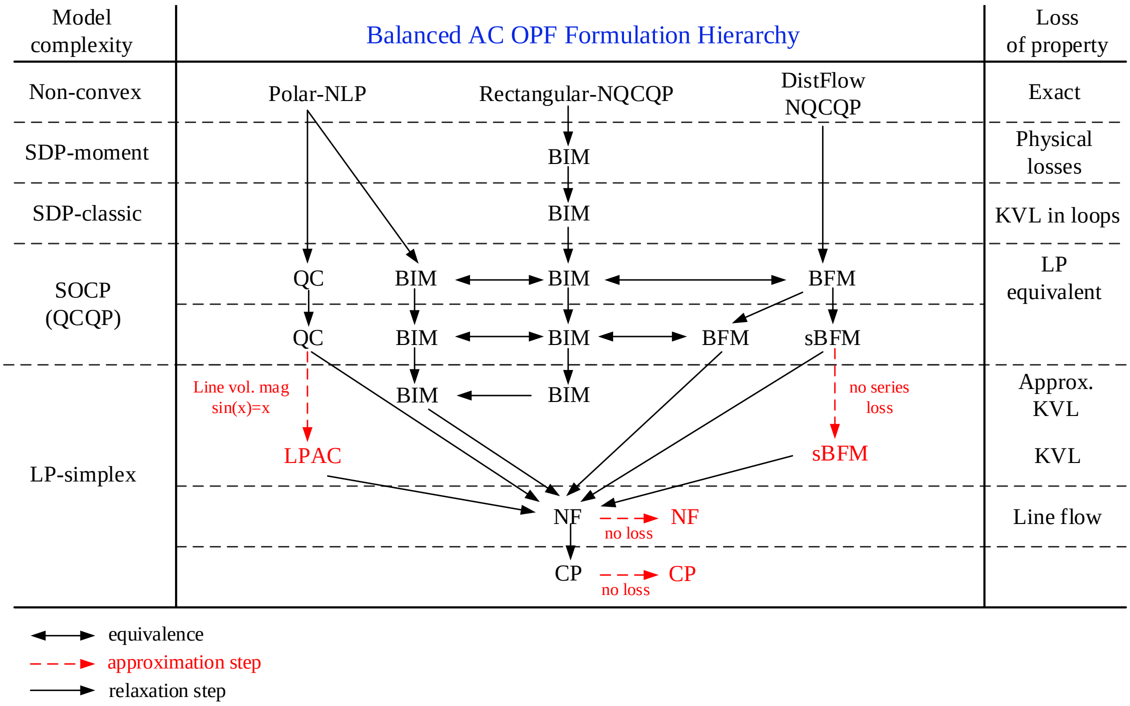

Figure 5.7: Relationship between different power flow formulations and relaxations [297].

is the only commercially available optimization tool which has the capability to solve this type of problem. Commercial Mixed Integer Semi-Definite Programming (MISDP) solvers, as of now, do not exist and consequently, these problems have to be reformulated by either relaxing the discrete variables into continuous variables or transforming the whole OP into a MISOCP/MILP domain. Since SDP solvers are based on the interior-point algorithm, researchers have also put significant efforts in improving the performance of this algorithm by proposing its parallel implementation which significantly improves the tractability and computational performance of an SPD-based relaxation [300].

5.5 Three-phase convex relaxation- based OPF models

To determine the optimal active and reactive power operational point of single- and three-phase DERs connected to MV and LV DNs, it is incumbent to solve a multi-phase OPF problem. Since these DNs exhibit significant unbalance loading, solving a single-phase OPF model for them provides an incomplete picture of the state variables of these DNs. However, due to the increased complexity and non-convexity of a multi-phase OPF problem in comparison to a single-phase OPF model, only few researchers have studied it for three-phase networks. Among the relaxation techniques, the single-phase SDP-based relaxation in its *primal* form is extended in [264] and solved through an ADMM-based distributed algorithm. The BIM- and BFM-based SOCP relaxations are extended in [257], [301] for three-phase unbalanced DNs. However, it must be noted that even for a radial system, these relaxations involve PSD constraints in their formulation due to the existence of mutual coupling among phases. However, the PSD constraints are defined over smaller matrices, which either involve node voltages (BIM) or node voltage along with the branch flow quantities (BFM), and as a result, the computational efficiency of these cheap SDP-based OPF models does not degrade too much from the single-phase SOCP-based relaxation. In fact, implementing PSD constraints only on the *edge minor*, *three cycle minor* or *four cycle minor* of a complete matrix variable significantly lowers the CT as compared to the case when only one PSD constraint is defined over a matrix variable. Furthermore, it must be noted that for single-phase radial DNs, both SDP- and SOCP-based relaxations are equivalent and, therefore, one can solve the SOCP-based relaxation without making any compromise on the solution quality. However, as per author knowledge, no such equivalence has been established between the primal SDP [264] and BIM-based SDP/BFM-based SDP [257], [301] relaxations in the case of three-phase DNs. Consequently, a general statement about the existence of equivalency between these relaxations would be an overstatement.

Quite recently, a chordal relaxation-based SDP model is proposed in [302] which exploits the chordal sparsity of a three-phase SDP-based relaxation to speed-up the computational process. Furthermore, in [303], the chordal relaxation is embedded inside a convex iterative algorithm which, on the one hand, increases the computational efficiency for large size DNs and, on the other hand, guarantees the global optimality of recovered solution when the trace of regularization terms becomes zero.

Finally, it must be noted that due to the complex analytical characterization of mutually coupled power injections in a multi-phase unbalanced DN, sufficient conditions related to the exactness, and lack thereof, of a multi-phase OPF model do not exist yet. Some attempts are made in [264] and [303] to define the FRs of a three-phase SDP-based OPF relaxation and its original non-convex AC-OPF model to show that under an increasing OF with respect to the active power injections, both regions coincide with each other and, therefore, one can expect a rank-1 solution for a three-phase SDP-based OPF relaxation. However, for monotone (non-increasing) and power injections independent OFs (economic values and cost related OFs), this might not be the case. Resultantly, it becomes important to tackle the analytical expression of line flows in such DNs intelligently to achieve the goal of developing sufficient conditions related to the exactness of a multi-phase OPF model.

CHAPTER 6

Centralized SDP based OPF Relaxation for Neutral-equipped Multi-Phase Distribution Networks

This chapter presents a multi-phase OPF model for neutral-equipped distribution networks hosting both wye- and delta-connected loads. The decoupling of power injections is carried out through a network admittance-based approach, whereas the incorporation of a full ZIP load is made possible through a novel complex voltage-based optimization variable. Furthermore, two modelling approaches are also introduced for handling the constant current component of a ZIP load. Finally, the exactness of proposed multi-phase OPF relaxation is tested against several load models for wye-, delta-, and mixed-load types, varying R/X ratio and a range of neutral-ground impedance values.

In chapter 5, an extensive literature review on single- and three-phase OPF relaxations is presented. Since the main focus of this thesis work revolves around neutral-equipped distribution networks, consequently, more attention is put on the latter OPF relaxations in this chapter. In the following, the major shortcomings of these models are discussed, which hinder their direct extension to DNNs, in order to set the path for the development of a convexified OPF model for such DNs.

1. In all the proposed single- and three-phase OPF relaxations except [301], phase-ground power injections have been taken into consideration by assuming only wye-connected loads. In [301], an attempt is made to solve the BFM-based SDP relaxation for mixed wye- and delta-connected loads. However, the relaxation variables related to the latter load type depict a large Eigen Value Ratio (EVR) which indicates the inexactness of the proposed relaxation. In the case of DNNs, which host shunt element either between phase-neutral (wye) or phase-phase (delta) conduc-

tors, the assumption of phase-ground power injection cannot be justified. In such cases, the power injections are coupled between two conductors and, therefore, the decoupling of these injections is a must requirement to develop an OPF model for such DNs.

2. In all the studies except [304], only constant power loads (power absorption/injection is independent of node voltage) are taken into consideration. In [304], a full ZIP LM is incorporated in a single-phase SDP-based OPF model; however, it is demonstrated in this chapter that the approach reported in [304] cannot be generalized for the loads connected in a multi-phase DNN. Due to the significant presence of constant impedance and constant current loads in such DNs, it is, therefore, equally important to model these load types in an OP since ignoring the impact of their voltage dependency can lead to sub-optimal results.

3. In [264], KR technique is utilized to implicitly add the impact of a neutral conductor in the developed OPF model. However, in the case of SPG and MPG DNs, as stated earlier in chapters 3 and 4, the unrealistic assumption of equal potential at both ends of a neutral conductor (which is the basis of KR approach) cannot be justified. Resultantly, it should be treated similarly as phase conductors and network quantities (power flow, voltage, losses etc.) must be expressed explicitly for these conductors. In this regard, it becomes incumbent to model neutral conductors and neutral-ground impedance explicitly in a multi-phase OPF model.

To address the above-mentioned short-comings, the following goals are set to derive an OPF model which can truly capture the characteristics of a DNN.

1. Proposal of a network admittance-based approach for the decoupling of coupled power injections between the conductors of a DNN and, subsequently, extension of a centralized three-phase SDP-based OPF model to such network

2. Examining the limitations of existing voltage magnitude-based approach [304] and development of a novel complex voltage variable-based methodology for the representation of a full ZIP load in the developed OPF model

3. Proposal of an approximate representation of the constant current component of a ZIP load in terms of the OV of proposed OPF relaxation

4. Depicting the impact of neutral-ground impedance on the quality of proposed OPF methodology under both SPG and MPG configurations

To achieve these objectives, CCI [81], [305], [306] concept is employed which facilitates the representation of a shunt load by a constant admittance and a suitable current injector, and, resultantly, makes it possible to explicitly represent the power injections (active and reactive) at each conductor of a network. For a ZIP load, the current injection terms of CCI methodology are used to express the voltage dependency behaviour of constant impedance and constant current components. The constant impedance component dependency on the square of voltage magnitude term allows its easy handling in a three-phase SDP-based

OPF relaxation. However, since constant current component depends on the linear voltage magnitude term which is not available in the OV of a three-phase OPF relaxation, two additional modelling techniques, based on the *first-order Taylor series* and *approximation of the first-order Taylor series*, are developed to incorporate this load component in the proposed OPF model. Finally, to demonstrate the negative impact of KR methodology on the optimality of the recovered solution, a detailed analysis is carried out between the proposed multi-phase and three-phase KR-based OPF models.

6.1 Modelling of a standard SDP-based OPF relaxation

In this section, the nomenclature, which will be used in the modelling of OPF problem throughout the rest of this thesis work, is presented. Moreover, the primal three-phase SDP-based OPF relaxation [264] along with its mathematical formulation is briefly recalled to point out the limitations which exist in the existing three-phase OPF models in order to set the basis of proposed MPSDP-based OPF relaxation.

6.1.1 Nomenclature

Consider a radial ADN comprising a set N of $n+1$ nodes as $N = \{0, 1, 2, \cdots, n\}$ and a set E of branches as $E = \{(i, j) \subset N \times N\}$ having τ conductors between any two nodes. Let $(j : i \sim j) \in E$ denotes a line connecting node i to node j. Let 0 represents the slack node and define N^+ as $N \backslash \{0\}$. Consider $G \subseteq N$ be the set of nodes where DGs are connected. Let $\phi_{ij} \subset \{a_{ij}, b_{ij}, c_{ij}, n_{1_{ij}}, \cdots, n_{m_{ij}}\}$ and $\phi_i \subset \{a_i, b_i, c_i, n_{1_i}, \cdots, n_{m_i}\}$ be the sets containing phase and neutral conductors of a line $(i \sim j) \in E$, and phase and neutral conductors of a node $i \in N$, respectively. Consider $\delta_i \subset \{n_{1_i}, \cdots, n_{m_i}\}$ and $\delta_{ij} \subset \{n_{1_{ij}}, \cdots, n_{m_{ij}}\}$ be the sets containing neutral conductor of a node $i \in N$ and line $(i \sim j) \in E$, respectively, and define $\eta_i = \phi_i \backslash \delta_i$ and $\eta_{ij} = \phi_{ij} \backslash \delta_{ij}$ be the sets containing only phase conductors of a node $i \in N$ and line $(i \sim j) \in E$, respectively. Consider $\psi_i \subset \{a_i - n_{1_i}, b_i - n_{1_i}, c_i - n_{1_i}, \cdots, a_i - n_{m_i}, b_i - n_{m_i}, c_i - n_{m_i}\}$ and $\chi_i \subset \{a_i - b_i, b_i - c_i, c_i - a_i\}$ be the sets containing phase-neutral and phase-phase connection of a node $i \in N$, respectively. Lines are modelled as π-equivalent representation and the complex series impedance and shunt admittance of a line $(i, j) \in E$ are represented by $\mathbf{Z}_{ij} \in \mathbb{C}^{|\phi_{ij}| \times |\phi_{ij}|}$ and $\mathbf{Y}_{ij} \in \mathbb{C}^{|\phi_{ij}| \times |\phi_{ij}|}$, respectively where $|\mathbf{A}|$ defines the cardinality of a set $\mathbf{A}$.

Consider V_i^{φ} be the complex phase-ground voltage of phase $\varphi \in \phi_i$ of a node i and let $\mathbf{V}_i = [V_i^{ag}\ V_i^{bg}\ V_i^{cg}\ V_i^{ng_1}\ \cdots\ V_i^{ng_m}]^T$ be the complex phase-ground voltage vector of a node i. Define $\mathbf{V} = [\mathbf{V}_1, \cdots, \mathbf{V}_n]^T$ be the vector of voltages of all nodes. Take $\mathbf{V}_0 = [1\angle 0^\circ, 1\angle -120^\circ, 1\angle 120^\circ, 0, \cdots, 0]^T$ be the slack node voltage vector, defined as a positive sequence voltage triplet for phases $\{a, b, c\}$ and 0 for neutrals $\{n_1, \cdots, n_m\}$. Let I_i^{φ} be the complex current injected into the phase $\varphi \in \phi_i$ of a node i and let I_{ij}^{φ} be the complex current flowing on the phase $\varphi \in \phi_{ij}$ of a line $(j : i \sim j)$. In a vector form, let $\mathbf{I}_{ij} = [I_{ij}^a\ I_{ij}^b\ I_{ij}^c\ I_{ij}^{n_1}\ , \cdots,\ I_{ij}^{n_m}]^T$ be the complex current flowing on a line between nodes i and j.

For $\upsilon \in \psi_i$, let $P^{\upsilon}_{l_i}/P^{\upsilon}_{g_i}$ and $Q^{\upsilon}_{l_i}/Q^{\upsilon}_{g_i}$ represent the active and reactive power demand/generation of a load/DG connected between the phase-neutral conductors of a node i having constant admittance $y^{\upsilon}_{l_i}/y^{\upsilon}_{g_i}$. Similarly, for $\upsilon \in \chi_i$, let $P^{\upsilon}_{l_i}/P^{\upsilon}_{g_i}$ and $Q^{\upsilon}_{l_i}/Q^{\upsilon}_{g_i}$ represent the active and reactive power demand/generation of a load/DG connected between the phase-phase conductors of a node i. Let $\mathbf{S}_{\varrho_i} = [S^{ag}_i \; S^{bg}_i \; S^{cg}_i \; S^{n_1 g}_i, \cdots, S^{n_m g}_i]$ be the complex phase-ground power injection vector at node i. For a DNN, let $y^{\alpha}_{gnd_i}$ be the admittance connected between the neutral and ground of a node i for $\alpha \in \delta_i$, and for capacitor banks, which are usually connected for end-users power factor correction [307] and voltage support, let $y^{\upsilon}_{c_j}$ be the admittance of a shunt capacitor connected between a particular phase and neutral of a node j for $\upsilon \in \psi_i$. Let $\theta^{\varphi_i \varphi_j}_{ij}$ be the angle difference between the phases of nodes i and j for $\varphi_i, \varphi_j \in \eta_{ij}$, whereas $\boldsymbol{\theta}_{ij} = [\theta^{aa}_{ij} \; \theta^{bb}_{ij} \; \theta^{cc}_{ij}]^T$ be the phase-angle difference vector related to a three-phase line between nodes i and j, and finally, let $\underline{x}$ and $\overline{x}$ denote the lower and upper limits on a variable x, respectively.

Before proceeding further, it is important to mention that for the sake of clarity, only one neutral conductor is considered in the rest of the work to derive a compact form of the proposed OPF model. Nevertheless, the presented approach can be generalized for any number of neutral conductors.

6.1.2 Non-convex AC-OPF problem formulation

The non-convex AC-OPF problem for a multi-phase DN is summarized in model **M6.1**, which solves the set of non-linear power and current balance constraints at each phase of a node by fulfilling the set of technical limits for a specific OF.

It can be observed, and as stated in chapter 5, that the equality constraints (6.1b)-(6.1d) correspond to the physics (power and current balance) of a network, whereas the inequality constraints (6.1e)-(6.1g) are imposed on certain network quantities (voltage

M6.1: Non-Convex AC-OPF Model

$$\textbf{M6.1}: \underset{\Psi}{\textbf{minimize}} \; f(\Psi) \tag{6.1a}$$

$$\textbf{variables}: P^{\upsilon}_{g_i}, Q^{\upsilon}_{g_i}, V^{\varphi}_i \qquad \forall (\upsilon \in \psi_i/\chi_i), \varphi \in \phi_i, i \in N$$

subject to :

$$V^{\varphi}_i I^{*\varphi}_i = (P^{\upsilon}_{g_i} - P^{\upsilon}_{l_i}) + j(Q^{\upsilon}_{g_i} - Q^{\upsilon}_{l_i}) \qquad \forall \varphi \in \phi_i, \upsilon \in \psi_i, i \in G \tag{6.1b}$$

$$V^{\varphi}_k I^{*\varphi}_k = (-P^{\upsilon}_{l_k} - jQ^{\upsilon}_{l_k}) + jy^{\upsilon}_{c_k}|V_k|^2 \qquad \forall \varphi \in \phi_k, \upsilon \in \psi_k, k \in N \setminus G \tag{6.1c}$$

$$I^{\varphi}_i = \sum_{(k:i\sim k)\in E} y^{\varphi}_{ik} V^{\varphi}_k \qquad \forall \varphi \in \phi_i, i, k \in N \tag{6.1d}$$

$$|\underline{V_k}|^2 \le |V^{\varphi}_k|^2 \le |\overline{V_k}|^2 \qquad \forall \varphi \in \eta_k, k \in N^+ \tag{6.1e}$$

$$\underline{P}_{g_k} \le P^{\upsilon}_{g_k} \le \overline{P}_{g_k} \qquad \forall \upsilon \in \psi_k, k \in G \tag{6.1f}$$

$$\underline{Q}_{g_k} \le Q^{\upsilon}_{g_k} \le \overline{Q}_{g_k} \qquad \forall \upsilon \in \psi_k, k \in G \tag{6.1g}$$

and DGs output) to ensure the secure and reliable operation of a DN. Similarly, other inequalities such as line flow limits, although not shown here, can also be added in the model. It can also be noted that (6.1d) can be eliminated from the model by substituting it in (6.1b) and (6.1c), which, consequently, restricts the non-convexity of the presented model in these constraints.

6.1.3 Convexification of a three-phase AC-OPF model

The core idea of utilizing an SDP methodology for AC-OPF problem is to represent both network equalities and inequalities (6.1b)-(6.1g), related to each phase of a node, in terms of a matrix variable $\mathbf{W}$. For three-phase DNs, $\mathbf{W}$ is defined as the product $\mathbf{V}\mathbf{V}^H$ where $\mathbf{V}$ is defined only for the phase conductors belonging to η set [264]. To this end, the following matrices are introduced to establish a linear relation between system constraints and OV $\mathbf{W}$,

$$\mathbf{Y}^{\varphi}_{k,nw} = \mathbf{e}^{\varphi}_k * \mathbf{e}^{\varphi T}_k * \mathbf{Y}_B \qquad \forall\varphi \in \eta_k, \forall k \in N \tag{6.2}$$

$$\mathbf{\Psi}^{\varphi}_{k,nw_p} = \frac{1}{2}\{\mathbf{Y}^{\varphi}_{k,nw} + (\mathbf{Y}^{\varphi}_{k,nw})^H\} \qquad \forall\varphi \in \eta_k, \forall k \in N \tag{6.3}$$

$$\mathbf{\Psi}^{\varphi}_{k,nw_q} = \frac{j}{2}\{\mathbf{Y}^{\varphi}_{k,nw} - (\mathbf{Y}^{\varphi}_{k,nw})^H\} \qquad \forall\varphi \in \eta_k, \forall k \in N \tag{6.4}$$

$$\mathbf{\Psi}^{\varphi}_{k,nw_v} = \mathbf{e}^{\varphi}_k * \mathbf{e}^{\varphi T}_k \qquad \forall\varphi \in \eta_k, \forall k \in N \tag{6.5}$$

where $\mathbf{Y}_B$ is the bus admittance matrix, $\mathbf{Y}^{\varphi}_{k,nw}$ represents the admittance matrix related to the phase φ of a node k, $\mathbf{\Psi}^{\varphi}_{k,nw_p}$ and $\mathbf{\Psi}^{\varphi}_{k,nw_q}$ are the Hermitian matrices which represent the network admittance, as seen by the phase φ of a node k, corresponding to the active and reactive power injections, respectively, $\mathbf{\Psi}^{\varphi}_{k,nw_v}$ is the Hermitian matrix corresponding to the voltage at phase φ of a node k and finally, $\mathbf{e}^{\varphi}_k$ denotes the standard canonical basis of $\mathbb{R}^{|\eta_k|\times 1}$ and is defined as $\mathbf{e}^{\varphi}_k = [\mathbf{0}^T_{|\eta_0|}, \cdots, \mathbf{0}^T_{|\eta_{k-1}|}, \mathbf{I}^{\varphi T}_{|\eta_k|}, \mathbf{0}^T_{|\eta_{k+1}|}, \cdots, \mathbf{0}^T_{|\eta_n|}]^T$.

Based on the above-mentioned matrices and OV $\mathbf{W}$, the active and reactive power injections, and voltage at each phase of a node, can be expressed as:

$$P^{\varphi}_{g_k} - P^{\varphi}_{l_k} = \Re(V^{\varphi}_k I^{*\varphi}_k) = \mathrm{Tr}(\mathbf{\Psi}^{\varphi}_{k,nw_p}\mathbf{W}) \qquad \forall\varphi \in \eta_k, \forall k \in N \tag{6.6}$$

$$Q^{\varphi}_{g_k} - Q^{\varphi}_{l_k} = \Im(V^{\varphi}_k I^{*\varphi}_k) = \mathrm{Tr}(\mathbf{\Psi}^{\varphi}_{k,nw_q}\mathbf{W}) \qquad \forall\varphi \in \eta_k, \forall k \in N \tag{6.7}$$

$$|V^{\varphi}_k|^2 = \mathrm{Tr}(\mathbf{\Psi}^{\varphi}_{k,nw_v}\mathbf{W}) \qquad \forall\varphi \in \eta_k, \forall k \in N \tag{6.8}$$

which leads to the formation of the three-phase SDP-based OPF model as presented in **M6.2**.

It can be noticed that the constraints (6.9c)-(6.9g) are linear equalities with respect to the OP variables P_g, Q_g and $\mathbf{W}$, and are, therefore, convex. The inequalities (6.9h) and (6.9i) are also linear in nature and are, therefore, convex as well. However, the quadratic equality constraint $\mathbf{W} = \mathbf{V}\mathbf{V}^H$, which is represented in the model through its equivalent representation (6.10), makes this model a non-convex formulation mainly due to the rank-1 constraint (6.9l). It can also be noticed that the model contains additional variables in the form of P_g and Q_g that can be eliminated by substituting (6.9e)-(6.9f) into (6.9h)-(6.9i)

M6.2: Three-phase SDP-based OPF model

$$\textbf{M6.2}: \underset{\Psi}{\textbf{minimize}}\ f(\Psi) \tag{6.9a}$$

$$\textbf{variables}: \quad \mathbf{W} \tag{6.9b}$$
$$P^{\varphi}_{g_k}, Q^{\varphi}_{g_k} \qquad \forall\varphi \in \eta_k, \forall k \in N$$

subject to :

$$\mathrm{Tr}(\mathbf{\Psi}^{\varphi}_{k,nw_p}\mathbf{W}) + P^{\varphi}_{l_k} = 0, \qquad \forall\varphi \in \eta_k, k \in N\backslash G \tag{6.9c}$$
$$\mathrm{Tr}(\mathbf{\Psi}^{\varphi}_{k,nw_q}\mathbf{W}) + Q^{\varphi}_{l_k} - y^{\varphi}_{c_k}\,\mathrm{Tr}(\mathbf{\Psi}^{\varphi}_{k,nw_v}\mathbf{W}) = 0, \qquad \forall\varphi \in \eta_k, k \in N\backslash G \tag{6.9d}$$
$$P^{\varphi}_{g_i} - P^{\varphi}_{l_i} - \mathrm{Tr}(\mathbf{\Psi}^{\varphi}_{i,nw_p}\mathbf{W}) = 0, \qquad \forall\varphi \in \eta_i, i \in G \tag{6.9e}$$
$$Q^{\varphi}_{g_i} - Q^{\varphi}_{l_i} - \mathrm{Tr}(\mathbf{\Psi}^{\varphi}_{i,nw_q}\mathbf{W}) = 0, \qquad \forall\varphi \in \eta_i, i \in G \tag{6.9f}$$
$$|\underline{V_k}|^2 \leq \mathrm{Tr}(\mathbf{\Psi}^{\varphi}_{k,nw_v}\mathbf{W}) \leq |\overline{V_k}|^2, \qquad \forall\varphi \in \eta_k, k \in N^+ \tag{6.9g}$$
$$\underline{P}_{g_i} \leq P^{\varphi}_{g_i} \leq \overline{P}_{g_i}, \qquad \forall\varphi \in \eta_i, i \in G \tag{6.9h}$$
$$\underline{Q}_{g_i} \leq Q^{\varphi}_{g_i} \leq \overline{Q}_{g_i}, \qquad \forall\varphi \in \eta_i, i \in G \tag{6.9i}$$
$$[\mathbf{W}]_{\eta_0\times\eta_0} = \mathbf{V}_0\mathbf{V}_0^H \tag{6.9j}$$
$$\mathbf{W} \succeq 0, \tag{6.9k}$$
$$\mathrm{rank}(\mathbf{W}) = 1 \tag{6.9l}$$

which, in turn, leads to the standard SDP-based OPF model **M6.3** as reported in [264].

$$\mathbf{W} = \mathbf{V}\mathbf{V}^H \Leftrightarrow \begin{cases} \mathbf{W} \succeq 0 \\ \mathrm{rank}(\mathbf{W}) = 1 \end{cases} \tag{6.10}$$

The non-convexity of the original AC-OPF problem **M6.1** is now restricted to the rank-1 constraint (6.9l) which, according to the lift-and-project based concept, can be dropped from the model **M6.3** to it a convex OPF model. The solution of model **M6.1**

M6.3: Three-phase SDP-based OPF formulation

$$\textbf{M6.3}: \underset{\Psi}{\textbf{minimize}}\ f(\Psi) \tag{6.11a}$$

variable : $\mathbf{W} = \mathbf{V}\mathbf{V}^H$

subject to : (6.9c)-(6.9d), (6.9g), (6.9j)-(6.9k) and

$$\underline{P}_{g_i} \leq \mathrm{Tr}(\mathbf{\Psi}^{\varphi}_{i,nw_p}\mathbf{W}) + P^{\varphi}_{l_i} \leq \overline{P}_{g_i}, \qquad \forall\varphi \in \eta_i, i \in G \tag{6.11b}$$
$$\underline{Q}_{g_i} \leq \mathrm{Tr}(\mathbf{\Psi}^{\varphi}_{i,nw_q}\mathbf{W}) + Q^{\varphi}_{l_i} \leq \overline{Q}_{g_i}, \qquad \forall\varphi \in \eta_i, i \in G \tag{6.11c}$$

can be successfully recovered from the solution of model **M6.3** if the latter results satisfies the rank-1 condition. Otherwise, as mentioned in chapter 5, it will be a lower bound to the optimal objective value of model **M6.1** in the case of a minimization problem. Two key observations can be noticed in the model **M6.3**:

1. Phase-ground power injections are considered for wye-connected loads in (6.9c)-(6.9d) and (6.11b)-(6.11c). Consequently, the active and reactive power injections at each phase of a network become decoupled from the injections at other network phases.

2. Constant power loads are considered in (6.9c)-(6.9d) and (6.11b)-(6.11c). As stated earlier at the start of this chapter, the published literature on convex relaxation-based OPF models, except [304], have considered this load type since its power absorption is voltage independent and, therefore, can be easily incorporated in any OPF model. In [304], ZIP loads are handled in the framework of a *single-phase equivalent representation* using voltage magnitude-based variables. However, it is comprehensively demonstrated in section 6.2.2 that this modelling technique fails to correctly take into account the behaviour of a ZIP load in the framework of multi-phase SPG and MPG DNs.

For DNs which incorporate a neutral conductor, it is not possible to extend the model **M6.3** by simply imposing additional active and reactive power balance constraints on the neutral conductor due to the fact that power injections in each phase of a node are not decoupled any more. In such DNs, loads and DGs are connected either between phase-neutral or phase-phase conductors, and, therefore, their apparent power is coupled between these conductors. Furthermore, for the sake of generalization, a full ZIP model should be used in an OPF model of such DNs to comprehensively take into account the voltage dependency of shunt elements. This is due to the fact that constant impedance and constant current loads are part of the overall load connected to a DN [308] and ignoring the impact of their voltage dependency would lead to sub-optimal results. Lastly, it is also important to represent the delta-loads in an OPF model since these elements also exist in a DN; however, up till now as per author's knowledge, no successful attempt has been made to incorporate this load type in an OPF relaxation.

These shortcomings are thoroughly tackled in the next sections where explicit power injections are proposed for each conductor of a network through the CCI approach. Furthermore, a novel complex voltage variable-based methodology is also introduced to incorporate a complete ZIP load in the proposed MPSDP-based OPF relaxation.

6.2 Multi-phase SDP-based OPF relaxation

Consider a typical branch of a 4-wire DN incorporating loads, DGs and grounding impedance as shown in Fig. 6.1. The core idea in CCI approach, as explained in [81], [306], is the representation of any shunt element by a combination of a constant admittance and a suitable current injector, if required. The advantage of this methodology is the easy incorporation of the constant admittance part in a network bus admittance matrix, whereas

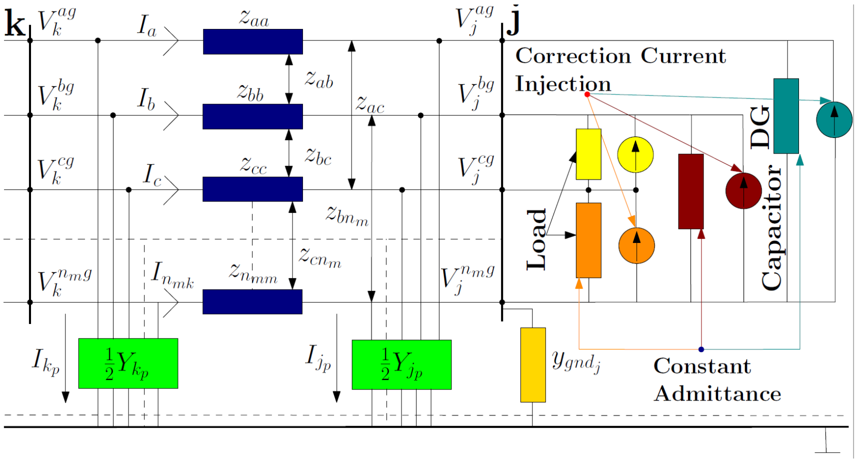

Figure 6.1: Distribution network representation with constant load admittances, correction current injections and earthing admittance.

voltage dependency of a shunt element can be customized by a suitable current injection term based upon its chosen model i.e., Z, I or P. Based on this approach, the apparent power of a single-phase shunt element, referred to the *t-th* iteration of a load-flow, can be written as:

$$S^{*\alpha}_{i_{(t)}} = Y^{\alpha}_{i_{(0)}} |V^{\alpha}_{i_{(t)}}|^2 - V^{\alpha}_{i_{(t)}} \Delta I^{\alpha}_{i_{(t)}} \tag{6.12}$$

where $i \in N$, $\alpha \in \{\upsilon, \sigma\}$, $\upsilon \in \psi_i$, $\sigma \in \chi_i$, ΔI is the correction current injection and $Y_{i(0)}$ is the constant admittance referred to the rated apparent power and voltage values. For wye- and delta-connected loads, $Y_{i_{(0)}}$ is defined as:

$$\text{Wye End-Users:} \quad Y^{\upsilon}_{i_{(0)}} = \frac{S^{*\upsilon}_{i_{(0)}}}{|V^{\upsilon}_{i_{(0)}}|^2} \tag{6.13}$$

$$\text{Delta End-Users:} \quad Y^{\sigma}_{i_{(0)}} = \frac{S^{*\sigma}_{i_{(0)}}}{|V^{\sigma}_{i_{(0)}}/\sqrt{3}|^2} \tag{6.14}$$

where subscript (0) refers to the rated value. On the other hand, the voltage dependency of each component of a ZIP load can be defined through the correction-current injection terms as follows:

$$\text{Constant Impedance} \quad \text{Z:} \quad \Delta I^{\alpha:Z\%}_{i_{(t)}} = 0 \tag{6.15}$$

$$\text{Constant Current} \quad \text{I:} \quad \Delta I^{\alpha:I\%}_{i_{(t)}} = k_I \frac{Y^{\alpha}_{i_{(0)}}}{V^{\alpha}_{i_{(t)}}} (|V^{\alpha}_{i_{(t)}}|^2 - |V^{\alpha}_{i_{(t)}}||V^{\alpha}_{i_{(0)}}|) \tag{6.16}$$

$$\text{Constant Power} \quad \text{P:} \quad \Delta I^{\alpha:P\%}_{i_{(t)}} = k_P \frac{Y^{\alpha}_{i_{(0)}}}{V^{\alpha}_{i_{(t)}}} (|V^{\alpha}_{i_{(t)}}|^2 - |V^{\alpha}_{i_{(0)}}|^2) \tag{6.17}$$

By substituting (6.15)-(6.17) in (6.12), the apparent power of a single-phase shunt element becomes:

$$S^{*\alpha}_{i_{(t)}} = Y^{\alpha}_{i_{(0)}} |V^{\alpha}_{i_{(t)}}|^2 - (\Delta I^{\alpha:I\%}_{i_{(t)}} + \Delta I^{\alpha:P\%}_{i_{(t)}}) V^{\alpha}_{i_{(t)}} \tag{6.18}$$

which can further be expressed for each component of a ZIP LM as follows:

$$S^{*\alpha:Z\%}_{i_{(t)}} = k_Z \cdot Y^{\alpha:Z\%}_{i_{(0)}} |V^{\alpha}_{i_{(t)}}|^2 \tag{6.19}$$

$$S^{*\alpha:I\%}_{i_{(t)}} = (1-k_I) \cdot Y^{\alpha:I\%}_{i_{(0)}} |V^{\alpha}_{i_{(t)}}|^2 + k_I Y^{\alpha:I\%}_{i_{(0)}} (|V^{\alpha}_{i_{(t)}}||V^{\alpha}_{i_{(0)}}|) \tag{6.20}$$

$$S^{*\alpha:P\%}_{i_{(t)}} = (1-k_P) \cdot Y^{\alpha:P\%}_{i_{(0)}} |V^{\alpha}_{i_{(t)}}|^2 + k_p Y^{\alpha:P\%}_{i_{(0)}} |V^{\alpha}_{i_{(0)}}|^2 \tag{6.21}$$

where $Y^{\alpha:(I/Z/P)\%}_{i_{(0)}}$ represent the constant admittance terms related to the constant current, constant impedance and constant power component of a ZIP load at node i, whereas parameters k_Z, k_I and k_P represent the coefficients corresponding to the active and reactive power injections of these components. The subscript t, which represents the t^{th}-iteration of a load flow, becomes irrelevant in the case of an OPF model formulation and, therefore, is dropped in the subsequent formulations. It must be noted that the same voltage dependency for active and reactive power injections i.e., $k_{(Z/I/P)_p} = k_{(Z/I/P)_q}$ is considered in (6.19)-(6.21) to derive a compact form of these injections, and subsequently, the OPF model. However, during the real-time application of proposed scheme, the active and reactive power injections related to the each component of a ZIP load are multiplied by the respective active $k_{(Z/I/P)_p}$ and reactive $k_{(Z/I/P)_q}$ power parameters to correctly take into account their voltage dependency i.e.,

$$\Delta I^{\alpha:I\%}_{i_{(t)}} = k_{I_p} \Re\left\{ \frac{Y^{\alpha}_{i_{(0)}}}{V^{\alpha}_{i_{(t)}}} (|V^{\alpha}_{i_{(t)}}|^2 - |V^{\alpha}_{i_{(t)}}||V^{\alpha}_{i_{(0)}}|) \right\} + k_{I_q} \Im\left\{ \frac{Y^{\alpha}_{i_{(0)}}}{V^{\alpha}_{i_{(t)}}} (|V^{\alpha}_{i_{(t)}}|^2 - |V^{\alpha}_{i_{(t)}}||V^{\alpha}_{i_{(0)}}|) \right\} \tag{6.22}$$

$$\Delta I^{\alpha:P\%}_{i_{(t)}} = k_{P_p} \Re\left\{ \frac{Y^{\alpha}_{i_{(0)}}}{V^{\alpha}_{i_{(t)}}} (|V^{\alpha}_{i_{(t)}}|^2 - |V^{\alpha}_{i_{(0)}}|^2) \right\} + k_{P_q} \Im\left\{ \frac{Y^{\alpha}_{i_{(0)}}}{V^{\alpha}_{i_{(t)}}} (|V^{\alpha}_{i_{(t)}}|^2 - |V^{\alpha}_{i_{(0)}}|^2) \right\} \tag{6.23}$$

6.2.1 Decoupling of apparent power injection between conductors

The apparent powers expressed in (6.19)-(6.21) do not represent the explicit power injections in the conductors (phase-phase or phase-neutral) because of the presence of coupled admittance between them. This suggests that the whole problem of an OPF model development is reduced to split the admittance between the conductors to obtain the explicit representation of power injections. To this extent, it can be achieved by defining load matrices $\mathbf{\Lambda}_{Y_i}$ and $\mathbf{\Lambda}_{\Delta_i}$, corresponding to each node, for both wye- and delta-connected loads, respectively, as reported below:

$$\mathbf{\Lambda}_{Y_i} = \tilde{I}^T_Y * \mathrm{diag}(\hat{L}_{Y_i}) * \tilde{I}_Y \tag{6.24}$$

$$\mathbf{\Lambda}_{\Delta_i} = \tilde{I}^T_\Delta * \mathrm{diag}(\hat{L}_{\Delta_i}) * \tilde{I}_\Delta \tag{6.25}$$

where $\tilde{I}_Y$ and $\tilde{I}_\Delta$ are the incidence matrices and are defined as:

$$\tilde{I}_Y = \begin{bmatrix} 1 & 0 & 0 & -1 \\ 0 & 1 & 0 & -1 \\ 0 & 0 & 1 & -1 \end{bmatrix}; \quad \tilde{I}_\Delta = \frac{1}{\sqrt{3}} \begin{bmatrix} 1 & -1 & 0 & 0 \\ 0 & 1 & -1 & 0 \\ -1 & 0 & 1 & 0 \end{bmatrix}$$

and $\hat{L}_{Y_i} = [Y^{an}_{i(0)}\, Y^{bn}_{i(0)}\, Y^{cn}_{i(0)}]^T$ and $\hat{L}_{\Delta_i} = [Y^{ab}_{i(0)}\, Y^{bc}_{i(0)}\, Y^{ca}_{i(0)}]^T$ are 3×1 vectors containing respective admittances of wye- and delta-connected shunt elements, calculated thorough (6.13)-(6.14), connected to each conductor of a node. Through $\mathbf{\Lambda}_{Y_i}$ and $\mathbf{\Lambda}_{\Delta_i}$, it becomes possible to obtain explicit power injections for each component of a ZIP load connected at node i as expressed below:

$$\mathbf{S}_i^{*Z\%} = \mathbf{V}_i^* \otimes \{\mathbf{\Lambda}_i^Z \mathbf{V}_i\} \tag{6.26}$$

$$\mathbf{S}_i^{*I\%} = \mathbf{V}_i^* \otimes \{(\mathbf{\Lambda}_i^{I_c} - \mathbf{\Lambda}_i^{I})\mathbf{V}_i\} + \mathbf{\Lambda}_i^I(|\mathbf{V}_i| \otimes |\mathbf{V}_{i_{(0)}}|) \tag{6.27}$$

$$\mathbf{S}_i^{*P\%} = \mathbf{V}_i^* \otimes \{(\mathbf{\Lambda}_i^{P_c} - \mathbf{\Lambda}_i^{P})\mathbf{V}_i\} + \mathbf{V}_{i_{(0)}}^* \otimes \{\mathbf{\Lambda}_i^P \mathbf{V}_{i_{(0)}}\} \tag{6.28}$$

where $\mathbf{\Lambda}^{I_c}, \mathbf{\Lambda}^{P_c}$ are the load matrices which are independent of ZIP parameters, whereas load matrices $\mathbf{\Lambda}^Z, \mathbf{\Lambda}^I$ and $\mathbf{\Lambda}^P$ are formed by multiplying the parameters k_Z, k_I and k_P to the admittances of respective load components. It must be noted that the additional OV for the representation of delta loads, as introduced in [301], is no longer needed in this modelling approach since the impact of phase-phase voltages is already included in the delta admittances.

Single-phase loads connected between two phases (e.g., phase a and b) are representable as delta loads. In such a case, the decoupled power injections in these conductors, corresponding to a constant impedance component, can now be expressed as:

$$S_i^{*ag} = Y_i^{ab} * |V_{ag_i}|^2 - Y_i^{ab} * \{V_{ag_i}^* V_{bg_i}\} \tag{6.29a}$$

$$S_i^{*bg} = -Y_i^{ab} * \{V_{bg_i}^* V_{ag_i}\} + Y_i^{ab} * |V_{bg_i}|^2 \tag{6.29b}$$

where voltages are referred to ground g. The above-mentioned equations clearly represent how one can obtain the decoupled power injections related to each conductor of a node. After obtaining these injections, the last step towards establishing a multi-phase OPF model for a DNN is to express them in terms of the OV of proposed approach. However, as shown in the next section, the approach reported in [304] is unable to handle ZIP loads in a multi-phase modelling framework due to the lack of availability of complex voltage variables. Consequently, a new methodology is proposed which generalizes the modelling of a full ZIP load in both single- and multi-phase representation of electrical networks.

Before proceeding further, it is important to mention one last point of equal importance regarding power injections related to constant power and constant current components. Consider the power injections related to constant power component for an end-user connected between phase a and neutral n as follows:

$$S_i^{*ag} = (1-k_P)\{Y_i^{an}|V_{ag_i}|^2 - Y_i^{an}\{V_{ag_i}^* V_{ng_i}\}\} + k_P\{Y_i^{an}|V_{ag_i}^{(0)}|^2 - Y_i^{an}\{V_{ag_i}^{*(0)} V_{ng_i}^{(0)}\}\} \tag{6.30a}$$

$$S_i^{*ng} = (1-k_P)\{Y_i^{an}|V_{ng_i}|^2 - Y_i^{an}\{V_{ng_i}^* V_{ag_i}\}\} + k_P\{Y_i^{an}|V_{ng_i}^{(0)}|^2 - Y_i^{an}\{V_{ng_i}^{*(0)} V_{ag_i}^{(0)}\}\} \tag{6.30b}$$

By substituting $|V_{ag}^{(0)}| = 1$ and $|V_{ng}^{(0)}| = 0$, (6.30a)-(6.30b) can be represented as:

$$S_i^{*ag} = (1 - k_P)\{Y_i^{an}|V_{ag_i}|^2 - Y_i^{an}\{V_{ag_i}^* V_{ng_i}\}\} + k_P\{Y_i^{an}|1|^2\} \tag{6.31a}$$

$$S_i^{*ng} = (1 - k_P)\{Y_i^{an}|V_{ng_i}|^2 - Y_i^{an}\{V_{ng_i}^* V_{ag_i}\}\} + k_P\{Y_i^{an}|0|^2\} \tag{6.31b}$$

It can be noticed that (6.31a) contains one extra term ($k_P\{Y_i^{an}\}$) as compared to (6.31b) and, hence, it can be *wrongly* perceived that the apparent power coming out of the conductor a is not flowing back through the conductor n. However, by setting initial neutral voltage to 0, neutral conductor becomes solidly grounded and, therefore, the apparent power coming out of the conductor a is completing its path by flowing through the ground. Therefore, it is rightly justified to set $V_{ng_i}^0$ in $\mathbf{V}_{i_{(0)}}$ to 0 in (6.27)-(6.28).

6.2.2 Limitation of voltage magnitude-based approach for the representation of a ZIP load

To incorporate a ZIP load, additional 2 × 2 rank-1 matrices Π_i (6.32) are introduced in [304] at each load bus i.

$$\Pi_i = \begin{bmatrix} 1 & |V_i| \\ |V_i| & |V_i|^2 \end{bmatrix} \tag{6.32}$$

In the case of single-phase equivalent representation of electrical networks, the apparent power injection corresponding to a ZIP load can be represented as:

$$S(V_i) = k_Z * |V_i|^2 + k_I * |V_i| + k_P \tag{6.33}$$

and it can be seen that such a power injection can be successfully handled by Π_i. The matrix Π_i, which contains the voltage magnitude terms $|V_i|$, allows to model the constant impedance and constant power components of (6.33) accurately. However, the constant current load only can be represented approximately through it. This is because of the additional PSD and voltage magnitude constraints imposed on the Π_i matrix and its components, respectively, which in turn upper and lower bound the convex feasible space in the Π_i^{22} versus Π_i^{12} plane on the curve $\Pi_i^{12} = \sqrt{\Pi_i^{22}}$. Resultantly, rather than necessarily lying on this curve, the components Π_i^{22} and Π_i^{12} must be within this feasible space and, as a result, the constant current loads can only be represented approximately through this approach. Furthermore, in the case of single-phase networks, voltage V_i is referred with respect to the ground which is at a fixed potential. However, in the case of multi-phase DNs, shunt elements are connected between two conductors whose potentials are floating and, as a result, even the modelling of constant impedance part, which is considered pretty straight forward in the case of single-phase equivalently represented electrical networks, cannot be done by utilizing (6.32) as explained below.

Consider a simple two-phase DN, as shown in Fig. 6.2, which is grounded through a finite impedance and contains a shunt element between phases α and β, respectively. For the sake of clarity, only constant impedance load is considered. For such load type, the apparent power flowing through it can be expressed as:

$$S_i^{\alpha\beta}(V_i) = k_Z * \frac{S_{i_{(0)}}^{\alpha\beta}}{|V_{i_{(0)}}^{\alpha\beta}|^2} * |V_i^{\alpha\beta}|^2 \tag{6.34}$$

It can be noticed in (6.34) that the apparent power, which is coupled between two phases, depends on a voltage magnitude term which is absent in the OV **W**. However, by expressing $|V_i^{\alpha\beta}|^2$ as the product of two complex numbers as shown below:

$$|V_i^{\alpha\beta}|^2 = |V_i^{\alpha g} - V_i^{\beta g}|^2 = (V_i^{\alpha g} - V_i^{\beta g}) * (V_i^{\alpha g} - V_i^{\beta g})^* \tag{6.35}$$

(6.34) can be expressed in terms of complex voltage variables, as can be seen in (6.36)-(6.37), for the active and reactive power injections at phase α.

$$P_i^{\alpha g} = Y_{i_r}^{\alpha\beta}(V_i^{\alpha g} * V_i^{\alpha g*}) + \left\{\frac{-Y_{i_r}^{\alpha\beta} + jY_{i_{im}}^{\alpha\beta}}{2}\right\}(V_i^{\alpha g*} * V_i^{\beta g}) + \left\{\frac{-Y_{i_r}^{\alpha\beta} - jY_{i_{im}}^{\alpha\beta}}{2}\right\}(V_i^{\alpha g} * V_i^{\beta g*}) \tag{6.36}$$

$$Q_i^{\alpha g} = -Y_{i_{im}}^{\alpha\beta}(V_i^{\alpha g} * V_i^{\alpha g*}) + \left\{\frac{Y_{i_{im}}^{\alpha\beta} + jY_{i_r}^{\alpha\beta}}{2}\right\}(V_i^{\alpha g*} * V_i^{\beta g}) + \left\{\frac{Y_{i_{im}}^{\alpha\beta} - jY_{i_r}^{\alpha\beta}}{2}\right\}(V_i^{\alpha g} * V_i^{\beta g*}) \tag{6.37}$$

where r and im represent the real and imaginary parts of a complex quantity. It can be clearly seen in (6.36)-(6.37) that besides the square of voltage magnitude term $(|V_i^{\alpha g}|^2)/(|V_i^{\beta g}|^2)$, these injections also depend on the product of two complex voltages. Since $(V_i^{\alpha g*} * V_i^{\beta g}) \neq (V_i^{\alpha g} * V_i^{\beta g*}) \neq |V_i^{\alpha g}||V_i^{\beta g}|$, (6.36)-(6.37) cannot be represented by (6.32) due to the absence of complex voltage variables in Π_i and, consequently, the approach presented in [304] cannot be directly generalized for ZIP loads connected in a multi-phase DN which generally exhibits high levels of unbalance i.e., significant neutral voltage as regard to the earth potential.

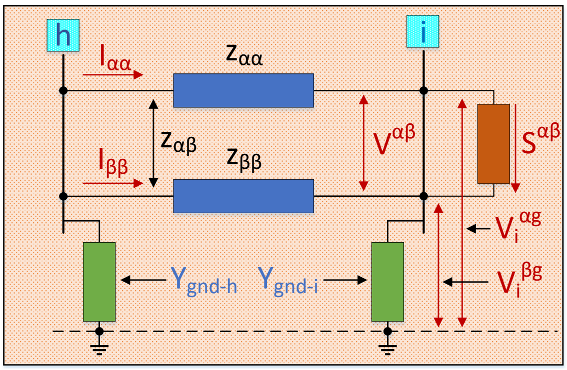

Figure 6.2: A fictitious multiple point grounded DN containing a load between two floating potential phases.

6.3 Complex voltage variable-based modelling of a ZIP load

To express the decoupled power injections (6.26-6.28) of a ZIP load in an OPF model, the following new OV $\hat{\mathbf{W}}$ is adopted.

$$\hat{\mathbf{W}} = \begin{bmatrix} 1_{1\times1} \\ \mathbf{V}_{(|\phi|\times n)\times1} \end{bmatrix} \begin{bmatrix} 1_{1\times1} & \mathbf{V}^H_{1\times(|\phi|\times n)} \end{bmatrix} = \begin{bmatrix} 1_{1\times1} & \mathbf{V}^H_{1\times(|\phi|\times n)} \\ \mathbf{V}_{(|\phi|\times n)\times1} & \mathbf{W}_{(|\phi|\times n)\times(|\phi|\times n)} \end{bmatrix} \tag{6.38}$$

Since this new OV consists of complex voltage variables, one can easily represent each component of a ZIP load through it as described in the following sections.

6.3.1 Representation of constant power element

The representation of constant power (6.28) component is pretty straight-forward due to the presence of square of voltage magnitude terms in their formulation, which are readily available in the sub-matrix $\mathbf{W}$ of new OV. In order to express the power injections, the following matrices are introduced

$$\mathbf{\Gamma}^{\varphi:P\%}_{k,l} = \mathbf{e}^{\varphi}_k * \mathbf{e}^{\varphi T}_k * \mathbf{Y}^P_L \qquad \forall\varphi \in \phi_k, \forall k \in N \tag{6.39}$$

$$\mathbf{\Psi}^{\varphi:P\%}_{k,l_p} = \frac{1}{2}\{\mathbf{\Gamma}^{\varphi:P\%}_{k,l} + (\mathbf{\Gamma}^{\varphi:P\%}_{k,l})^H\} \qquad \forall\varphi \in \phi_k, \forall k \in N \tag{6.40}$$

$$\mathbf{\Psi}^{\varphi:P\%}_{k,l_q} = \frac{j}{2}\{\mathbf{\Gamma}^{\varphi:P\%}_{k,l} - (\mathbf{\Gamma}^{\varphi:P\%}_{k,l})^H\} \qquad \forall\varphi \in \phi_k, \forall k \in N \tag{6.41}$$

where $\mathbf{Y}^P_L$ is the $(n \times \tau) \times (n \times \tau)$ load matrix formed by $\mathbf{\Lambda}^P_{Y/\Delta_i}$ of all nodes and $\mathbf{\Psi}^{\varphi:P\%}_{k,l_p}/\mathbf{\Psi}^{\varphi:P\%}_{k,l_q}$ are the Hermitian matrices related to the active/reactive power injections at each phase of a node. Based upon these matrices, the active and reactive power injections in (6.28) become:

$$P^{\varphi:P\%}_{k,l} = \mathrm{Tr}(\mathbf{\Psi}^{\varphi:P_c\%}_{k,l_p}\mathbf{W}) - \mathrm{Tr}(\mathbf{\Psi}^{\varphi:P\%}_{k,l_p}\mathbf{W}) + \mathrm{Tr}(\mathbf{\Psi}^{\varphi:P\%}_{k,l_p}\mathbf{W}_0) \tag{6.42}$$

$$Q^{\varphi:P\%}_{k,l} = \mathrm{Tr}(\mathbf{\Psi}^{\varphi:P_c\%}_{k,l_q}\mathbf{W}) - \mathrm{Tr}(\mathbf{\Psi}^{\varphi:P\%}_{k,l_q}\mathbf{W}) + \mathrm{Tr}(\mathbf{\Psi}^{\varphi:P\%}_{k,l_q}\mathbf{W}_0) \tag{6.43}$$

where $\mathbf{W}_0 = \mathbf{V}_{int}\mathbf{V}^H_{int}$ and $\mathbf{V}_{int}$ is defined as the vector of initial voltages at all nodes. It can be noticed that $\mathbf{\Psi}^{\varphi:P_c\%}_{k,l_p}/\mathbf{\Psi}^{\varphi:P_c\%}_{k,l_q}$ can be formed by simply replacing $\mathbf{\Lambda}^P_{Y/\Delta_i}$ with $\mathbf{\Lambda}^{P_c}_{Y/\Delta_i}$ in $\mathbf{Y}^P_L$ in (6.39).

6.3.2 Representation of constant impedance element

Following the similar approach as shown above for the constant power element representation, the active and reactive power injections corresponding to constant impedance part can be defined by replacing $\mathbf{Y}^P_L$ with $\mathbf{Y}^Z_L$ (formed by $\mathbf{\Lambda}^Z_{Y/\Delta_i}$) in (6.39) and omitting $\mathrm{Tr}(\mathbf{\Psi}^{\varphi:P_c\%}_{k,l_{p/q}}\mathbf{W})$and $\mathrm{Tr}(\mathbf{\Psi}^{\varphi:P\%}_{k,l_{p/q}}\mathbf{W}_0)$ terms from (6.42) and (6.43), respectively. Resultantly, with the introduction of following matrices (6.44)-(6.46),

$$\mathbf{\Gamma}^{\varphi:Z\%}_{k,l} = \mathbf{e}^{\varphi}_k * \mathbf{e}^{\varphi T}_k * \mathbf{Y}^Z_L \qquad \forall\varphi \in \phi_k, \forall k \in N \tag{6.44}$$

$$\mathbf{\Psi}^{\varphi:Z\%}_{k,l_p} = \frac{1}{2}\{\mathbf{\Gamma}^{\varphi:Z\%}_{k,l} + (\mathbf{\Gamma}^{\varphi:Z\%}_{k,l})^H\} \qquad \forall\varphi \in \phi_k, \forall k \in N \tag{6.45}$$

$$\mathbf{\Psi}^{\varphi:Z\%}_{k,l_q} = \frac{j}{2}\{\mathbf{\Gamma}^{\varphi:Z\%}_{k,l} - (\mathbf{\Gamma}^{\varphi:Z\%}_{k,l})^H\} \qquad \forall\varphi \in \phi_k, \forall k \in N \tag{6.46}$$

the active and reactive power injections related to this component can be defined as:

$$P^{\varphi:Z\%}_{k,l} = \mathrm{Tr}(\mathbf{\Psi}^{\varphi:Z\%}_{k,l_p}\mathbf{W}) \tag{6.47}$$

$$Q^{\varphi:Z\%}_{k,l} = \mathrm{Tr}(\mathbf{\Psi}^{\varphi:Z\%}_{k,l_q}\mathbf{W}) \tag{6.48}$$

6.3.3 Representation of constant current element

The injection related to constant current component contain both linear and square of the voltage magnitude terms in its formulation as shown below.

- Square of the voltage magnitude term $\Rightarrow \mathbf{V}^*_i \otimes \{(\mathbf{\Lambda}^{I_c}_i - \mathbf{\Lambda}^{I}_i)\mathbf{V}_i\}$
- Linear voltage magnitude term $\Rightarrow \mathbf{V}^*_i \otimes \mathbf{\Lambda}^I_i(|\mathbf{V}_i| \otimes |\mathbf{V}_{i_{(0)}}|)$

The first part i.e., the square of voltage magnitude term, is similar to the constant power and constant impedance parts and can, therefore, be expressed in a similar fashion by replacing $\mathbf{Y}^P_L$ with $\mathbf{Y}^I_L$ (formed by $\mathbf{\Lambda}^I_i$) in (6.39). The second part, however, contains a voltage magnitude term which is not available in $\hat{\mathbf{W}}$. Consequently, two additional modelling formulations are proposed in this work which are based on a *first-order Taylor series* and *approximation of the first-order Taylor series* to express the complete injection related to constant current component in terms of the OV $\hat{\mathbf{W}}$.

To express this part, consider the last term in (6.20) for a load connected between the phase a and neutral n of node i.

$$\begin{aligned} S^{*an}_i &= k_I Y^{an}_{i_{(0)}}\{|V^{an}_{i_{(t)}}| \cdot |V^{an}_{i_{(0)}}|\} \\ &= k_I Y^{an}_{i_{(0)}}\left\{\sqrt{(V^{ag}_{i_r} - V^{ng}_{i_r})^2 + (V^{ag}_{i_{im}} - V^{ng}_{i_{im}})^2}\right\} \end{aligned} \tag{6.49}$$

$$S^{*an}_i \approx k_I Y^{an}_{i_{(0)}}\{V^{ag}_{i_r} - V^{ng}_{i_r}\} + k_I Y^{an}_{i_{(0)}}\{V^{ag}_{i_{im}} - V^{ng}_{i_{im}}\} \tag{6.50}$$

$$S^{*an}_i = k_I Y^{an}_{i_{(0)}}\{V^{ag}_{i_r} + V^{ag}_{i_{im}}\} - k_I Y^{an}_{i_{(0)}}\{V^{ng}_{i_r} + V^{ng}_{i_{im}}\} \tag{6.51}$$

It can be noticed that (6.50) is obtained through a *first-order Taylor series* approximation which is evaluated at V_{a_0}. Based on (6.50), the power injected into phase a and neutral n of node i can then be expressed as:

$$S^{*ag}_i = k_I Y^{an}_{i_{(0)}}(\frac{V^{ag}_i + V^{ag*}_i}{2}) + j * k_I Y^{an}_{i_{(0)}}(\frac{-V^{ag}_i + V^{ag*}_i}{2}) \tag{6.52}$$

$$S^{*ng}_i = k_I Y^{an}_{i_{(0)}}(\frac{V^{ng}_i + V^{ng*}_i}{2}) + j * k_I Y^{an}_{i_{(0)}}(\frac{-V^{ng}_i + V^{ng*}_i}{2}) \tag{6.53}$$

It can be noted that (6.52)-(6.53) involve the subtraction of voltage terms which can lead to the poor numerical data input to optimization solver due to the fact that computing softwares, such as MATLAB, do not produce a hard zero and, consequently, an extremely small number ($< 10^{-7}$) causes the solver to either report Numerical Problem (NP) in the optimization model or produce sub-optimal results or make the OP infeasible. The impact of this term on the quality of developed relaxation is discussed in detail in section 6.5.

Fortunately, the second term in (6.52) and (6.53) belongs to the imaginary component of a phase and neutral voltage, and can be dropped under the assumption that in the case of lightly and moderately unbalanced DNs, this term would be small as compared to the real component of these voltages. Moreover, the term $(V_{i_{im}}^{ag} - V_{i_{im}}^{ng})$ in (6.50) can also be ignored in the case of wye-connected loads in these DNs since the imaginary component of a neutral voltage becomes extremely small in comparison to the imaginary component of a phase voltage under such scenario i.e., $V_{i_{im}}^{ng} \ll V_{i_{im}}^{ag}$. Under these assumptions, the explicit power injections at phase a and neutral n can be expressed as:

$$S_i^{*ag} = k_I Y_{i_{(0)}}^{an} (\frac{V_i^{ag} + V_i^{ag*}}{2}) \tag{6.54}$$

$$S_i^{*ng} = -k_I Y_{i_{(0)}}^{an} (\frac{V_i^{ng} + V_i^{ng*}}{2}) \tag{6.55}$$

Theoretically, (6.54)-(6.55) appear to be less accurate as compared to (6.52)-(6.53). However, it is demonstrated in section 6.5 that these injections surpass the OPF relaxation based on (6.52)-(6.53) in terms of exactness, and provide a rank-1 solution in almost all the cases. Before proceeding further, it is important to mention that in order to develop (6.52)-(6.55) for other phases b and c, their voltage vectors in $\hat{\mathbf{W}}$ must be rotated towards the reference position of phase a to have the equivalent power injection in these phases corresponding to the same load attached to them as connected to the phase a. Furthermore, it must also be kept in mind that in the case of highly unbalanced DNs and a large contribution from constant current loads, the approximated power injections related to both wye- and delta-connected loads would lead to sub-optimal results.

The injections in (6.52)-(6.55) can readily be seen as the decoupled injections which can be expressed through $\hat{\mathbf{W}}$ by introducing the following matrix.

$$\boldsymbol{\Upsilon}_{k,l}^{\varphi:I\%} = \hat{\boldsymbol{\Theta}}_k * \mathbf{e}_k^{\varphi} * \mathbf{e}_k^{\varphi T} * \mathbf{Y}_L^{I_D} \qquad \forall \varphi \in \phi_k, \forall k \in N \tag{6.56}$$

where $\mathbf{Y}_L^{I_D}$ is a matrix formed by the diagonal elements of $\mathbf{Y}_L^{I}$ and $\hat{\boldsymbol{\Theta}}_k$ is defined as:

$$\hat{\boldsymbol{\Theta}}_k = \begin{bmatrix} \mathbf{0}_{11} & \cdots & \mathbf{c}_{1k}^{a} * \mathbf{c}_{1k}^{\varphi T} & \cdots & \mathbf{0}_{1n} \\ \vdots & \ddots & \vdots & \ddots & \vdots \\ \mathbf{0}_{n1} & \cdots & \mathbf{0}_{nk} & \cdots & \mathbf{0}_{nn} \end{bmatrix} \tag{6.57}$$

where $\mathbf{c}_k^{\varphi}$ is a standard canonical basis vector of $\mathbb{R}^{|\phi_k| \times 1}$ corresponding to phase φ. Based on (6.38) and (6.56), the active and reactive power injections corresponding to (6.52) for phase a can be written as:

$$P_k^{a:I_{Abs}} = \mathrm{Tr}\left\{\frac{\Re(\mathbf{\Upsilon}_{k,l}^{a:I\%} + \mathbf{\Upsilon}_{k,l}^{a:I\%^T})}{2}\hat{\mathbf{W}}\right\} + j * \mathrm{Tr}\left\{\frac{\Re(-\mathbf{\Upsilon}_{k,l}^{a:I\%} + \mathbf{\Upsilon}_{k,l}^{a:I\%^T})}{2}\hat{\mathbf{W}}\right\} \tag{6.58}$$

$$Q_k^{a:I_{Abs}} = \mathrm{Tr}\left\{\frac{-\Im(\mathbf{\Upsilon}_{k,l}^{a:I\%} + \mathbf{\Upsilon}_{k,l}^{a:I\%^T})}{2}\hat{\mathbf{W}}\right\} + j * \mathrm{Tr}\left\{\frac{\Im(\mathbf{\Upsilon}_{k,l}^{a:I\%} - \mathbf{\Upsilon}_{k,l}^{a:I\%^T})}{2}\hat{\mathbf{W}}\right\} \tag{6.59}$$

whereas the active and reactive power injections related to (6.54) for phase a can be expressed as:

$$P_k^{a:I_{Abs}} = \mathrm{Tr}\left\{\frac{\Re(\mathbf{\Upsilon}_{k,l}^{a:I\%} + \mathbf{\Upsilon}_{k,l}^{a:I\%^T})}{2}\hat{\mathbf{W}}\right\} \tag{6.60}$$

$$Q_k^{a:I_{Abs}} = \mathrm{Tr}\left\{\frac{-\Im(\mathbf{\Upsilon}_{k,l}^{a:I\%} + \mathbf{\Upsilon}_{k,l}^{a:I\%^T})}{2}\hat{\mathbf{W}}\right\} \tag{6.61}$$

In a similar fashion, the expressions for active and reactive power injections can be derived for other phases and neutral conductors as well. The complete injections related to constant current element can now be expressed as:

$$P_{k,l}^{\varphi:I\%} = \mathrm{Tr}(\mathbf{\Psi}_{k,l_p}^{\varphi:I_c\%}\mathbf{W}) - \mathrm{Tr}(\mathbf{\Psi}_{k,l_p}^{\varphi:I\%}\mathbf{W}) + P_{k_{(r)}}^{\varphi:I_{Abs}} \tag{6.62}$$

$$Q_{k,l}^{\varphi:I\%} = \mathrm{Tr}(\mathbf{\Psi}_{k,l_q}^{\varphi:I_c\%}\mathbf{W}) - \mathrm{Tr}(\mathbf{\Psi}_{k,l_q}^{\varphi:I\%}\mathbf{W}) + Q_{k_{(r)}}^{\varphi:I_{Abs}} \tag{6.63}$$

where $P_{k,l}^{\varphi:I_{Abs}}$ and $Q_{k,l}^{\varphi:I_{Abs}}$ become equal to either (6.58)-(6.59) or (6.60)-(6.61) for the *first-order Taylor series-* and *approximation of the first-order Taylor series*-based relaxations, respectively. Lastly, it has to be noted that the diagonal entry in (6.56) for a neutral conductor must be removed before applying (6.58)-(6.61) since it does not appear in the neutral component of (6.53) and (6.55).

6.3.4 Incorporation of grounding impedance

In [21], it has been assumed that the neutral conductor is solidly grounded at each node in a multi-phase DN and, therefore, its impact can be implicitly taken into account through the application of KR methodology. However, this leads to the non-availability of neutral conductor state variables such as voltages and current. Furthermore, in the case of SPG and MPG DNs, the application of KR approach cannot be justified due to the existence of significant neutral voltages and current in this conductor [309], [310]. Therefore, in this work, the grounding impedance connected between a neutral conductor and ground is considered explicitly and, resultantly, the power injections related to it, as expressed below, are incorporated in the proposed OPF model.

$$P_{k,gnd}^{\varphi} = \mathrm{Tr}(\mathbf{\Psi}_{k,gnd_p}^{\varphi}\mathbf{W}) \tag{6.64}$$

$$Q_{k,gnd}^{\varphi} = \mathrm{Tr}(\mathbf{\Psi}_{k,gnd_q}^{\varphi}\mathbf{W}) \tag{6.65}$$

where $\mathbf{\Psi}^{\varphi}_{k,gnd_p}/\mathbf{\Psi}^{\varphi}_{k,gnd_q}$ are determined from (6.40)-(6.41) by replacing $\mathbf{Y}^P_L$ with $\mathbf{Y}_{gnd}$ in (6.39) where $\mathbf{Y}_{gnd}$ is the admittance matrix containing only neutral-ground admittances.

6.4 Convexified OPF model for multi-phase neutral equipped active distribution networks

The centralized MPSDP-based OPF relaxation for DNNs can now be expressed since all active and reactive power injections corresponding to a full ZIP load have been represented explicitly for each phase and neutral conductor. However, it must be noted that all power injections except those shown in (6.58)-(6.61) must be expressed using $\hat{\mathbf{W}}$ instead of $\mathbf{W}$ which can be easily done by appending all Hermitian matrices of the corresponding active and reactive power injections with an additional row and column of zeros. Based on $\hat{\mathbf{W}}$ and extended Hermitian matrices, the resultant injections for a complete ZIP load become:

$$\begin{aligned} P^{\varphi}_{k,l_{inj}} &= \mathrm{Tr}(\hat{\mathbf{\Psi}}^{\varphi:Z\%}_{k,l_p}\hat{\mathbf{W}}) + \mathrm{Tr}(\hat{\mathbf{\Psi}}^{\varphi:P_c\%}_{k,l_p}\hat{\mathbf{W}}) - \mathrm{Tr}(\hat{\mathbf{\Psi}}^{\varphi:P\%}_{k,l_p}\hat{\mathbf{W}}) + \mathrm{Tr}(\hat{\mathbf{\Psi}}^{\varphi:P\%}_{k,l_p}\hat{\mathbf{W}}_0) \\ &+ \mathrm{Tr}(\hat{\mathbf{\Psi}}^{\varphi:I_c\%}_{k,l_p}\hat{\mathbf{W}}) - \mathrm{Tr}(\hat{\mathbf{\Psi}}^{\varphi:I\%}_{k,l_p}\hat{\mathbf{W}}) + P^{\varphi:I_{Abs}}_{k(r)} \end{aligned} \tag{6.66}$$

$$\begin{aligned} Q^{\varphi}_{k,l_{inj}} &= \mathrm{Tr}(\hat{\mathbf{\Psi}}^{\varphi:Z\%}_{k,l_q}\hat{\mathbf{W}}) + \mathrm{Tr}(\hat{\mathbf{\Psi}}^{\varphi:P_c\%}_{k,l_q}\hat{\mathbf{W}}) - \mathrm{Tr}(\hat{\mathbf{\Psi}}^{\varphi:P\%}_{k,l_q}\hat{\mathbf{W}}) + \mathrm{Tr}(\hat{\mathbf{\Psi}}^{\varphi:P\%}_{k,l_q}\hat{\mathbf{W}}_0) \\ &+ \mathrm{Tr}(\hat{\mathbf{\Psi}}^{\varphi:I_c\%}_{k,l_q}\hat{\mathbf{W}}) - \mathrm{Tr}(\hat{\mathbf{\Psi}}^{\varphi:I\%}_{k,l_q}\hat{\mathbf{W}}) + Q^{\varphi:I_{Abs}}_{k(r)} \end{aligned} \tag{6.67}$$

which can be combined with (6.64)-(6.65) to express the multi-phase OPF model for DNNs as shown in **M6.4**. Please note that this model is still a non-convex model but the non-convexity is constrained in (6.68j) which can be dropped to obtain a convexified OPF model. The solution of relaxed model **M6.4** also becomes the solution of model **M6.1** if it satisfies the rank-condition (6.68j), otherwise, it provides a lower bound to the optimal objective value.

6.4.1 Objective functions

The OFs chosen in this study are the minimization of slack-bus power ($\mathbf{OF_1}$) and system active power losses ($\mathbf{OF_2}$) which can be expressed in terms of $\hat{\mathbf{W}}$ as follows:

$$f_{\mathbf{OF_1}}(\hat{\mathbf{W}}) = \sum_{\varphi\in\phi_0} \{\mathrm{Tr}(\hat{\mathbf{\Psi}}^{\varphi}_{0,nw_p}\hat{\mathbf{W}}) + \mathrm{Tr}(\hat{\mathbf{\Psi}}^{\varphi}_{0,nw_q}\hat{\mathbf{W}})\} \tag{6.69}$$

$$f_{\mathbf{OF_2}}(\hat{\mathbf{W}}) = \sum_{(i\sim j)\in E}\sum_{\varphi\in\phi_i} \{(\mathrm{Tr}(\mathbf{\Psi}^{\varphi,nw_p}_{i\longrightarrow j}\hat{\mathbf{W}}) + \mathrm{Tr}(\mathbf{\Psi}^{\varphi,nw_p}_{j\longrightarrow i}\hat{\mathbf{W}})\} \tag{6.70}$$

where $\mathbf{\Psi}^{nw_p}_{i\longrightarrow j}$ represents the line flow and is calculated as:

$$\mathbf{\Psi}^{nw_p}_{i\longrightarrow j} = \frac{1}{2}(\mathbf{A}^H_{i\longrightarrow j}\mathbf{B}_i + \mathbf{B}^H_i\mathbf{A}_{i\longrightarrow j}) \tag{6.71}$$

M6.4: Centralized MPSDP-based OPF formulation

$$\mathbf{M6.4}:\underset{\Psi}{\mathbf{minimize}}\ f(\Psi) \tag{6.68a}$$

variable : $\hat{\mathbf{W}}$

subject to :

$$\mathrm{Tr}(\hat{\mathbf{\Psi}}^{\varphi}_{k,nw_p}\hat{\mathbf{W}}) + \mathrm{Tr}(\hat{\mathbf{\Psi}}^{\varphi}_{k,gnd_p}\hat{\mathbf{W}}) + P^{\varphi}_{k,l_{inj}} = 0, \qquad \forall\varphi \in \phi_k, k \in N \setminus G \tag{6.68b}$$

$$\mathrm{Tr}(\hat{\mathbf{\Psi}}^{\varphi}_{k,nw_q}\hat{\mathbf{W}}) + \mathrm{Tr}(\hat{\mathbf{\Psi}}^{\varphi}_{k,gnd_q}\hat{\mathbf{W}}) + Q^{\varphi}_{k,l_{inj}} = 0, \qquad \forall\varphi \in \phi_k, k \in N \setminus G \tag{6.68c}$$

$$\underline{P}_{g_i} \leq \mathrm{Tr}(\hat{\mathbf{\Psi}}^{\varphi}_{i,nw_p}\hat{\mathbf{W}}) + \mathrm{Tr}(\hat{\mathbf{\Psi}}^{\varphi}_{i,gnd_p}\hat{\mathbf{W}}) + P^{\varphi}_{i,l_{inj}} \leq \overline{P}_{g_i}, \quad \forall\varphi \in \phi_i, i \in G \tag{6.68d}$$

$$\underline{Q}_{g_i} \leq \mathrm{Tr}(\hat{\mathbf{\Psi}}^{\varphi}_{i,nw_q}\hat{\mathbf{W}}) + \mathrm{Tr}(\hat{\mathbf{\Psi}}^{\varphi}_{i,gnd_q}\hat{\mathbf{W}}) + Q^{\varphi}_{i,l_{inj}} \leq \overline{Q}_{g_i}, \quad \forall\varphi \in \phi_i, i \in G \tag{6.68e}$$

$$|\underline{V_k}|^2 \leq \mathrm{Tr}(\hat{\mathbf{\Psi}}^{\varphi}_{k,nw_v}\hat{\mathbf{W}}) \leq |\overline{V_k}|^2, \qquad \forall\varphi \in \eta_k, k \in N^+ \tag{6.68f}$$

$$\hat{\mathbf{W}}_{(1,1)} = 1,\ \hat{\mathbf{W}}_{(2:|\phi_0|,1)} = \mathbf{V}_0,\ \hat{\mathbf{W}}_{(1,2:|\phi_0|)} = \mathbf{V}_0^H \tag{6.68g}$$

$$\hat{\mathbf{W}}_{(2:|\phi_0|,2:|\phi_0|)} = \mathbf{V}_0\mathbf{V}_0^H \tag{6.68h}$$

$$\hat{\mathbf{W}} \succeq 0, \tag{6.68i}$$

$$\mathrm{rank}(\hat{\mathbf{W}}) = 1 \tag{6.68j}$$

where $\mathbf{A}_{i\longrightarrow j}$ and $\mathbf{B}_i$ are defined as:

$$\mathbf{A}_{i\longrightarrow j} = \Big[\mathbf{0}_{|\phi_{ij}|\times\sum_{k=0}^{i-1}|\phi_k|}, \mathbf{Z}_{ij}^{-1}, \mathbf{0}_{|\phi_{ij}|\times\sum_{k=i+1}^{j-1}|\phi_k|}, -\mathbf{Z}_{ij}^{-1}, \mathbf{0}_{|\phi_{ij}|\times\sum_{k=j+1}^{n}|\phi_k|}\Big] \tag{6.72}$$

$$\mathbf{B}_i = \Big[\mathbf{0}_{|\phi_{ij}|\times\sum_{k=0}^{i-1}|\phi_k|}, \mathbf{I}_{|\phi_{ij}|}, \mathbf{0}_{|\phi_{ij}|\times\sum_{k=i+1}^{n}|\phi_k|}\Big] \tag{6.73}$$

Lastly, a detailed derivation representing the link between electrical quantities and mathematical OVs related to the power injections, line flow and both OFs are presented in appendix A.1 for better clarity.

6.5 Quality assessment of the proposed relaxation

In this section, the quality of proposed MPSDP-based OPF relaxation **M6.4** in terms of recovered solution and CT is reported for several combinations of ZIP load parameters and grounding impedance values. For this purpose, five different ADNs, varying in size and degree of unbalance, are chosen. The networks, in addition to the two test networks which are reported in chapters 3 and 4, include three additional networks termed as MG-10 bus, CIGRE-13 bus and IT-111 bus. The degree of unbalance of these DNs is reported in Table 6.2, whereas their complete data can be found in appendices B-F. For all simulation scenarios, $\underline{V}$ and $\overline{V}$ are set to 0.90 and 1.05pu, respectively and lastly, the simulations are carried out using MATLAB-based tool box YALMIP [311] along with the MOSEK solver.

6.5.1 Criteria for numerical exactness

Three metrics namely EVR [302], [312], power mismatch at load (PQ) buses [246] and Cumulative Normalized Constraint Violation (CNCV) [313] are used to check the optimality and feasibility of the recovered solution provided by the proposed relaxation for several combinations of LMs [308] which are shown in Table 6.1.

The EVR is defined as the ratio between the two largest eigenvalues of the obtained solution ($\hat{\lambda}_P$ and $\hat{\lambda}_{P-1}$) which are recovered from the Hermitian matrix $\hat{\mathbf{W}}$ having dimensions equal to $P = n \times \tau + 1$. Ideally, all eigenvalues except one of this matrix should be zero if its recovered rank is 1. However, due to the limited numerical precision of SDP solvers, it is not possible to satisfy the rank-1 condition (6.68j) even though the relaxed problem is exact. The EVR is calculated as $|\hat{\lambda}_{P-1}|/|\hat{\lambda}_P|$ where $|\hat{\lambda}_{P-1}|/|\hat{\lambda}_P| \geq 0$ and the obtained solution is considered as a rank-1 solution for $|\hat{\lambda}_{P-1}|/|\hat{\lambda}_P| \leq 10^{-5}$. It is important to mention that %Optimality Gap (OG) is another metric [276], [278] which is normally used to check the difference between the objective values of a relaxation and its non-convex model which is normally solved by a non-linear solver such as IPOPT [314] etc. However, in this work, several open source non-convex solvers such as IPOPT [314], FMINCON, FilterSD [315] and SNOPT [316] failed to solve the multi-phase non-convex OPF model. Consequently, the %OG metric is not used to check the optimality of the obtained solution.

Due to the heuristic nature of EVR criterion (selection of 10^{-5} is user dependent) and the inability of implementing %OG metric, power mismatch and CNCV metrics are utilized as additional criteria to check the feasibility of proposed relaxation. The power mismatch criterion checks the power balance constraint at each load bus once the relaxation is solved. In case of a feasible recovered solution, the active and reactive power mismatch at each load bus must be zero.

In the original CNCV criterion, the distance to AC feasibility is calculated if convex relaxation provides an infeasible solution. For this purpose, a simple power flow is run by setting the *initial voltages* at network buses and *active/reactive power set-points* of DGs equal to the values obtained from the *infeasible* solution and after obtaining the feasible

Table 6.1: Active and reactive power absorption/injection coefficients of ZIP load models.

Load Models and their Parameters													
LMs	$\mathbf{P_L}$			$\mathbf{Q_L}$			**LMs**	$\mathbf{P_L}$			$\mathbf{Q_L}$		
	k_Z	k_I	k_P	k_Z	k_I	k_P		k_Z	k_I	k_P	k_Z	k_I	k_P
LM:1	1	0	0	1	0	0	**LM:6**	1.21	-1.61	1.41	4.35	-7.08	3.72
LM:2	0	1	0	0	1	0	**LM:7**	1.21	-1.61	1.41	1.21	-1.61	1.41
LM:3	0	0	1	0	0	1	**LM:8**	0.3	0	0.7	0.5	0	0.5
LM:4	1.56	-2.49	1.93	10.1	-16.75	7.65	**LM:9**	0.88	-0.21	0.34	0.83	-0.05	0.22
LM:5	0.57	-0.22	0.65	0.57	-0.22	0.65	**LM:10**	0.07	-0.26	1.19	0.59	0.65	-0.24

solution from power flow, the following CNCV parameter is determined.

$$x_{viol} = \sum_{k \in \mathbf{X}} \frac{max(x_k^{AC-PF} - \overline{x}_k, \underline{x}_k - x_k^{AC-PF}, 0)}{\overline{x}_k - \underline{x}_k} \times 100\% \tag{6.74}$$

where $x = \{P_g^{\varphi}, Q_g^{\varphi}, |V^{\varphi}|\}$ and $\mathbf{X} = \{G, G, N\}$. However, in this work, this criterion is slightly modified by replacing the state variables values obtained from the power flow (x_k^{AC-PF}) with the state variables values obtained from the OPF relaxation ($x_k^{OPF-Rlx}$) to determine if the voltage at any phase of a node and the active/reactive power set-points of DGs have violated the constraints (6.68f), and (6.68d)-(6.68e), respectively. A cumulative value of 0 indicates that a state variable has not violated its FR and, therefore, the obtained optimal value is a feasible one. In the case of non-zero cumulative value, (6.74) can, subsequently, be used to determine the distance of state variables to the feasibility point.

6.5.2 Exactness in terms of eigen-value ratio criterion

Table 6.2 summarizes the results on the exactness, and lack thereof, of proposed relaxation in terms of EVR criterion. Please note that the ***bold-italic*** faced values represent the cases where relaxation becomes inexact. The following observations can be made from the obtained results:

1. For all LMs which involve constant current components, the relaxation based on the *first-order Taylor-series approximation* either fails to converge (NP/bad conditioning) or reports Rank-2 (R2) or greater than R2 solution. This is mainly due to the subtraction of same voltage terms in (6.52)-(6.53) which leads to extremely small coefficients in the power balance constraints and, consequently, solvers, such as MOSEK, fails to compute a meaningful solution. The relaxation based on the *first-order Taylor-series approximation* is reported only for the OF1 since almost the same results are obtained in the case of OF2, and therefore, they are not reported here.

2. For the sake of avoiding repetition about the approach used for constant current component modelling, it should be noted that in the following points, the exactness, and lack-thereof, of proposed MPSDP-based OPF relaxation is discussed when it is modelled through the *approximation of the first-order Taylor series* approach.
   For all LMs which are independent of constant current component, an exact solution is obtained for all load types and DNs irrespective of their degree of unbalance.

3. For wye-connected loads in lightly and moderately unbalanced DNs, the proposed relaxation provides an exact solution for all LMs when tested for both OFs. However, in the case of delta loads, the same trend is not observed for the LMs 4 and 6 in the case of OF2. Since these LMs contain a large contribution from the constant current component, ignoring the imaginary component of phases voltage leads to the inaccurate power injections in phase conductors and, consequently, a poor EVR is

Table 6.2: Quality of the proposed MPSDP-based OPF relaxation for $R_{gnd} = 1\Omega$.

LMs	**EigenValue Ratio $\lvert\hat{\lambda}_{P-1}\rvert/\lvert\hat{\lambda}_{P}\rvert \times 10^{-5}$**														
	Y End-Users					**Δ End-Users**					**Y-Δ End-Users**				
	MG	IT-37	IT-111†	CIGRE	IEEE	MG	IT-37	IT-111†	CIGRE	IEEE	MG	IT-37	IT-111†	CIGRE	IEEE
	LuB	*MuB*	*MuB*	*HuB*	*HuB*	*LuB*	*MuB*	*MuB*	*HuB*	*HuB*	*LuB*	*MuB*	*MuB*	*HuB*	*HuB*
OF:1 Slack Bus Power (kVA) based on the first-order Taylor Series Relaxation															
LM:1	0.32	0.34	-	1.09	0.66	2.86	0.11	-	1.58	3.17	1.12	0.47	-	0.93	1.17
LM:2	>R2	R2	-	R2	>R2	>R2	>R2	-	>R2	>R2	>R2	>R2	-	>R2	>R2
LM:3	0.16	0.84	-	0.72	1.50	1.18	0.51	-	0.92	0.74	0.17	0.48	-	1.27	2.21
LM:4	NP	R2	-	R2	NP	NP	>R2	-	R2	>R2	>R2	>R2	-	>R2	>R2
LM:5	>R2	R2	-	R2	>R2	>R2	>R2	-	>R2	>R2	>R2	>R2	-	>R2	>R2
LM:6	>R2	R2	-	R2	NP	>R2	>R2	-	R2	>R2	NP	>R2	-	>R2	>R2
LM:7	>R2	R2	-	R2	NP	NP	>R2	-	>R2	>R2	NP	>R2	-	>R2	>R2
LM:8	1.27	0.65	-	0.83	4.10	0.11	0.15	-	1.50	1.85	0.28	0.35	-	1.20	9.20
LM:9	>R2	>R2	-	>R2	>R2	NP	>R2	-	>R2	>R2	>R2	R2	-	>R2	>R2
LM:10	>R2	>R2	-	>R2	>R2	>R2	>R2	-	>R2	>R2	>R2	>R2	-	>R2	NP
OF:1 Slack Bus Power (kVA) based on Approximation of the first-order Taylor Series Relaxation															
LM:1	0.32	0.34	6.43	1.09	0.66	2.86	0.11	0.17	1.58	3.17	1.12	0.47	4.96	0.93	1.17
LM:2	0.15	1.34	3.18	1.02	0.54	0.72	0.28	0.87	1.39	4.91	1.65	0.93	2.88	0.90	1.69
LM:3	0.16	0.84	2.33	0.72	1.50	1.18	0.51	0.20	0.92	0.74	0.17	0.48	1.94	1.27	2.21
LM:4	0.30	1.96	6.93	***13.1***	3.26	0.05	1.87	9.34	***1680***	***5870***	***55.2***	***110***	***52.4***	***120***	2.79
LM:5	0.15	0.56	0.89	0.77	1.36	2.26	0.46	2.42	0.78	0.53	0.17	0.53	1.73	1.25	2.02
LM:6	0.28	1.47	1.32	7.03	***11.4***	0.15	0.36	8.78	***63.3***	***170***	0.40	0.93	6.23	4.44	3.78
LM:7	0.04	0.44	1.87	3.11	1.34	0.16	0.18	3.44	1.93	0.40	1.53	0.28	3.77	2.21	1.15
LM:8	1.27	0.66	9.85	0.82	4.89	0.11	0.15	0.63	1.52	0.14	0.28	0.34	1.90	1.18	3.84
LM:9	0.10	0.14	6.07	1.32	4.13	3.81	0.22	1.32	1.59	1.20	0.03	0.77	1.31	0.85	1.02
LM:10	0.18	0.19	5.35	1.16	3.33	0.32	0.17	0.87	0.88	0.89	0.25	0.18	3.47	1.84	5.97
OF:2 Network Losses (kW) based on Approximation of the first-order Taylor Series Relaxation															
LM:1	0.73	1.50	6.66	6.95	3.71	0.06	0.49	0.87	1.43	0.84	0.31	0.74	8.04	1.62	4.23
LM:2	0.70	0.48	5.09	1.90	0.75	0.03	0.22	1.34	3.67	1.87	0.20	0.24	7.25	1.38	0.54
LM:3	0.25	0.43	6.96	0.42	0.36	0.11	0.24	0.51	3.64	0.66	0.20	0.61	5.53	1.86	4.09
LM:4	0.06	0.43	9.20	1.46	***30.0***	0.36	***26.4***	***611***	***581***	***6028***	***71.0***	***69.6***	***78.3***	***89.1***	***76.5***
LM:5	0.03	0.22	8.91	2.31	2.51	0.54	0.33	2.92	0.43	0.95	0.15	1.17	6.34	1.32	2.00
LM:6	0.24	0.90	9.07	2.37	***32.0***	0.23	0.60	***527***	1.86	***317***	0.52	3.00	8.89	1.15	7.42
LM:7	0.10	0.25	6.60	1.13	1.01	0.25	0.21	6.04	3.04	1.03	0.46	0.55	8.98	0.77	3.58
LM:8	0.93	2.14	9.20	1.98	1.79	1.13	0.28	0.17	1.31	0.34	1.24	0.25	7.59	0.34	0.65
LM:9	0.12	0.45	2.85	2.19	0.78	0.83	0.43	0.98	0.85	0.28	0.07	0.57	2.32	1.02	1.02
LM:10	0.27	0.54	3.08	5.66	1.56	0.46	0.52	3.93	0.21	0.65	1.23	0.65	3.53	0.38	3.58

R2: rank-2 †: Memory Limit *LuB*: Lightly Unbalanced *MuB*: Moderately Unbalanced *HuB*: Highly Unbalanced

obtained as can be noticed for the IT-37 bus DN. On the other hand, in the case of wye-connected loads, since the neutral voltage is relatively small as compared to the phase voltage, the proposed relaxation remains valid for these LMs.

4. In the case of highly unbalanced DNs, rank-2 solution is obtained for the wye-connected loads in the case of LMs 4 and 6, whereas for the delta-connected loads, the relaxation fails to provide a meaningful solution as can be noticed by the large EVR which, consequently, makes the rank of $\hat{\mathbf{W}}$ greater than 2.

5. In the case of mixed wye- and delta-connected loads, the proposed methodology exhibits the same behaviour as reported in the case of explicit load types i.e., for a small power injection/absorption from a constant current load, the relaxation is exact for both OFs, whereas under a large contribution from this load, the relaxation

gives a sub-optimal solution.

6. It is also worth mentioning that the exactness, and lack thereof, of proposed relaxation also depends upon the quality of the OF i.e., if the polynomial of OF contains coefficients ranging from extremely small values to extremely high values, the solver has a higher tendency to produce sub-optimal results. For example, in the case of IEEE-13 and CIGRE DNs, the network losses OF ranges from (1.14×10^{-13} - 3.13×10^{5}) and (3.5×10^{-15} - 1.4×10^{4}), respectively, and therefore, apart from being highly unbalanced DNs, the poor numerical input data to optimization solver also leads to the rank-2 or completely meaningless solution. YALMIP provides a *clean* command which can remove lower coefficients from the polynomial of OF and system constraints and it has been observed that in some cases, implementing this function leads to the exact solution. However, this is not always the case since this command removes useful information from the OF and, consequently, makes the OP infeasible as experienced in some other cases. Therefore, its usage cannot be generally encouraged.

6.5.3 Exactness in terms of power mismatch and CNCV criteria

As stated earlier EVR is a heuristic criterion i.e., selection of 10^{-5} as a threshold value, for classifying the obtained solution as a rank-1 or higher than rank-1 solution, is totally user dependent. Therefore, to categorize a solution for which the obtained EVR is close to 10^{-4} as a rank-1 or higher than rank-1 solution, additional criteria must be utilized. In this context, power mismatch and CNCV criteria are also evaluated in this study to determine the exactness of obtained solution. The threshold value for power mismatch criterion is chosen as 10^{-2} [W/VAr], which is lower than the usually specified tolerance value of 10^{-1} in power flow solution packages such as PSS/E, and any recovered solution which violates this threshold at any of the load buses is considered as a suboptimal (rank-2) or a completely meaning less (higher than rank-2) solution. On the other hand, the obtained solution which indeed satisfies the power balance equalities at all load buses (6.68b)-(6.68c) as well as the voltage constraints at all network buses (6.68f) but has an EVR very close to 10^{-4} can be considered as rank-1 solution. To evaluate the feasibility and optimality of proposed relaxation using these criteria, Figs. 6.3-6.5 represent the active and reactive power mismatch and recovered voltage values at all phases for all load types (wye, delta and mixed wye-delta). The following observations can be made from the presented results.

1. For wye-connected loads, in the case of lightly and moderately unbalanced DNs, the *apparent* exactness of proposed relaxation, as perceived by the satisfaction of EVR criterion, is further supported by the non-violation of other two criteria for all LMs. Consequently, the obtained solution is regarded as an optimal and feasible solution. On the other hand, for highly unbalanced DNs specifically IEEE-13 bus network, a higher EVR is obtained in the case of LMs 4 and 6 which makes the relaxation inexact and, consequently, as per expectation, the active and reactive power mismatch for

these LMs have also violated the specified threshold level as can be noticed by the extreme quartiles (Figs. 6.3a-6.3b), which indicate that the constraints (6.68b)-(6.68c) are weakly satisfied. However, in the case of CNCV criterion, a value of 0 is obtained for all test cases. Since this criterion is satisfied for all LMs and DNs, it is, therefore, pointless to represent a table showing 0 values for all the state variables. Instead voltage feasibility is presented in Fig. 6.3c which clearly shows that the recovered voltages at all nodes remain within the prescribed voltage limits. The obtained value of CNCV criterion *apparently* contradicts the results obtained from EVR and power mismatch criteria in a sense that one should also expect the network voltages, in the case of LMs 4 and 6, to violate the voltage FR. However, this is not the case due to the fact that initial voltages are set to 1.05pu at all buses in this case, rather than 1.0pu as per the given IEEE data sheet, and this allows the voltages at all buses to stay above the lower limit value[1]. Consequently, the obtained solution, although remains feasible with respect to the voltage values, is considered as a suboptimal solution due to the violation of EVR and power mismatch criteria. However, in the case of LMs having lower contribution from the constant current load, all three criteria are satisfied for this network, and, therefore, the obtained optimal solution is considered exact for all such cases.

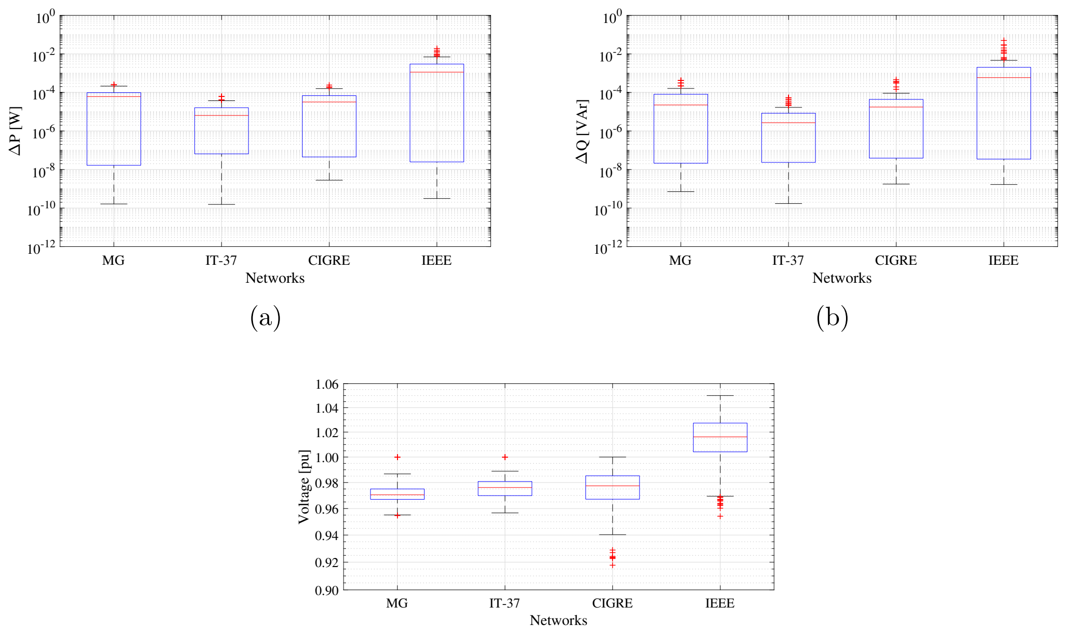

(a) (b) (c)

Figure 6.3: Impact of wye-connected loads on power mismatch and CNCV criteria (a) active power mismatch (b) reactive power mismatch (c) phase voltages.

[1]The initial voltage level is set to 1.05pu due to the fact that network is heavily loaded and setting an initial value equal to 1.0pu causes the voltage to violate the lower limit even in the case of a simple power flow study. Therefore, in order to obtain a feasible solution, the voltages on secondary side of RG60 are raised to 1.05pu.

2. For delta-connected loads, the obtained EVR is well below the threshold level in the case of lightly unbalanced DN and, resultantly, as per expectation, the active and reactive power mismatch criterion is also satisfied as well as the voltages at all nodes remain within the prescribed FR for all tested LMs. Consequently, the relaxation is considered exact for this DN. However, for the moderately and highly unbalanced DNs, the lower voltage limit is violated at multiple buses in the case of LMs 4 and 6 as can be seen in Fig. 6.4c. Similarly, the active and reactive power constraints at few of the load buses are weakly satisfied as can be observed by the extreme quartiles in Figs. 6.4a-6.4b which are above or very close to the specified threshold value. In the case of moderately unbalanced networks, although all three criteria are violated but it can be noticed that the recovered solution is still close to the specified tolerance levels of these criteria and, therefore, can be considered as a rank-2 solution. However, this is not the case for the latter DNs and, consequently, the extremely large EVR and the severe violation of lower voltage limit classify the obtained solution as a higher than rank-2 solution. On the other hand, the relaxation provides an exact solution for these DNs under moderate contribution from the constant current loads as evident by the satisfaction of all feasibility and optimality criteria.

3. In the case of mixed wye- and delta-connected loads, the same trend, as shown in Figs. 6.5a-6.5c, is observed as reported in points 1 and 2 for the explicit load

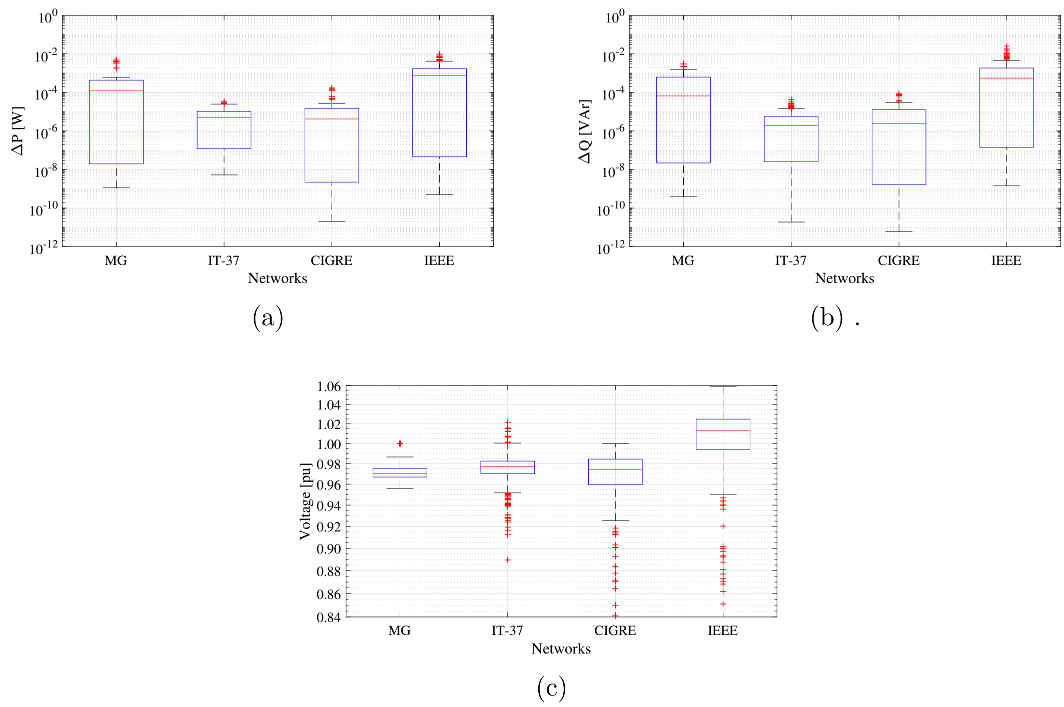

Figure 6.4: Impact of delta-connected loads on power mismatch and CNCV criteria (a) active power mismatch (b) reactive power mismatch (c) phase voltages.

types. The relaxation is exact for all LMs having lower contribution, in terms of power injection/absorption, from the constant current load since no violation of the selected criteria is observed for any test network. However, in the case of LM 4, a higher EVR is obtained for all DNs and, consequently, the apparent inexactness (due to the high EVR) is also supported by the violation of lower voltage limit and power mismatch threshold. Consequently, the obtained solutions for all DNs can easily be categorized as suboptimal solutions.

4. The power mismatch and CNCV criteria also suggest that in the case of a *perceived* rank-2 solution on the basis of a higher but relatively close EVR to the specified threshold value i.e., 10^{-5}, it is plausible that the obtained solution might not violate the other two criteria. In such a case, the recovered solution can be considered as a rank-1 solution and it is justified to say that the chosen EVR criterion is quite stringent in terms of characterizing the obtained solution as a rank-1 or higher than rank-1 solution.

5. With the increase in degree of unbalance i.e., from IT-37 to IEEE-13, an interesting observation can be made about the median value of power mismatch criterion which starts increasing with an increase in the degree of unbalance for all load types. In the case of IT-37 and CIGRE DNs, which are relatively less unbalanced in comparison to IEEE-13, the median value of both active and reactive mismatch remains within $10^{-6} - 10^{-4}$ [W/VAr], whereas in the case of IEEE-13 bus network, the median

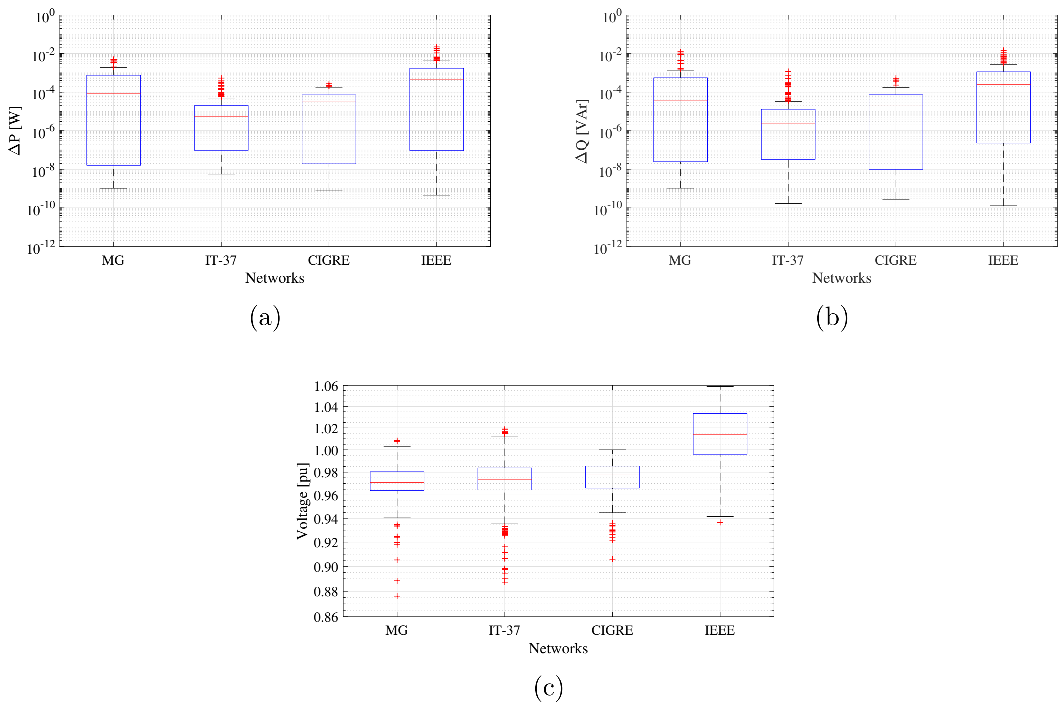

Figure 6.5: Impact of mixed wye/delta-connected loads on power mismatch and CNCV criteria (a) active power mismatch (b) reactive power mismatch (c) phase voltages.

value stays between $10^{-4} - 10^{-3}$ [W/VAr] range. Consequently, it is perceivable that a higher rank solution can be obtained for a highly unbalanced DN particularly if it is serving a large load of constant current type. However, the same trend is not observed for the lightly unbalanced MG DN which represents a higher median value of power mismatch as compared to the value obtained in the case of IT-37 and CIGRE DNs. This is due to the fact that some branches/lines in the network are extremely short and, as a result, the poor numerical data in the admittance matrix (high admittance values related to these lines) of this network causes the solver to provide an inferior solution.

6. For IT-111 bus system, MOSEK is unable to solve the developed OPF relaxation due to the large dimensions of $\hat{\mathbf{W}}$ which, in turn, leads to the formation of extremely large number of internally generated constraints (∼130k) and causes the solver to hit its memory limit. Consequently, for this network, a cheap conic SDP-based OPF relaxation termed as BFM-based SDP relaxation, which is presented in chapter 7, is solved. Please note that the proposed MPSDP-based OPF relaxation generalizes (more tighter) the cheap conic SDP-based OPF relaxation even in the case of RDNs unless an equivalence is established between them for this network type. Despite being weaker, an exact solution is obtained in almost all cases (two delta load cases are inexact) through the cheap conic relaxation as evident by the results shown in Table 6.2. These results clearly indicate that being more tighter than the cheap conic relaxation, MPSDP-based OPF relaxation will definitely provide an exact solution with the emergence of more stable and advanced SDP solvers.

7. It must be noted that other SDP solvers such as SeDuMi [317], CSDP [315], DSDP [315] and SDPT3 [318] are been utilized to solve the model **M6.4** but all of them reported either NP or produced sub-optimal results. It is expected that with the advancements in SDP solvers, a higher EVR and, consequently, a more accurate solution will be obtained, but as per author knowledge, MOSEK is the only commercially available and widely used solver for SDP problems because of its reliability (even in the case of poor numerical data) and high computational efficiency.

6.5.4 Exactness of the proposed relaxation under time varying load and DG profiles

In previous sections, the exactness of MPSDP-based OPF relaxation is tested under extreme loading conditions i.e., rated load and generation profiles are used which put maximum stress on DNs. However, in real-time, load profiles rarely touch their peak levels and remain well below their rated level. Resultantly, a more realistic case study is presented in this section to evaluate the exactness of proposed relaxation under two LMs 4 and 9 for time-varying loads and DGs profiles. The chosen LMs represent two extremes in terms of contribution from the constant current load. For each LM, the following two case studies are carried out.

Case-1: Time varying loads and DGs profiles

Case-2: Time varying loads and rated DGs profiles

The simulations are carried out for one day and the same three criteria, as reported in section 6.5.1, are utilized for the evaluation of both case studies. Figs. 6.6-6.9 show the results for LM 4 whereas Figs. 6.10-6.13 show the results for LM 9. The following observations can be made from the obtained results.

1. With respect to the case study 1 and LM 4, the relaxation appears to be exact in the case of CIGRE DN as evident by the satisfaction of all criteria i.e., the EVR is less than 1×10^{-4}, the extreme quartiles in the case of power mismatch remain well below the specified threshold value and the recovered voltages at all nodes stay within the FR over the whole simulation period as can be noticed from the obtained results shown in Figs. 6.6a-6.9a. In the case of MG DN, the relaxation remains exact over a large number of time instants with inexactness observed only at those few instants when either there is no output from the connected DGs or the system is heavily loaded without enough output from DGs to support the system voltage locally. Consequently, the active and reactive power constraints at load buses are weakly satisfied (Figs. 6.7a and 6.8a) and voltage violations are also noticed at few network buses (Fig. 6.9a). In the case of IEEE-13 node network, which is highly unbalanced, the EVR remains above the specified threshold level over the complete simulated time period except at few instants. Consequently, one can also notice that the active and reactive power mismatch values become as large as 10^{0} in the case of extreme quartiles. Furthermore, the median value of power mismatch has also increased and lies in the range of $10^{-3} - 10^{-2}$ [W/VAr], which is significantly higher than the median value observed in the case of MG $(10^{-4} - 10^{-3})$ [W/VAr] and CIGRE $(10^{-5} - 10^{-4})$ [W/VAr] DNs. These findings, therefore, confirm the previously reported statement that in a highly unbalanced DN which is serving large constant current loads, the approximate modelling of such loads leads to extremely poor and suboptimal solutions.

2. With respect to the case study 2 and LM 4, it can be noticed in Fig. 6.6b that the

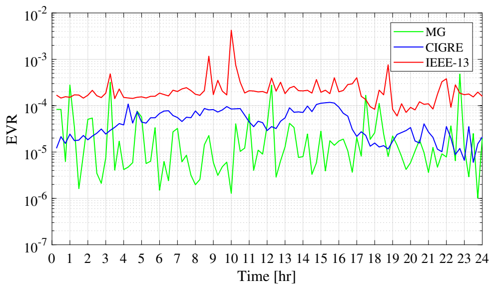

(a)

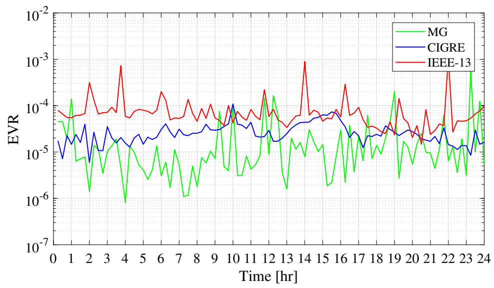

(b)

Figure 6.6: Impact of end-users profiles on eigenvalue ratio for load model 4 (a) both load and generation profiles are time varying (b) time varying load and rated (fixed) generation profiles.

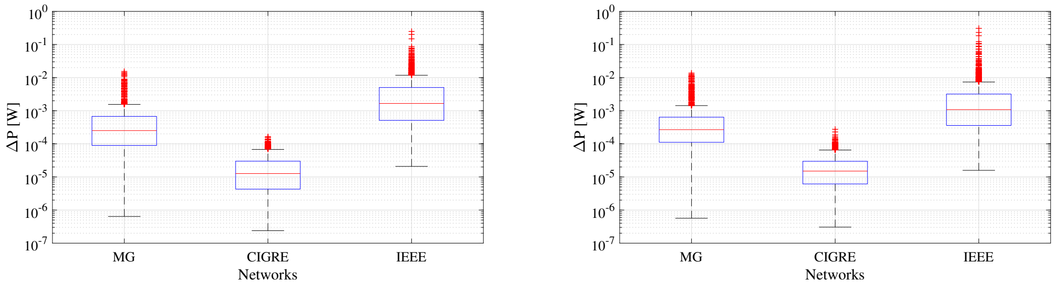

(a) (b)

Figure 6.7: Impact of end-users profiles on active power mismatch for load model 4 (a) both load and generation profiles are time varying (b) time varying load and rated (fixed) generation profiles.

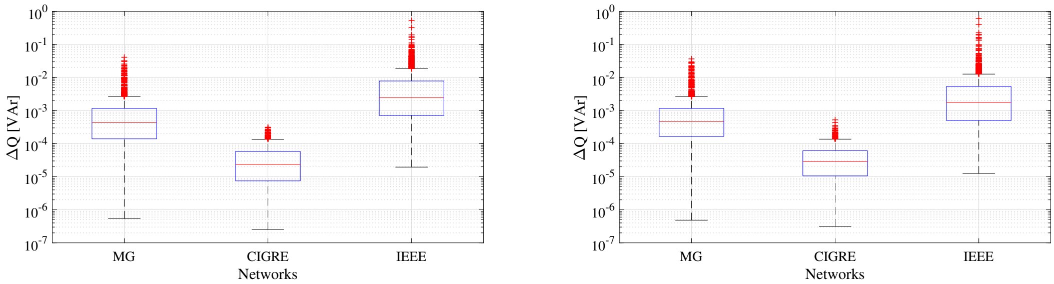

(a) (b)

Figure 6.8: Impact of end-users profiles on reactive power mismatch for load model 4 (a) both load and generation profiles are time varying (b) time varying load and rated (fixed) generation profiles.

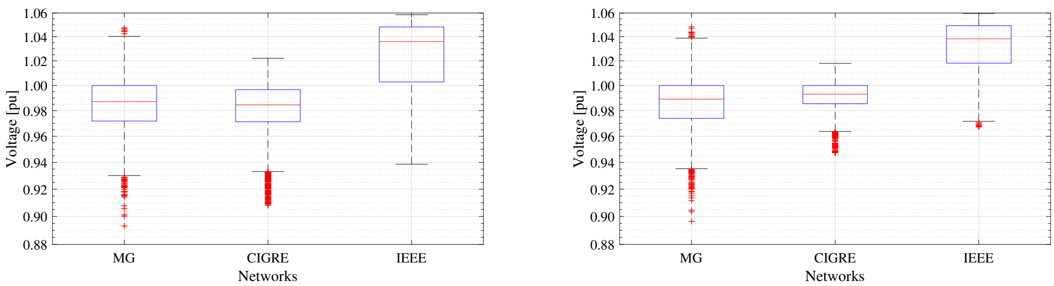

(a) (b)

Figure 6.9: Impact of end-users profiles on recovered voltages for load model 4 (a) both load and generation profiles are time varying (b) time varying load and rated (fixed) generation profiles.

EVR has improved for all DNs and, in particular, less violations have been observed for MG and IEEE-13 bus DNs. Furthermore, the median value of power mismatch has also reduced slightly, as can be seen in Figs. 6.7b-6.8b, despite the fact that extreme quartiles in this case still have the same value as observed in case study 1. Similarly, the median value of recovered voltages has also increased for all DNs and fewer extreme quartiles are observed indicating less voltage violations. These results clearly indicate that the proposed relaxation has tightened as compared to the case study 1 which involves both time-varying load and DG profiles.

3. The previous discussion shows that even for LM 4, which involves a large contribution from the constant current load and shows inexactness in the extreme network loading scenario, the MPSDP-based OPF relaxation has a tendency to remain exact under realistic time-varying load and rated DG profiles. However, the *degree of unbalance* and *network physical characteristics* play a significant role in this matter. With respect to the network physical characteristics, both MG and IEEE-13 bus DNs contain some branches of extremely short length[2] and, as a result, the violation of EVR criterion is observed for these DNs. Moreover, the relaxation is further exacerbated for the IEEE-13 node network because of its highly unbalanced nature. On the other hand, although the CIGRE network is also highly unbalanced, the relaxation provides an optimal solution over the whole simulation range in both case studies due to its well connected graph. These results show that one can expect an exact solution even in the case of a large injection/absorption from a constant current load being served by a highly unbalanced network, provided it is well connected and does not provide any ill-conditioned data to an SDP solver.

4. With respect to LM 9, it can be noticed in Figs. 6.10-6.13 that under the mild contribution from constant current load, the relaxation provides an exact solution for both MG and CIGRE DNs in both case studies as evident from the satisfaction of all three criteria. In the case of CIGRE DN, one instance can be noticed in Fig. 6.10b where EVR is above the specified set limit; however, no violation of power

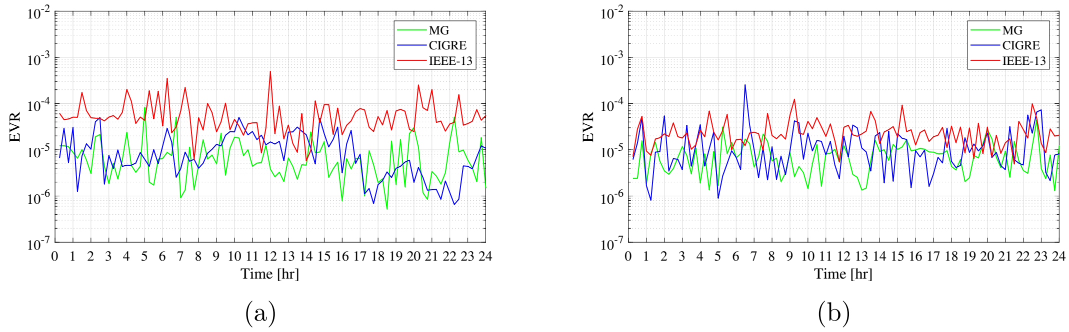

Figure 6.10: Impact of end-users profiles on eigenvalue ratio for load model 9 (a) both load and generation profiles are time varying (b) time varying load and rated (fixed) generation profiles.

[2]In the case of IEEE-13 bus network, the switch connected between the buses 671 and 692 is replaced by a line of almost negligible impedance.

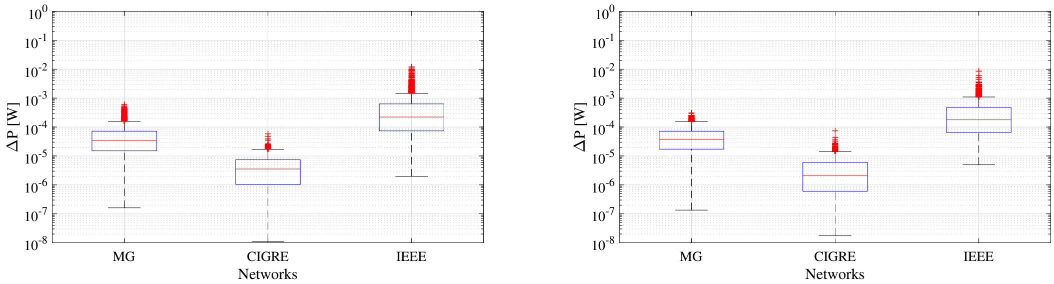

(a) (b)

Figure 6.11: Impact of end-users profiles on active power mismatch for load model 9 (a) both load and generation profiles are time varying (b) time varying load and rated (fixed) generation profiles.

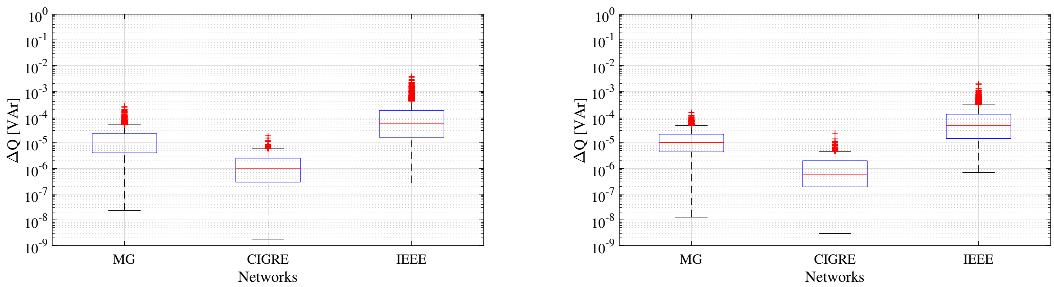

(a) (b)

Figure 6.12: Impact of end-users profiles on reactive power mismatch for load model 9 (a) both load and generation profiles are time varying (b) time varying load and rated (fixed) generation profiles.

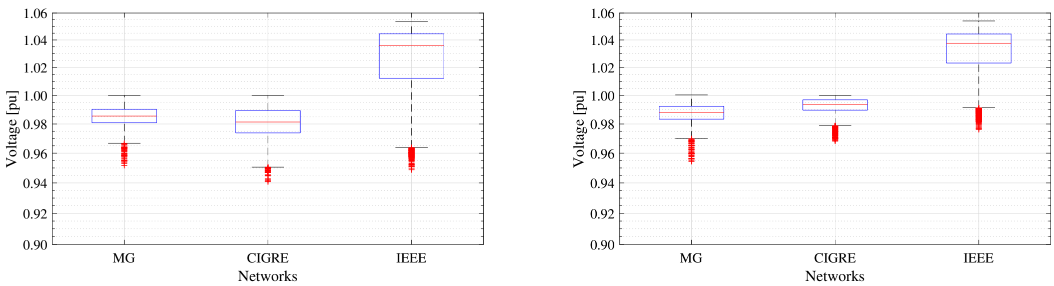

(a) (b)

Figure 6.13: Impact of end-users profiles on recovered voltages for load model 9 (a) both load and generation profiles are time varying (b) time varying load and rated (fixed) generation profiles.

mismatch and CNCV criteria is observed corresponding to this EVR. Consequently, the obtained solution, which is perceived as a rank-2 solution, can be considered as a rank-1 solution and this finding also endorses the statement reported in the point 4 of section 6.5.3 that in the case of a *perceived* rank-2 solution on the basis of EVR criterion, it is equally important to check other criteria to classify the obtained solution as an optimal or a sub-optimal solution.

5. In the case of IEEE-13 node DN, it is expected that the developed OPF relaxation would remain exact under both time-varying and rated DG profiles since the connected ZIP load has dominant constant impedance and constant power components. However, a higher value of EVR is observed at few instants under time-varying DG profiles, as can be seen in Fig. 6.10a, which indicates that the obtained solution is a rank-2 solution. Nevertheless, a closer look at the active power mismatch (Fig. 6.11a) shows that it is violated only for one EVR value which is observed at 12^{th}hr time instant. For all the other time instants, the active power mismatch remains below the threshold value. Moreover, the reactive power mismatch criterion is satisfied as well as the nodes voltages remain within the FR throughout the simulation range. Furthermore, in the case of case study 2, no violation is observed for any of the chosen criterion and, therefore, it can be concluded that under small contribution from a constant current load, an exact solution should be expected even for highly unbalanced DNs.

6.5.5 Theoretical guarantees of MPSDP-based OPF relaxation

The proposed relaxation is also tested for other LMs (not reported in this chapter) which consist of large k_I values and it has been found that in majority of the cases, a high rank solution is obtained. Although, there exists some rank-recovery methods as reported in [245], [319], [320], these methods have only been tested for single-phase equivalent networks. Since the non-convexity of a multi-phase OPF problem is much stronger than the non-convexity of a single-phase OPF problem, the ability of these methods to recover a rank-1 solution in the case of an unbalanced multi-phase OPF problem is still an open research task. Furthermore, there does not exist any theoretical guarantee for the exactness of MPSDP-based OPF relaxation due to the extremely complex analytical characterization of power injections, which represent strong mutual coupling among line power flows. In [264] and [303], some attempts are made to exhibit the FR of a two-bus three-phase network. For a strictly increasing OF with respect to the power injections, the FRs of non-convex AC-OPF and relaxed problems are shown to coincide with each other in [264] and, resultantly, it is expected that a rank-1 solution can be obtained for a three-phase unbalanced OPF problem. However, a counter example is provided in [303] which shows that the FR of relaxed problem of the same network can become greater than the FR of non-convex AC-OPF problem under a non-increasing OF and, therefore, the obtained solution can have a higher rank. These two counter examples clearly indicate that there is a strong need to propose sufficient condition(s) which can guarantee the exactness, and lack thereof, of a MPSDP-based OPF relaxation.

6.5.6 Impact of R/X ratio on the accuracy of proposed relaxation

Figs. 6.14-6.15 show the exactness, and lack thereof, of proposed relaxation for several R/X ratio values. The nominal R/X ratio of all branches in the aforementioned DNs, for which the results are mentioned in Table 6.2, is considered as a base case which is then multiplied by a coefficient μ, as shown in (6.75), to get a lower and a higher R/X ratio of the network branch.

$$(R/X)_{NC} = \mu * (R/X)_{BC} \tag{6.75}$$

where NC and BC stand for New Case and Base Case, respectively. In this study, the value of μ is changed between 0.1-3 range, where $\mu = 1$ represents the base case R/X ratio. For the scope of simplicity, the R/X ratio is modified by changing only the R component since the variation of X component is limited in practice for a wide range of line sizing (in the case, the line type (aerial/cable) is not modified).

The following observations can be made from the obtained results.

1. For a small R/X ratio (0.1), the relaxation gives a R2 solution under both OFs. This is because of the fact that at a small R/X ratio, the graph induced by $\Re(\mathbf{Z})$ (correspondingly $\Re(\mathbf{Y})$) is not strongly connected [245] and as stated earlier, the extremely small resistance value of a branch leads to poor numerical data in bus admittance matrix and, consequently, ill-conditioned data is given as an input to SDP solver. However, with an increase in the ratio i.e., from 0.1-0.5, the relaxation starts to become exact as evident from the decreasing EVR.

2. For R/X ratio between 0.5-1.5 range, an exact solution is obtained for both OFs. This indicates that in the case of real DNs where the R/X ratio is neither too small nor too large, the proposed relaxation can provide a global optimal solution.

3. For a large R/X ratio, the relaxation starts to become inexact and a large EVR is obtained in the case of MG and CIGRE DNs due to the fact that a significant voltage

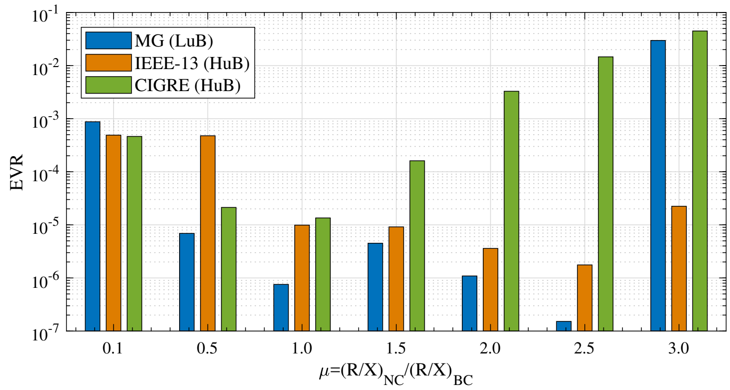

Figure 6.14: Impact of varying R/X ratio on the exactness of proposed relaxation solved for OF1.

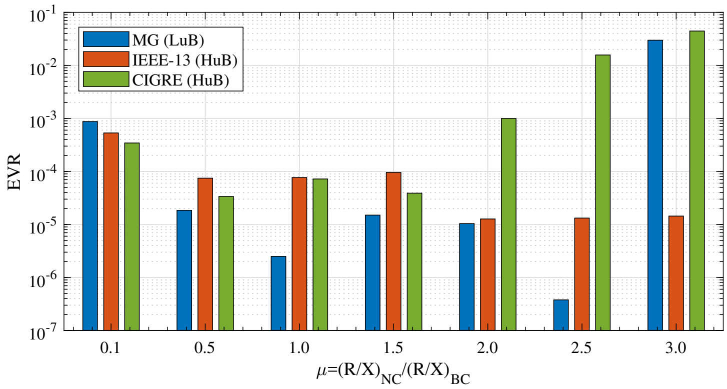

Figure 6.15: Impact of varying R/X ratio on the exactness of proposed relaxation solved for OF2.

drop occurs in these networks which leads to the violation of lower voltage limit at network buses. The same trend is not observed in the case of IEEE-13 node DN due to the fact, which has already been explained comprehensively in the previous section, that the initial voltage at all buses is set to 1.05pu in this case as compared to 1.0pu (set for all other DNs). This causes the voltage to stay above the lower voltage limit even for the large R/X ratio values in this network. Furthermore, it is also observed that by setting the lower voltage limit to a hypothetical (even if unrealistic) lower value (0.6pu), the relaxation becomes exact again for both MG and CIGRE DNs.

4. It has also been observed that by slightly increasing the slack node voltage in the range of 1.0-1.05, the relaxation becomes exact again for μ equal to 1.5 in the case of CIGRE DN for OF1. Similarly, in the case of MG DN, an exact solution is obtained as well at a high R/X ratio value for both OFs. This clearly indicates that under realistic (and allowed) network operating conditions, the proposed methodology is able to provide an exact solution.

These results show that the inexactness issues are mostly related to the extremely low or high value of R/X ratio of each network branch which, consequently, leads to an infeasible solution. By decreasing the R/X ratio of a branch which already has a small ratio value, or vice versa can lead to the situation where even the *simple power flow* results deviate from the standard limits and become infeasible. Therefore, it is justified to conclude that the proposed relaxation can provide an exact solution at the typical value of R/X ratio of DNs at which they are usually designed.

6.5.7 Computational performance

The CT of proposed approach is shown in Fig. 6.16a and reported in Table 6.3 for each LM in the case of wye-connected loads. Please note that the CT is reported only for OF1 since almost the same CT is observed in the case of OF2. Furthermore, the time observed

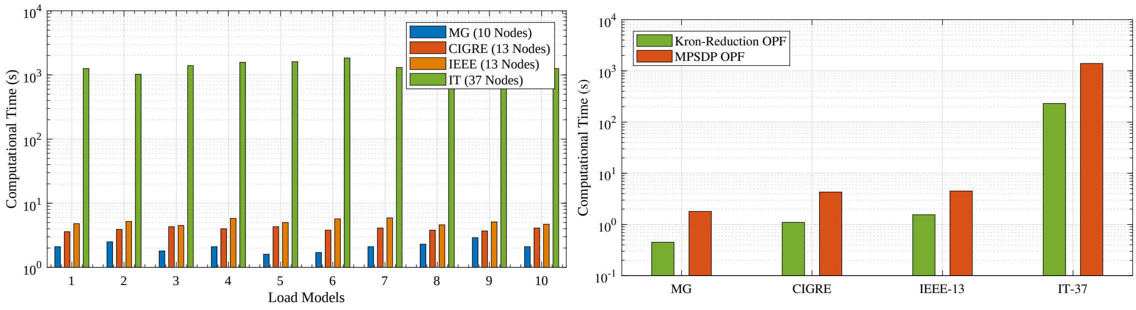

(a) (b)

Figure 6.16: Computational performance of MPSDP-based OPF relaxation (a) impact of increasing network size (b) impact of Kron reduction.

for delta and mixed loads is almost identical to the wye-connected loads and, therefore, is not reported here. It can be noticed that the CT increases remarkably with an increase in network size as can be observed for IT-37 bus system. With such a large CT, the real-time implementation of MPSDP-based OPF relaxation for medium and large size DNs is practically non-viable. Moreover, it can also be noted that the CT increases significantly when the dimension of an OPF problem increases by one i.e., from 3-phase to 4-conductor system as shown in Fig. 6.16b. In the case of small DNs such as MG, CIGRE and IEEE, the CT increases almost by a factor of 3-4, whereas in the case of IT-37 bus network, a 6-7% increase in the time is observed.

The CT of IT-111 bus system cannot be compared with the CT of other networks due to the formation of OPF problem through the cheap conic relaxation methodology. However, it can be observed that this relaxation can practically be realized due to its low

Table 6.3: Computational time of the proposed scheme under wye-connected end-users.

LMs	Computational Time (s)									
	OF:1 Slack Bus Power					OF:2 Network Losses				
	MG	IT-37	IT-111†	CIGRE	IEEE	MG	IT-37	IT-111†	CIGRE	IEEE
Three-Phase Kron-Reduced Network										
LM:3	0.45	231	-	1.10	1.55	0.60	235	-	1.18	1.65
Multi-Phase (Four Conductor) Network										
LM:1	2.1	1257	1.35	3.6	4.8	1.6	1411	1.50	3.9	4.9
LM:2	2.5	1023	1.40	3.9	5.2	1.4	1458	1.52	4.6	5.5
LM:3	1.8	1397	1.48	4.3	4.5	1.5	1760	1.55	4.0	5.1
LM:4	2.1	1571	1.70	4.0	5.8	1.5	1247	1.80	3.7	6.4
LM:5	1.6	1608	1.39	4.3	5.0	1.8	1407	1.48	3.6	5.1
LM:6	1.7	1835	1.50	3.8	5.7	1.7	1514	1.59	3.7	5.9
LM:7	2.1	1307	1.45	4.1	5.9	1.7	1535	1.68	3.6	6
LM:8	2.3	1357	1.41	3.8	4.6	1.8	1298	1.49	3.1	6.1
LM:9	2.9	1139	1.53	3.7	5.1	1.9	1457	1.57	3.8	4.9
LM:10	2.1	1257	1.46	4.1	4.7	2.1	1534	1.63	4.1	6.1

†: Memory Limit

computational requirements, provided it computes the exact solution. The high CT associated with a large-scale SDP problem is a well known problem in the literature and several techniques based on sparsity exploitation [246], [250], [256], [259], [321] and distributed algorithms [260], [262]–[264], [322] have been proposed for CT reduction which can, in turn, be adopted for medium and large size DNs to realize the real-time implementation of proposed relaxation for these networks.

6.5.8 Effect of grounding impedance on the quality of proposed relaxation

The grounding impedance also has a strong impact on the quality of proposed relaxation as evident from the results reported in Tables 6.4 and 6.5. The first table shows the results when relaxation is tested by varying the grounding impedance from $1 \times 10^{-6}\Omega$ to $1 \times 10^{5}\Omega$ for MPG DNs and set to $1 \times 10^{10}\Omega$ for SPG DNs under a fixed constant power LM, whereas the second table represents the exactness (quality) of relaxation for all wye-connected LMs under a fixed grounding impedance which is set to 1Ω. In both tables, the objective value of MPSDP-based OPF relaxation is compared with the optimal value obtained from KR-based OPF model through a %RD criterion as represented in (6.76). Please note that the **bold** values reported in both tables represent the cases where all evaluation criteria are satisfied and %RD is grater than 1%.

$$\%\text{Relative Difference} = \frac{|obj_{MP} - obj_{KR}|}{obj_{MP}} \times 100 \tag{6.76}$$

The following key observations can be made with respect to the first case study:

1. Emulating KR scenario by putting an extremely small value of grounding impedance leads to a high EVR as can be seen in the first three cases when proposed relaxation is solved for OF1. However, the same trend is not observed in the case of OF2 where a less than 1%RD is observed. Since OF1 deals with the apparent power injection at slack bus to which no load is attached, the grounding impedance value, as a result, becomes significantly relevant in this case. An extremely small value of it (e.g., $1 \times 10^{-6}\Omega$) sets the values of extreme (smallest and largest) coefficients in the OF polynomial equal to 6.8×10^{-13} and 5.3×10^{7}, respectively, whereas in the case of 1Ω value, these coefficients take the value 6.8×10^{-13} and 1.3×10^{4}, respectively. A significant reduction in the range of OF polynomial coefficients can be noticed with an increase in the value of grounding impedance, which in turn stabilises the input numerical data from the solver perspective and, as a result, a meaningful solution is obtained in the latter case. These results indicates that for DNNs, the proposed multi-phase relaxation can mimic an OPF model based on the KR approach, provided the SDP solver is capable of handling poor numerical data.

2. With the increase in grounding impedance value from $1 \times 10^{-2}\Omega$ to $1 \times 10^{5}\Omega$, the %RD starts to increase due to the rise in neutral current, and consequently, the values of OFs, particularly network losses, start deviating significantly from the

Table 6.4: Impact of grounding impedance on the quality of proposed scheme in comparison to the Kron-reduction based three-phase OPF model.

	MG		IEEE-13		CIGRE		MG		IEEE-13		CIGRE	
Grounding Impedance	**OF:1 Slack Bus Power (kVA)**						**OF:2 Network Losses (kW)**					
	Three-Phase Kron Reduced Network						*Three-Phase Kron Reduced Network*					
	Value (kVA)	**Time** (s)	**Value** (kVA)	**Time** (s)	**Value** (kVA)	**Time** (s)	**Value** (kW)	**Time** (s)	**Value** (kW)	**Time** (s)	**Value** (kW)	**Time** (s)
	3048.7	0.43	4057.8	1.55	162.8	1.10	105.0	0.60	307.2	1.65	7.76	1.10
	Multi-Phase (Four Conductor) Network						*Multi-Phase (Four Conductor) Network*					
Ω	**Diff.** %	**EVR** $\times10^{-5}$	**Diff.** %	**EVR** $\times10^{-5}$	**Diff.** %	**EVR** $\times10^{-5}$	**Diff.** %	**EVR** $\times10^{-5}$	**Diff.** %	**EVR** $\times10^{-5}$	**Diff.** %	**EVR** $\times10^{-5}$
1×10^{-6}	93.0	$> 10^4$	87.4	$> 10^4$	80.0	$> 10^4$	0.47	0.21	**1.38**	0.75	0.53	0.15
1×10^{-5}	90.2	$> 10^4$	86.4	$> 10^4$	6.91	66.3	0.14	1.06	**2.10**	0.52	**1.65**	0.25
1×10^{-4}	88.3	$> 10^4$	76.6	$> 10^4$	0.49	1.38	0.24	0.05	**2.46**	0.45	**2.82**	0.04
1×10^{-3}	3.30	12.3	11.5	79.4	0.54	2.03	0.29	0.26	**4.66**	5.10	**3.49**	0.26
1×10^{-2}	0.12	1.35	0.50	5.10	0.57	4.00	0.41	0.06	**3.65**	2.50	**2.96**	0.01
1	0.91	0.16	**2.56**	1.50	**2.26**	0.72	**2.07**	0.25	**9.67**	0.36	**1.42**	0.42
5	0.31	0.04	**1.11**	5.30	**1.15**	4.50	**2.08**	1.50	**3.78**	15.5	**3.38**	1.77
10	0.60	1.60	**1.40**	21.3	**1.16**	1.75	**2.33**	3.35	45.4	***22.3***	**3.33**	3.36
1×10^{2}	0.81	3.70	**1.21**	13.1	**1.18**	2.05	**2.52**	1.93	42.3	***26.2***	**3.87**	2.99
1×10^{5}	**1.32**	7.40	1.69	47.1	**1.13**	3.02	**3.40**	1.18	10.1	***19.7***	**3.10**	2.25
SPG	**1.47**	2.79	**1.94**	6.14	**3.27**	15.6	**2.44**	0.08	**11.7**	9.80	**9.16**	13.4

values obtained from the Kron-reduced network since in such DN, the current tends to flow through the ground rather than taking the neutral conductor path. It can be noticed that in the case of OF1, the %RD is as large as 2% whereas in the case of OF2, it has reached to 9%. Similarly, in the case of SPG DN, an 11% RD is observed. These results clearly indicate that applying KR on DNNs leads to suboptimal results and, therefore, its application on neutral-equipped DNs cannot be justified.

3. With the increase in degree of unbalance, putting a high neutral-ground impedance to mimic an open circuit condition leads to a high rank solution as can be noticed in few cases of IEEE-13 node and CIGRE DNs. In all such cases, all three evaluation criteria are violated.

With respect to the second case study, a large %RD, as per expectation, is observed between the optimal solutions of above-mentioned OPF relaxations. In the case of constant impedance load, the %RD has reached to 14% for IEEE-13 node network. Similarly, under different contributions from each component of a ZIP load, a notable %RD is obtained for all test networks in the case of both OFs.

The presented results in Tables 6.4 and 6.5 clearly demonstrate that the different values of grounding impedance lead to the objective values which can differ significantly from the results obtained from KR-based OPF model and, therefore, solving an OPF model for DNs which are not solidly grounded through the application of KR technique is practically non-viable. Similarly, the degree of unbalance and LMs also have a strong impact on the exactness of proposed relaxation and even for a moderate grounding impedance value, a large %RD can be obtained in a highly unbalanced network scenario hosting ZIP loads.

Table 6.5: %Relative difference between the objective values of MPSDP- and KR-based OPF relaxations.

% Relative Difference between Objective Values												
LMs	**MG**			**IT-37**			**CIGRE**			**IEEE**		
	KR	*MP*	*%Diff*	*KR*	*MP*	*%Diff*	*KR*	*MP*	*%Diff*	*KR*	*MP*	*%Diff*
OF:1 Minimization of Slack Bus Power (kVA)												
LM:1	2813.0	2828.6	0.55	97.9	98.0	0.14	146.5	143.5	**2.05**	4018.2	3782.0	**6.25**
LM:2	2922.2	2918.3	0.13	100.9	102.0	**1.13**	153.9	153.4	0.36	4061.3	3852.9	**5.41**
LM:3	3048.7	3021.2	0.91	104.1	106.5	**2.26**	162.8	166.5	**2.26**	4057.8	4164.4	**2.56**
LM:4	2888.1	3123.1	**7.52**	100.2	99.9	0.28	151.3	149.6	**1.17**	4144.1	3733.4	**11.0**
LM:5	2935.6	2929.5	0.21	101.2	102.5	**1.22**	154.8	154.9	0.03	4076.5	3860.8	**5.59**
LM:6	2940.6	2940.7	0.00	101.7	101.8	0.14	155.3	154.3	0.61	4121.5	3781.2	**9.00**
LM:7	2987.6	2943.0	**1.52**	102.8	102.9	0.03	159.0	157.0	**1.26**	4145.7	3882.1	**6.79**
LM:8	2958.1	2946.8	0.38	101.9	103.4	**1.47**	156.4	157.0	0.42	4066.8	3909.7	**4.02**
LM:9	2861.2	2862.7	0.05	99.2	99.7	0.49	150.0	147.8	**1.43**	4088.1	3803.9	**7.47**
LM:10	3022.1	2999.4	0.76	103.7	105.9	**2.02**	160.8	163.6	**1.69**	4062.3	4051.8	0.26
OF:2 Minimization of Network Losses (kW)												
LM:1	91.1	90.2	**1.04**	2.46	2.23	**10.2**	6.34	5.78	**9.68**	252.4	221.4	**14.0**
LM:2	93.6	100.6	**6.96**	2.71	2.79	**3.17**	6.97	6.46	**7.85**	272.4	245.9	**10.8**
LM:3	105.0	107.2	**2.07**	2.79	3.09	**9.86**	7.76	7.65	**1.42**	307.2	280.1	**9.67**
LM:4	97.0	133.1	**27.1**	2.86	2.96	**3.36**	6.76	6.50	**4.05**	288.4	262.1	**10.0**
LM:5	95.3	100.5	**5.13**	2.94	2.88	**1.88**	7.04	6.63	**6.24**	288.4	252.8	**14.1**
LM:6	99.6	127.6	**22.0**	2.69	2.89	**7.13**	7.00	6.74	**3.95**	290.9	280.9	**3.53**
LM:7	102.0	101.2	0.77	2.69	2.96	**9.18**	7.32	6.82	**7.30**	248.7	267.6	**7.07**
LM:8	96.1	101.5	**5.36**	2.82	2.92	**3.31**	7.16	6.78	**5.61**	286.1	258.7	**10.6**
LM:9	96.9	95.2	**1.78**	2.63	2.72	**3.20**	6.61	6.08	**8.66**	246.4	222.9	**10.6**
LM:10	101.5	106.4	**4.65**	2.68	3.13	**14.1**	7.66	7.38	**3.88**	288.8	274.8	**5.10**

Since DNs contain such type of loads in abundance, it can be expected that the KR-based OPF model for DNNs would lead to sub-optimal solution. Consequently, it is unrealistic to adopt this reduction approach for DNs in which neutral is either ungrounded or grounded through a finite resistance at a single or multiple points, and containing ZIP loads as well.

6.5.9 Concluding remarks

To summarize the findings regarding the quality of proposed multi-phase relaxation with respect to the degree of unbalance, LM type (wye/delta), contribution of ZIP load components, R/X ratio, grounding impedance value and CT, a brief discussion is carried out in this section.

- In the case of solely Z, I or P loads, the relaxation recovers an exact solution for both wye- and delta-connected load types under any degree of unbalance in a DN.

- In the case of wye-connected ZIP loads, the relaxation provides an exact solution for lightly and moderately unbalanced DNs for all LMs as evident by the satisfaction of all three criteria. However, in the case of highly unbalanced DNs, the contribution of constant current load plays a significant role in the exactness of proposed relaxation, which remains exact under low and moderate contribution from this load component. However, in the case of dominant injections from this load component, a higher EVR is obtained as per expectation along with the weak satisfaction of power mismatch and CNCV criteria.

- In the case of delta-connected ZIP loads, the relaxation provides an exact solution in the case of lightly unbalanced DNs for all LMs, whereas in the case of moderately and highly unbalanced DNs, the relaxation provides a rank-2 and completely meaningless solution, respectively when the constant current component dominates the other components of a ZIP load. For all other LMs, which involve either low or moderate contribution from a constant current load, an exact solution is obtained for this load type.

- In the case of mixed wye-delta loads, the same trend with respect to the degree of unbalance and constant current load contribution is observed as noted for the solely wye- and delta-connected loads. The relaxation remains exact, irrespective of the degree of unbalance, under small contribution from the constant current load. In the case of dominant participation of wye-connected constant current loads in the mix, the relaxation remains exact for moderately unbalanced DNs and a rank-2 solution is obtained in the case of highly unbalanced DNs. On the other hand, the dominance of delta-connected loads in the mix can make the relaxation inexact even for moderately unbalanced DNs. Furthermore, the probability of obtaining a completely meaningless solution in the case of highly unbalanced DNs, serving dominant constant current delta loads, increases significantly as compared to the wye-connected loads.

- The proposed relaxation appears to provide an exact solution in the presence of realistic time-varying loads and DGs profiles i.e., in a realistic loading scenario, an optimal solution can be obtained even for LMs having large contributions from constant current loads and DNs exhibiting a high degree of unbalance.

- With respect to the R/X ratio, the relaxation becomes inexact at small ratio value due to weakly connected network graph, whereas in the case of large ratio value, given the unrealistic hypothesis of assuming the same change (increase/decrease) in the R/X ratio of each network branch, the technical constraints (e.g., lower voltage limit) are violated and consequently, an inexact solution is obtained. On the other hand for real DNs having a realistic value of R/X ratio corresponding to each network branch, the proposed relaxation provides an exact solution.

- The KR methodology, when applied to MPG and SPG DNs, leads to an optimal value which differs significantly from the optimal value obtained from MPSDP-based OPF relaxation. The grounding impedance, chosen OF and varying parameters of a ZIP load strongly impact the optimal solution value. However, under KR approach, the impact of these characteristics are lost completely. Consequently, the obtained solution from KR-based OPF relaxation should be considered as a sub-optimal solution.

- The CT of proposed relaxation increases to such an extent for a real DN containing moderate number of nodes that its real-time implementation cannot be practically realized unless additional strategies such as sparsity exploitation and/or distributed OPF algorithms are exploited for such network.

6.6 Summary

In this chapter, a novel MPSDP-based OPF relaxation for neutral-equipped distribution networks is proposed. The main bottleneck in the development of an OPF model for such DNs is the coupled power injection across phase-neutral and phase-phase conductors for both wye- and delta-connected loads. In order to overcome this problem, a network admittance-based representation of shunt-elements is adopted which ultimately leads to explicit power injections at each conductor of a DNN.

The proposed relaxation provides an exact solution for both wye- and delta-connected loads under *moderate* values of constant current components and for *any* values of the parameters representing constant impedance and constant power components. On the other hand, when constant current component of a ZIP load dominates the other components, the relaxation has a tendency to provide a sub-optimal solution due to the approximate modelling of this load component. Nevertheless, the sub-optimal solution, obtained in the case of wye-connected loads, is still a rank-2 solution from which the meaningful results can be derived by using rank-recovery techniques, provided the single-phase rank-recovery methods are applicable to multi-phase networks. Furthermore, the modelling of constant current component through *first-order Taylor series*, despite being theoretically more accurate than the representation based on the *approximation of the first-order Taylor series* approach, provides an inexact solution for all load models because of the solver inability to handle poor numerical data.

The degree of unbalance of a DN also influences the exactness of proposed relaxation. For lightly and moderately unbalanced DNs, the developed relaxation appears to be tight. However, in the case of highly unbalanced DNs, the probability of getting a low-rank solution increases under a large contribution from constant current loads. Finally, the application of KR methodology either on a SPG or MPG DNs leads to an optimal solution which differs significantly from the results obtained through the OPF model of a multi-phase DNN.

The computational efficiency of developed scheme strongly depends upon the network size and, as expected, the computing time increases significantly for medium size DNs in comparison to the CT observed for three-phase OPF model for the same networks. For large size DNs, MOSEK fails to solve the relaxation due to the violation of its internal memory limit but, nevertheless, a large CT can be perceived for such DNs provided a solver is capable to solve the proposed relaxation. Such a large CT impedes the implementation of this scheme on a real-time basis for medium and large size DNs and, therefore, in the next chapter, a cheap conic SDP-based relaxation is adopted for such DNs which facilitates the practical realization of a multi-phase OPF model.

Published papers

The presented work in this chapter led to the publication of following papers.

1. Usman, M., A. Cervi, M. Coppo, F. Bignucolo, and R. Turri. "Centralized OPF in Unbalanced Multi-Phase Neutral equipped Distribution Networks hosting ZIP Loads" in *IEEE Access*, 7, 177890-177908.

2. Usman, M., A. Cervi, M. Coppo, F. Bignucolo, and R. Turri. "Bus injection relaxation based OPF in multi-phase neutral equipped distribution networks embedding wye-and delta-connected loads and generators." *International Journal of Electrical Power & Energy Systems* 114 (2020): 105394.

3. Usman, M., A. Cervi, M. Coppo, F. Bignucolo, and R. Turri. "Convexified OPF in Multiphase Low Voltage Radial Distribution Networks including Neutral Conductor" in *IEEE Power and Energy Society General Meeting, 2019.*

CHAPTER 7

Cheap Conic Relaxation for Practical Realization of Multi-Phase SDP based OPF Relaxation

This chapters presents a new conic SDP-based OPF relaxation aiming at overcoming the high computational requirements of multi-phase SDP-based OPF relaxation which is presented in the previous chapter. For the incorporation of constant current load in the proposed OPF relaxation, three novel propositions are presented along with the computation of novel bounds for phase and neutral voltage variables. Finally, the quality assessment of developed relaxation, in terms of exactness and computational time, is tested against several load models for wye, delta, and mixed load types, voltage angle deviation parameter and imposition of neutral envelopes.

In chapter 6, a MPSDP-based OPF relaxation is developed for neutral-equipped DNs which successfully incorporates both wye- and delta-connected loads and DGs without reducing the network configuration from four conductors to three phases. However, it suffers from a high CT requirement and, therefore, cannot be practically realized even for medium-size real LV ADNs, let alone the large-size DNs. Since LV DNs are rapidly transforming from passive to active networks and, therefore, can play a significant role in the near future in day-ahead and ancillary services market, it is therefore necessary to *optimally* control and manage these networks on a real-time basis.

To realize the real-time implementation of an OPF model for large size networks, SOCP-based OPF methodology provides an alternative to SDP-based OPF technique since both methodologies are proven to be equivalent in the case of single-phase equivalently represented RDNs [255], [284]. Consequently, both OPF models provide the same optimal solution but SOCP-based OPF relaxation can be solved in a significantly reduced time. However, in the case of multi-phase unbalanced DNs, the Second Order Cone (SOC) constraint takes the form of a *cheap* PSD constraint since solving a matrix-based SOC constraint is practically impossible due to the non-existence of any solver which can handle this type of constraint. This means that in a multi-phase DN, PSD constraints have to be defined for matrices having dimensions equal to $(\tau \times 2) \times (\tau \times 2)$ instead of setting SOC constraints on the OVs. Furthermore, in comparison to the *primal* MPSDP-based OPF relaxation which involve only one stringent PSD constraint on a $(n \times \tau) \times (n \times \tau)$ matrix, PSD constraints have to be defined for each node- and branch-related matrix variables in the cheap SDP relaxation. However, the CT of this relaxation is significantly lower as compared to the CT of MPSDP-based relaxation and, as a result, the practical implementation of an OPF model for DNN can be realized through this approach. Resultantly, to enjoy the benefits of this relaxation, the following goals are set and successfully achieved in this chapter.

1. Development of a novel centralized cheap SDP-based OPF model, which utilizes the BFM-based power system representation, for DNNs containing both wye- and delta-connected ZIP loads

2. Proposal of three novel strategies for the approximate modelling of constant current load in order to incorporate it in the proposed OPF model

3. Developing tighter limits for complex phase-voltage variables and proposal of a novel approach for determining the bounds on neutral voltage variable at each node

4. Demonstrating the impact of neutral envelopes and voltage-angle limit on the exactness of proposed relaxation

To achieve these objectives, the existing BFM-based cheap OPF model for a three-phase DN is recalled first which pinpoints the shortcomings in that model; followed by the introduction of novel propositions and modifications in that model in the context of a DNN. Please note that the same nomenclature as reported in section 6.1.1 is used in this chapter.

7.1 Recap of existing three-phase BFM-based cheap OPF relaxation

The existing three-phase OPF model which utilizes the concept of *cheap* PSD constraints is shown in model **M7.1**. In the context of this relaxation, the following variables are introduced for representing the Ohm's law and power balance constraints.

$$
\begin{aligned}
&\mathbf{II}_{ij} = \mathbf{I}_{ij}\mathbf{I}_{ij}^{H}, \;\; \mathbf{S}_{ij} = \mathbf{V}_{i}\mathbf{I}_{ij}^{H} && \forall (j : i \sim j) \in E \\
&\mathbf{W}_{ii} = \mathbf{V}_{i}\mathbf{V}_{i}^{H} && \forall i \in N
\end{aligned}
$$

The above-mentioned variables are sufficient for the modelling of wye-connected shunt elements (loads/DGs). However, for the modelling of delta elements, additional variables, as shown below, are needed which led to the additional constraints as reported in (7.1i) and (7.1l).

$$\mathbf{X}_i = \mathbf{V}_i \mathbf{I}_{\Delta_i}^H \qquad \forall i \in N$$
$$\mathbf{\Phi}_i = \mathbf{I}_{\Delta_i} \mathbf{I}_{\Delta_i}^H \qquad \forall i \in N$$

where $\mathbf{I}_{\Delta_i}$ is defined as $[I_i^{ab}, I_i^{bc}, I_i^{ca}]$. It can be noticed in **M7.1** that OVs are defined for each node and branch which is a significant departure from the MPSDP-based OPF model. Consequently, the coupling has to be established between these variables in the form of a rank-1 matrices which, ultimately, leads to the cheap PSD constraints as shown in (7.1h) and (7.1i). Furthermore, it can be noted that only constant power load is taken

M7.1: Cheap conic OPF relaxation for a three-phase DN

$$\textbf{M7.1}: \underset{\Upsilon}{\textbf{minimize}} \; f(\Upsilon) \tag{7.1a}$$

$$\begin{aligned}
\textbf{variables}: & \mathbf{S}_{g_i}, \in \mathbb{C}^{|\eta_i|}, \mathbf{X}_i \in \mathbb{C}^{|\eta_i|\times|\eta_i|} && (\forall i \in N)\\
& \mathbf{W}_{ii} \in \mathbb{H}^{|\eta_i|\times|\eta_i|}, \mathbf{\Phi}_i \in \mathbb{H}^{|\eta_i|\times|\eta_i|} && (\forall i \in N)\\
& \mathbf{S}_{ij} \in \mathbb{C}^{|\eta_{ij}|\times|\eta_{ij}|}, \mathbf{\amalg}_{ij} \in \mathbb{H}^{|\eta_{ij}|\times|\eta_{ij}|} && (\forall i \sim j \in E)
\end{aligned}$$

subject to :

$$\mathbf{W}_{jj} = \mathbf{W}_{ii} - (\mathbf{S}_{ij}\mathbf{Z}_{ij}^H + \mathbf{Z}_{ij}\mathbf{S}_{ij}^H) + \mathbf{Z}_{ij}\,\mathbf{\amalg}_{ij}\,\mathbf{Z}_{ij}^H \qquad \forall (j : i \sim j) \in E \tag{7.1b}$$

$$\sum_{k:k\sim i} \text{diag}(\mathbf{S}_{ki} - \mathbf{Z}_{ki}\mathbf{\amalg}_{ki}) - \sum_{j:i\sim j} \text{diag}(\mathbf{S}_{ij}) = \mathbf{S}_{g_i} - (\mathbf{S}_{\varrho_i} + \mathbf{S}_{\Delta_i}) \qquad \forall i \in N \tag{7.1c}$$

$$\underline{\mathbf{S}}_{g_i} \leq \mathbf{S}_{g_i} \leq \overline{\mathbf{S}}_{g_i} \qquad \forall i \in N \tag{7.1d}$$

$$|\underline{\mathbf{V}}|_i^2 \leq \text{diag}(\mathbf{W}_{ii}) \leq |\overline{\mathbf{V}}|_i^2 \qquad \forall i \in N^+ \tag{7.1e}$$

$$[\mathbf{W}]_{\eta_0\times\eta_0} = \mathbf{V}_0\mathbf{V}_0^H \tag{7.1f}$$

$$\mathbf{W}_{ii} \succeq 0 \qquad \forall i \in N^T \tag{7.1g}$$

$$\begin{bmatrix} \mathbf{W}_{ii} & \mathbf{S}_{ij} \\ \mathbf{S}_{ij}^H & \mathbf{\amalg}_{ij} \end{bmatrix} \succeq 0 \qquad \forall (j : i \sim j) \in E \tag{7.1h}$$

$$\begin{bmatrix} \mathbf{W}_{ii} & \mathbf{X}_i \\ \mathbf{X}_i^H & \mathbf{\Phi}_i \end{bmatrix} \succeq 0 \qquad \forall i \in N \tag{7.1i}$$

$$\text{rank}(\mathbf{W}_{ii}) = 1 \qquad \forall i \in N^T \tag{7.1j}$$

$$\text{rank}\left\{ \begin{bmatrix} \mathbf{W}_{ii} & \mathbf{S}_{ij} \\ \mathbf{S}_{ij}^H & \mathbf{\amalg}_{ij} \end{bmatrix} \right\} = 1 \qquad \forall (j : i \sim j) \in E \tag{7.1k}$$

$$\text{rank}\left\{ \begin{bmatrix} \mathbf{W}_{ii} & \mathbf{X}_i \\ \mathbf{X}_i^H & \mathbf{\Phi}_i \end{bmatrix} \right\} = 1 \qquad \forall i \in N \tag{7.1l}$$

into consideration. However, it has been comprehensively explained in chapter 6 that other LMs also exist in a DN in a significant quantity and, therefore, they should also be incorporated in an OPF model. From the observation of the structure of this model, two key questions arise:

1. Can the same approach as reported in section 6.3 be utilized for the incorporation of ZIP shunt-elements in a multi-phase version (phase and neutral conductors) of **M7.1**?

2. Is there a way to avoid using additional variables for the incorporation of delta loads/DGs in a multi-phase model?

Although the presented model **M7.1** is defined with respect to a three-phase network configuration, the responses to the above-mentioned questions can only be found by extending this model to a four-conductor network framework.

7.1.1 Modified BFM-based cheap SDP-OPF formulation

The approach reported in section 6.3 is based on the extension of OV $\mathbf{W}$ by appending it with a row and column of complex voltage variables to form a new OV $\hat{\mathbf{W}}$. These variables appear in the first row and column of OV $\hat{\mathbf{W}}$ and are used for the modelling of constant current component of a ZIP load. Please note that due to the extensive repetition of these variables in the following discussion, they are simply termed as *First-Row/First-Column Variables* (FR/FC Vs) for easy understanding.

With regard to the first question, an additional row and column of complex voltage variables is appended at each node matrix $\mathbf{W}_{ii}$ of **M7.1**, and a new OV $\hat{\mathbf{W}}_{ii}$ having dimensions equal to $(\tau + 1) \times (\tau + 1)$, is defined for each node as follows:

$$\hat{\mathbf{W}}_{ii} = \begin{bmatrix} 1 \\ V_i^{ag} \\ \vdots \\ V_i^{ng} \end{bmatrix} \begin{bmatrix} 1 & V_i^{*ag} & \cdots & V_i^{*ng} \end{bmatrix} = \begin{bmatrix} 1 & V_i^{*ag} & \cdots & V_i^{*ng} \\ V_i^{ag} & V_i^{ag} V_i^{*ag} & \cdots & V_i^{ag} V_i^{*ng} \\ \vdots & \vdots & \ddots & \vdots \\ V_i^{ng} & V_i^{cg} V_i^{*ag} & \cdots & V_i^{ng} V_i^{*ng} \end{bmatrix} \tag{7.2}$$

A careful observation of $\hat{\mathbf{W}}_{ii}$ reveals that although the constant current component of a ZIP load can be defined through the FR/FC Vs, (7.1b) can no longer be defined due to the dimension mismatch between $\hat{\mathbf{W}}_{ii/jj}$ and $\mathbf{S}_{ij}$, $\mathbf{Z}_{ij}$, $\mathbf{II}_{ij}$ OVs since the latter OVs ($\mathbf{S}_{ij}$, $\mathbf{Z}_{ij}$, $\mathbf{II}_{ij}$) have dimensions equal to $(\tau \times \tau)$. Resultantly, in order to satisfy (7.1b), one has to increase the dimensions of $\mathbf{S}_{ij}$ and $\mathbf{II}_{ij}$ by appending an additional scalar 1 in the voltage and current vectors, whereas the dimensions of $\mathbf{Z}_{ij}$ has to be increased by appending an additional row and column of zeros. Consequently, these extended variables are represented as $\hat{\mathbf{S}}_{ij}$, $\hat{\mathbf{II}}_{ij}$ and $\hat{\mathbf{Z}}_{ij}$ in the context of **MM1**. With the introduction of these new variables, PSD constraint (7.1h) has to be enforced on a larger matrix as shown below:

$$\begin{bmatrix} 1 \\ V_i^{ag} \\ \vdots \\ V_i^{ng} \\ 1 \\ I_{ij}^{a} \\ \vdots \\ I_{ij}^{n} \end{bmatrix} \begin{bmatrix} 1 & V_i^{*ag} & \cdots & V_i^{*ng} & 1 & I_{ij}^{*a} & \cdots & I_{ij}^{*n} \end{bmatrix} = \begin{bmatrix} 1 & \mathbf{V}_i^* & 1 & \mathbf{I}_{ij}^* \\ \mathbf{V}_i & \mathbf{V}_i\mathbf{V}_i^* & \mathbf{V}_i & \mathbf{V}_i\mathbf{I}_{ij}^* \\ 1 & \mathbf{V}_i^* & 1 & \mathbf{I}_{ij}^* \\ \mathbf{I}_{ij} & \mathbf{I}_{ij}\mathbf{V}_i^* & \mathbf{I}_{ij} & \mathbf{I}_{ij}\mathbf{I}_{ij}^* \end{bmatrix} \succeq 0 \quad (7.3)$$

The formulation of new variables ($\hat{\mathbf{W}}_{ii/jj}, \hat{\mathbf{S}}_{ij}, \hat{\mathbf{\amalg}}_{ij}, \hat{\mathbf{Z}}_{ij}$) and the enforcement of PSD constraint on rank-1 matrix (7.3) led to a modified version of three-phase cheap conic relaxation which is termed as Modified Model 1 (MM1) in the subsequent discussion. A detailed analysis of **MM1** reveals that:

1. The increase in the dimensions of OVs $\mathbf{S}_{ij}$, $\mathbf{Z}_{ij}$ and $\mathbf{\amalg}_{ij}$ due to the extension of $\mathbf{W}_{ii}$ causes an unnecessary complexity in the model.

2. While solving (7.1b) and (7.1c) with new variables ($\hat{\mathbf{W}}_{ii}$, $\hat{\mathbf{S}}_{ij}$, $\hat{\mathbf{\amalg}}_{ij}$ and $\hat{\mathbf{Z}}_{ij}$), the top most row and element has to be discarded from both equations, respectively, due to their redundancy (non-physical relation between the network quantities) after the formulation of these equation.

3. The rank-1 matrix (7.3) has dimensions equal to $\{(\tau \times 2) + 2\} \times \{(\tau \times 2) + 2\}$ as compared to the dimensions $(\tau \times 2) \times (\tau \times 2)$ of rank-1 matrix in **M7.1** which, resultantly, leads to an increase in the CT of **MM1** due to the imposition of PSD constraint on a larger-size matrix. Furthermore, the probability of getting a rank-1 solution for (7.3) decreases with an increase in its size.

4. The FR/FC Vs in (7.3) require additional *complex* bounds since it has been observed that leaving them unbounded lead to the unrealistic values of these variables after the relaxation is solved. Please note that no extra constraints are needed for the OV of MPSDP-based OPF relaxation even after the extension of $\mathbf{W}$ to $\hat{\mathbf{W}}$. The reason is that a SDP solver while enforcing the PSD constraint on rank-1 matrix $\hat{\mathbf{W}}$ bounds the FR/FC Vs automatically. However, there is a catch in this statement that there is no guarantee that the square of magnitude of FR/FC Vs will be equal to the value of voltage terms ($V_i^{\varphi g} V_i^{*\varphi g}$) appearing on the diagonal of $\hat{\mathbf{W}}$. In the case of MPSDP-based OPF relaxation, the solver is able to determine such values of FR/FC Vs of $\hat{\mathbf{W}}$ which are equal to the values of the terms appearing on the diagonal of this matrix, in terms of the square of magnitude, for all LMs and load types. Based on the experience with MPSDP-based OPF relaxation, it was expected that an optimal solution can also be obtained in the case of *cheap* **MM1** relaxation by keeping the complex voltage and current variables, which appear in $\hat{\mathbf{W}}_{ii}$ and $\hat{\mathbf{\amalg}}_{ij}$, unbounded. However, the same trend was not observed and instead of obtaining an

optimal solution when constant current loads were simulated, a completely meaningless solution was obtained and no correlation between the values of FR/FC Vs and diagonal terms in $\hat{\mathbf{W}}_{ii}$ was observed. The reason for this behaviour lies in the *mathematical manifold technique* which states that solvers tend to find such values of all OVs that satisfy a PSD constraint(s) and it is possible that the resulting values may or may not have any correlation among them. In the case of MPSDP-based OPF relaxation, the recovered values are strongly correlated whereas in the case of **MM1** relaxation, no correlation is found. These findings suggests that i) FR/FC Vs must be linked to the diagonal and off-diagonal terms of the extended variables and ii) extra bounds should be put on the FR/FC Vs (both voltages and current) if one wants to use the **MM1** for the incorporation of a full ZIP load.

The discussion in the above-mentioned points clearly reveals the difficulties associated with the modelling of a full ZIP load through **MM1**. Apart from extending $\mathbf{W}_{ii}$ to incorporate constant current loads, the dimensions of other OVs appearing in **M7.1** have to be extended as well and, furthermore, additional bounds have to be defined for each extended variable. Consequently, instead of taking this route, a new path is chosen in this work where new OVs, as reported in section 7.2.2, are introduced only at those nodes which host constant current loads/DGs and all equalities and inequalities shown in the model **M7.1** are expressed through the same OVs reported in it. With this strategy, only few extra bounds are needed for the complex voltage variables, whereas no additional constraints are required for the complex line current variables due to their non-existence in the proposed propositions for the constant current load modelling. In brief, the proposed methodology simplifies the whole process of constant current load modelling without increasing the CT and model complexity.

With respect to the second question, there is no need of any additional variable in the proposed approach for the modelling of delta loads/DGs and, as a result, the variables $\mathbf{X}_i$ and $\mathbf{\Phi}_i$, and their corresponding constraints (7.1i) and (7.1l) which are introduced in **M7.1** become redundant in the new cheap OPF relaxation and are, therefore, discarded.

7.2 Modelling of ZIP loads in cheap SDP-based OPF framework

The main bottleneck of coupled power injections in DNNs is successfully solved in chapter 6 through a network admittance matrix-based approach which leads to the following decoupled power injections at each phase and neutral conductor of a node i corresponding to a ZIP load.

$$\mathbf{S}_i^{*Z\%} = \mathbf{V}_i^* \otimes \{\mathbf{\Lambda}_i^Z \mathbf{V}_i\} \tag{7.4}$$

$$\mathbf{S}_i^{*I\%} = \mathbf{V}_i^* \otimes \{(\mathbf{\Lambda}_i^{I_c} - \mathbf{\Lambda}_i^I)\mathbf{V}_i\} + \mathbf{\Lambda}_i^I(|\mathbf{V}_i| \otimes |\mathbf{V}_{i_{(0)}}|) \tag{7.5}$$

$$\mathbf{S}_i^{*P\%} = \mathbf{V}_i^* \otimes \{(\mathbf{\Lambda}_i^{P_c} - \mathbf{\Lambda}_i^P)\mathbf{V}_i\} + \mathbf{V}_{i_{(0)}}^* \otimes \{\mathbf{\Lambda}_i^P \mathbf{V}_{i_{(0)}}\} \tag{7.6}$$

Since in cheap OPF relaxation, the OV $\mathbf{W}_{ii}$ $(\forall i = 1, \cdots, n)$ is defined for each node, the representation of constant impedance, constant power and the first term of constant current injection can be easily done through this variable. However, for the latter part i.e., the term involving absolute voltage variable, three novel propositions are proposed in this section which, ultimately, allow to complete the modelling of constant current component of a ZIP load. The representation of each ZIP component in terms of the relaxation OVs is presented in the subsequent sections. Please note that the variables involved in the following formulations have dimensions with respect to a four conductor network framework i.e., the dimension of $\mathbf{W}_{ii}$ is 4×4 rather than 3×3 as used in **M7.1**.

7.2.1 Representation of constant impedance and constant power element

The presence of the product of same and different phases voltage terms in $\mathbf{W}_{ii}$ allows the quick representation of constant impedance and constant power components without requiring any new OV. To this extent, the decoupled power injections related to these components can be defined as:

$$\mathbf{S}_{\varrho i}^{Z\%} = \text{diag}\left\{\mathbf{\Lambda}_{Y/\Delta_i}^{Z}\mathbf{W}_{ii}\right\}^* \tag{7.7}$$

$$\mathbf{S}_{\varrho i}^{P\%} = \text{diag}\{(\mathbf{\Lambda}_{Y/\Delta_i}^{P_c} - \mathbf{\Lambda}_{Y/\Delta_i}^{P})\mathbf{W}_{ii} + (\mathbf{\Lambda}_{Y/\Delta_i}^{P}\mathbf{W}_{0_{ii}})\}^* \tag{7.8}$$

where $\mathbf{W}_0 = \mathbf{V}_{int}\mathbf{V}_{int}^H$, $\mathbf{V}_{int}$ is defined as the vector of initial voltage at each node and $\mathbf{\Lambda}_{Y/\Delta_i}^{Z/P/Pc}$ matrices are reported in (6.24) and (6.25).

7.2.2 Representation of constant current element

Since constant current injection (7.5) contains both absolute and square of the absolute of phase-voltage terms, additional mathematical modelling is required to represent the injection of this component. The representation of the latter term (square of the absolute voltage term) is pretty straightforward and it takes the same form as shown for the constant impedance and constant power components. To this end, it can be modelled as follows:

$$\mathbf{S}_{\varrho i}^{I^{sq}} = \text{diag}\left\{(\mathbf{\Lambda}_{Y/\Delta_i}^{I_c}\mathbf{W}_{ii}) - (\mathbf{\Lambda}_{Y/\Delta_i}^{I}\mathbf{W}_{ii})\right\}^* \tag{7.9}$$

For the modelling of first part containing absolute voltage terms, the explicit power injections based on *approximation of first order Taylor series* are derived in (6.54)-(6.55). Since injections based on the *first order Taylor series* result in NP or greater than rank-2 solution, they are not treated here. To incorporate the injections (6.54)-(6.55) in a cheap OPF relaxation, three novel independent mathematical models are developed due to the difficulties associated with the generalization of the approach presented in section 6.3 for MPSDP-based OPF relaxation.

7.2.2.1 Proposition-1 (P1)

In this proposition, an additional matrix variable $\mathbf{\Pi}_{ii}$ (7.10) is introduced at each node i containing constant current loads as follows:

$$\mathbf{\Pi}_{ii} = \begin{bmatrix} 1 \\ \mathbf{V}_i \end{bmatrix} \begin{bmatrix} 1 & \mathbf{V}_i^H \end{bmatrix} = \begin{bmatrix} 1 & \mathbf{V}_i^H \\ \mathbf{V}_i & \mathbf{W}_{ii} \end{bmatrix} \tag{7.10}$$

Based on (7.10), the injections related to the real part of (6.52) and (6.53) can be expressed as:

$$S_i^{\varphi, I_{P1}} = \left\{ \mathrm{Tr} \left(\frac{\hat{\mathbf{L}}_{i,l}^{\varphi,I} + \hat{\mathbf{L}}_{i,l}^{T\varphi,I}}{2} \right) \mathbf{\Pi}_{ii} \right\}^* \quad \forall \varphi \in \phi_i, i \in N_{IL} \tag{7.11}$$

where $\hat{\mathbf{L}}_{i,l}^{\varphi:I}$ is calculated as follows:

$$\hat{\mathbf{L}}_{i,l}^{\varphi,I} = (\mathbf{c}_i^a * \mathbf{c}_i^{\varphi T}) * (\mathbf{e}_i^{\varphi} * \mathbf{e}_i^{\varphi T}) * \mathbf{\Lambda}_{Y/\Delta_i}^{I_D} \tag{7.12}$$

where $\mathbf{e}_i^{\varphi}/\mathbf{c}_i^{\varphi}$ is a standard canonical basis vector of $\mathbb{R}^{|\phi_i| \times 1}$ corresponding to phase φ and $\mathbf{\Lambda}_{Y/\Delta_i}^{I_D}$ is a diagonal matrix formed by the diagonal elements of $\mathbf{\Lambda}_{Y/\Delta_i}^{I}$ which, in turn, is obtained from (6.24) and (6.25). It should be kept in mind that after obtaining $\hat{\mathbf{L}}_{i,l}^{\varphi:I}$, it has to be appended by an additional row and column of zeros to have the same dimensions as $\mathbf{\Pi}_{ii}$.

Since $\mathbf{\Pi}_{ii}$ is not used in any other equality or inequality constraints of the proposed cheap OPF relaxation, it has to be coupled with the other OVs of this relaxation. Consequently, to enforce the coupling between $\mathbf{\Pi}_{ii}$ and $\mathbf{W}_{ii}$, the following additional constraints are introduced.

$$\mathbf{\Pi}_{ii_{(1,1)}} = 1 \qquad \forall i \in N_{IL} \tag{7.13}$$

$$\mathbf{\Pi}_{ii_{(2:|\phi_i|,2:|\phi_i|)}} = \mathbf{W}_{ii} \quad \forall i \in N_{IL} \tag{7.14}$$

$$\mathbf{\Pi}_{ii} \succeq 0 \qquad \forall i \in N_{IL} \tag{7.15}$$

However, constraints (7.13)-(7.15) do not enforce any coupling between the FR/FC Vs of $\mathbf{\Pi}_{ii}$ and $\mathbf{W}_{ii}$ which is extremely important due to the involvement of these variables in the power injection (7.11). Consequently, additional bounds (7.16)-(7.17) are enforced in this regard which restrict the real and imaginary part of each phase voltage within the specified limits. These bounds, in turn, are based on the chosen value of the maximum angle deviation of a phase-ground voltage parameter. The bound calculation approach is comprehensively explained in the next section.

$$\underline{\mathbf{V}}_{r_i} \leq \frac{(\mathbf{\Gamma}_i + \mathbf{\Gamma}_i^*)}{2} \leq \overline{\mathbf{V}}_{r_i} \tag{7.16}$$

$$\underline{\mathbf{V}}_{im_i} \leq \frac{-j(\mathbf{\Gamma}_i - \mathbf{\Gamma}_i^*)}{2} \leq \overline{\mathbf{V}}_{im_i} \tag{7.17}$$

In (7.16)-(7.17), $\mathbf{\Gamma}_i$ represents the sub-vector $\mathbf{\Pi}_{ii(2:|\eta|,1)}$ and $\mathbf{V}_{r/im_i}$ is a 3×1 vector containing the maximum and minimum bounds on real and imaginary components of phase-voltages. Based on (7.13)-(7.17), each term of $\mathbf{\Pi}_{ii}$ is bounded and coupled with the other OVs of proposed OPF relaxation.

7.2.2.2 Bounds on linear complex voltage variables

In practice, bounds on the magnitude of a phase voltage are readily available and are specified by the technical standards. However, as it can be seen in (7.16)-(7.17), the real and imaginary bounds are required for a complex variable which are usually not available. Resultantly, a methodology is presented in [278] which derives the bounds on a complex voltage variable V_i and, subsequently, limits its real and imaginary components between $-|\overline{V}_i|$ and $|\overline{V}_i|$. However, as shown in Fig. 7.1, this approach encloses a large FR (green region) for V_i and allows the solver to calculate the value of V_i anywhere between 0° and 360°. However, this is not the case in real DNs where each phase voltage vector remains within a small region around the balanced condition *phase voltage vector* position. This region, in turn, depends on the maximum deviation of *phase voltage vector* in terms of voltage angle deviation δ parameter with respect to its reference position which is taken as ground potential. Therefore, it is expected that the maximum value of δ at each phase of a node will remain in a small symmetrical range i.e., ±10° and, resultantly, the bounds presented in [278] can be tightened by making use of δ parameter. It is extremely important to emphasize that in $\mathbf{W}_{ii}$ and $\mathbf{\Pi}_{ii}$, phase-ground voltage variables are involved and these variables must not be confused with the phase-neutral voltage variables. In an unbalanced DN, phase-neutral voltage angle can assume any value depending upon the degree of unbalance in a network. However, in the presented OP phase-ground voltage variables are involved and, therefore, the assumed range of δ can be used with a higher level of confidence. Based on δ, the following lower and upper bounds on real and imaginary

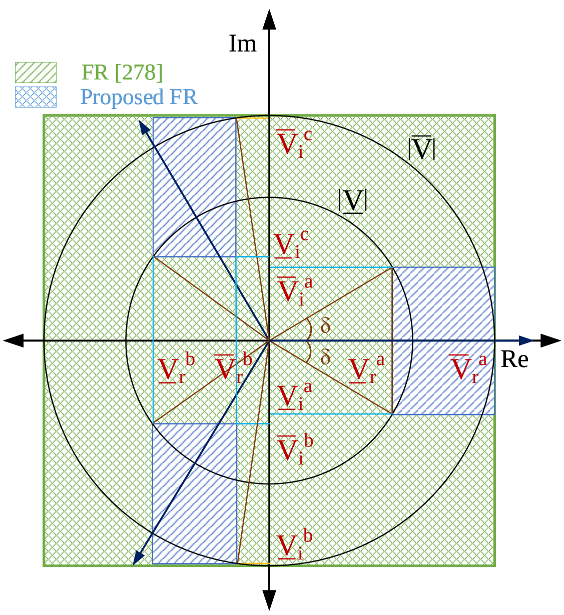

Figure 7.1: Proposed complex voltage variable bounds and associated feasible region.

voltage components are derived for each phase voltage variable in $\mathbf{\Pi}_{ii}$.

- Phase A:

$$|\underline{V_i}| \cdot cos(\delta_i) \leq \Re(V_i^a) \leq |\overline{V_i}| \tag{7.18}$$

$$-|\underline{V_i}| \cdot sin(\delta_i) \leq \Im(V_i^a) \leq |\underline{V_i}| \cdot sin(\delta_i) \tag{7.19}$$

- Phase B:

$$|\underline{V_i}| \cdot cos(240^\circ - \delta_i) \leq \Re(V_i^b) \leq |\overline{V_i}| \cdot cos(240^\circ + \delta_i) \tag{7.20}$$

$$|\overline{V_i}| \cdot sin(240^\circ - \delta_i) \leq \Im(V_i^b) \leq |\underline{V_i}| \cdot sin(240^\circ + \delta_i) \tag{7.21}$$

- Phase C:

$$|\underline{V_i}| \cdot cos(120^\circ + \delta_i) \leq \Re(V_i^c) \leq |\overline{V_i}| \cdot cos(120^\circ - \delta_i) \tag{7.22}$$

$$|\underline{V_i}| \cdot sin(120^\circ + \delta_i) \leq \Im(V_i^c) \leq |\overline{V_i}| \cdot sin(120^\circ - \delta_i) \tag{7.23}$$

It can be noted that the FR of each phase voltage variable is tightened by utilizing these new bounds which leads to a more accurate solution, as reported in section 7.3, in comparison to the solution obtained by setting the bounds proposed in [278].

The last point to be discussed in this section is the determination of bounds that can be put on the terms involving neutral voltage variables in $\mathbf{\Pi}_{ii}$. The technical standards usually provide the maximum limit on voltage unbalance but do not provide any guidelines on the maximum value of voltage appearing on a neutral conductor. However, the information about this voltage term may be of significant importance, for example, in the assessment and allocation of the losses as shown in the previous chapters. Consequently, in this work, the following procedure is adopted to set the minimum and maximum bounds on the real and imaginary component of a neutral voltage. To determine these bounds, a CCI-based load flow model is solved first and the real and imaginary components of neutral voltage are obtained at each node. Based on these components, the parameter $\sigma_{r/im}$ is set to the specified $max(|max(V_{nt_{r/im}})|, |min(V_{nt_{r/im}})|)$ value, which leads to bound each component of a neutral voltage within $(-\sigma_{r/im}, \sigma_{r/im})$ limits. This is equivalent to impose that neutral voltage after solving an OPF problem is not higher than its initial condition value.

7.2.2.3 Proposition-2 (P2)

Since P1 involves an additional matrix $\mathbf{\Pi}_{ii}$ variable at each node, setting additional McCormick constraints on the bilinear product of two terms of $\mathbf{\Pi}_{ii}$, corresponding to two different phases i.e., $\mathbf{\Pi}_{ii}^{(2,1)} \times \mathbf{\Pi}_{ii}^{(1,3)}$, leads to a quadratic matrix inequality which cannot be solved due to the lack of availability of any solver for handling this type of constraint. Consequently, to enforce the coupling between the voltage variables corresponding to the different phases of a same node, scalar complex voltage variables V_i^{φ} $\{\forall \varphi \in \phi, i \in N\}$ are introduced in P2 since the bilinear product of two scalar variables can, subsequently, be replaced by the McCormick envelopes [292], and, as a result, a convex region can ultimately be constituted through these linear inequalities. Following the introduction of new scalar variables, additional constraints are enforced in P2 to link V_i^{φ} with the terms of $\mathbf{W}_{ii}$ as shown below:

$$V_i^{\varphi'} V_i^{\varphi' *} \leq \mathbf{W}_{ii}^{\varphi'\varphi'} \qquad \forall \varphi' \in \phi_i, i \in N_{IL} \tag{7.24}$$

$$\begin{aligned} \langle V_{i_r}^{\varphi'} V_{i_r}^{\varphi''} \rangle^M + \langle V_{i_{im}}^{\varphi'} V_{i_{im}}^{\varphi''} \rangle^M &= \Re\{\mathbf{W}_{ii}(\varphi', \varphi'')\} \\ \langle V_{i_{im}}^{\varphi'} V_{i_r}^{\varphi''} \rangle^M - \langle V_{i_r}^{\varphi'} V_{i_{im}}^{\varphi''} \rangle^M &= \Im\{\mathbf{W}_{ii}(\varphi', \varphi'')\} \\ \forall \{\varphi', \varphi''\} &\in \phi_i, i \in N \& \varphi' \neq \varphi'' \end{aligned} \tag{7.25}$$

where M stands for McCormick envelope. Eq. (7.24) sets the limit on voltage magnitude of each complex variable V_i^{φ} by linking it to the diagonal terms of $\mathbf{W}_{ii}$. Please note that the equality constraint cannot be set in (7.24) since it leads to a quadratic constraint which is non-convex. Furthermore, (7.25) links the off-diagonal terms of $\mathbf{W}_{ii}$ with the bilinear product of scalar variables. Interestingly, it has been observed that setting only the constraint (7.24) results in a real value for each complex voltage variable after solving the OP, whereas the collective enforcement of (7.24)-(7.25) leads to the correct complex value of phase and neutral voltages. It is also important to emphasize that the bilinear product of phase and neutral voltages is also replaced by the convex region imposed by the McCormick envelopes, where upper and lower bounds on the neutral voltage are obtained as defined in section 7.2.2.2. Based on this proposition, the apparent power injection corresponding to the real term in (7.5) can be written as:

$$S_i^{\varphi, I_{P2}} = \left[\frac{1}{2} \left\{ (\hat{\mathbf{L}}_{i,l}^{\varphi,I} * \mathbf{V}_i) + (\hat{\mathbf{L}}_{i,l}^{T\varphi,I} * \mathbf{V}_i^*) \right\}^* \right]^{\circledast} \tag{7.26}$$

where $\circledast$ represents only the first element of vector on the right-hand side of (7.26).

7.2.2.4 Proposition-3 (P3)

In propositions P1 and P2, additional variables and constraints are introduced which increase the complexity of OPF relaxation. Consequently, to keep the relaxation as simple as possible, a further approximation in (6.50) is introduced which models the constant current component using only $\mathbf{W}_{ii}$ without introducing any new OV.

In the following discussion, the derivation is shown only for phase a; however, it is equally applicable for the injections at other phases and neutral conductors. For phase a, (6.50) can be re-written as:

$$S_i^{*ag} = k_I Y_{i_{(0)}}^{an} * \sqrt{(V_{i_r}^{ag} - V_{i_{im}}^{ag})^2} \tag{7.27}$$

$$= k_I Y_{i_{(0)}}^{an} * \sqrt{V_{i_r}^{2ag} + V_{i_{im}}^{2ag} - 2V_{i_r}^{ag} V_{i_{im}}^{ag}} \tag{7.28}$$

$$S_i^{*ag} \approx k_I Y_{i_{(0)}}^{an} * \sqrt{V_{i_r}^{2ag} + V_{i_{im}}^{2ag}} \tag{7.29}$$

$$= k_I Y_{i_{(0)}}^{an} * \sqrt{V_i^{ag} V_i^{*ag}} \tag{7.30}$$

$$S_i^{*ag} \approx k_I Y_{i_{(0)}}^{an} * (\mu_i + \mu_i * V_i^{ag} V_i^{*ag}) \tag{7.31}$$

It can be noted that an approximation is introduced in (7.29) under the assumption that for lightly and moderately unbalanced DNs, the imaginary part of phase a voltage would be small as compared to its real part i.e., $V_{i_{im}}^{2ag} \leq |2V_{i_r} V_{i_{im}}| \leq V_{i_r}^{2ag}$ and, therefore, these terms $V_{i_{im}}^{2ag}$ and $2V_{i_r}^{ag} V_{i_{im}}^{ag}$ can be dropped. Nevertheless, the former term is kept in (7.29) in order to have the product of variables $V_i^{ag} V_i^{*ag}$, which, in turn, is readily available in $\mathbf{W}_{ii}$. Furthermore, it can also be noticed that a further approximation is introduced in (7.31) by applying the *first-order Taylor* series on (7.30), evaluated at V_{a_0}, which leads to a linear-equation that can be easily realized through $\mathbf{W}_{ii}$. In (7.31), μ is a constant which depends on the point at which Taylor-series is evaluated. In this work, its value is chosen as 0.5. Based on (7.31), the approximate injection related to the absolute term in (7.5) can be written as:

$$\mathbf{S}_i^{\varphi, I_{P3}} = \mu_i * \text{diag}\{\mathbf{\Lambda}_{Y/\Delta_i}^{I_D} + (\mathbf{\Lambda}_{Y/\Delta_i}^{I_D} * \mathbf{W}_{ii})\}^* \tag{7.32}$$

It must be noted that to develop (7.11), (7.26) and (7.32) for other phases b and c, their voltage vectors must be rotated towards the reference position of phase a to have the equivalent power injection in these phases corresponding to the same load attached to them as connected to the phase a. It can also be noted that no additional constraints and variables are needed in this proposition. However, the introduction of two additional approximations i.e., (7.29) and (7.31), can lead to a suboptimal solution in the case of highly unbalanced DNs serving a large constant current load since imaginary component of a phase voltage cannot be ignored under such circumstances.

The complete injection related to a constant current component can now be expressed as:

$$\mathbf{S}_{\varrho_i}^{I\%} = \mathbf{S}_{\varrho_i}^{I^{sq}} + \mathbf{S}_i^{\varphi, \hat{I}} \tag{7.33}$$

where $\mathbf{S}_i^{\varphi, \hat{I}}$ is a $\mathbb{C}^{|\phi| \times 1}$ vector representing the injections obtained from P1 (7.11) or P2 (7.26) or P3 (7.32)-based approaches.

7.2.3 Modelling of grounding impedance

The grounding impedance can be incorporated in the proposed cheap OPF relaxation by formulating a ground matrix $\mathbf{\Lambda}_{ii}^{gnd}$, having dimensions equal to $\tau \times \tau$, at each node i which contains only neutral-ground admittance value at the diagonal position corresponding to a neutral conductor. Based on this matrix, the power injections related to the impedance connected between a neutral conductor and ground can be defined as:

$$\mathbf{S}_i^{gnd} = \text{diag}\{\mathbf{\Lambda}_{ii}^{gnd} * \mathbf{W}_{ii}\}^* \tag{7.34}$$

Similarly, bus shunt admittances or any shunt element which is connected between a particular phase and ground can be incorporated in the OPF model by formulating a $\mathbf{\Lambda}_{ii}^{sh}$ matrix which contains the respective admittance at the diagonal entry corresponding to the phase to which the shunt element is connected and, subsequently, the power injections related to it can be expressed in the same way as reported in (7.34).

$$\mathbf{S}_i^{sh} = \text{diag}\{\mathbf{\Lambda}_{ii}^{sh} * \mathbf{W}_{ii}\}^* \tag{7.35}$$

7.2.4 Convexified cheap OPF model for neutral-equipped networks

The cheap SDP-based OPF model for multi-phase active DNNs containing both wye- and delta-connected loads can now be developed since explicit (decoupled) power injections for each phase and neutral conductor have been derived in the previous sections corresponding to a full ZIP load which finally lead to the model **M7.2**. Please note that $\mathbf{S}_{\varrho_i}$ in (7.36b) represents the summation of power injections from each component of a ZIP load. The model **M7.2** contains three sub-models related to the modelling technique utilized for a constant current load. Furthermore, the model is still non-convex due to the presence of (7.36h) and (7.36i) constraints which are finally dropped to make it a convex model.

7.2.5 Objective functions

The same OFs as mentioned in chapter 6 are chosen for the evaluation of proposed cheap OPF relaxation. In terms of the OVs of **M7.2**, these OFs can be represented as follows:

$$f_{\mathbf{OF_1}}(\mathbf{S}_{g_1}) = \sum_{\varphi=1}^{r} \Big\{ \Re(\mathbf{S}_{g_1}^{\varphi}) + \Im(\mathbf{S}_{g_1}^{\varphi}) \Big\} \tag{7.37}$$

$$f_{\mathbf{OF_2}}(\mathbf{\Pi}) = \Re\Big\{ \sum_{j:i\sim j} \text{Tr}(\mathbf{Z}_{ij}\boldsymbol{\lambda}_{ij}) \Big\} \tag{7.38}$$

7.3 Quality assessment of the proposed relaxation

The quality assessment of the proposed relaxation **M7.2** in terms of recovered solution, maximum voltage angle limits, neutral envelopes and CT is reported in this section for several combinations of ZIP load parameters. The same LMs, as mentioned in chapter 6, are used in this case study. Furthermore, four additional LMs are also introduced, as reported in Table 7.1, to evaluate the exactness of all propositions (P1-P3) under $+k_I$ coefficients. The relaxation **M7.2** is applied on MG, IT-37 and CIGRE DNs and finally, for all the simulation scenarios, $\underline{V}$ and $\overline{V}$ are set to 0.90 and 1.05pu, respectively.

The exactness, and lack thereof, of **M7.2** is determined on the basis of %RD criterion which is defined as:

$$\%RD = \frac{|obj|_{MPSDP} - |obj|_{cheap-SDP}}{|obj|_{MPSDP}} \times 100 \tag{7.39}$$

M7.2: Cheap conic OPF relaxation for a multi-phase DNN

Proposition 1 :

variables : $\mathbf{S}_{g_i} \in \mathbb{C}^{|\phi_i|}, \mathbf{W}_{ii} \in \mathbb{H}^{|\phi_i|\times|\phi_i|}, \quad (\forall i \in N)$

$\mathbf{\Pi}_{ii} \in \mathbb{H}^{|\phi_i|\times|\phi_i|}, \quad (\forall i \in N_{IL})$

$\mathbf{S}_{ij} \in \mathbb{C}^{|\phi_{ij}|\times|\phi_{ij}|}, \mathbf{\Pi}_{ij} \in \mathbb{H}^{|\phi_{ij}|\times|\phi_{ij}|} \quad (\forall i \sim j \in E)$

subject to : (7.13)-(7.15), (7.16)-(7.17), (7.36a)-(7.36g)

$$\mathbf{W}_{jj} = \mathbf{W}_{ii} - (\mathbf{S}_{ij}\mathbf{Z}_{ij}^H + \mathbf{Z}_{ij}\mathbf{S}_{ij}^H) + \mathbf{Z}_{ij}\,\mathbf{\Pi}_{ij}\,\mathbf{Z}_{ij}^H \qquad \forall(j : i \sim j) \in E \tag{7.36a}$$

$$\sum_{k:k\sim i} \text{diag}(\mathbf{S}_{ki} - \mathbf{Z}_{ki}\mathbf{\Pi}_{ki}) - \sum_{j:i\sim j} \text{diag}(\mathbf{S}_{ij}) = \mathbf{S}_{g_i} - (\mathbf{S}_{\varrho_i} + \mathbf{S}_i^{gnd} + \mathbf{S}_i^{sh}) \quad \forall i \in N \tag{7.36b}$$

$$\underline{\mathbf{S}}_{g_i} \leq \mathbf{S}_{g_i} \leq \overline{\mathbf{S}}_{g_i} \qquad \forall i \in N \tag{7.36c}$$

$$|\underline{\mathbf{V}}|_i^2 \leq \text{diag}(\mathbf{W}_{ii}) \leq |\overline{\mathbf{V}}|_i^2 \qquad \forall i \in N^+ \tag{7.36d}$$

$$[\mathbf{W}]_{\eta_0\times\eta_0} = \mathbf{V}_0\mathbf{V}_0^H \tag{7.36e}$$

$$\mathbf{W}_{ii} \succeq 0 \qquad \forall i \in N \tag{7.36f}$$

$$\begin{bmatrix} \mathbf{W}_{ii} & \mathbf{S}_{ij} \\ \mathbf{S}_{ij}^H & \mathbf{\Pi}_{ij} \end{bmatrix} \succeq 0 \qquad \forall(j : i \sim j) \in E \tag{7.36g}$$

$$\text{rank}(\mathbf{W}_{ii}) = 1 \qquad \forall i \in N^T \tag{7.36h}$$

$$\text{rank}\left(\begin{bmatrix} \mathbf{W}_{ii} & \mathbf{S}_{ij} \\ \mathbf{S}_{ij}^H & \mathbf{\Pi}_{ij} \end{bmatrix}\right) = 1 \qquad \forall(j : i \sim j) \in E \tag{7.36i}$$

Proposition 2 :

variables : $\mathbf{S}_{g_i} \in \mathbb{C}^{|\phi_i|}, \mathbf{W}_{ii} \in \mathbb{H}^{|\phi_i|\times|\phi_i|} \quad (\forall i \in N)$

$V_i^{\varphi} \in \mathbb{C}^{1\times 1} \quad (\forall \varphi \in \phi, i \in N)$

$\mathbf{S}_{ij} \in \mathbb{C}^{|\phi_{ij}|\times|\phi_{ij}|}, \mathbf{\Pi}_{ij} \in \mathbb{H}^{|\phi_{ij}|\times|\phi_{ij}|} \quad (\forall i \sim j \in E)$

subject to : (7.36a)-(7.36g), (7.24)-(7.25)

Proposition 3 :

variables : $\mathbf{S}_{g_i} \in \mathbb{C}^{|\phi_i|}, \mathbf{W}_{ii} \in \mathbb{H}^{|\phi_i|\times|\phi_i|} \quad (\forall i \in N)$

$\mathbf{S}_{ij} \in \mathbb{C}^{|\phi_{ij}|\times|\phi_{ij}|}, \mathbf{\Pi}_{ij} \in \mathbb{H}^{|\phi_{ij}|\times|\phi_{ij}|} \quad (\forall i \sim j \in E)$

subject to : (7.36a)-(7.36g)

It can be seen that the optimal solution of cheap SDP-based relaxation is compared with the optimal solution of MPSDP-based relaxation and the former approach is considered

Table 7.1: Types of load models.

Load Models and their Parameters													
LMs	$\mathbf{P_L}$			$\mathbf{Q_L}$			**LMs**	$\mathbf{P_L}$			$\mathbf{Q_L}$		
	k_Z	k_I	k_P	k_Z	k_I	k_P		k_Z	k_I	k_P	k_Z	k_I	k_P
LM:11	0.05	0.31	0.63	-0.56	2.20	-0.65	**LM:12**	0.23	0.61	0.16	-1.21	3.47	-1.26
LM:13	-1.60	3.58	-0.98	0.79	-0.16	0.36	**LM:14**	-2.78	6.06	-2.28	-2.78	6.06	-2.28

exact if %RD remains within 2%. The exactness of MPSDP-based relaxation is checked using EVR criterion, $|\hat{\lambda}_{P-1}|/|\hat{\lambda}_P| \leq 10^{-5}$, which raises the natural question *why the same criterion is not used for establishing the exactness of cheap SDP-based OPF relaxation?* The reason is the lack of existence of any theoretical guarantee(s), as of now, that obtaining a rank-1 solution for each matrix in (7.36g) also provides a rank-1 solution for MPSDP-based relaxation if it (recovered solution from **M7.2**) is substituted in $\hat{\mathbf{W}}$ matrix. Although, few published works [257] consider the cheap SDP-based relaxation exact if EVR of each matrix in (7.36g) is below the specified threshold value. However, it has been observed in this work that extremely short branches/lines (small impedance value) can lead to an EVR which can be as large as 10^{-3}. But even in such cases, the obtained %RD is within 2% range. Therefore, in this work, the comparison between the optimal solutions of MPSDP- and cheap SDP-based OPF relaxations is considered as a more suitable criterion to ensure the exactness of latter relaxation, provided the former relaxation is exact. Due to the dominance of MPSDP-based relaxation over cheap SDP-based model, unless an equivalence is established between the two in the case of RDNs, the latter relaxation will be considered inexact for all such cases where the former relaxation fails to provide a meaningful solution.

Tables 7.3 and 7.4 compare the exactness of each proposition (P1-P3)-based OPF model with the standard MPSDP-based OPF relaxation for OF1 and OF2, respectively. In all the test cases, MPG configuration is considered by setting $R_{gnd} = 1\Omega$ at each node. Finally, to ease the reading process and better clarification of the results, font styles used in Tables 7.3 and 7.4 are mentioned in Table 7.2 along with their interpretation.

7.3.1 Exactness in terms of eigen-value ratio criterion

In the context of exactness, and lack-thereof, of the proposed approach, the following observations can be made based upon the chosen criterion. Please note that the results reported in Tables 7.3 and 7.4 are based on the angle limit δ value equal to 5° for P1- and P2-based OPF relaxations.

Table 7.2: Font styles and their interpretation.

Style	Interpretation	Style	Interpretation
Bold	SDP is inexact	<u>**Bold-Underline**</u>	P3 is exact; P1 and P2 are inexact
Bold-Italic	P2 dominates P1 (P1 is inexact)	<u>*Italic-Underline*</u>	MPSDP is exact, BFM-SDP is inexact
<u>Underline</u>	P1 dominates P2	*Italic*†	P2 dominates P3

Table 7.3: Comparison of MPSDP- and cheap SDP-based OPF relaxations under OF1 for $R_{gnd} = 1\Omega$.

OF:1 Slack Bus Power (kVA)															
LMs	*Y-connected End-Users*					*Δ-connected End-Users*					*Y-Δ connected End-Users*				
	SDP		**BFM-SDP**			**SDP**		**BFM-SDP**			**SDP**		**BFM-SDP**		
	EVR $\lvert\hat{\lambda}_{P-1}\rvert/\lvert\hat{\lambda}_P\rvert$ $\times 10^{-5}$	*Obj. Value*	*% Relative Difference*			*EVR* $\lvert\hat{\lambda}_{P-1}\rvert/\lvert\hat{\lambda}_P\rvert$ $\times 10^{-5}$	*Obj. Value*	*% Relative Difference*			*EVR* $\lvert\hat{\lambda}_{P-1}\rvert/\lvert\hat{\lambda}_P\rvert$ $\times 10^{-5}$	*Obj. Value*	*% Relative Difference*		
MG: Lightly Unbalanced DN															
LM:1	0.32	2828.6	0.01	0.01	0.01	2.86	2823.8	0.56	0.56	0.56	1.12	2824.8	0.17	0.18	0.17
LM:2	0.15	2918.3	***9.09***	***0.57***	0.08	0.72	2917.6	***9.10***	***0.58***	0.08	1.65	2906.5	***8.94***	***0.20***	0.49
LM:3	0.16	3021.2	0.03	0.03	0.03	1.18	3020.3	0.22	0.22	0.22	0.17	3018.5	0.04	0.04	0.04
LM:4	0.30	3123.1	0.05	*0.06*†	*0.40*†	0.05	2881.6	0.11	*0.12*†	*0.46*†	**55.2**	2881.4	**5.18**	**15.7**	**1.34**
LM:5	0.15	2929.5	0.01	0.00	0.01	2.26	2929.1	0.42	0.42	0.43	0.17	2927.8	0.00	0.01	0.02
LM:6	0.28	2940.7	0.01	0.01	0.16	0.15	2919.3	0.07	*0.07*†	*0.24*†	0.40	2922.6	0.07	*0.03*†	*0.32*†
LM:7	0.04	2943.0	0.03	0.03	0.12	0.16	2944.5	0.00	0.00	0.09	1.53	2950.3	0.02	0.02	0.08
LM:8	1.27	2946.8	0.24	0.24	0.24	0.11	2943.3	0.02	0.02	0.02	0.28	2952.0	0.11	0.09	0.10
LM:9	0.10	2862.7	0.03	0.03	0.03	3.81	2866.3	0.51	0.51	0.52	0.03	2868.3	0.01	0.01	0.02
LM:10	0.18	2999.4	0.01	0.01	0.03	0.32	2998.1	0.03	0.03	0.02	0.25	2999.5	0.01	0.01	0.01
LM:11	0.18	2953.2	***7.95***	***0.04***	*0.65*†	3.50	2935.5	***8.52***	***0.57***	0.03	0.39	2953.8	***8.49***	***0.51***	0.09
LM:12	0.07	2914.1	***14.7***	***0.91***	0.09	0.13	2911.0	***14.7***	***0.89***	0.11	0.04	2910.4	***14.4***	***0.85***	0.10
LM:13	1.24	2940.2	***22.6***	***1.39***	0.16	0.21	2942.4	***22.8***	***1.63***	0.08	1.22	2949.7	***23.3***	***1.32***	0.31
LM:14	3.45	2972.6	**72.4**	**3.56**	**0.46**	0.45	2955.6	**72.5**	**3.38**	**0.66**	0.53	2949.9	**70.1**	**3.48**	**0.19**
IT-37: Moderately Unbalanced DN															
LM:1	0.34	98.04	0.14	0.14	0.14	0.11	98.4	0.02	0.02	0.02	0.47	97.60	0.03	0.03	0.03
LM:2	1.34	102.0	***10.15***	***0.68***	0.21	0.28	102.1	***10.3***	***0.57***	0.18	0.93	102.0	***10.2***	***0.65***	0.26
LM:3	0.84	106.5	0.12	0.12	0.12	0.51	106.3	0.10	0.10	0.10	0.48	107.0	0.30	0.30	0.30
LM:4	1.96	99.94	0.64	0.86	0.37	1.87	123.7	**6.75**	**14.5**	**1.46**	**110.0**	128.3	**30.2**	**57.5**	**4.79**
LM:5	0.56	102.5	0.15	0.15	0.14	0.46	102.5	0.03	0.03	0.04	0.53	102.4	0.14	0.14	0.13
LM:6	1.47	101.8	0.30	0.31	0.17	0.36	105.1	0.26	*0.27*†	*0.46*†	0.93	105.4	***10.1***	***11.4***	***0.01***
LM:7	0.44	102.9	0.31	0.32	0.24	0.18	103.1	0.09	0.09	0.02	0.28	102.9	0.04	0.04	0.07
LM:8	0.66	103.4	0.25	0.25	0.25	0.15	103.3	0.04	0.04	0.04	0.34	103.4	0.14	0.14	0.14
LM:9	0.14	99.73	0.14	0.14	0.13	0.22	100.0	0.31	0.31	0.30	0.77	99.40	0.36	0.36	0.35
LM:10	0.19	105.9	*6.25*	*6.25*	*6.24*	0.17	105.7	*5.91*	*5.91*	*5.90*	0.18	106.3	*7.12*	*7.12*	*7.11*
LM:11	0.31	103.8	***11.0***	***1.82***	0.05	0.03	103.9	***7.38***	***0.30***	0.28	0.08	103.9	***7.82***	***0.56***	0.12
LM:12	0.24	101.8	***19.5***	***2.02***	0.11	0.11	102.3	***13.0***	***0.83***	0.13	0.03	102.0	***13.7***	***0.93***	0.17
LM:13	0.30	103.4	**46.1**	**3.19**	**0.24**	0.59	103.4	***30.5***	***1.78***	0.16	0.32	103.8	***30.2***	***1.93***	0.43
LM:14	0.29	102.1	**135.4**	**4.80**	**0.36**	0.30	103.6	**77.3**	**3.87**	**0.40**	0.21	101.2	***83.1***	***1.92***	1.01
CIGRE: Highly Unbalanced DN															
LM:1	1.09	143.5	0.07	0.07	0.07	1.58	144.0	0.01	0.01	0.01	0.93	143.7	0.02	0.02	0.02
LM:2	1.02	153.4	***15.7***	***0.75***	0.14	1.39	153.3	***15.1***	***0.68***	0.13	0.90	153.3	***15.5***	***0.71***	0.16
LM:3	0.72	166.5	0.04	0.04	0.04	0.92	166.4	0.02	0.02	0.02	1.27	166.6	0.07	0.07	0.07
LM:4	**13.0**	149.6	**0.05**	**0.47**	**8.70**	**1680**	191.9	**0.56**	**10.6**	**32.0**	**120.0**	166.3	**0.90**	**1.76**	**13.1**
LM:5	0.77	154.9	0.02	0.02	0.01	0.78	155.3	0.18	0.47	0.00	1.25	155.1	0.05	0.05	0.02
LM:6	7.03	154.3	0.02	0.07	0.59	**63.3**	176.0	**2.51**	**6.03**	**2.89**	4.44	158.6	0.90	0.74	0.79
LM:7	3.11	157.0	0.01	*0.02*†	*023*†	1.93	159.2	1.40	1.73	0.39	2.21	157.8	0.24	0.25	0.54
LM:8	0.82	157.0	0.02	0.02	0.02	1.52	157.2	0.00	0.00	0.00	1.18	157.1	0.00	0.00	0.00
LM:9	1.32	147.8	0.02	0.02	0.00	1.59	148.3	0.12	0.41	0.01	0.85	148.0	0.01	0.01	0.01
LM:10	1.16	163.6	0.01	0.01	0.03	0.88	163.7	0.22	0.50	0.01	1.84	163.8	0.07	0.07	0.03
LM:11	0.50	157.4	***14.3***	***0.68***	0.15	0.58	157.1	***14.3***	***0.67***	0.18	0.62	157.2	***14.3***	***0.65***	0.18
LM:12	1.70	152.3	***25.5***	***1.15***	0.25	0.79	152.2	***25.6***	***1.24***	0.28	0.78	152.1	***25.6***	***1.14***	0.28
LM:13	0.69	155.4	***41.4***	***1.73***	0.46	0.76	156.2	***38.7***	***1.37***	0.39	1.26	155.6	***40.4***	***1.73***	0.37
LM:14	1.59	153.3	**136.7**	**3.72**	**1.15**	1.72	155.6	**144.0**	**5.03**	**0.95**	0.61	154.0	**138.4**	**4.51**	**0.84**

1. For all LMs which are independent of constant current component i.e., LMs 1, 3 and 8, the proposed relaxation provides an exact solution when tested for both OFs. Since in the absence of constant current load, the OPF model **M7.2** becomes same for all propositions, therefore, the same %RD, as per expectation, is obtained in all cases as can be noted from the presented results.

2. For LMs which contain large active and reactive power contributions from constant current load such as LMs 4, 6 and 14, the MPSDP-based relaxation becomes inexact

Table 7.4: Comparison of MPSDP- and cheap SDP-based OPF relaxations under OF2 for $R_{gnd} = 1\Omega$.

OF:2 Power Losses (kW)															
LMs	*Y-connected End-Users*					*Δ-connected End-Users*					*Y-Δ connected End-Users*				
	SDP		BFM-SDP			SDP		BFM-SDP			SDP		BFM-SDP		
	EVR $\lvert\hat{\lambda}_{P-1}\rvert/\lvert\hat{\lambda}_P\rvert$ $\times 10^{-5}$	*Obj. Value*	*% Relative Difference*			*EVR* $\lvert\hat{\lambda}_{P-1}\rvert/\lvert\hat{\lambda}_P\rvert$ $\times 10^{-5}$	*Obj. Value*	*% Relative Difference*			*EVR* $\lvert\hat{\lambda}_{P-1}\rvert/\lvert\hat{\lambda}_P\rvert$ $\times 10^{-5}$	*Obj. Value*	*% Relative Difference*		
MG: Lightly Unbalanced DN															
LM:1	0.73	90.2	0.05	0.05	0.05	0.06	93.6	0.13	0.13	0.13	0.31	91.1	0.26	0.26	0.26
LM:2	0.70	100.6	***16.6***	***1.41***	0.16	0.03	96.9	***16.2***	***0.89***	0.32	0.20	96.3	***17.1***	***1.33***	0.01
LM:3	0.25	107.2	0.41	0.41	0.41	0.11	104.5	0.00	0.00	0.00	0.20	104.4	0.23	0.23	0.24
LM:4	0.06	133.1	0.17	0.34	0.31	0.36	96.7	0.80	0.99	0.16	**71.0**	96.2	**34.3**	**113.0**	**1.10**
LM:5	0.03	100.5	0.07	0.07	0.04	0.54	98.2	0.08	0.07	0.10	0.15	98.4	0.01	0.00	0.04
LM:6	0.24	127.6	1.05	0.37	0.18	0.23	98.0	0.69	*0.67*†	*1.08*†	0.52	99.2	**4.62**	**3.07**	**1.37**
LM:7	0.10	101.2	0.18	0.23	0.03	0.25	99.2	0.39	0.41	0.19	0.46	106.0	1.61	1.67	1.36
LM:8	0.93	101.5	0.95	0.95	0.95	1.13	101.0	0.73	0.73	0.73	1.24	99.2	0.42	0.43	0.43
LM:9	0.12	95.2	1.10	1.11	1.08	0.83	91.7	0.04	0.05	0.02	0.07	94.0	0.50	0.50	0.47
LM:10	0.27	106.4	0.92	0.91	0.94	0.46	102.1	0.08	0.08	0.11	1.23	101.4	0.38	0.38	0.12
LM:11	0.05	101.8	***11.4***	***0.31***	0.59	0.30	100.1	***11.8***	***0.73***	0.12	0.09	100.6	***11.3***	***0.53***	0.38
LM:12	0.70	102.9	***18.3***	***0.73***	1.28	1.31	95.1	***19.6***	***0.81***	0.67	0.27	96.6	***20.5***	***1.79***	1.47
LM:13	1.11	104.5	**40.9**	**3.59**	**0.22**	0.45	100.7	**40.2**	**2.38**	**1.01**	0.38	99.5	**41.1**	**3.19**	**0.49**
LM:14	0.22	111.5	**85.8**	**9.79**	**0.04**	0.71	103.9	**85.9**	**8.00**	**0.65**	1.06	101.9	*70.5*	*3.94*	*2.23*
IT-37: Moderately Unbalanced DN															
LM:1	1.50	2.65	0.79	0.80	0.80	0.49	2.51	0.26	0.26	0.26	0.74	2.80	0.11	0.12	0.12
LM:2	0.48	2.79	**18.6**	**3.05**	**1.41**	0.22	2.67	***17.8***	***1.10***	0.34	0.24	2.93	***17.1***	***1.76***	0.13
LM:3	0.43	3.09	0.32	0.32	0.32	0.24	2.91	0.66	0.66	0.66	0.61	3.44	2.03	2.03	2.03
LM:4	0.43	2.96	0.39	0.39	0.01	**26.4**	19.3	**8.25**	**68.1**	**0.47**	**69.6**	25.3	**76.0**	**161.1**	**5.54**
LM:5	0.22	2.88	0.10	0.09	0.12	0.33	2.75	0.13	0.13	0.11	1.17	3.10	1.04	1.03	1.00
LM:6	0.90	2.89	0.94	*0.95*†	*1.16*†	0.60	5.29	0.49	*0.55*†	*1.12*†	3.00	6.64	**64.5**	**80.2**	**1.11**
LM:7	0.25	2.96	0.00	0.00	0.16	0.21	3.04	0.60	0.65	0.46	0.55	3.51	0.03	0.02	0.24
LM:8	2.14	2.92	0.27	0.27	0.27	0.28	2.83	0.67	0.67	0.67	0.25	3.21	0.94	0.94	0.94
LM:9	0.45	2.72	0.22	0.21	0.20	0.43	2.56	0.19	0.19	0.17	0.57	2.85	0.88	0.88	0.90
LM:10	0.54	3.13	1.89	3.73	1.81	0.52	3.05	0.84	2.69	0.75	0.65	3.41	**3.15**	**3.15**	**1.05**
LM:11	0.25	2.99	**5.69**	**2.79**	**1.43**	0.22	2.92	***4.94***	***0.94***	1.23	0.60	3.14	**6.09**	**8.92**	**1.93**
LM:12	0.56	2.80	**10.8**	**3.75**	**1.90**	0.87	2.89	**6.45**	**3.41**	**1.34**	0.57	3.10	**13.6**	**37.6**	**1.85**
LM:13	0.92	2.99	***51.0***	***1.20***	1.30	0.69	2.90	**54.0**	**2.26**	**1.72**	0.52	3.53	**40.3**	**3.50**	**1.37**
LM:14	0.46	3.00	**90.8**	**6.34**	**1.84**	0.18	3.68	*50.5*	*25.5*	*2.20*	0.27	4.20	**75.0**	**169.1**	**1.75**
CIGRE: Highly Unbalanced DN															
LM:1	6.95	5.78	0.36	0.37	0.37	1.43	5.77	0.56	0.56	0.56	1.62	5.76	0.97	0.97	0.97
LM:2	1.90	6.46	***17.9***	***1.18***	0.06	3.67	6.27	***17.7***	***0.82***	0.41	1.38	6.40	***18.2***	***1.53***	0.15
LM:3	0.42	7.65	1.73	1.73	1.73	3.64	7.38	0.81	0.81	0.81	1.86	7.59	0.52	0.52	0.52
LM:4	5.55	6.50	***2.11***	***1.82***	0.27	**581.8**	20.59	**3.35**	**23.7**	**5.08**	**89.1**	12.18	**0.79**	**3.35**	**2.19**
LM:5	2.31	6.63	0.64	1.16	0.53	0.43	6.60	1.45	1.01	1.60	1.32	6.65	0.06	0.23	0.18
LM:6	2.25	6.74	1.37	1.24	0.29	1.86	10.7	0.06	1.56	1.13	1.15	8.11	*0.88*†	*0.82*†	*3.92*†
LM:7	1.13	6.82	1.30	1.59	0.28	3.04	7.38	0.95	0.93	0.02	0.77	7.04	1.00	1.51	0.33
LM:8	1.98	6.78	0.19	0.18	0.18	1.31	6.68	0.10	0.10	0.10	0.34	6.79	1.13	1.12	1.12
LM:9	2.19	6.08	0.03	0.42	0.04	0.85	6.07	0.69	0.34	0.77	1.02	6.08	0.17	0.18	0.24
LM:10	5.66	7.38	0.92	1.41	0.76	0.21	7.18	0.08	0.72	0.14	0.38	7.33	0.08	0.59	0.13
LM:11	2.69	6.86	***17.6***	***1.08***	0.36	1.20	6.63	**21.2**	**3.80**	**0.50**	2.86	6.77	**20.9**	**3.67**	**0.69**
LM:12	6.83	6.41	***29.6***	***1.95***	0.51	2.54	6.35	**36.1**	**6.14**	**1.11**	5.10	6.36	**35.6**	**6.81**	**0.43**
LM:13	4.41	6.66	**31.4**	**2.50**	**1.21**	3.98	6.51	**35.9**	**8.18**	**1.54**	5.73	6.47	**36.1**	**8.92**	**1.67**
LM:14	**17.55**	6.67	**86.0**	**6.93**	**2.82**	5.12	6.89	**87.4**	**20.9**	**1.67**	**28.1**	6.79	**90.1**	**22.5**	**2.44**

(as indicated by the **bold** font style) and, resultantly, a high EVR (10^{-2}) for each matrix in (7.36g) is also observed in the case of cheap SDP-based relaxation which confirms its inexactness as well.

3. The MPSDP-based relaxation dominates the cheap SDP-based OPF model since a large %RD is observed in few cases (LM 10 and LM 14 in the case of OF1 and OF2, respectively) for the latter relaxation, whereas the former methodology has

provided the exact solution for these cases as well. This points out that the cheap conic relaxation might not be equivalent to the MPSDP-based relaxation even in the case of RDNs. However, further investigation in this regard is necessary.

4. The dominance of proposed P1-, P2- and P3-based relaxations over each other strongly depends on the sign of k_I coefficient i.e., whether constant current load injects ($-k_I$) or absorbs ($+k_I$) power into/from the system. With respect to $-k_I$ coefficient, P3-based relaxation provides an exact solution in all such LMs and becomes inexact only when MPSDP-based relaxation fails to provide a meaningful solution. Furthermore, it dominates the P1- and P2-based OPF models as can be noted in the bold-underline cases (OF2) where these OPF models exhibit a large %RD, and are, therefore, considered inexact in comparison to the P3-based OPF model which provides a very close solution to the MPSDP-based relaxation results. However, few cases, as identified by the *italic* style, are also observed where P2-based relaxation provides a more tighter solution as compared to the P3-based model. Nevertheless, the exactness of P3-based model even in these cases, with a considerably small difference between the results of these propositions (P2 and P3) and given the fact that P1- and P2-based relaxations can fail for some LMs, makes it a stronger model among all propositions.

5. With respect to the same coefficients ($+k_I$), P1- and P2-based OPF models almost provide the same identical solution in majority of the cases. However, few cases as mentioned by the underline style shows the superiority of P1 over P2, especially in the case of OF2 where P2-based OPF relaxation provides an inexact solution in the case of LM 10. This is an unexpected observation since P2-based relaxation is supposed to be more tighter than the P1-based model. The reason for this unanticipated behaviour lies in the chosen value of δ which appears too tight for the scalar voltage variable of proposition P2. However, it has been noted that by slightly relaxing the angle limit from 5° to 7°, the exact solution is obtained again for P2-based relaxation which dominates the solution recovered from the P1-based OPF model.

6. With respect to the positive k_I coefficients, P1-based OPF model fails for all such LMs as indicated by the extremely large %RD and obtained poor EVR. P2-based relaxation brings down the %RD within the specified 2% (providing an exact solution) in majority of the cases as indicated by the ***bold-italic*** style and, therefore, exhibits a superior performance over the P1-based relaxation.

7. The P3-based relaxation further tightens the model **M7.2** and provides a more accurate solution in comparison to the P2-based approach. Furthermore, it remains exact and provides a meaningful solution even in the case of large power absorbing constant current LMs for which the inexactness is observed in the case of P2-based OPF relaxation as outlined by the **bold-underline** style. Nevertheless, under large contribution from the constant current component, P3 fails as well as observed in the case of OF2 for LMs 13 and 14. However, the MPSDP-based relaxation provides an

exact solution in few instances of such cases which further confirms the dominance of this relaxation over cheap conic relaxation.

8. To conclude the discussion with respect to the propositions for constant current component modelling, it is justified to say that the P3-based OPF model appears to be the strongest among all the presented OPF models. It has the tendency to remain exact under all LMs having power absorbing as well as power injecting constant current loads. However, its general dominance cannot be established due to the presence of few cases where P2-based relaxation dominates it. On the other hand, the P2-based OPF model dominates the P1-based OPF approach in the case of positive coefficient-based constant current loads, whereas for negative coefficient-based loads, the P1-approach can be adopted due to its easy and simple implementation in comparison to the P2-based OPF model.

9. With respect to the degree of unbalance, the P3-based relaxation provides an optimal solution for wye-connected loads in the case of lightly and moderately unbalanced DNs for all LMs. However, for delta and mixed load types, the relaxation becomes inexact under largely dominated constant current LMs (4, 6, 14) due to the fact that ignoring imaginary component of phases voltage has a more negative impact on the accuracy of proposed relaxation as compared to the dropping of imaginary component of a neutral voltage.

10. In the case of highly unbalanced DNs, the MPSDP-based relaxation becomes inexact and, therefore, it is expected that a suboptimal solution would also be obtained from the cheap conic P3-based relaxation. Finally, to conclude this point, it is sufficient to say that with an increase in the degree of unbalance, a relatively large %RD should be expected particularly in the case of LMs having dominating constant current load participation.

7.3.2 Impact of voltage angle deviation limits and neutral envelopes on the exactness of proposed relaxation

The voltage angle deviation parameter δ plays a significant role in the exactness of P1- and P2-based relaxations when tested for LMs having $+k_I$ values, as can be seen from the results reported in Table 7.5. It can be noted that for such LMs, tightening the angle limit from 15° to 5° reduces the %RD for both propositions; in particular, P2-based relaxation becomes exact in majority of the cases for δ value equal to 5°. In the case of P1-based OPF model, setting small angle limit does reduce the %RD; however, the obtained solution is still far from the solution obtained from MPSDP-based relaxation and, consequently, cannot be considered as an exact solution. It can also be observed that imposing the limits on voltage variables as suggested by [278] fails to provide a meaningful solution.

On the other hand, in the case of LMs which inject active/reactive power in DNs i.e., $-k_I$ values, the impact of angle limit on the exactness of P1- and P2-based relaxation is minimal. For such LMs, almost same %RD is observed for both relaxations. These results, therefore, suggest that a moderate value of δ parameter can be selected if an OP involves

Table 7.5: Exactness of P1- and P2-based OPF relaxations under the influence of varying voltage angle limit.

LMs	*Y-connected End-Users*								*Δ-connected End-Users*							
	%RD with respect to MPSDR value for OF2															
	Ref	*δ for P1*			**Ref**	*δ for P2*			**Ref**	*δ for P1*			**Ref**	*δ for P2*		
	[278]	15°	10°	5°	[278]	15°	10°	5°	[278]	15°	10°	5°	[278]	15°	10°	5°
MG																
LM:2	99.9	23.6	20.2	16.6	99.8	9.09	5.02	1.41	99.9	21.6	17.9	16.2	99.9	6.59	2.75	0.89
LM:11	52.8	15.3	12.8	11.4	52.4	4.65	2.13	0.31	53.9	15.4	12.9	11.8	53.0	4.62	1.84	0.73
LM:12	56.1	26.3	22.7	18.3	58.4	10.3	6.44	0.73	59.3	24.6	20.7	19.6	56.8	6.63	2.10	0.81
LM:13	73.2	53.0	46.8	40.9	72.6	20.0	9.84	3.59	73.6	51.8	45.2	40.2	72.6	19.2	9.73	2.38
LM:14	89.4	84.4	76.4	85.8	90.4	34.7	16.2	9.79	99.8	96.7	91.3	85.9	98.8	42.3	23.8	8.00
IT-37																
LM:2	100.0	32.6	29.3	18.6	100.0	8.17	3.26	3.05	100.0	32.0	28.7	17.8	100.0	6.17	1.75	1.10
LM:11	44.4	14.3	12.8	5.69	44.8	3.42	1.13	2.79	44.1	14.3	12.9	4.94	46.1	3.07	1.00	0.94
LM:12	52.6	24.7	22.4	10.8	53.1	5.97	1.81	3.75	48.8	23.3	21.0	6.45	54.6	4.40	0.69	3.41
LM:13	90.6	82.6	78.7	51.0	90.7	29.0	14.9	1.20	88.6	80.5	76.6	54.0	89.1	24.6	12.3	2.26
LM:14	100.0	100.0	100.0	90.8	100.0	51.0	28.3	6.34	75.4	76.2	76.2	50.5	75.8	34.6	18.0	25.5
CIGRE																
LM:2	100.0	35.4	31.5	17.9	100.0	8.44	3.74	1.18	100.0	33.9	30.0	17.7	100.0	7.40	3.03	0.82
LM:11	69.3	33.0	29.4	17.6	70.4	8.16	3.76	1.08	70.2	33.9	30.3	21.2	71.8	8.11	3.62	3.80
LM:12	73.4	53.0	48.5	29.6	74.1	12.9	5.66	1.95	73.4	55.1	50.9	36.1	76.5	13.9	6.27	6.14
LM:13	48.6	45.5	44.1	31.4	49.6	19.6	9.92	2.50	46.6	42.7	41.4	35.9	47.9	16.3	7.85	8.18
LM:14	100.0	100.0	100.0	86.0	100.0	45.4	24.31	6.93	92.4	92.2	92.1	87.4	92.7	42.0	22.7	20.9

only such LMs. However, it must be kept in mind that putting an extremely tight angle bound can make the P2-based OPF model inexact as observed in few cases reported in the bold-italic format in Tables 7.3 and 7.4. Consequently, in such cases, the angle limit has to be relaxed to such value where the relaxation becomes exact again.

In Table 7.6, the impact of introducing neutral envelopes on the phase-neutral terms of P2-based OPF model is reported. It can be noted that by imposing the envelopes on these terms, a moderate reduction in the %RD can be obtained. However, it must be noted that the bounds on neutral voltage variable has a strong impact on the exactness

Table 7.6: Impact of imposing neutral envelopes on the quality of P2-based OPF relaxation.

Network	LMs	%RD in the case of OF-1					
		Y		Δ		*Y*-Δ	
		NE	*WE*	*NE*	*WE*	*NE*	*WE*
IT-37	**LM:2**	2.00	0.68	2.33	0.57	2.72	0.65
	LM:5	2.31	0.15	1.25	0.03	1.60	0.14
	LM:7	1.70	0.32	1.47	0.09	2.73	0.04
	LM:9	2.78	0.14	2.96	0.31	2.96	0.36
	LM:12	5.15	2.02	4.19	0.83	10.35	0.93
CIGRE	**LM:2**	1.24	0.75	2.60	0.68	1.91	0.71
	LM:5	1.91	0.02	5.65	0.47	3.07	0.05
	LM:7	1.58	0.02	7.35	1.73	3.08	0.25
	LM:9	1.68	0.02	1.01	0.41	1.76	0.01
	LM:12	3.70	1.15	6.84	1.24	4.98	1.14

NE: No Envelope WE: With Envelope

of the relaxation since imposing very tight bounds in the case of highly unbalanced DNs causes the relaxation to become infeasible.

The inexactness of P1-based OPF models under LMs having positive k_I coefficients demands a further investigation of this behaviour. Resultantly, the next section is dedicated completely to understand the reasons behind this unexpected outcome of P1-based OPF relaxation.

7.3.3 Inexactness of P1-based OPF relaxation under power absorbing constant current load

The sub-optimality of P1-based OPF relaxation largely depends upon the choice of OF. In order to understand this, it is fully important to clarify first *what does the sign of a load coefficient mean*? Normally, loads are considered passive and absorb power from a network. For all such loads, the active and reactive power coefficients have positive value which make the power injection equations (7.4)-(7.6) positive and, as per standards, these injections are considered as a withdrawal of power from the system. However, it has been reported in [308] that the majority of constant current household appliances have negative power coefficient and, therefore, these loads inject power into a network. Furthermore, the power injection/absorption of a constant current load is voltage dependent and is, therefore, highly influenced by the node voltage to which it is connected.

Now, under OF2 (power losses minimization), solver tends to go towards the lower voltage limits, which is put on the additional variables ($\mathbf{\Pi}_{ii}$) of P1-based OPF model for constant current load modelling, of the FR to reduce the power absorption of these components. The reduction in power drawn by these loads, subsequently, reduces the power flow in the lines/branches of a network and, as a result, the whole system losses are reduced which is the objective of OP. Similarly, in the case of OF1 which deals with the minimization of slack bus power injection, lowering the voltage on the load buses leads to a reduced power absorption by the constant current loads which ultimately reduces the power injection into the system from the slack bus.

To better understand this point, consider the results presented in Table 7.8 which reports the OF2 value obtained in the case of power absorption and injection from a purely constant current load i.e., LM 2, along with the voltages value recovered from $\mathbf{\Pi}_{ii}$ and V_i^{φ} variables used in the P1- and P2-based relaxations, respectively. Furthermore, the minimum and maximum values of real and imaginary bounds related to $\delta = 5°$ and $\delta = 10°$ are also presented in Table 7.7 as reference values to cross-check the recovered

Table 7.7: Bounds on real and imaginary components of phase-ground node voltages.

Phase	$\boldsymbol{\delta = 5°}$				$\boldsymbol{\delta = 10°}$			
	$\underline{V}_r$	$\overline{V}_r$	$\underline{V}_{im}$	$\overline{V}_{im}$	$\underline{V}_r$	$\overline{V}_r$	$\underline{V}_{im}$	$\overline{V}_{im}$
a	0.897	1.050	-0.0784	0.078	0.886	1.050	-0.156	0.156
b	-0.516	-0.443	-0.951	-0.737	-0.587	-0.359	-0.986	-0.689
c	-0.516	-0.443	0.737	0.951	-0.587	-0.359	0.689	0.986

Table 7.8: Recovered voltages from P1- and P2-based OPF relaxations for load model 2.

LM:2 $(+k_I)$				
Phase	**OF2 (kW):**5.67		**OF2 (kW):**6.38	
	Voltages from P1		**Voltages from P2**	
	$\mathbf{\Pi}_{ii}$	$\boldsymbol{W}_{ii}$	V_i^{φ}	$\boldsymbol{W}_{ii}$
V_a	0.896+j0.002 (0.89∡0.11)	0.982+j0.002 (0.98∡0.11)	0.967+j0.001 (0.97∡0.05)	0.979+j0.002 (0.98∡0.11)
V_b	-0.446-j0.787 (0.90∡-119.5)	-0.491-j0.864 (0.99∡-119.6)	-0.481-j0.866 (0.99∡-119.1)	-0.491-j0.861 (0.99∡-119.6)
V_c	-0.452+j0.772 (0.89∡120.3)	-0.497+j0.847 (0.98∡120.4)	-0.501+j0.844 (0.98∡120.7)	-0.497+j0.846 (0.98∡120.4)
-LM:2 $(-k_I)$				
	OF2 (kW):5.81		**OF2 (kW):**5.81	
V_a	0.981-j0.002 (0.98∡-0.11)	0.981-j0.002 (0.98∡-0.11)	0.981-j0.001 (0.98∡-0.05)	0.981-j0.002 (0.98∡-0.11)
V_b	-0.495-j0.862 (0.99∡-119.8)	-0.492-j0.863 (0.99∡-119.6)	-0.496-j0.861 (0.99∡-119.9)	-0.492-j0.863 (0.99∡-119.6)
V_c	-0.494+j0.848 (0.98∡120.2)	-0.497+j0.846 (0.98∡120.4)	-0.492+j0.849 (0.98∡120.1)	-0.498+j0.846 (0.98∡120.4)

voltages. Please note that the voltages are presented only for node 8 of CIGRE network due to the fact that the same trend is observed for other nodes voltages.

It can be noticed that in the case of $+k_I$ coefficient, the real and imaginary components of complex voltages appearing in the first column of $\mathbf{\Pi}_{ii}$ are almost identical to the maximum and minimum bounds presented in Table 7.7, whereas the voltages recovered from $\mathbf{W}_{ii}$ of P1-based relaxation are quite far away from the voltages of $\mathbf{\Pi}_{ii}$ and do not lie at the extreme bounds of FR. In terms of polar coordinates, both recovered voltages share the same angle position but their magnitudes are quite different. The voltages magnitudes in the case of $\mathbf{\Pi}_{ii}$ are almost equal to the minimum bound value, whereas in the case of $\mathbf{W}_{ii}$ of P1-based relaxation, they are almost identical to the values recovered from MPSDP-based OPF model. Since constant current loads are modelled through $\mathbf{\Pi}_{ii}$ variable, the calculated lower value of the voltages by the solver leads to a reduced power absorption by these loads which, in turn, lowers down the power system losses to an unrealistic value. On the other hand, the voltages obtained from V_i^{φ} and $\mathbf{W}_{ii}$ in the case of P2-based relaxation are almost identical to each other as well as to the values obtained from the MPSDP-based relaxation as shown in Table 7.9. These results show that the solver calculates the voltages values of V_i^{φ} which are not close to the extreme bounds and, therefore the value of OF is very close to the value obtained in the case of MPSDP-based relaxation. This is because of the fact that convex region of complex voltage variables in P1-based relaxation is further tightened by the application of McCormick envelopes in P2-based model which introduces further coupling between the off-diagonal elements of

Table 7.9: Recovered voltages from MPSDP-based OPF relaxations for load model 2.

Phase	**LM:2** $(+k_I)$	**-LM:2** $(-k_I)$
	OF2 (kW): 6.46	**OF2 (kW):** 5.71
	Voltages from MPSDP-based OPF relaxation	
V_a	0.979+0.002j (0.98∡0.88)	0.981+0.002j (0.98∡0.61)
V_b	-0.490-0.861j (0.99∡-118.9)	-0.491-0.861j (0.99∡-119.2)
V_c	-0.497+0.846j (0.98∡121.2)	-0.491+0.846j (0.98∡120.8)

$\mathbf{W}_{ii}$ and V_i^{φ} terms. Since voltages recovered for V_i^{φ} are very close to the values of $\mathbf{W}_{ii}$ of P2-based relaxation, consequently, the power absorbed by constant current loads i.e., OF2 value, in this relaxation is almost identical to the optimal solution value of MPSDP-based OPF model.

In the case of $-k_I$ coefficient, constant current load injects power into a system and, therefore, can be considered as a local power source. In such a case, the solver tends to increase the power injections from these loads to reduce the power drawn from the slack bus in order to bring down the overall system losses. Resultantly, the optimal voltages values calculated for $\mathbf{\Pi}_{ii}$ and V_i^{φ} variables in P1- and P2-based relaxations, respectively are almost identical to each other as well as equal to the voltages value obtained from $\mathbf{W}_{ii}$ matrices of these approaches and MPSDP-based model. These results clearly explain that why in the case of negative coefficients P1-based OPF approach works well and gives the same optimal solution as obtained from the other OPF models.

7.3.4 Computational performance

The real strength of cheap SDP-based relaxation in comparison to the MPSDP-based relaxation is its superior computational performance which can be clearly noticed from the CT reported in Table 7.10 and shown in Fig. 7.2. For a medium-size DN (e.g., IT-37 bus), MPSDP-based relaxation takes an exceptionally large CT as shown in chapter 6 and, consequently, the real-time implementation of such an OPF model in the context of DMS seems hard to realize. On the other hand, a remarkable reduction in the CT can be observed when cheap relaxation is solved for such DNs. It can also be noted that CT is invariably independent of load types and LMs, and, therefore, no additional techniques such as sparsity exploitation [256], [273] or distributed algorithms [264] are required for the real-time implementation of proposed approach. Furthermore, for large-size real DNs (IT-111 node network), MPSDP-based OPF model is difficult to solve, as of now, due to immature SDP solving technology. Consequently, in such cases, cheap SDP-based relaxation provides an alternative for the real-time control of these networks.

Table 7.10: Comparison between the computational time of P3- and MPSDP-based OPF relaxations.

Network	LMs	SDP (s)			SOCP-P3 (s)		
		Y	Δ	Y-Δ	Y	Δ	Y-Δ
CIGRE	**LM:1**	5.41	3.92	5.11	0.68	0.57	0.59
	LM:2	4.14	3.87	4.64	0.58	0.56	0.59
	LM:3	4.36	4.45	4.38	0.69	0.59	0.58
	LM:5	5.49	4.18	4.79	0.57	0.67	0.64
	LM:9	4.37	3.83	4.12	0.60	0.54	0.56
IT-37	**LM:1**	1069	932	1073	1.06	0.85	1.01
	LM:2	907	1030	1003	0.81	0.71	0.72
	LM:3	993	910	1205	0.82	0.86	0.68
	LM:5	923	928	942	0.96	0.86	0.96
	LM:9	1066	932	1004	1.09	0.78	1.28

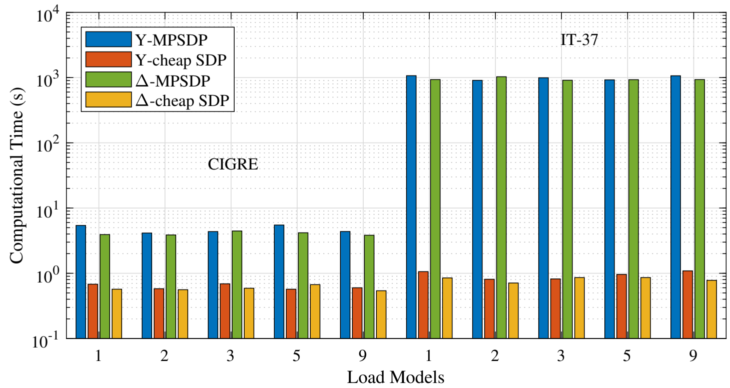

Figure 7.2: Comparison of computational time between MPSDP- and cheap SDP-based OPF relaxations.

7.3.5 Comparison of the proposed relaxation with delta approach

In Table 7.11, a comparison is made between the P3-based relaxation and OPF scheme reported in [301], referred here as delta approach, in terms of exactness, computational performance and RMSE in the context of delta-load modelling. It can be noted that P3-based OPF scheme outperforms the delta approach in the case of both OFs as evident by a reduced %RD, lower CT and a small value of RMSE parameter. This is due to the fact that additional OVs ($\mathbf{\Phi}_i$) are introduced in the delta approach to incorporate delta loads in the OP; however, these variables are not coupled to the network power balance equations. Consequently, the obtained EVR for all constraints (7.1i) has a value equal to 1, which shows that the recovered solution has failed to satisfy all rank-1 constraints (7.1l). Resultantly, a large %RD can be observed in Table 7.11 under both OFs, thereby indicating a better performance by the proposed relaxation.

Table 7.11: Comparison of P3-based OPF relaxation with delta approach reported in [301].

Networks	**SDP**		**Delta Approach [301]**			**Proposed BFM-SDP**		
	EVR	Obj. Value	%RD	RMSE	CT	%RD	RMSE	CT
OF:1 Slack Bus Power (kVA)								
CIGRE	0.41	166.4	1.81	30.2	0.52	0.00	1.40	0.44
IT-37	0.48	106.3	1.58	10.2	0.91	0.04	0.60	0.76
OF:2 Power Losses (kW)								
CIGRE	3.57	7.38	15.1	42.3	0.55	0.31	1.30	0.59
IT-37	0.79	2.91	25.6	14.5	0.95	1.78	1.00	0.86

7.4 Summary

In this chapter, a novel cheap SDP-based OPF relaxation is presented which provides an alternative to the MPSDP-based OPF relaxation for realizing the real-time optimal control and management of DNNs hosting both wye- and delta-connected ZIP loads. Furthermore, three novel modelling methodologies are presented for the incorporation of constant current loads in the proposed OPF model due to the fact that the complex voltage variable approach which is presented in chapter 6 for the handling of these loads cannot be generalized for this relaxation.

The proposed relaxation provides an exact solution for all those LMs which do not include constant current component. For LMs which consist of constant current component, P2-based relaxation dominates the P1-based model, whereas P3-based relaxation neither dominates nor is dominated by the P2-based approach. For LMs which consist of constant current component having positive k_I values, P1-relaxation fails to provide a meaningful optimal solution. For such LMs, P2-approach significantly reduces the relative difference; however, it is even surpassed by the P3-based approach in terms of the provision of an optimal solution.

The angle deviation limit strongly affects the quality of P1- and P2-based relaxations since setting a large value for the angle deviation parameter leads to a weaker relaxation and, subsequently, to suboptimal results. The incorporation of neutral envelopes in the P2-based approach further tightens the model; however, it is at the expense of introducing a large number of additional constraints which causes YALMIP to take a significant amount of time for the internal modelling of OPF problem before solving it.

With respect to the CT, the developed relaxation provides an optimal solution in just a fraction of second time even for medium size DNs (MPSDP-based technique can take up to three-orders of magnitude for these DNs). Although the MPSDP-based relaxation dominates the cheap SDP-based OPF model due to the involvement of a more stringent PSD constraint, the optimistic behaviour of the latter relaxation in terms of the provision of an exact solution, under a range of realistic ZIP load parameters and in a significantly reduced time, allows the practical realization of an OPF model for ADNs to ensure their optimal management.

Published paper

The presented work in this chapter led to the publication of following paper.

1. Usman, M., A. Cervi, M. Coppo, F. Bignucolo, and R. Turri. "SOCP-based OPF Model for Multi-Phase Neutral-equipped Networks containing ZIP loads." submitted in *IEEE Transactions on Control of Network Systems*

CHAPTER 8

Tightening Cheap Conic Relaxation through Convex Envelopes

This chapter presents a new methodology aiming to tighten the bus-injection model-based cheap conic relaxation through the introduction of convex envelopes. The resultant relaxation, termed as three-phase quadratic convex model, involves the polar form representation of power flow equations and convex envelopes in its formulation for the quadratic, bilinear and trigonometric terms. Preliminary results show that the proposed OPF relaxation provides an optimal solution which is as tight as the three-phase SDP-based OPF relaxation solution, without sacrificing the advantages of lower computational time of cheap conic relaxation.

The MPSDP- and cheap SDP-based OPF relaxations presented in chapters 6 and 7, respectively successfully solve an OPF problem for a DNN. Nevertheless, there are some shortcomings associated with both of them. The former methodology suffers from a high CT requirement, whereas the latter relaxation is dominated by the former relaxation and, as of now, no theoretical guarantees exist with respect to the equivalence between these two models even in the case of a RDN. Consequently, the cheap OPF relaxation can provide a sub-optimal solution in the case of highly unbalanced DNs and, as a result, there is a need to develop a convexified OPF model which combines the advantages of both approaches i.e., its computational efficiency should be equal or close to the computational efficiency of cheap SDP-based relaxation and it should be as tight as MPSDP-based relaxation. Resultantly, in this chapter, a new relaxation is proposed which tightens a cheap SDP-based OPF relaxation, which utilizes the BIM-based power flow representation in its formulation, by introducing additional constraints on the individual terms of OVs of this relaxation. A Cheap BIM-based Semi-Definite Relaxation (CBSDR) (without additional constraints) is proposed in [257] but because of its inferior numerical performance, due to the subtraction of voltage variables, in comparison to the BFM-based cheap SDR (which is utilized in chapter 7), it is not studied in the latter studies.

The original CBSDR is based on power flow equations which are modelled in rectangular form. However, by expressing the OVs of this relaxation in polar form, it is possible to enforce additional constraints in the original model which, ultimately, tightens it. This concept is utilized in [276] in the framework of single-phase equivalently represented electrical networks. The resultant relaxation termed as QC relaxation strengthens an SOCP-based OPF model by enclosing the non-convex hull of polar variables through linear and quadratic inequalities which, in turn, constitute a convex region around the original FR of these variables.

In the context of this thesis work, the above-mentioned concept is extended to a multi-phase network modelling framework and a novel Three-Phase Quadratic Convex (TPQC) OPF relaxation is proposed in this chapter. The preliminary study, which is carried out on a three-phase network configuration, could set the path for the development of a complete multi-phase (four conductor) QC relaxation if promising results are achieved in the case of TPQC-based OPF relaxation. To this end, the novel contributions with respect to the above-mentioned discussion can be specified as:

1. Detailed mathematical modelling of convex envelopes for the trigonometric functions involving variables of same and different phases

2. Proposal of novel upper and lower bounds for the above-mentioned envelopes and recursive application of McCormick envelopes to constitute the FR of a trilinear term

3. Collective application of all the relevant envelopes which, resultantly, leads to the proposed TPQC-based OPF relaxation

Before proceeding further, a natural question arises that *why the cheap BFM-based relaxation (introduced in chapter 7) is not tightened through this approach*? In [257], it has been shown that the cheap SDP-based relaxation which is based on BIM is numerically weaker than the BFM-based OPF relaxation and since promising results are achieved for the latter relaxation as shown in chapter 7, therefore, the former relaxation is chosen in this work as significant improvement in the performance of this relaxation can be expected. Nevertheless, the proposed approach can readily be applied to a BFM-based OPF relaxation and is left for the future study if TPQC relaxation shows promising results in the case of CBSDR.

8.1 Recap of existing three-phase BIM-based cheap OPF relaxation

The existing three-phase CBSDR OPF model is shown in the model **M8.1**. Please note that the same nomenclature is used in this chapter as reported in chapter 6. It can be noted that the model **M8.1** is similar to the model **M7.1** in a sense that both models

M8.1: Bus Injection Model based cheap Semi-Definite Relaxation

$$\textbf{M1}: \underset{\Psi}{\textbf{minimize}}\ f(\Psi) \tag{8.1a}$$

$$\textbf{variables}: \mathbf{S}_{g_i} \in \mathbb{C}^{|\eta_i|}, \mathbf{W}_{ii} \in \mathbb{H}^{|\eta_i|\times|\eta_i|} \qquad (\forall i \in N)$$

$$\mathbf{W}_{ij} \in \mathbb{C}^{|\eta_{ij}|\times|\eta_{ij}|} \qquad (\forall i \sim j \in E)$$

subject to :

$$\mathbf{S}_i = \sum_{k:k\rightarrow i} \mathrm{diag}(\mathbf{W}_{ii} - \mathbf{W}_{ik}^H)\mathbf{Y}_{ik}^H + \sum_{j:i\rightarrow j} \mathrm{diag}(\mathbf{W}_{ii} - \mathbf{W}_{ij})\mathbf{Y}_{ij}^H \qquad \forall i \in N \tag{8.1b}$$

$$|\underline{\mathbf{V}}|_i^2 \leq \mathrm{diag}(\mathbf{W}_{ii}) \leq |\overline{\mathbf{V}}|_i^2 \qquad \forall i \in N^+ \tag{8.1c}$$

$$\tan(\underline{\boldsymbol{\theta}}_{ij}) \otimes \Re(\mathbf{W}_{ij}^D) \leq \Im(\mathbf{W}_{ij}^D) \leq \tan(\overline{\boldsymbol{\theta}}_{ij}) \otimes \Re(\mathbf{W}_{ij}^D) \qquad \forall (i\sim j) \in E \tag{8.1d}$$

$$\underline{\mathbf{S}}_{g_i} \leq \mathbf{S}_{g_i} \leq \overline{\mathbf{S}}_{g_i} \qquad \forall i \in N \tag{8.1e}$$

$$\mathbf{W}_{ij} = \mathbf{W}_{ji}^H \qquad \forall (i\sim j) \in E \tag{8.1f}$$

$$\begin{bmatrix} \mathbf{W}_{ii} & \mathbf{W}_{ij} \\ \mathbf{W}_{ij}^H & \mathbf{W}_{jj} \end{bmatrix} \succeq 0 \qquad \forall (i\sim j) \in E \tag{8.1g}$$

$$\mathrm{rank}\begin{bmatrix} \mathbf{W}_{ii} & \mathbf{W}_{ij} \\ \mathbf{W}_{ij}^H & \mathbf{W}_{jj} \end{bmatrix} = 1 \qquad \forall (i\sim j) \in E \tag{8.1h}$$

D: Diagonal $\otimes$: Element wise multiplication

enforce PSD constraints on small size matrices which are based on the OVs of both models. However, it can be seen in (8.1b) that the power balance equality involves the subtraction of voltage terms present in $\mathbf{W}_{ii}$ and $\mathbf{W}_{ik}$, and, consequently, poor numerical data is given as an input to the optimization solver which, resultantly, causes the relaxation to fail in the majority of test cases. This aspect has already been shown in chapter 6 in the case of *first-order Taylor series* based modelling of a constant current load. Furthermore, the model **M8.1** is still a non-convex model due to the presence of constraint (8.1h), which can be dropped, subsequently, to make it a convex relaxation[1].

As reported in chapters 5 and 7 in the case of single-phase equivalently represented RDNs, both SOCP- and SDP-based OPF relaxations are equivalent and, therefore, the former approach can replace the latter relaxation. However, due to the non-existence of sufficient condition(s) which can ensure the equivalency between the multi-phase SDP- and cheap SDP-based relaxations (both BIM- and BFM-based representation) in a multi-phase network framework, the former approach would be considered as a dominant relaxation, and, therefore, there would always be room to tighten the latter relaxation. Consequently,

[1]It can be noted that (8.1g) takes the form of a SOC constraint in the case of a single-phase equivalent representation of a DN. However, the formation of (8.1g) in the matrix SOC form $\mathbf{W}_{ij}\mathbf{W}_{ij}^H \leq \mathbf{W}_{ii}\mathbf{W}_{jj}$ cannot be done since it becomes a quadratic matrix inequality and no solver exists which can solve this inequality.

in the context of this chapter, a natural question arises *how to enclose the non-convex region associated with the individual non-linear terms of* $\mathbf{W}_{ii}$ *and* $\mathbf{W}_{ij}$ *to strengthen the model* **M8.1**? Please note that the model **M8.1** is a convex model (after dropping the rank constraints) due to the presence of linear and PSD constraints. However, the individual terms of OVs still constitute a non-convex region which can be replaced by a convex region and is the main topic of the following sections.

8.2 Three-phase quadratic convex relaxation

To answer the above-mentioned question, consider the real and imaginary parts of $\mathbf{W}_{ii}$ and $\mathbf{W}_{ij}$ as shown in (8.2)-(8.5).

$$\Re(\mathbf{W}_{ii}) \Rightarrow \begin{bmatrix} |V_i^a|^2 & V_i^aV_i^b cos(\theta_{ii}^{ab}) & V_i^aV_i^c cos(\theta_{ii}^{ac}) \\ V_i^bV_i^a cos(\theta_{ii}^{ba}) & |V_i^b|^2 & V_i^bV_i^c cos(\theta_{ii}^{bc}) \\ V_i^cV_i^a cos(\theta_{ii}^{ca}) & V_i^cV_i^b cos(\theta_{ii}^{cb}) & |V_i^c|^2 \end{bmatrix} \tag{8.2}$$

$$\Im(\mathbf{W}_{ii}) \Rightarrow \begin{bmatrix} 0 & V_i^aV_i^b sin(\theta_{ii}^{ab}) & V_i^aV_i^c sin(\theta_{ii}^{ac}) \\ V_i^bV_i^a sin(\theta_{ii}^{ba}) & 0 & V_i^bV_i^c sin(\theta_{ii}^{bc}) \\ V_i^cV_i^a sin(\theta_{ii}^{ca}) & V_i^cV_i^b sin(\theta_{ii}^{cb}) & 0 \end{bmatrix} \tag{8.3}$$

$$\Re(\mathbf{W}_{ij}) \Rightarrow \begin{bmatrix} V_i^aV_j^a cos(\theta_{ij}^{aa}) & V_i^aV_j^b cos(\theta_{ij}^{ab}) & V_i^aV_j^c cos(\theta_{ij}^{ac}) \\ V_i^bV_j^a cos(\theta_{ij}^{ba}) & V_i^bV_j^b cos(\theta_{ij}^{bb}) & V_i^bV_j^c cos(\theta_{ij}^{bc}) \\ V_i^cV_j^a cos(\theta_{ij}^{ca}) & V_i^cV_j^b cos(\theta_{ij}^{cb}) & V_i^cV_j^c cos(\theta_{ij}^{cc}) \end{bmatrix} \tag{8.4}$$

$$\Im(\mathbf{W}_{ij}) \Rightarrow \begin{bmatrix} V_i^aV_j^a sin(\theta_{ij}^{aa}) & V_i^aV_j^b sin(\theta_{ij}^{ab}) & V_i^aV_j^c sin(\theta_{ij}^{ac}) \\ V_i^bV_j^a sin(\theta_{ij}^{ba}) & V_i^bV_j^b sin(\theta_{ij}^{bb}) & V_i^bV_j^c sin(\theta_{ij}^{bc}) \\ V_i^cV_j^a sin(\theta_{ij}^{ca}) & V_i^cV_j^b sin(\theta_{ij}^{cb}) & V_i^cV_j^c sin(\theta_{ij}^{cc}) \end{bmatrix} \tag{8.5}$$

It can be observed that these matrices are formed by defining the voltage vector entries in the polar form. The rectangular form of voltage vectors can also be used to define the envelopes but due to the non-availability of the bounds on real and imaginary components of a complex voltage variable in technical standards, this path has not been taken. Although, these bounds are successfully derived in chapter 7 but they strongly depend on the assumed value of voltage angle deviation δ parameter which has to be chosen with great care. Furthermore, it is shown that complex bounds alone in the case of P1-based OPF relaxation provide a loose convex region. Therefore, it is more appropriate to use the polar form representation of voltage vectors due to the readily available bounds on voltage magnitude and angle deviation terms.

It can be noted that the real and imaginary parts of $\mathbf{W}_{ii}$ and $\mathbf{W}_{ij}$ consist of quadratic ($|V_i^{\varphi_i}|^2$), trigonometric $\{cos(\theta_{ii}^{\varphi_i\varphi_i}), sin(\theta_{ii}^{\varphi_i\varphi_i})\}$ and bilinear ($V_i^{\varphi_i}V_i^{\varphi_i}$) terms. By enclosing the non-convex FR of these non-linear terms, the original model **M8.1**, on the one hand, is strengthened and, on the other hand, is still solvable in a polynomial time. To this extent, the envelopes can be formed by introducing additional lifted variables $\breve{\alpha}$, $\breve{\beta}$, $\breve{cs}$ and $\breve{sn}$ for the quadratic, bi-linear, cosine and sine terms, respectively. Based on these variables, the first two terms of $\mathbf{W}_{ii}$ can be expressed as follows:

$$\Re(W_{ii}^{aa}) = |V_i^a|^2 = \langle |V_i^a|^2 \rangle^Q = \breve{\alpha}_{ii}^{aa} \tag{8.6}$$

$$\Re(W_{ii}^{ab}) = V_i^a V_i^b cos(\theta_{ii}^{ab}) = \langle \langle V_i^a V_i^b \rangle^M \langle cos(\theta_{ii}^{ab}) \rangle^C \rangle^M = \langle \breve{\beta}_{ii}^{ab}.\breve{cs}_{ii}^{ab} \rangle^M \tag{8.7}$$

$$\Im(W_{ii}^{ab}) = V_i^a V_i^b sin(\theta_{ii}^{ab}) = \langle \langle V_i^a V_i^b \rangle^M \langle sin(\theta_{ii}^{ab}) \rangle^S \rangle^M = \langle \breve{\beta}_{ii}^{ab}.\breve{sn}_{ii}^{ab} \rangle^M \tag{8.8}$$

where Q, M, C and S stand for quadratic, McCormick, cosine and sine envelopes and $\langle \cdot \rangle$ represent the convex envelope on $f()$. These envelopes, thus, convexify the FR of each non-linear term in $\mathbf{W}_{ii}$ and, consequently, lead to a stronger relaxation. Similar envelopes can also be derived for the other terms of $\mathbf{W}_{jj}$ and $\mathbf{W}_{ij}$ matrices by introducing the lifted variables for each node and branch of a network. In the following sections, the above-mentioned envelopes are described in detail in the context of TPQC relaxation.

8.2.1 Envelopes on quadratic function

The non-convexity associated with a quadratic function is shown in Fig. 8.1 (red line) which can be transformed into a convex region by defining the appropriate lower and upper envelopes around it through the following inequalities:

$$\text{Quadratic Envelope: } \langle z^2 \rangle^Q = \begin{cases} \breve{\alpha} & \geq \; z^2 \\ \breve{\alpha} & \leq \; (\underline{z} + \overline{z})z - \underline{z}\overline{z} \end{cases}$$

It can be noted that with the introduction of a new lifted variable $\breve{\alpha}$, which is lower bounded by z^2 (red line) and upper bounded by the straight line (green line), the non-convex region of z^2 can be replaced by the convex region of $\breve{\alpha}$ which is shown between the green and red curves. Instead of strictly lying on the red curve, the values of phases voltages can now be inside this FR.

8.2.2 Envelopes on bilinear function

The convex envelopes for bilinear terms, which are well known in literature [292] and are already utilized in chapter 7 in P2-based OPF relaxation, are reported below for a quick recap. For variables $x \in \{\underline{x}, \overline{x}\}$ and $y \in \{\underline{y}, \overline{y}\}$, the envelopes on a bilinear term $z = xy$

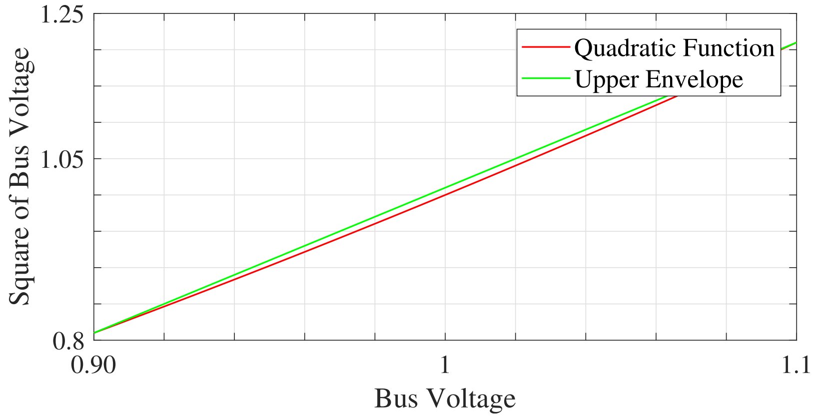

Figure 8.1: Envelopes on a quadratic function.

can be defined by the set of following four inequalities:

$$\text{McCormick Envelope: } \langle xy \rangle^M = \begin{cases} \breve{\beta} & \geq \underline{x}y + \underline{y}x - \underline{x}\underline{y} \\ \breve{\beta} & \geq \overline{x}y + \overline{y}x - \overline{x}\overline{y} \\ \breve{\beta} & \leq \underline{x}y + \overline{y}x - \underline{x}\overline{y} \\ \breve{\beta} & \leq \overline{x}y + \underline{y}x - \overline{x}\underline{y} \end{cases}$$

Fig. 8.2 represents the lower envelopes (red and blue) on the original FR of bilinear term (green one). It can easily be perceived that the resultant region enclosed by the two upper and two lower envelopes would be a convex region.

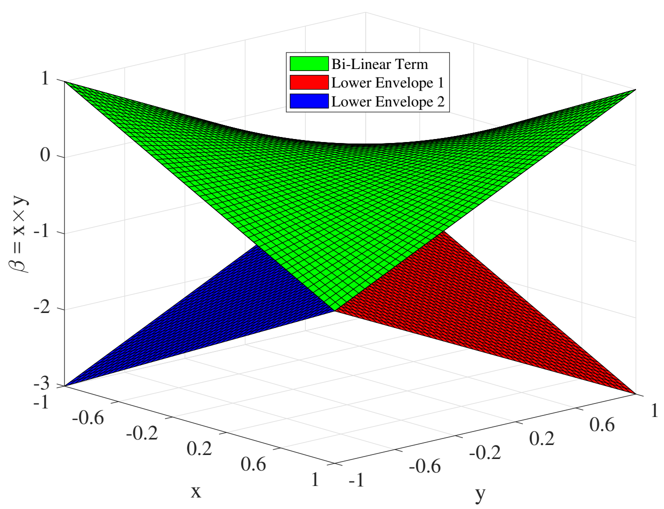

Figure 8.2: Envelopes on a bilinear function.

8.2.3 Trigonometric functions relaxation

The envelopes of trigonometric terms are based on the *first-order Taylor series* expansion and *cosecant/secant functions* as represented below.

For angle difference variable $\theta \in \{\underline{\theta}, \overline{\theta}\}$, the *first-order Taylor series* expansion of a cosine (c) and sine (s) function around θ_0 is expressed as:

$$f^c(\theta) = cos(\theta_0) - sin(\theta_0)(\theta - \theta_0) \tag{8.9}$$

$$f^s(\theta) = sin(\theta_0) + cos(\theta_0)(\theta - \theta_0) \tag{8.10}$$

Similarly, the cosecant (csc) and secant (sec) function are expressed as:

$$f^{csc}(\underline{\theta}, \overline{\theta}) = \frac{cos(\overline{\theta}) - cos(\underline{\theta})}{\overline{\theta} - \underline{\theta}}(\theta - \underline{\theta}) + cos(\underline{\theta}) \tag{8.11}$$

$$f^{sec}(\underline{\theta}, \overline{\theta}) = \frac{sin(\overline{\theta}) - sin(\underline{\theta})}{\overline{\theta} - \underline{\theta}}(\theta - \underline{\theta}) + sin(\underline{\theta}) \tag{8.12}$$

Apart from the above mentioned functions, a quadratic function on cosine is also defined as:

$$f^{cq}(\theta) = 1 - \frac{1 - cos(\theta^{\gamma})}{(\theta^{\gamma})^2}(\theta)^2 \tag{8.13}$$

where cq stands for convex-quadratic and $\theta^{\gamma} = \max\{|\underline{\theta}|, |\overline{\theta}|\}$. The cosecant and secant functions are termed as polyhedral relaxations of cosine and sine functions, respectively which either upper or lower bound the given trigonometric function depending upon the angle difference θ value.

8.2.4 Key findings on the envelopes of trigonometric terms

Figs. 8.3 and 8.4 show the cosine and sine waveforms over the period $(-2\pi, 2\pi)$ which are lower and upper bounded by (8.9)-(8.13) in five different intervals. These intervals are reported in Table 8.1, whereas the lower and upper bounds on the lifted variables related

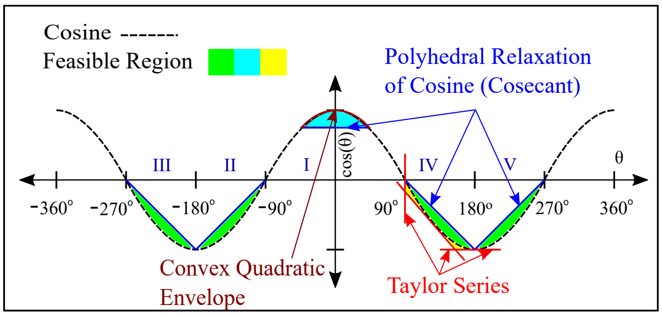

Figure 8.3: Convex quadratic, Taylor and polyhedral relaxations on a cosine function.

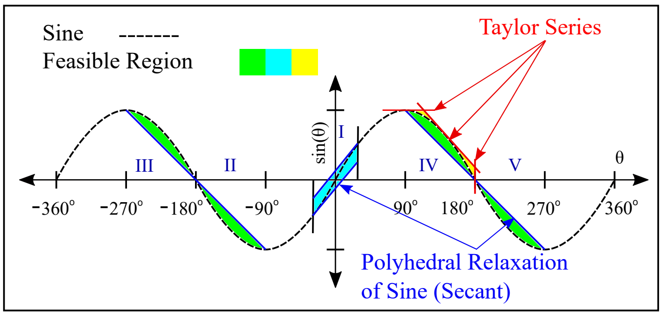

Figure 8.4: Taylor and polyhedral relaxations on a sine function.

to each trigonometric term of $\mathbf{W}_{ii}$ and $\mathbf{W}_{ij}$ are reported in Tables 8.2 and 8.3. It can be noted that:

1. The Taylor series for both cosine and sine functions is defined at three points, i.e., $\underline{\theta}$, $\overline{\theta}$ and $\tilde{\theta} = (\underline{\theta} + \overline{\theta})/2$, to provide a tighter envelope as compared to evaluating the Taylor series at a single point in the interval $(\underline{\theta}, \overline{\theta})$ i.e., either at $\underline{\theta}$ or $\overline{\theta}$ or $\tilde{\theta}$.

2. The cosine function in the upper diagonal part of $\mathbf{W}_{ii}$ is lower bounded by the Taylor series and upper bounded by the cosecant function for all phases. However, in the case of sine function, the bounds are reversed for the phase $a - c$.

3. The lower and upper bounds on cosine terms in the lower diagonal part of $\mathbf{W}_{ii}$ are the same as reported for the cosine terms in Table 8.2 due to the even nature of cosine function.

4. The lower and upper bounds on sine terms in the lower diagonal part of $\mathbf{W}_{ii}$ are negative of the bounds reported for sine terms in Table 8.2 due to the odd nature of sine function.

5. The diagonal terms of $\mathbf{W}_{ii}$ are independent of trigonometric functions and are bounded by the quadratic envelope.

6. The cosine terms on the diagonal of $\mathbf{W}_{ij}$ are upper bounded by the cosine-quadratic function which is defined at θ^{γ}, and are lower bounded by the polyhedral relaxation based on the angle limit belonging to the interval I.

7. The sine terms on the diagonal of $\mathbf{W}_{ij}$ are upper and lower bounded by the Taylor series evaluated at $\theta^{\gamma}/2$ and $-\theta^{\gamma}/2$, respectively.

8. The cosine and sine terms in the upper diagonal part of $\mathbf{W}_{ij}$ have the same lower and upper bounds as reported in Table 8.2.

9. The cosine terms in the lower diagonal part of $\mathbf{W}_{ij}$ are still lower and upper bounded by the Taylor series and cosecant function. However, these bounds are now defined for theta ranges belonging to the intervals IV and V due to the fact that $cos(\theta_i^a - \theta_j^b) \neq cos(\theta_i^b - \theta_j^a)$.

Table 8.1: Intervals over which envelopes are determined.

Intervals and their ranges					
Interval	**Phases**	**Range**	**Interval**	**Phases**	**Range**
I	*pp*	{-30,30}	-	-	-
II	*ab*	{-180,-90}	IV	*ba*	{90,180}
	bc	{-180,-90}		*cb*	{90,180}
III	*ac*	{-270,-180}	V	*ca*	{180,270}

Table 8.2: Lower and upper bounds on the elements of W_{ii}.

Bounds on trigonometric terms in the upper diagonal part of $\mathbf{W}_{ii}$				
Ph.	**Bounds on $\breve{\mathbf{cs}}_{ii}^{\varphi_i\varphi_i}$**		**Bounds on $\breve{\mathbf{sn}}_{ii}^{\varphi_i\varphi_i}$**	
	LB	*UB*	*LB*	*UB*
ab	$f^c(\hat{\theta}_{ab})$	$f^{csc}(\underline{\theta}_{ab}, \overline{\theta}_{ab})$	$f^s(\hat{\theta}_{ab})$	$f^{sec}(\underline{\theta}_{ab}, \overline{\theta}_{ab})$
bc	$f^c(\hat{\theta}_{bc})$	$f^{csc}(\underline{\theta}_{bc}, \overline{\theta}_{bc})$	$f^s(\hat{\theta}_{bc})$	$f^{sec}(\underline{\theta}_{bc}, \overline{\theta}_{bc})$
ac	$f^c(\hat{\theta}_{ac})$	$f^{csc}(\underline{\theta}_{ac}, \overline{\theta}_{ac})$	$f^{sec}(\underline{\theta}_{ac}, \overline{\theta}_{ac})$	$f^s(\hat{\theta}_{ac})$

Table 8.3: Lower and upper bounds on the elements of W_{ij}.

Bounds on trigonometric terms in the upper diagonal part of $\mathbf{W}_{ij}$				
Ph.	**Bounds on $\breve{\mathbf{cs}}_{ii}^{\varphi_i\varphi_i}$**		**Bounds on $\breve{\mathbf{sn}}_{ii}^{\varphi_i\varphi_i}$**	
	LB	*UB*	*LB*	*UB*
pp	f^{Λ}	$f^{cq}(\theta_{pp}^{M})$	$f^s(-\theta_{pp}^{M/2})$	$f^s(\theta_{pp}^{M/2})$
ba	$f^c(\hat{\theta}_{ba})$	$f^{csc}(\underline{\theta}_{ba}, \overline{\theta}_{ba})$	$f^{sec}(\underline{\theta}_{ba}, \overline{\theta}_{ba})$	$f^s(\hat{\theta}_{ba})$
cb	$f^c(\hat{\theta}_{cb})$	$f^{csc}(\underline{\theta}_{cb}, \overline{\theta}_{cb})$	$f^{sec}(\underline{\theta}_{cb}, \overline{\theta}_{cb})$	$f^s(\hat{\theta}_{cb})$
ca	$f^c(\hat{\theta}_{ca})$	$f^{csc}(\underline{\theta}_{ca}, \overline{\theta}_{ca})$	$f^s(\hat{\theta}_{ca})$	$f^{sec}(\underline{\theta}_{ca}, \overline{\theta}_{ca})$

$pp \in \{aa, bb, cc\}$, $\hat{\theta}_{pp} \in \{\underline{\theta}_{pp}, \overline{\theta}_{pp}, \tilde{\theta}_{pp}\}$, $f^{\Lambda} : f^{csc}(\underline{\theta}_{pp}, \overline{\theta}_{pp})$, Ph: Phases, LB: Lower Bound, UB: Upper Bound

10. The bounds on sine terms in the lower diagonal part of $\mathbf{W}_{ij}$ are reversed as compared to the bounds mentioned for these terms in the upper diagonal part. Moreover, the bounds are now defined for theta ranges related to the intervals IV and V due to the fact that $sin(\theta_i^a - \theta_j^b) \neq -sin(\theta_i^b - \theta_j^a)$.

8.2.5 Relaxation of bilinear function of lifted variables through the recursive application of McCormick envelopes

The introduction of lifted variables for bilinear and trigonometric terms leads to another bilinear function of the lifted variables ($\breve{\beta}_{ii}^{ab}\breve{cs}_{ii}^{ab}$ and $\breve{\beta}_{ii}^{ab}\breve{sn}_{ii}^{ab}$) which is still non-convex and, therefore, can be relaxed by the further application of McCormick envelopes. However, during the recursive application of McCormick envelopes, new bounds related to the lifted variables are needed which are comprehensively reported in Table 8.4. It can be noted that the bounds on lifted variable $\breve{\beta}_{ii}^{\varphi\varphi}$ is simply the product of lower/upper voltage magnitude

Table 8.4: Lower and upper bounds on the lifted variables.

Bounds on lifted variables				
Variables	*LB*	*UB*	*LB*	*UB*
$\breve{\beta}_{ii}^{\varphi_i\varphi_i}$	$\underline{V}_i^{\varphi_i} \cdot \underline{V}_i^{\varphi_i}$	$\overline{V}_i^{\phi_i} \cdot \overline{V}_i^{\phi_i}$	-	-
	$\theta_{ab}/\theta_{bc} < 0$		$\theta_{ab}/\theta_{bc} > 0$	
$\breve{cs}_{ii}^{ab}$	$cos(\underline{\theta}_{ii}^{ab})$	$cos(\overline{\theta}_{ii}^{ab})$	$cos(\overline{\theta}_{ii}^{ab})$	$cos(\underline{\theta}_{ii}^{ab})$
$\breve{sn}_{ii}^{ab}$	$sin(\overline{\theta}_{ii}^{ab})$	$sin(\underline{\theta}_{ii}^{ab})$	$sin(\overline{\theta}_{ii}^{ab})$	$sin(\underline{\theta}_{ii}^{ab})$
	$\theta_{ba}/\theta_{cb} < 0$		$\theta_{ba}/\theta_{cb} > 0$	
$\breve{cs}_{ii}^{ba}$	$cos(\underline{\theta}_{ii}^{ba})$	$cos(\overline{\theta}_{ii}^{ba})$	$cos(\overline{\theta}_{ii}^{ba})$	$cos(\underline{\theta}_{ii}^{ba})$
$\breve{sn}_{ii}^{ba}$	$sin(\overline{\theta}_{ii}^{ba})$	$sin(\underline{\theta}_{ii}^{ba})$	$sin(\overline{\theta}_{ii}^{ba})$	$sin(\underline{\theta}_{ii}^{ba})$
	$\theta_{ac} < 0$		$\theta_{ac} > 0$	
$\breve{cs}_{ii}^{ac}$	$cos(\overline{\theta}_{ii}^{ac})$	$cos(\underline{\theta}_{ii}^{ac})$	$cos(\underline{\theta}_{ii}^{ac})$	$cos(\overline{\theta}_{ii}^{ac})$
$\breve{sn}_{ii}^{ac}$	$sin(\overline{\theta}_{ii}^{ac})$	$sin(\underline{\theta}_{ii}^{ac})$	$sin(\overline{\theta}_{ii}^{ac})$	$sin(\underline{\theta}_{ii}^{ac})$
	$\theta_{ca} < 0$		$\theta_{ca} > 0$	
$\breve{cs}_{ii}^{ca}$	$cos(\overline{\theta}_{ii}^{ca})$	$cos(\underline{\theta}_{ii}^{ca})$	$cos(\underline{\theta}_{ii}^{ca})$	$cos(\overline{\theta}_{ii}^{ca})$
$\breve{sn}_{ii}^{ca}$	$sin(\overline{\theta}_{ii}^{ca})$	$sin(\underline{\theta}_{ii}^{ca})$	$sin(\overline{\theta}_{ii}^{ca})$	$sin(\underline{\theta}_{ii}^{ca})$

limit. However, in the case of lifted trigonometric variables, the lower and upper bounds are strongly dependent on the interval of angle difference ($\theta_{ii/ij}^{\varphi\varphi}$) and, therefore, special attention must be paid while putting bounds on the lifted trigonometric variables since bounds belonging to a wrong interval can simply lead the OP towards infeasibility.

Once the recursive application of McCormick envelope is done, the complete TPQC-based OPF relaxation can be formulated as shown in model **M8.2**. It can be observed that apart from the OVs which appear in the model **M8.1**, a significant number of new lifted variables, and correspondingly additional constrains related to them, are introduced in the proposed model.

8.2.6 Objective functions

The OFs chosen in this study are the same as defined in chapter 6 and are formulated below in terms of the OVs of proposed relaxation.

- Slack Bus Power (OF1)

$$f_{\mathbf{OF_1}}(\mathbf{S}_{g_0}) = \sum_{\phi_0 \in \{a_0, b_0, c_0\}} (P_{g_0}^{\phi_0} + Q_{g_0}^{\phi_0}) \tag{8.15}$$

- Power Network Losses (OF2)

$$f_{\mathbf{OF_2}}(\mathbf{W}_{ii}, \mathbf{W}_{ij}) = \sum_{E} \sum_{i:i\sim j} \Re(\mathrm{diag}\{(\mathbf{W}_{ii} - \mathbf{W}_{ij})\mathbf{Y}_{ij}^H + (\mathbf{W}_{jj} - \mathbf{W}_{ij}^H)\mathbf{Y}_{ij}^H\}) \tag{8.16}$$

8.3 Quality assessment of the proposed relaxation

The quality assessment of the proposed relaxation **M8.2** is reported in this section in terms of %Optimality Gap (OG), RMSE and CT for all the test networks which are reported

Model 8.2: Three-Phase Quadratic Convex OPF relaxation

$$\textbf{M2}: \underset{\Psi}{\textbf{minimize}}\ f(\Psi) \tag{8.14a}$$

variables :

$\mathbf{S}_{g_i} \in \mathbb{C}^{|\phi_i|}, \mathbf{W}_{ii} \in \mathbb{H}^{|\phi_i|\times|\phi_i|}$ $(\forall i \in N)$

$\mathbf{W}_{ij} \in \mathbb{C}^{|\phi_{ij}|\times|\phi_{ij}|}$ $(\forall i \sim j \in E)$

$\{\mathbf{V}_i, \theta_i, \breve{\alpha}_i, \breve{\beta}_i, \breve{\mathbf{cs}}_i, \breve{\mathbf{sn}}_i, \gamma_i, \eta_i\} \in \mathbb{R}^{|\phi_i|}$ $(\forall i \in N)$

$\{\breve{\beta}_{ij}, \breve{\mathbf{cs}}_{ij}, \breve{\mathbf{sn}}_{ij}, \gamma_{ij}, \eta_{ij}\} \in \mathbb{R}^{|\phi_{ij}|\times|\phi_{ij}|}$ $(\forall i \sim j \in E)$

subject to : (8.1b)-(8.1g) &

$$\text{diag}\{\Re(\mathbf{W}_{ii})\} = \langle\breve{\alpha}_i\rangle^Q \qquad \forall i \in N \tag{8.14b}$$
$$\Re(\mathbf{W}_{ii})^{\triangle} = \gamma_i = \langle\breve{\beta}_i \otimes \breve{\mathbf{cs}}_i\rangle^M \qquad \forall i \in N \tag{8.14c}$$
$$\Im(\mathbf{W}_{ii})^{\triangle} = \eta_i = \langle\breve{\beta}_i \otimes \breve{\mathbf{sn}}_i\rangle^M \qquad \forall i \in N \tag{8.14d}$$
$$\Re(\mathbf{W}_{ii})^{\triangledown} = \Re(\mathbf{W}_{ii})^{\triangle} \qquad \forall i \in N \tag{8.14e}$$
$$\Im(\mathbf{W}_{ii})^{\triangledown} = -\Im(\mathbf{W}_{ii})^{\triangle} \qquad \forall i \in N \tag{8.14f}$$
$$\Re(\mathbf{W}_{ij}) = \gamma_{ij} = \langle\breve{\beta}_{ij} \otimes \breve{\mathbf{cs}}_{ij}\rangle^M \qquad \forall (i \sim j) \in E \tag{8.14g}$$
$$\Im(\mathbf{W}_{ij}) = \eta_{ij} = \langle\breve{\beta}_{ij} \otimes \breve{\mathbf{sn}}_{ij}\rangle^M \qquad \forall (i \sim j) \in E \tag{8.14h}$$

$\triangle$: Upper diagonal part $\triangledown$: Lower diagonal part $\otimes$: Element wise multiplication

in chapter 6. Furthermore, the three-phase non-linear OPF model is also solved using FilterSD solver [315] for all the test cases. Resultantly, %OG, as defined below, is used as a metric instead of EVR criterion to evaluate the performance of TPQC-based relaxation. Furthermore, the chosen metric value is also calculated for Three-Phase Semi-Definite Programming (TPSDP) and CBSDR-based OPF models, and a detailed comparison is made between all the OPF relaxations as shown in Table 8.5. A value of up to 1% for the chosen criterion allows to classify an OPF model as an exact relaxation. Lastly, please note that constant power loading is considered in this preliminary study.

$$\%\text{Optimality Gap} = \frac{(\text{AC-OPF}) - (\text{OPF-Relaxation})}{(\text{AC-OPF})} \times 100 \tag{8.17}$$

8.3.1 Exactness in terms of optimality gap and root-mean-square-error

In terms of optimality gap, the following observations can be made from the obtained results:

1. For OF1, the developed relaxation provides an exact solution for all the test cases. The obtained OG is exactly 0 in the case of CIGRE and MG DNs, whereas for all the other networks, it is extremely close to zero. However, it can be noted that the

Table 8.5: Comparison of the exactness and computational time of TPQC relaxation with MPSDP- and cheap SDP-based OPF relaxations.

Test Networks		**Optimality Gap** (%)			**RMSE** ($\times 10^{-4}$)			**Computational Time** (s)			
	AC-OPF	TPSDP	TPQC	CBSDP	TPSDP	TPQC	CBSDP	AC-OPF	TPSDP	TPQC	CBSDP
OF:1 Slack Bus Power (kVA)											
MG	3021	0	0	0	0.05	0.90	0.90	3.04	0.78	0.82	0.53
IT-37	80.3	0.09	0.19	0.34	0.08	0.32	1.55	8.56	230.4	0.80	0.56
IT-111	71.2	†	*0.08*	*3.10*	†	4.80	84.8	42.5	†	2.41	1.32
CIGRE	162.7	0	0	0	0.13	0.01	0.10	2.46	1.40	0.85	0.52
IEEE-13	4057.6	0	0.07	0.02	0.63	37.3	5.00	2.03	1.50	0.97	0.50
OF:2 Power System Losses (kW)											
MG	41.4	0.46	*1.03*	*3.09*	0.84	9.01	99.9	3.27	0.76	0.65	0.61
IT-37	2.36	**2.31**	***0.91***	*2.47*	1.11	0.17	6.13	8.78	232.4	0.93	0.66
IT-111	4.08	†	2.80	52.3	†	4.50	32.9	43.4	†	2.19	1.15
CIGRE	4.64	0.86	1.22	1.31	8.59	0.89	6.87	2.51	1.35	0.68	0.51
IEEE-13	73.4	**2.58**	***0.47***	*3.48*	79.0	3.81	95.0	4.46	1.94	0.71	0.51

TPSDP-based OPF model dominates the proposed approach since it further closes the OG and provides a more accurate solution.

2. With respect to OF2, the proposed relaxation dominates the TPSDP-based OPF model in IT-37 and IEEE-13 DNs cases, as shown in the bold values, where latter relaxation fails to provide a meaningful solution and produces a large OG. However, the TPQC-based relaxation is dominated by the TPSDP-based approach in the case of MG and CIGRE DNs where the proposed OPF model shows inexactness. Nevertheless, it can be noticed that even in these cases, the OG value is close to its threshold level, indicating that the obtained solution is not far from the global optimal solution. These results clearly indicate that while TPSDP-based OPF relaxation is considered as the tightest approach in literature, there exists some cases in which it is dominated by the developed relaxation.

3. The TPQC-based OPF relaxation dominates the CBSDR in both OFs. On the one hand, it further reduces the OG in those cases where CBSDR provides an exact solution and, on the other hand, it also makes CBSDR exact in the majority of cases where it shows inexactness and provides a large OG. Furthermore, it can also be noticed that the TPSDP-based model fails in the case of IT-111 node network (due to the violation of solver's internal memory limit) and CBSDR shows inexactness in this case. However, the proposed model provides an exact solution for OF1 and significantly reduces the OG in the case of OF2. These findings show that the quality of CBSDR can significantly be improved by imposing additional constraints on it in the form of convex envelopes.

In terms of RMSE parameter, the maximum error between the voltages recovered from the AC-OPF model and TPQC-based OPF relaxation is of order 10^{-3} which occurs only in the case of IEEE-13 node system. For all other cases, the RMSE lies between $10^{-5} - 10^{-4}$ range, which indicates that the proposed relaxation recovers the voltages with a high accuracy. The same trend is observed in the case of TPSDP-based relaxation. However, a higher value of this parameter is observed in the case of CBSDR which further confirms its inexactness and lower performance as compared to the proposed relaxation.

8.3.2 Computational performance

The CT of AC-OPF model and all OPF relaxations is reported in the last four columns of Table 8.5 and shown in Fig. 8.5. It can be noticed that the CBSDR model surpasses the AC-OPF model and both TPSDP- and TPQC-based OPF relaxations and solves the problem in a fraction of a second. The CT of proposed relaxation increases by a factor of 1.5-2 in comparison to the CBSDR since it imposes additional linear and quadratic inequalities in its formulation. However, the CT of AC-OPF and TPSDP-based models increases significantly with an increase in the network size. For smaller networks, it can be seen that the relaxation takes less time as compared to the time taken by the original non-convex model. However, for real-size DNs, the CT of TPSDP-based relaxation even surpasses the CT of AC-OPF model and, therefore, it makes less sense to solve this particular relaxation for medium size DNs provided the non-convex AC-OPF model of such networks can be solved successfully through a non-linear solver.

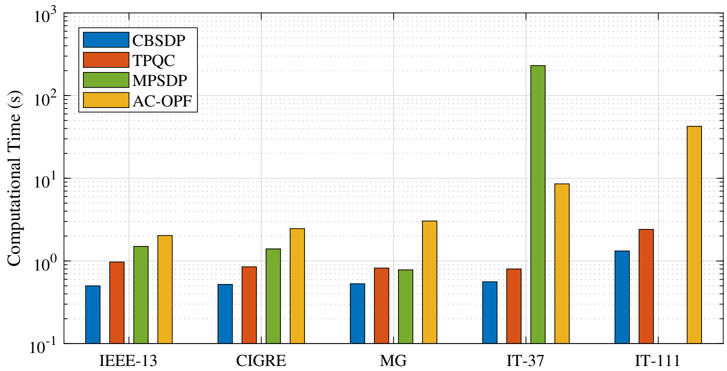

Figure 8.5: Comparison of computational time of proposed scheme with other relaxations.

8.4 Summary

In this chapter, a new TPQC-based OPF relaxation is proposed which combines the benefits of both CBSDR and TPSDP-based OPF model and, therefore, provides an alternative path for the solution of a non-convex AC-OPF problem. The significance of the proposed approach is quite evident as, on the one hand, it significantly tightens the CBSDR and, on the other hand, it even surpasses the standard TPSDP-based OPF model in few scenarios and, resultantly, provides a more accurate and exact solution.

From the computational point of view, the proposed relaxation has a significant advantage over the TPSDP-based relaxation since it can be solved in a significantly reduced time even for medium- and large-size networks. For such networks, as shown in the previous chapters as well as in this chapter, a large CT should be expected for TPSDP-based model which, resultantly, hinders its practical implementation. Consequently, the developed relaxation can be utilized for such networks since not only it can be solved in a fraction of a second time, an exact solution can also be obtained from it. However, it must be noted that for large-size systems, the total number of constraints related to the convex envelopes in the proposed approach increases exponentially (in the case of IT-111 node system, ~30k constraints are formed) and, as a result, the modelling environment, i.e., YALMIP, can take a significant amount of modelling time before solving the OPF relaxation. Therefore, an efficient way of defining the constraints, such as vectorizing the cone constraints, must be utilized to retain the advantages of proposed relaxation.

Published paper

The presented work in this chapter led to the publication of following paper.

1. Usman, Muhammad, Massimiliano Coppo, Fabio Bignucolo, and Roberto Turri. "Quadratic Convex Relaxation based centralized OPF for Multi-Phase Active Distribution Networks." in *2019 IEEE International Conference on Environment and Electrical Engineering and 2019 IEEE Industrial and Commercial Power Systems Europe (EEEIC/I&CPS Europe)*, pp. 1-6. IEEE, 2019.

CHAPTER 9

Conclusions and Future Perspectives

9.1 Main goals and objectives

Due to the detrimental impact of fossil-fuel-based electricity generation on the environment and, consequently, the adoption of renewable energy-based policies by governments and key industrial players has led to the swift integration of green energy resources in electricity grids worldwide, with special emphasis has been laid on MV and LV DNs for the installation of these resources. Resultantly, these systems can no longer be considered as passive networks and, therefore, a special focus must be put in the management of these active networks to ensure reliable delivery of electricity to end-users. Furthermore, the continuous reliance on *fit-and-forget* policy is no more suitable since these networks have started facing technical challenges like voltage unbalance, fault detection failure, reverse power flow or undesired islanded operation etc., which can jeopardize the stability of whole power system, and as a result, the active participation of renewable DERs in ensuring a safe and reliable operation of these networks, in the light of updated grid codes, is deemed necessary.

In this regard, the first and foremost step involves a detailed analysis of DNs through a numerical simulation tool which must be capable to model each aspect of these systems and should provide information about each state variable. Since MV and, in particular, LV DNs are unbalanced in nature and host both single- and three-phase end-users, their single-phase equivalent representation by assuming balanced loading and symmetrical configuration cannot be justified since it can lead to the loss of extremely important information. Consequently, the analysis of both MV and LV DNs should be based on their multi-phase configuration to properly evaluate the impact of DERs, which would, in turn, set the path for innovative solutions to carry out their efficient management. Furthermore, in the context of LV ADNs which exhibit significant unbalanced loading, neutral conductor gains special importance since it carries large unbalance current and, therefore, must be treated like phase conductors while carrying out the analysis of such networks. The application of KR approach in the case of single- and multiple-point grounded LV DNs provides over/under-estimated results and, therefore, undermines the accurate analysis of these networks. Since LV ADNs can play a significant role in the near-future in day-ahead and ancillary services electricity markets and can become a prominent pillar of a decentralized electrical grid, their analysis should be carried out by considering both phase and neutral conductors.

In view of the presented discussion, the aim of this thesis is to propose novel analysis and management methodologies for LV ADNs by modelling ***neutral conductors*** in addition to phases conductors in the context of LsMag schemes. Since LsMag is a broad concept which includes the ideas of LsMin, LA to end-users and effect of other network management strategies, such as load management and operating cost/profit optimization etc., on system losses in its scope, the extent of this thesis work, however, is confined to the first two above-mentioned approaches and following goals are set in this regard.

1. ***Proposal of a novel LAP for a multi-phase LV ADN by explicitly taking into account both phase and neutral conductors in its mathematical formulation, and, subsequently, development of a novel unbalance reduction management scheme by utilizing neutral losses allocation factors***

2. ***Modelling of an OPF problem for a neutral-equipped LV ADN hosting a mix of wye- and delta-connected end-users through convex optimization techniques with the aim of improving network operating conditions such as losses reduction etc.***

9.2 Summary and conclusions

Multi-phase losses allocation procedure

In the context of first goal, a novel MPLAP is presented in chapter 3 which belongs to the category of tracing LA methods and decomposes each branch current into the respective nodes current which are being fed by that branch. The main features of MPLAP include the (i) explicit allocation of branch losses to phase and neutral conductors at each node which, resultantly, leads to the novel concepts of PLAFs and NLAFs and (ii) segregation of cross-terms induced losses through self- and mutual-VLCs, which, in turn, address the shortcomings of equal segregation of these losses by the solely existed three-phase RCLP-based BCDLA. Consequently, the proposed approach successfully takes into consideration the impact of unbalanced loading through these coefficients. The self VLCs segregate the losses between phase/neutral currents of different nodes being fed by the ***same phase/neutral*** of an upstream branch, whereas mutual VLCs segregate the losses between phase/neutral currents of different nodes being fed the ***mutually coupled phases/neutral*** of an upstream branch. Furthermore, these coefficients are calculated not only between the currents of same end-users type i.e., load or DG, but are also developed between the currents of different end-users type i.e., load and DG. In this way, the impact of each end-user current on the losses in its phase and mutually coupled phases/neutral conductors is taken into account while allocating losses to it. Resultantly, the equal segregation of losses is avoided between the two mutually coupled conductors which, ultimately, leads to fair allocation of losses to passive and active end-users. Lastly, due to the quadratic relation between branch losses and its current, the self- and mutual-VLCs are determined through two LP approaches, termed as QLP and GLP techniques, to demonstrate the arbitrariness caused by this quadratic relation in the segregation of cross-terms induced losses.

The application of MPLAP on a test system reveals its superior performance over RCLP-based BCDLA scheme since the proposed scheme avoids negative LA to non-controllable passive end-users, which is seen in the case of RCLP-based LAP, and allocates positive losses to DGs in the case of their negative impact on system losses. Furthermore, no reconciliation factor is needed for the proposed approach since total allocated losses are equal to the total system losses and finally, additional information in the form of NLAFs is available which can be effectively used for the management of a DN.

Neutral losses allocation factors-based network management scheme

Since NLAFs provides pivotal information about the degree of unbalance at each node of a network, they can be practically utilized by DSOs to take respective corrective measures to improve network balancing. In this regard, a novel unbalance reduction strategy is proposed in chapter 4 which depends on three key factors (i) identification of HUNs (ii) phase switching algorithm and (iii) chosen OF. The recognition and selection of HUNs is based on positive NLAFs since these factors are assigned to those nodes which are responsible for an increase in network unbalance. Once identified, these nodes can serve as potential locations for the installation of PhSDs which commutate either individual or combined load from the heavily loaded phase(s) to the lightly loaded phase(s) of these critical nodes to reduce network unbalance. In this regard, two phase switching algorithms, termed as PSA-1 and PSA-2, are proposed. The first algorithm has the capability to transfer each ***individual load*** from one phase to another; however, it requires a three-phase connection and PhSD at each household premise and, therefore, is difficult to realize practically as per existing power system status. The second algorithm, on the other hand, requires a PhSD only at a node level rather than at each point of coupling and, therefore, can be implemented practically but it allows only ***combined load*** to be commutated across the phases of HUNs. Furthermore, this algorithm requires an information exchange, which can flow either in a forward or backward network sweep manner, between network nodes. However, in the case of PSA-1, each PhSD acts independently without relying on any information from other nodes.

The application of proposed approach, as per expectation, exhibits the superior performance of PSA-1 over PSA-2 in the case of lightly and moderately unbalanced feeders, whereas in the case of highly unbalanced feeder, a significant improvement is noted in the performance of PSA-2 in comparison to its performance with respect to the previous case. Nevertheless, both algorithms result in improving the network balancing and reducing its overall losses, and, therefore, can be utilized by DSOs in efficacious planning and management of their networks. Lastly, the developed approach can easily be incorporated in DMS with currently available controllable devices, such as three-phase converters connected to

PV systems or EV charging batteries, which have the ability to modulate their phase(s) active power.

Multi-phase semi-definite programming based OPF relaxation

Concerning losses minimization in LV ADNs, a large variety of ***rule-based*** ANM schemes exists in the published literature. However, ***optimization-based*** techniques are less often developed due to the complexity of resultant problem and, in particular, an OPF model for such networks have not been discussed in the literature yet. Due to the non-convex and NP-hard nature of an OPF problem, mathematical tools from the convex optimization theory is utilized in this work and a MPSDP-based OPF relaxation is proposed for LV ADNs.

The inclusion of a neutral conductor in an OPF model leads to power injections which are coupled between phase and neutral conductors in the case of wye-connected end-users. Similarly, in the case of a delta shunt element, the power injection is coupled between two phases conductors. Consequently, the existing three-phase OPF models which consider power injection in each phase conductor with respect to the ground cannot be considered in the context of this work unless the decoupling of active and reactive power injections is carried out and an explicit representation of these injections is developed for each phase and neutral conductor. Furthermore, due to significance presence of ZIP loads in LV ADNs, it is inappropriate to consider only constant power loads in an OP which is always the case in the previous studies.

Based on the existing shortcomings, the unique features of proposed MPSDP-based OPF relaxation involve the (i) explicit representation of neutral conductors in an OPF model and, subsequently, decoupling of coupled power injections between network conductors for both wye- and delta-connected loads and DGs, and (ii) incorporation of a complete ZIP load and neutral-ground impedance in an OPF model. Regarding the first point, the coupled power injections between two conductors are decoupled through the utilization of a network admittance-based approach which models a shunt element through constant admittance and current injection terms. Based on this approach, the resultant problem is reduced to split the admittance of a shunt element between two conductors which is successfully done by the introduction of incidence matrices for both wye- and delta-connected end-users. For the incorporation of a ZIP load, a novel ***complex voltage variable-based*** methodology is developed since existing ***voltage magnitude-based*** approach, which is proposed in the framework of a single-phase equivalently represented networks, cannot be generalized for multi-phase networks. The proposed methodology, however, successfully generalizes the ZIP load modelling in the framework of both single- and multi-phase networks. Furthermore, two additional approximations based on the *first-order Taylor series* and *approximation of a first-order Taylor series* are proposed for the modelling of a constant current load, which allow representing it through the optimization variable of MPSDP-based OPF relaxation.

The application of proposed multi-phase OPF model on a range of DNs, varying in size and degree of unbalance, shows that global optimal solution can be obtained under a large combination of ZIP load parameters and a range of neutral-ground impedance. The relaxation provides an optimal solution for all LMs which are independent of constant current loads irrespective of the degree of unbalance in a DN. However, in the presence of constant current load which are modelled approximately, the exactness of relaxation strongly depends on the degree of unbalance and type of end-users connected in a DN. In the case of wye-connected loads, the relaxation shows inexactness only in the case of a highly unbalanced DN serving large constant current loads, whereas in the case of delta-connected loads, the quality of relaxation can be compromised in the case of moderately and highly unbalanced DNs under a significant contribution from constant current loads. The neutral to ground impedance strongly impacts the optimal objective value and a completely different result can be obtained in the case of SPG and MPG DNs under a range of LMs and grounding impedance value in comparison to the KR-based OPF approach. These findings further support the case of treating neutral conductors independently without imposing the unrealistic KR methodology to LV ADNs. From computational point of view, the MPSDP-based approach, however, cannot be practically realized due to its high CT requirement for medium- and large-size DNs.

Cheap conic semi-definite programming based OPF relaxation

To realize an OPF model for real DNs on a practical basis, a new cheap SDP-based OPF methodology is presented in chapter 7 which exploits the sparsity of a RDN and imposes PSD constraints on several small size matrices as compared to the stringent PSD constraint which is imposed on a single large matrix in the case of MPSDP-based OPF relaxation. Furthermore, for the modelling of constant current load in the cheap SDP-based OPF model, three novel propositions (P1, P2 and P3) are proposed as well. Although the complex voltage variable-based approach can be generalized to the case of cheap relaxation, however, it leads to an unnecessary complexity caused by the extension of OVs dimensions. Regarding new constant current modelling propositions, novel bounds on complex phase voltage variables are also presented and a procedure is reported as well which determines the minimum and maximum limits on neutral voltage variable.

The evaluation of proposed OPF relaxation demonstrates a significant reduction in the CT for medium- and large-size DNs which can now be solved in a fraction of a second time. Consequently, the proposed relaxation sets the path for the practical implementation of an OPF model for such networks. In terms of exactness, the P3-based OPF model dominates the P1- and P2-based OPF relaxations especially in the case of LMs which involve power absorbing constant current loads, whereas in the case of power injecting constant current loads, a general dominance of P3-based approach over P1- and P2-based models cannot be established due to the existence of few cases where P2 dominates it. Nevertheless, in all such cases, an exact solution is still obtained by the P3-based relaxation. The P2-based OPF model, on the other hand, dominates the P1-based relaxation under all cases provided the selected value of phase-voltage angle deviation parameter is not too tight with respect to the degree of unbalance and network loading. Moreover, the imposition of neutral envelopes further improves the quality of proposed relaxation. However, it should be kept in mind that neutral bounds calculation procedure is based on the assumption of improved network conditions after solving an OPF model and, as a result, tight bounds are calculated for this variable. This is true in the case of an OF which reduces the unbalance in a network; however, for a completely different OF (which can lead to an increase in network unbalance), the calculated neutral bounds can become too tight and may drive the OP towards infeasibility.

Finally, it has been shown that MPSDP-based OPF relaxation dominates the cheap SDP-based OPF model since the latter relaxation shows inexactness in few cases where the former methodology provides an exact solution. Although an equivalency is established between the SDP- and SOCP-based OPF models in the case of single-phase equivalently represented electrical networks, there does not exist any equivalent relation between the MPSDP- and cheap SDP-based models in a multi-phase network modelling framework and this assertion is further supported by the obtained results. Consequently, the cheap SDP-based methodology can be strengthened through a tightening approach which is reported in chapter 8.

Three-phase quadratic convex OPF relaxation

The resultant relaxation, termed as TPQC relaxation, introduces additional constraints in the form of convex envelopes which enclose the non-convex region of the individual terms of cheap SDP-based OPF approach OVs through quadratic, McCormick, polyhedral and Taylor series-based convex envelopes. The first two envelopes are introduced for the quadratic and bilinear terms of OVs, whereas the last two types of envelopes are developed for the trigonometric functions of these variables. The preliminary results shows that this approach combines the advantages of previously reported MPSDP- and cheap SDP-based methodologies since it can be solved in a significantly reduced time and is as tight as MPSDP-based approach. Furthermore, it exhibits a promising potential of even surpassing the MPSDP-based relaxation in few test cases and, therefore, suggests a further investigation of its application on a four-conductor network framework by involving a complete ZIP load in its formulation.

9.3 Perspectives for future work

The work presented in this thesis has opened a number of different directions for future research, some of which are discussed below.

The first aspect involves the formulation of NLAFs-based management strategy through an optimization-based rule. Since rule-based management scheme has shown promising results in improving network balancing, the optimal allocation (number and location) of PhSDs could further improve the network conditions as well as the performance of PSA-2. Furthermore, the proposed MPLAP also opens the room for the development of a financial policy to fairly penalize or reward the end-users based on their negative or positive impact on network balancing.

The second aspect focuses on tightening the cheap SDP-based OPF relaxation, which involves BFM for power system representation, through the introduction of convex envelopes on line currents. Since BFM-based cheap SDR has already shown impressive results for a four conductor network and ZIP LMs, a further improvement in its exactness can potentially rule out the tight MPSDP-based OPF relaxation. On a similar basis, the performance of cheap SDP-based OPF relaxation which is based on BIM has also improved through the enforcement of convex envelopes. Consequently, its effectiveness could also be explored in the case of neutral equipped DNs hosting ZIP loads.

The third aspect revolves around the inclusion of binary variables in the proposed OPF models since in this work, only continuous variables have been considered. The selective inclusion of PV inverters, batteries and demand response change the nature of OPF problem from continuous to binary. Since MISDP-based OPF relaxation cannot be solved in reality due to the non-availability of any solver to handle this type of problem, the future work could involve the reformulation of multi-phase OPF problem through a sparsity-regularization technique which relaxes the binary variables into continuous domain and, as a result, the reformulated problem can be solved through a cheap SDP-based modelling approach. Following this, the energy storage resources and uncertainty associated with DERs can further be modelled and incorporated in the OPF model and, resultantly, a multi-period OPF model can be developed for LV networks. This multi-period OPF model can subsequently be added in centralized LV distribution management systems which would, ultimately, provide the optimal control of these resources and, consequently, LV ADNs by ensuring the active participation of all types of end-users. Since it is likely that LV ADNs would become the central pillar of modern electricity networks, it is, therefore, expected to have centralized/de-centralized management systems in the near-future for the real-time optimal control and management of these networks. Finally, once a multi-period OPF model for LV ADNs is available, an optimal bidding strategy for the active participation of these networks in day-ahead and ancillary services electricity and energy markets can be explored and developed.

To conclude this thesis, it is also important to remark that, currently, the transformation of LV DNs in majority of the countries is in early stages. The advanced ICT infrastructure, SCADA systems and DMSs exist only to a limited extend as of now for these networks. Additionally, the end-users are not equipped with the advanced controllers and, therefore, the participation of active end-users in the provision of grid-services is limited mainly to a local voltage control and in some cases to a decentralized one. Quite recently, a new generation of smart-meters have been put in service in Italy which have the possibility of storing and transmitting the 15 min resolution-based active and reactive power consumption to DSOs. Consequently, an offline OPF model can be solved on the basis of stored and developed *aggregated* end-users profiles to determine the optimal set-points of DSOs owned, if any, DERs. Nevertheless, due to the rapid installation of green energy resources in LV DNs along with the pervasive deployment of modern technical infrastructure capable of handling big data as well as providing real-time control of each end-user, it is just a matter of time of realizing the real-time implementation of advanced analysis tools and management strategies for these networks.

Appendices

Appendix A

Relation between Network Physical Quantities and MPSDP-based OPF Variables

A.1 Representation of bus power injection in terms of an optimization variable

Consider a simple two phase two node network as shown in Fig. A.1 containing a constant impedance load. To express the apparent power $S_i^{\alpha\beta}$ drawn by the load in terms of $\mathbf{W}$, the starting point would be:

$$S_i^{*\alpha\beta} = k_Z * Y_i^{\alpha\beta} * |V_i^{\alpha\beta}|^2 \tag{A.1}$$
$$S_i^{*\alpha\beta} = k_Z * Y_i^{\alpha\beta} * (V_i^{\alpha g} - V_i^{\beta g})(V_i^{\alpha g} - V_i^{\beta g})^* \tag{A.2}$$
$$S_i^{*\alpha\beta} = \underbrace{\{k_Z * Y_i^{\alpha\beta} * [V_i^{*\alpha g} * (V_i^{\alpha g} - V_i^{\beta g})]\}}_{S_i^{*\alpha g}} + \underbrace{\{k_Z * Y_i^{\alpha\beta} * [V_i^{*\beta g} * (V_i^{\beta g} - V_i^{\alpha g})]\}}_{S_i^{*\beta g}} \tag{A.3}$$

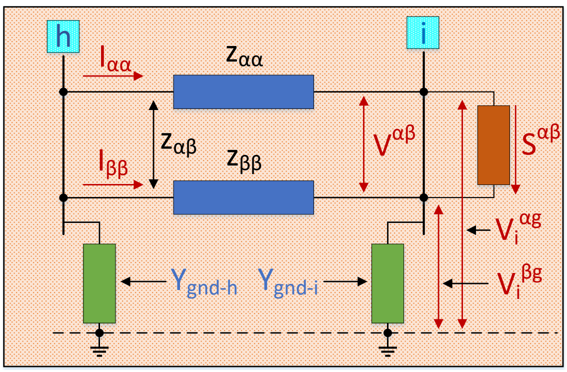

Figure A.1: A simple two bus network

It can be noticed that the first term $S_i^{*\alpha g}$ in (A.3) represents the power flowing out of the phase α whereas second term $S_i^{*\beta g}$ represents the power flowing into the phase β. In the following, the derivation is restricted only to $S_i^{*\alpha g}$; however, the concepts are readily applicable to $S_i^{*\beta g}$.
Starting from:

$$S_i^{*\alpha g} = k_Z * Y_i^{\alpha\beta} * [V_i^{*\alpha g} * (V_i^{\alpha g} - V_i^{\beta g})] \tag{A.4}$$

$$S_i^{*\alpha g} = k_Z * (g_i^{\alpha\beta} + jb_i^{\alpha\beta}) * (V_i^{\alpha g} V_i^{*\alpha g} - V_i^{\beta g} V_i^{*\alpha g}) \tag{A.5}$$

$$S_i^{*\alpha g} = k_Z * (g_i^{\alpha\beta} + jb_i^{\alpha\beta}) * \{(V_{i_R}^{\alpha g} + jV_{i_{IM}}^{\alpha g})(V_{i_R}^{\alpha g} - jV_{i_{IM}}^{\alpha g}) - (V_{i_R}^{\beta g} + jV_{i_{IM}}^{\beta g})(V_{i_R}^{\alpha g} - jV_{i_{IM}}^{\alpha g})\} \tag{A.6}$$

$$\begin{aligned} S_i^{\alpha g} = {} & k_Z * \{g_i^{\alpha\beta}(V_{i_R}^{\alpha g^2} + V_{i_{IM}}^{\alpha g^2}) - g_i^{\alpha\beta}(V_{i_R}^{\alpha g} V_{i_R}^{\beta g} + V_{i_{IM}}^{\alpha g} V_{i_{IM}}^{\beta g}) - b_i^{\alpha\beta}(V_{i_R}^{\beta g} V_{i_{IM}}^{\alpha g} - V_{i_{IM}}^{\beta g} V_{i_R}^{\alpha g})\} \\ & + jk_Z * \{-b_i^{\alpha\beta}(V_{i_R}^{\alpha g^2} + V_{i_{IM}}^{\alpha g^2}) + b_i^{\alpha\beta}(V_{i_R}^{\alpha g} V_{i_R}^{\beta g} + V_{i_{IM}}^{\alpha g} V_{i_{IM}}^{\beta g}) \\ & - g_i^{\alpha\beta}(V_{i_R}^{\beta g} V_{i_{IM}}^{\alpha g} - V_{i_{IM}}^{\beta g} V_{i_R}^{\alpha g})\} \end{aligned} \tag{A.7}$$

$$S_i^{\alpha g} = P_i^{\alpha g} + jQ_i^{\alpha g} \tag{A.8}$$

After obtaining explicit expressions for active and reactive power, they can be easily represented in terms of **W**. In the following, only active power is shown to be represented in terms of **W**.

$$P_i^{\alpha g} = k_Z * \{g_i^{\alpha\beta}(V_i^{\alpha g} V_i^{*\alpha g}) - g_i^{\alpha\beta}\Re(V_i^{\alpha g} V_i^{*\beta g}) - b_i^{\alpha\beta}\Im(V_i^{\alpha g} V_i^{*\beta g})\} \tag{A.9}$$

$$P_i^{\alpha g} = k_Z * \left\{ g_i^{\alpha\beta}(V_i^{\alpha g} V_i^{*\alpha g}) - g_i^{\alpha\beta}\left[\frac{(V_i^{\alpha g} V_i^{*\beta g}) + (V_i^{\alpha g} V_i^{*\beta g})^*}{2}\right] + jb_i^{\alpha\beta}\left[\frac{(V_i^{\alpha g} V_i^{*\beta g}) - (V_i^{\alpha g} V_i^{*\beta g})^*}{2}\right]\right\} \tag{A.10}$$

$$P_i^{\alpha g} = k_Z * \left\{ g_i^{\alpha\beta}(V_i^{\alpha g} V_i^{*\alpha g}) + \left[\frac{-g_i^{\alpha\beta} + jb_i^{\alpha\beta}}{2}(V_i^{\alpha g} V_i^{*\beta g})\right] + \left[\frac{-g_i^{\alpha\beta} - jb_i^{\alpha\beta}}{2}(V_i^{\alpha g} V_i^{*\beta g})^*\right]\right\} \tag{A.11}$$

$$P_i^{\alpha g} = k_Z * \left\{ \frac{Y_i^{\alpha\beta} + Y_i^{*\alpha\beta}}{2}(V_i^{\alpha g} V_i^{*\alpha g}) + \left[\frac{-Y_i^{*\alpha\beta}}{2}(V_i^{\alpha g} V_i^{*\beta g})\right] + \left[\frac{-Y_i^{\alpha\beta}}{2}(V_i^{\alpha g} V_i^{*\beta g})^*\right]\right\} \tag{A.12}$$

which can be written in terms of matrix form as follows:

$$P_i^{\alpha g} = \mathrm{Tr}\left\{ k_Z * \left\{ \underbrace{\begin{bmatrix} \frac{Y_i^{\alpha\beta} + Y_i^{*\alpha\beta}}{2} & \frac{-Y_i^{\alpha\beta}}{2} \\ \frac{-Y_i^{*\alpha\beta}}{2} & 0 \end{bmatrix}}_{\mathbf{\Psi}_{i,l_p}^{\alpha}} \underbrace{\begin{bmatrix} V_i^{\alpha g} V_i^{*\alpha g} & V_i^{\alpha g} V_i^{*\beta g} \\ V_i^{\beta g} V_i^{*\alpha g} & V_i^{\beta g} V_i^{*\beta g} \end{bmatrix}}_{\mathbf{W}} \right\} \right\} \tag{A.13}$$

It can be noticed that $\mathbf{\Psi}^{\alpha}_{i,l_p}$ can further be represented as summation of matrices $\mathbf{Y}^{\alpha}_{i,l_p}$ and $\mathbf{Y}^{H\alpha}_{i,l_p}$ which leads to:

$$\mathbf{\Psi}^{\alpha}_{i,l_p} = \frac{1}{2}\underbrace{\begin{bmatrix} Y_i^{\alpha\beta} & -Y_i^{\alpha\beta} \\ 0 & 0 \end{bmatrix}}_{\mathbf{Y}^{\alpha}_{i,l_p}} + \underbrace{\begin{bmatrix} Y_i^{\alpha\beta} & -Y_i^{\alpha\beta} \\ 0 & 0 \end{bmatrix}^H}_{\mathbf{Y}^{H\alpha}_{i,l_p}} \tag{A.14}$$

where $\mathbf{Y}^{\alpha}_{i,l_p}$ can be obtained from the load matrix $\mathbf{Y}_{L_i}$ as follows:

$$\begin{bmatrix} Y_i^{\alpha\beta} & -Y_i^{\alpha\beta} \\ 0 & 0 \end{bmatrix} = \underbrace{\begin{bmatrix} 1 & 0 \\ 0 & 0 \end{bmatrix}}_{\mathbf{e}_i^{\alpha} * \mathbf{e}_i^{\alpha T}} * \underbrace{\begin{bmatrix} Y_i^{\alpha\beta} & -Y_i^{\alpha\beta} \\ -Y_i^{\alpha\beta} & Y_i^{\alpha\beta} \end{bmatrix}}_{\mathbf{Y}_{L,i}} \tag{A.15}$$

and, consequently, $\mathbf{\Psi}^{\alpha}_{i,l_p}$ can finally be written in the matrix notation as:

$$\mathbf{\Psi}^{\alpha}_{i,l_p} = \frac{1}{2}\Big\{(\mathbf{e}_i^{\alpha} * \mathbf{e}_i^{\alpha T} * \mathbf{Y}_{L,i}) + (\mathbf{e}_i^{\alpha} * \mathbf{e}_i^{\alpha T} * \mathbf{Y}_{L,i})^H\Big\} \tag{A.16}$$

Based upon (A.16), (A.13) can now be expressed in terms of $\mathbf{W}$ as:

$$P_i^{\alpha g} = \mathrm{Tr}\{k_Z(\mathbf{\Psi}^{\alpha}_{i,l_p}\mathbf{W})\} \tag{A.17}$$

which completes the derivation. Following the same direction, injected reactive power at phase α can be represented as:

$$Q_i^{\alpha g} = \mathrm{Tr}\{k_Z(\mathbf{\Psi}^{\alpha}_{i,l_q}\mathbf{W})\} \tag{A.18}$$

A.1.1 Representation of slack-bus power

Consider node h in Fig. A.1 as a slack node. Consequently, power injected from the slack node into the system can be obtained on a similar basis as shown in (A.1)-(A.17) by replacing $\mathbf{\Psi}^{\alpha}_{i,l_{p/q}}$ with $\mathbf{\Psi}^{\alpha}_{h,nw_{p/q}}$ where $\mathbf{\Psi}^{\alpha}_{h,nw_{p/q}}$ is obtained by replacing $\mathbf{Y}_{L,i}$ in (A.15) with bus admittance matrix $\mathbf{Y}_B$ as shown in (6.3)-(6.4). This leads to the definition of slack-bus power objective function as reported below:

$$f_{\mathbf{OF_1}}(\mathbf{W}) = P_h^{\alpha g} + P_h^{\beta g} + Q_h^{\alpha g} + Q_h^{\beta g} \tag{A.19}$$

$$f_{\mathbf{OF_1}}(\mathbf{W}) = \mathrm{Tr}(\mathbf{\Psi}^{\alpha}_{h,nw_p}\mathbf{W}) + \mathrm{Tr}(\mathbf{\Psi}^{\beta}_{h,nw_p}\mathbf{W}) + \mathrm{Tr}(\mathbf{\Psi}^{\alpha}_{h,nw_q}\mathbf{W}) + \mathrm{Tr}(\mathbf{\Psi}^{\beta}_{h,nw_q}\mathbf{W}) \tag{A.20}$$

$$f_{\mathbf{OF_1}}(\mathbf{W}) = \sum_{\varphi\in\phi_0}\{\mathrm{Tr}(\mathbf{\Psi}^{\varphi}_{h,nw_p}\mathbf{W}) + \mathrm{Tr}(\mathbf{\Psi}^{\varphi}_{h,nw_q}\mathbf{W})\} \tag{A.21}$$

A.2 Representation of line flow in terms of an optimization variable

For the network shown in Fig. A.1, the series impedance matrix of the line from node h to node i can be defined as:

$$\mathbf{Z}_{hi} = \begin{bmatrix} z_{hi}^{\alpha\alpha} & z_{hi}^{\alpha\beta} \\ z_{hi}^{\beta\alpha} & z_{hi}^{\beta\beta} \end{bmatrix} \tag{A.22}$$

and the line admittance matrix can be defined as:

$$\mathbf{Y}_{hi} = \mathbf{z}_{hi}^{-1} \tag{A.23}$$

Based on $\mathbf{Y}_{hi}$, the line flow from node h to node i can represented as:

$$S_{h\to i} = V_h^{\alpha g}(I_{h\to i}^{\alpha})^* + V_h^{\beta g}(I_{h\to i}^{\beta})^* \tag{A.24}$$

$$\begin{aligned} S_{h\to i} &= V_h^{\alpha g}\left\{ y_{hi}^{*\alpha\alpha}(V_h^{*\alpha g} - V_i^{*\alpha g}) + y_{hi}^{*\alpha\beta}(V_h^{*\beta g} - V_i^{*\beta g}) \right\} \\ &\quad + V_i^{\beta}\left\{ y_{hi}^{*\beta\alpha}(V_h^{*\alpha g} - V_i^{*\alpha g}) + y_{hi}^{*\beta\beta}(V_h^{*\beta g} - V_i^{*\beta g}) \right\} \end{aligned} \tag{A.25}$$

$$\begin{aligned} S_{h\to i} &= y_{hi}^{*\alpha\alpha}(V_h^{\alpha g}V_h^{*\alpha g} - V_h^{\alpha g}V_i^{*\alpha g}) + y_{hi}^{*\beta\alpha}(V_h^{\beta g}V_h^{*\alpha g} - V_h^{\beta g}V_i^{*\alpha g}) \\ &\quad + y_{hi}^{*\alpha\beta}(V_h^{\alpha g}V_h^{*\beta g} - V_h^{\alpha g}V_i^{*\beta g}) + y_{hi}^{*\beta\beta}(V_h^{\beta g}V_h^{*\beta g} - V_h^{\beta g}V_i^{*\beta g}) \end{aligned} \tag{A.26}$$

which can be represented in terms of matrices as:

$$S_{h\to i} = \mathrm{Tr}\left\{ \underbrace{\begin{bmatrix} y_{hi}^{*\alpha\alpha} & y_{hi}^{*\beta\alpha} & 0 & 0 \\ y_{hi}^{*\alpha\beta} & y_{hi}^{*\beta\beta} & 0 & 0 \\ -y_{hi}^{*\alpha\alpha} & -y_{hi}^{*\beta\alpha} & 0 & 0 \\ -y_{hi}^{*\alpha\beta} & -y_{hi}^{*\beta\beta} & 0 & 0 \end{bmatrix}}_{\mathbf{X}_{line}} \underbrace{\begin{bmatrix} V_h^{\alpha g}V_h^{*\alpha g} & V_h^{\alpha g}V_h^{*\beta g} & V_h^{\alpha g}V_i^{*\alpha g} & V_h^{\alpha g}V_i^{*\beta g} \\ V_h^{\beta g}V_h^{*\alpha g} & V_h^{\beta g}V_h^{*\beta g} & V_h^{\beta g}V_i^{*\alpha g} & V_h^{\beta g}V_i^{*\beta g} \\ V_i^{\alpha g}V_h^{*\alpha g} & V_i^{\alpha g}V_h^{*\beta g} & V_i^{\alpha g}V_i^{*\alpha g} & V_i^{\alpha g}V_i^{*\beta g} \\ V_i^{\beta g}V_h^{*\alpha g} & V_i^{\beta g}V_h^{*\beta g} & V_i^{\beta g}V_i^{*\alpha g} & V_i^{\beta g}V_i^{*\beta g} \end{bmatrix}}_{\mathbf{W}} \right\} \tag{A.27}$$

where $\mathbf{X}_{line}$ can be defined as a product of two matrices $\mathbf{A}_{h\to i}$ and $\mathbf{B}_h$:

$$\begin{bmatrix} y_{hi}^{*\alpha\alpha} & y_{hi}^{*\beta\alpha} & 0 & 0 \\ y_{hi}^{*\alpha\beta} & y_{hi}^{*\beta\beta} & 0 & 0 \\ -y_{hi}^{*\alpha\alpha} & -y_{hi}^{*\beta\alpha} & 0 & 0 \\ -y_{hi}^{*\alpha\beta} & -y_{hi}^{*\beta\beta} & 0 & 0 \end{bmatrix} = \underbrace{\begin{bmatrix} y_{hi}^{*\alpha\alpha} & y_{hi}^{*\beta\alpha} \\ y_{hi}^{*\alpha\beta} & y_{hi}^{*\beta\beta} \\ -y_{hi}^{*\alpha\alpha} & -y_{hi}^{*\beta\alpha} \\ -y_{hi}^{*\alpha\beta} & -y_{hi}^{*\beta\beta} \end{bmatrix}}_{\mathbf{A}_{h\to i}^{H}} \underbrace{\begin{bmatrix} 1 & 0 & 0 & 0 \\ 0 & 1 & 0 & 0 \end{bmatrix}}_{\mathbf{B}_h} \tag{A.28}$$

and $\mathbf{A}_{h\to i}$ and $\mathbf{B}_h$ can be represented in a compact form as:

$$\mathbf{A}_{h\to i} = \begin{bmatrix} \mathbf{Z}_{hi}^{-1} & -\mathbf{Z}_{hi}^{-1} \end{bmatrix} \tag{A.29}$$

$$\mathbf{B}_h = \begin{bmatrix} \mathbf{I} & \mathbf{0} \end{bmatrix} \tag{A.30}$$

For an n node network, (A.29) and (A.30) will take the form as mentioned in (6.72) and (6.73) respectively. Based on $\mathbf{A}_{h\to i}$, $\mathbf{B}_h$ and $\mathbf{W}$, the apparent power flow from node h to node i can be represented as:

$$S_{h\to i} = \mathrm{Tr}(\mathbf{A}_{h\to i}^H \mathbf{B}_h \mathbf{W}) \tag{A.31}$$

A.2.1 Representation of network active power losses

The active network losses in any branch of a network can be represented as:

$$P_{loss}^{hi} = \Re(S_{h\to i}) + \Re(S_{i\to h}) \tag{A.32}$$

Substituting (A.31) in (A.32) leads to

$$P_{loss}^{hi} = \Re\{\mathrm{Tr}(\mathbf{A}_{h\to i}^H \mathbf{B}_h \mathbf{W})\} + \Re\{\mathrm{Tr}(\mathbf{A}_{i\to h}^H \mathbf{B}_i \mathbf{W})\} \tag{A.33}$$

$$P_{loss}^{hi} = \mathrm{Tr}\{\frac{1}{2}(\mathbf{A}_{h\to i}^H \mathbf{B}_h + \mathbf{B}_h^H \mathbf{A}_{h\to i})\mathbf{W}\} + \mathrm{Tr}\{\frac{1}{2}(\mathbf{A}_{i\to h}^H \mathbf{B}_i + \mathbf{B}_i^H \mathbf{A}_{i\to h})\mathbf{W}\} \tag{A.34}$$

By defining

$$\mathbf{\Psi}_{h\to i}^{nw_p} = \frac{1}{2}(\mathbf{A}_{h\to i}^H \mathbf{B}_h + \mathbf{B}_h^H \mathbf{A}_{h\to i}) \tag{A.35}$$

(A.34) can be represented as

$$P_{loss}^{hi} = \mathrm{Tr}\,(\mathbf{\Psi}_{h\to i}^{nw_p} \mathbf{W}) + \mathrm{Tr}\,(\mathbf{\Psi}_{i\to h}^{nw_p} \mathbf{W}) \tag{A.36}$$

which can be extended to arbitrary number of branches to get the formula reported in (6.70).

Appendix B

Medium Voltage Microgrid Distribution Network

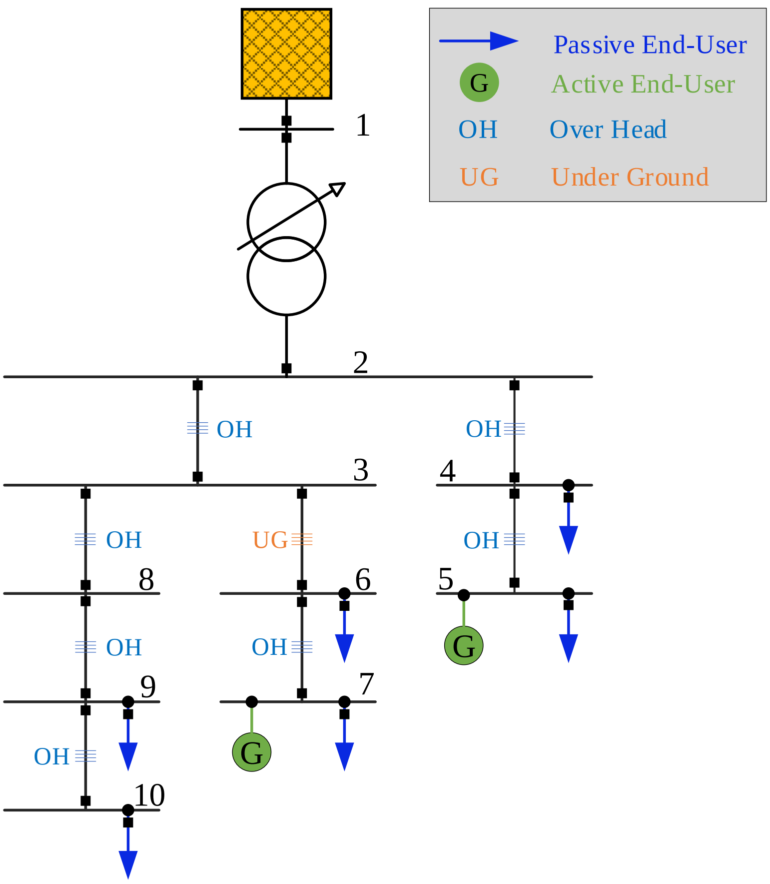

Figure B.1: Single line diagram of medium voltage microgrid distribution network.

Table B.1: Wire data.

Wire Type	d [mm]	GMR [mm]	Rc [Ω]	g [S]	Imax [A]
1	0.0235	0.8104	0.1155	0	730
2	0.0143	0.3470	0.3679	0	340
3	0.0101	0.2689	0.6959	0	230
4	0.0144	0.7238	0.2548	0	260
5	0.0016	18.196	0.7107	0	260
6	0.0093	0.7239	0.6027	0	310
7	0.0093	0.7259	0.3772	0	310

d = diameter R_c = DC-Resistance g = conductance

Table B.2: Line configuration data.

Configuration	No. of Phases	PC Type	NC Type	Mutual Distance [m]							
				Type	a	b	c	n	d	x	y
1	3	1	2	OH	0.30	0.77	1.07	0.15	1.21	-	-
2	3	2	2	OH	0.30	0.77	1.07	0.15	1.21	-	-
3	3	3	3	OH	0.30	0.77	1.07	0.15	1.21	-	-
4	3	3	3	OH	0.30	0.77	1.07	0.15	1.21	-	-
5	3	3	3	OH	0.30	0.77	1.07	0.15	1.21	-	-
6	3	4	5	UG	-	-	-	-	-	0.30	3.05
7	3	6	7	OH	0.30	0.77	1.07	0.15	1.21	-	-

PC = Phase Conductor/Cable Type NC = Neutral Conductor/Cable Type OH = Over Head
UG = Under Ground

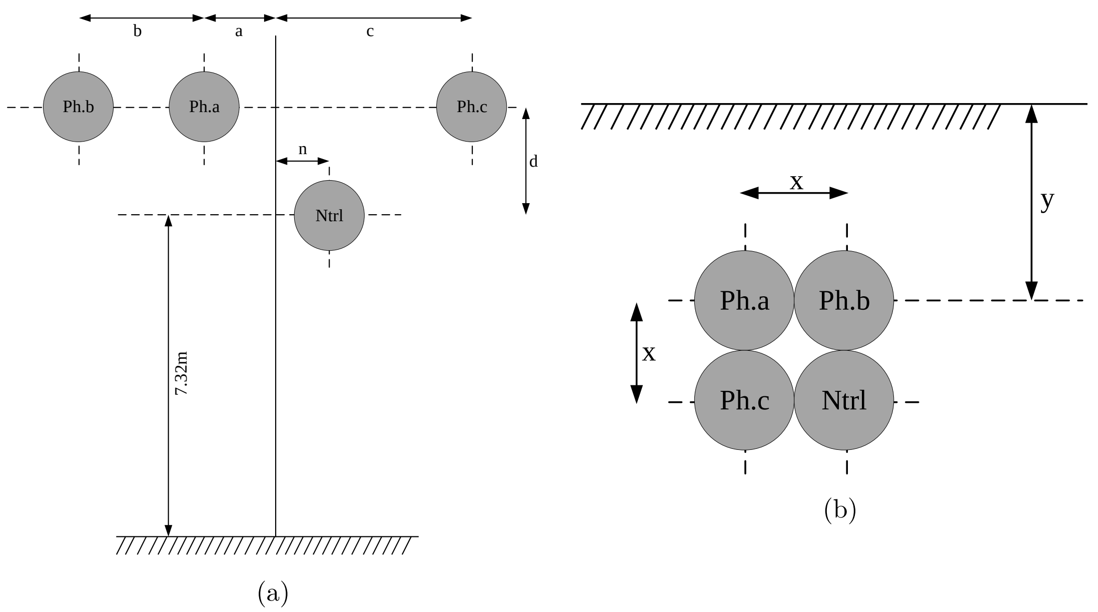

Figure B.2: Configuration of a 4-wire (a) overhead conductor (b) underground cable.

Table B.3: Branches connection data.

From Bus	To Bus	Line Type	Length [km]	From Bus	To Bus	Line Type	Length [km]
1	2	1	0.50	3	8	1	0.20
2	3	3	0.20	6	7	5	0.10
2	4	3	0.20	8	9	4	0.35
4	5	2	0.40	9	10	7	0.20
3	6	1	0.15	–	–	–	–

Table B.4: Installed load power data.

Bus	Phase	P [kW]	Q [kVAr]	p.f.	Bus	Phase	P [kW]	Q [kVAr]	p.f.
2	1	50	20	0.95	6	1	110	60	0.95
2	2	50	20	0.95	7	1	110	60	0.95
2	3	50	20	0.95	7	2	110	60	0.95
4	3	130	82	0.95	7	3	110	60	0.95
4	1	130	82	0.95	9	2	90	30	0.95
4	3	130	82	0.95	9	2	90	30	0.95
5	2	130	82	0.95	9	3	90	30	0.95
5	2	130	82	0.95	10	3	90	30	0.95
5	3	130	82	0.95	10	2	90	30	0.95
6	1	130	60	0.95	10	3	90	30	0.95
6	2	130	60	0.95	–	–	–	–	

Table B.5: Installed generator power data.

Bus	Phase	P [kW]	Q [kVAr]	Bus	Phase	P [kW]	Q [kVAr]
5	1	50	1	7	1	50	1
5	2	50	1	7	2	50	1
5	3	50	1	7	3	50	1

Appendix C

Low Voltage CIGRE Distribution Network

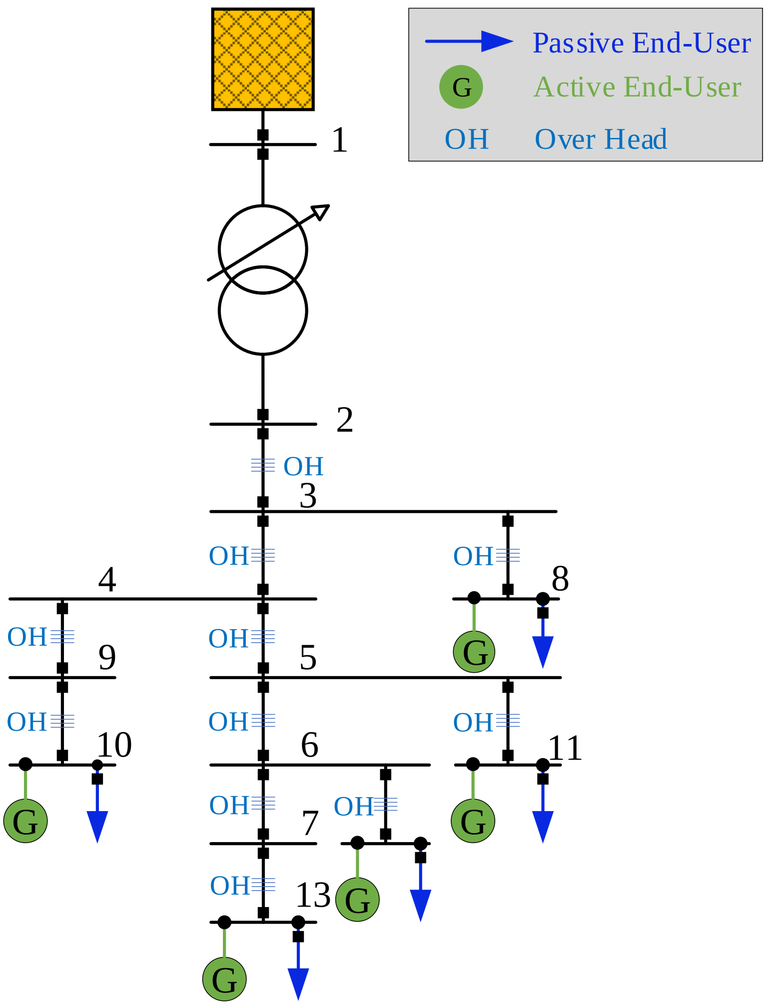

Figure C.1: Single line diagram of low voltage CIGRE distribution network.

Table C.1: Wire data.

Wire Type	d [mm]	GMR [mm]	Rc [Ω]	g [S]	Imax [A]
1	0.0175	0.7669	0.1620	0	240
2	0.0138	0.7696	0.2650	0	240
3	0.0124	0.7661	0.3250	0	240
4	0.0056	0.7801	1.5400	0	240
5	0.0067	0.7784	1.1100	0	240
6	0.0094	0.7797	0.5680	0	240
7	0.0051	0.7788	1.1500	0	240

Table C.2: Line configuration data.

Configuration	No. of Phases	PC Type	NC Type	Mutual Distance [m]		
				Type	a	b
1	3	1	2	OH	0.05	0.05
2	3	2	3	OH	0.04	0.04
3	3	3	2	OH	0.04	0.04
4	3	4	7	OH	0.02	0.02
5	3	5	7	OH	0.03	0.03
6	3	6	5	OH	0.03	0.03

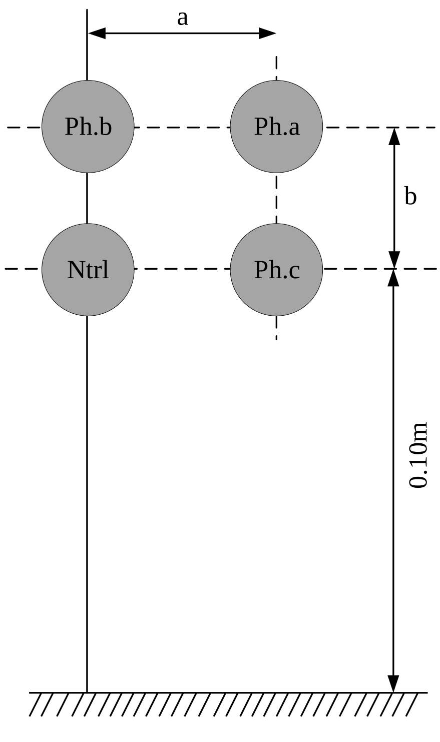

Figure C.2: Configuration of a 4-wire conductor.

Table C.3: Branches connection data.

From Bus	To Bus	Line Type	Length [km]	From Bus	To Bus	Line Type	Length [km]
1	2	1	0.02	3	8	4	0.03
2	3	1	0.07	4	9	2	0.105
3	4	1	0.035	9	10	3	0.03
4	5	1	0.07	5	11	6	0.03
5	6	1	0.105	6	12	4	0.03
6	7	1	0.035	7	13	5	0.03

Table C.4: Installed load power data.

Bus	Phase	P [kW]	Q [kVAr]	p.f.	Bus	Phase	P [kW]	Q [kVAr]	p.f.
8	1	8.0	3.8	0.95	11	3	14.0	6.7	0.95
8	2	6.0	2.9	0.95	12	1	16.0	7.7	0.95
8	3	3.5	1.6	0.95	12	2	19.0	9.2	0.95
10	1	19.5	9.4	0.95	12	3	15.5	7.5	0.95
10	2	20.5	9.9	0.95	13	1	3.5	1.6	0.95
10	3	24.0	11.6	0.95	13	2	6.0	2.9	0.95
11	1	12.5	6.1	0.95	13	3	8.0	3.8	0.95
11	2	16.5	7.9	0.95	–	–	–	–	–

Table C.5: Installed generator power data.

Bus	Phase	P [kW]	Q [kVAr]	Bus	Phase	P [kW]	Q [kVAr]
8	2	10	0	11	2	10	0
10	1	20	0	12	1	15	0
10	2	20	0	13	3	21	0
10	3	35	0	–	–	–	–

Appendix D

Medium Voltage IEEE-13 Bus Distribution Network

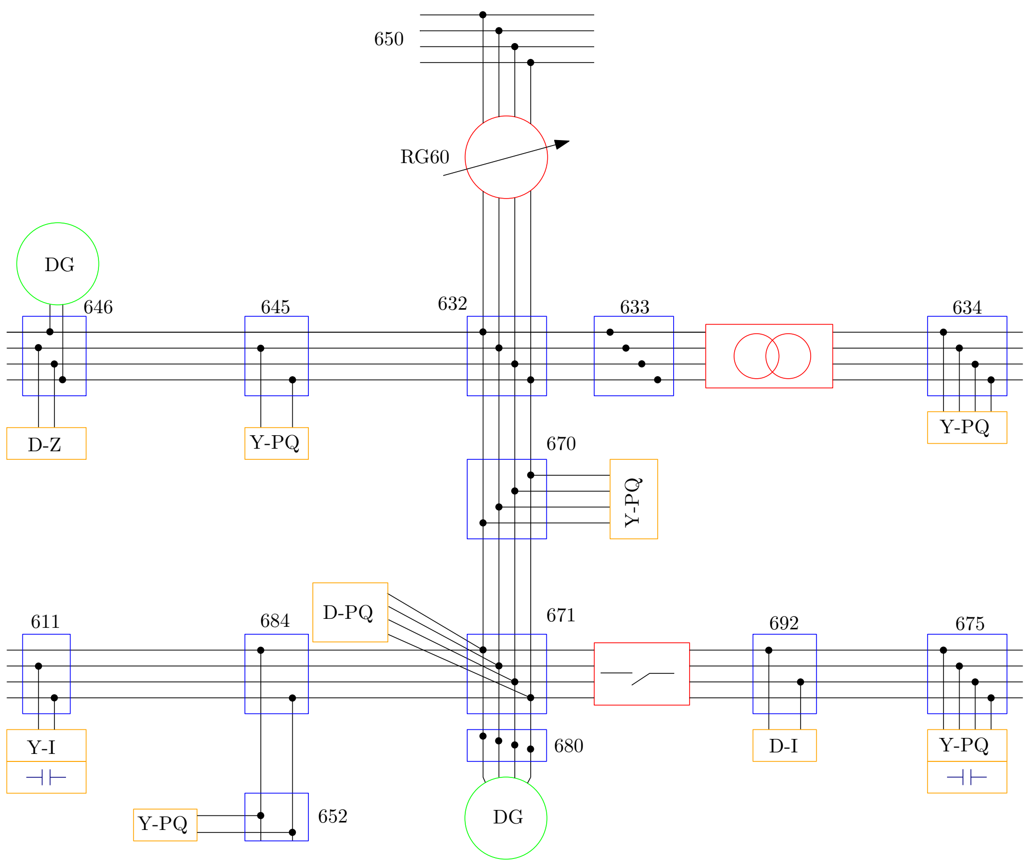

Figure D.1: Single line diagram of medium voltage IEEE-13 node distribution network.

Table D.1: Wire data.

Wire Type	d [mm]	GMR [mm]	Rc [Ω]	g [S]	Imax [A]
1	0.0235	0.8104	0.1155	0	730
2	0.0143	0.3470	0.3679	0	340
3	0.0101	0.2689	0.6959	0	230
4	0.0144	0.7238	0.2548	0	260
5	0.0016	18.196	0.7107	0	260
6	0.0093	0.7239	0.6027	0	310
7	0.0093	0.7259	0.3772	0	310
8	0.0000	0.0000	0.0000	0	500

Table D.2: Line configuration data.

Configuration	No. of Phases	Phase Cable Type	Neutral Cable Type	Type
1	3 [b-c-a-n]	1	2	OH
2	3 [c-a-b-n]	2	2	OH
3	2 [c-b-n]	3	3	OH
4	2 [c-a-n]	3	3	OH
5	1 [c-n]	3	3	OH
6	3 [a-b-c-n]	4	5	UG
7	1 [a-n]	6	7	UG
8	3	8	8	OH

Table D.3: Branches connection data.

From Bus	To Bus	Line Type	Length [km]	From Bus	To Bus	Line Type	Length [km]
1	2	1	0.6096	7	8	1	0.4572
2	3	2	0.1524	8	9	6	0.1524
3	4	1	0.1000	8	10	4	0.0914
2	5	3	0.1524	10	11	5	0.0914
5	6	3	0.0914	8	12	1	0.3048
2	7	1	0.1524	10	13	7	0.2438

Table D.4: Installed load power data.

Bus	Phase	P [kW]	Q [kVAr]	p.f.	Bus	Phase	P [kW]	Q [kVAr]	p.f.
634	1	160.0	110.0	-	675	2	68.0	-160.0	-
634	2	120.0	90.0	-	675	3	290.0	-8.0	-
634	3	120.0	90.0	-	611	3	170.0	-20.0	-
645	2	170.0	125.0	-	652	1	128.0	86.0	-
671	1	390.7	223.3	-	670	1	11.33	666.7	-
671	2	407.0	232.7	-	670	2	44.0	25.33	-
671	3	594.0	393.7	-	670	3	78.0	45.33	-
675	1	485.0	-30.0	-	646	2	230.0	132.0	-

Table D.5: Installed generator power data.

Bus	Phase	P [kW]	Q [kVAr]	Bus	Phase	P [kW]	Q [kVAr]
12	1	200.0	100.0	12	3	200.0	100.0
12	2	200.0	100.0	6	2	100.0	50.0

Appendix E

Low Voltage IT-37 Bus Distribution Network

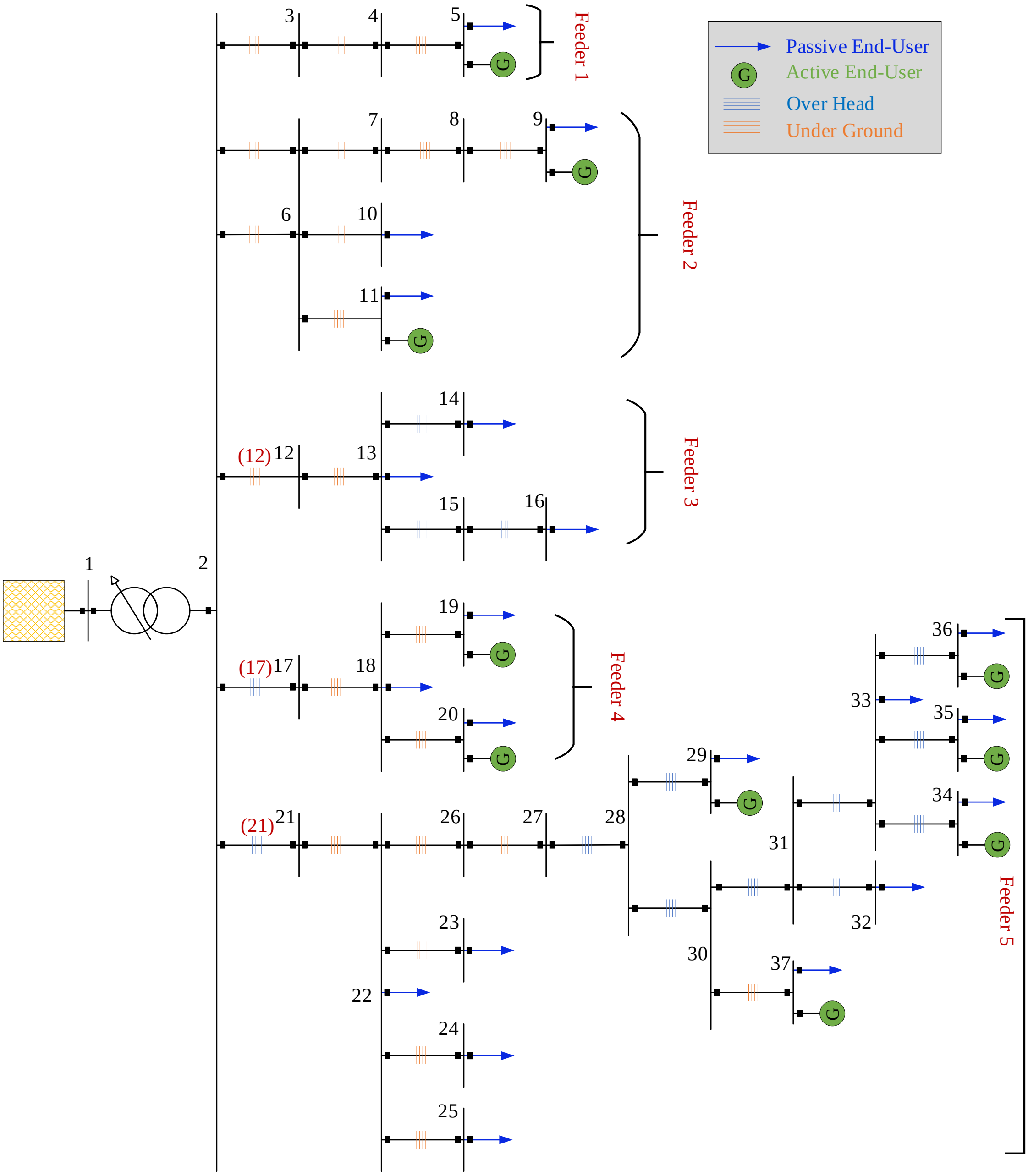

Figure E.1: Single line diagram of real low voltage IT-37 node distribution network.

Table E.1: Wire data.

Wire Type	**d** [mm]	**GMR** [mm]	**Rc** [Ω]	**g** [S]	**Imax** [A]
1	0.0055	0.78	0.734	0	166
2	0.0076	0.78	0.391	0	166
3	0.0035	0.78	1.840	0	55
4	0.0055	0.78	0.734	0	166
5	0.0076	0.78	0.390	0	166
6	0.0076	0.78	0.391	0	249
7	0.0108	0.78	0.195	0	249
8	0.0108	0.78	0.195	0	311
9	0.0133	0.78	0.127	0	311
10	0.0076	0.78	0.628	0	180
11	0.0090	0.78	0.443	0	180
12	0.0056	0.78	0.719	0	140
13	0.0027	0.78	3.060	0	53
14	0.0044	0.78	1.160	0	91
15	0.0055	0.78	0.734	0	166
16	0.0076	0.78	0.391	0	166
17	0.0044	0.78	1.140	0	105
18	0.0065	0.78	0.529	0	195
19	0.0106	0.78	0.320	0	195
20	0.0106	0.78	0.320	0	245
21	0.0132	0.78	0.206	0	245
22	0.0027	0.78	3.060	0	62
23	0.0043	0.78	1.910	0	65
24	0.0044	0.78	1.160	0	97
25	0.0055	0.78	1.200	0	97
26	0.0055	0.78	0.734	0	137
27	0.0075	0.78	0.641	0	137
28	0.0043	0.78	1.910	0	70
29	0.0043	0.78	1.910	0	65

Table E.2: Line configuration data.

Configuration	No. of Phases	PC Type	NC Type	Mutual Distance [m]		
				Type	x	y
1	3	2	1	UG	0.0081	0.0081
2	3	3	3	UG	0.0047	0.0047
3	3	5	4	UG	0.0131	0.0131
4	3	7	6	UG	0.0174	0.0174
5	3	9	8	UG	0.0203	0.0203
6	3	11	10	OH	0.0076	0.0153
7	3	12	12	OH	0.0052	0.0104
8	3	13	13	OH	0.0023	0.0046
9	3	14	14	OH	0.0028	0.0056
10	3	16	15	OH	0.0045	0.0091
11	3	17	17	OH	0.0045	0.0091
12	3	19	18	UG	0.0112	0.0112
13	3	21	20	UG	0.0201	0.0201
14	3	22	22	OH	0.0024	0.0048
15	3	23	23	OH	0.0037	0.0074
16	3	25	24	UG	0.0067	0.0068
17	3	27	26	UG	0.0079	0.0079
18	3	28	28	UG	0.0083	0.0083
19	3	29	29	UG	0.0074	0.0074

Table E.3: Branches connection data.

From Bus	To Bus	Line Type	Length [km]	From Bus	To Bus	Line Type	Length [km]
2	3	5	0.030	2	21	9	0.020
3	4	5	0.070	21	22	4	0.066
4	5	19	0.015	22	23	2	0.037
2	6	5	0.070	22	24	18	0.023
6	7	5	0.060	22	25	2	0.025
7	8	16	0.081	22	26	4	0.078
8	9	16	0.033	26	27	12	0.057
6	10	17	0.095	27	28	10	0.020
6	11	17	0.036	28	29	15	0.020
2	12	9	0.020	28	30	10	0.021
12	13	1	0.021	30	31	11	0.023
13	14	9	0.043	31	32	8	0.022
13	15	6	0.048	31	33	7	0.014
15	16	8	0.045	33	34	14	0.019
2	17	9	0.020	33	35	7	0.040
17	18	3	0.035	33	36	7	0.042
18	19	3	0.014	30	37	6	0.046
18	20	18	0.022	-	-	-	-

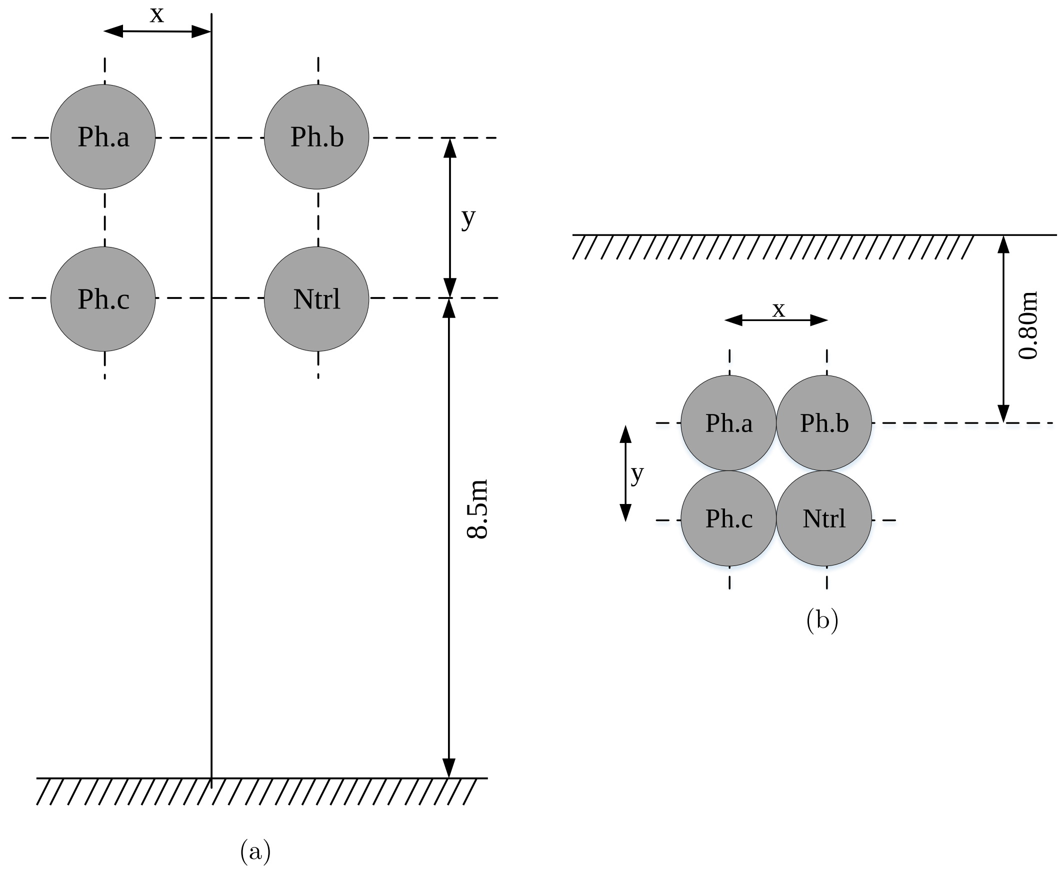

Figure E.2: Configuration of a 4-wire (a) overhead conductor and (b) underground cable.

Table E.4: Installed generator power data.

Bus	**Phase**	**P [W]**	**Q [VAr]**	**Bus**	**Phase**	**P [W]**	**Q [VAr]**
5	1	4.6	0	29	1	3.0	0
5	2	4.6	0	29	1	3.0	0
5	3	4.6	0	29	1	3.0	0
9	2	3.0	0	34	1	3.0	0
11	1	3.0	0	34	1	3.0	0
19	1	3.0	0	34	1	3.0	0
19	1	3.0	0	35	1	3.0	0
19	1	3.0	0	35	1	3.0	0
20	2	2.0	0	36	1	3.0	0
20	1	3.0	0	36	1	3.0	0
20	1	3.0	0	36	1	3.0	0
20	2	3.0	0	37	1	2.0	0
20	2	3.0	0	37	1	3.0	0

Table E.5: Installed load power data.

Bus	Phase	P [kW]	Q [kVar]	p.f.	Bus	Phase	P [kW]	Q [kVAr]	p.f.
5	1	3.33	0.68	0.95	14	3	3.00	1.45	0.95
5	2	3.33	0.68	0.95	14	3	3.00	1.45	0.95
5	3	3.33	0.68	0.95	14	3	2.00	0.97	0.95
9	1	2.00	0.97	0.95	14	3	3.00	1.45	0.95
9	2	2.00	0.97	0.95	18	2	3.00	1.45	0.95
9	3	2.00	0.97	0.95	18	2	2.00	0.97	0.95
9	1	4.50	2.18	0.95	18	2	1.00	0.48	0.95
9	2	3.00	1.45	0.95	18	2	2.00	0.97	0.95
10	1	4.50	2.18	0.95	18	2	3.00	1.45	0.95
10	2	4.50	2.18	0.95	18	3	3.00	1.45	0.95
10	3	4.50	2.18	0.95	18	3	1.00	0.48	0.95
10	2	4.50	2.18	0.95	18	3	1.00	0.48	0.95
11	1	3.33	1.61	0.95	18	3	2.00	0.97	0.95
11	2	3.33	1.61	0.95	18	3	1.00	0.48	0.95
11	3	3.33	1.61	0.95	18	3	1.00	0.48	0.95
11	1	3.00	1.45	0.95	18	3	2.00	0.97	0.95
11	2	3.00	1.45	0.95	19	1	3.00	1.45	0.95
11	3	3.00	1.45	0.95	19	1	3.00	1.45	0.95
13	1	2.00	0.97	0.95	19	1	2.00	0.97	0.95
13	1	3.00	1.45	0.95	19	2	3.00	1.45	0.95
13	1	3.00	1.45	0.95	19	2	3.00	1.45	0.95
13	1	3.00	1.45	0.95	19	2	3.00	1.45	0.95
13	1	2.00	0.97	0.95	19	2	3.00	1.45	0.95
13	2	3.00	1.45	0.95	19	3	3.00	1.45	0.95
13	2	3.00	1.45	0.95	19	3	1.00	0.48	0.95
13	3	3.00	1.45	0.95	19	3	1.00	0.48	0.95
13	3	3.00	1.45	0.95	19	3	2.00	0.97	0.95
13	3	3.00	1.45	0.95	19	3	3.00	1.45	0.95
16	1	2.00	0.97	0.95	20	1	3.00	1.45	0.95
16	1	3.00	1.45	0.95	20	1	3.00	1.45	0.95
16	1	3.00	1.45	0.95	20	1	3.00	1.45	0.95
16	1	3.00	1.45	0.95	20	1	1.00	0.48	0.95
16	2	3.00	1.45	0.95	20	1	2.00	0.97	0.95
16	3	3.00	1.45	0.95	20	1	3.00	1.45	0.95
16	3	3.00	1.45	0.95	20	2	2.00	0.97	0.95
14	1	3.00	1.45	0.95	20	2	3.00	1.45	0.95
14	1	3.00	1.45	0.95	20	2	3.00	1.45	0.95
14	1	3.00	1.45	0.95	20	2	1.50	0.73	0.95
14	1	3.00	1.45	0.95	20	2	1.00	0.48	0.95
14	2	3.00	1.45	0.95	20	2	3.00	1.45	0.95
14	2	2.00	0.97	0.95	20	2	3.00	1.45	0.95
14	2	3.00	1.45	0.95	20	2	3.00	1.45	0.95

20	2	3.00	1.45	0.95	32	2	1.00	0.48	0.95
20	2	2.00	0.97	0.95	32	2	2.00	0.97	0.95
20	2	1.00	0.48	0.95	32	2	1.00	0.48	0.95
20	3	1.50	0.73	0.95	32	2	3.00	1.45	0.95
20	3	3.00	1.45	0.95	32	3	2.00	0.97	0.95
20	3	1.00	0.48	0.95	32	3	3.00	1.45	0.95
20	3	3.00	1.45	0.95	34	1	3.00	1.45	0.95
20	3	1.00	0.48	0.95	34	1	3.00	1.45	0.95
20	3	1.00	0.48	0.95	34	1	2.00	0.97	0.95
20	3	1.00	0.48	0.95	34	1	2.00	0.97	0.95
20	3	1.00	0.48	0.95	34	1	1.00	0.48	0.95
20	3	1.00	0.48	0.95	34	2	3.00	1.45	0.95
20	3	1.00	0.48	0.95	34	2	3.00	1.45	0.95
20	3	1.00	0.48	0.95	34	2	3.00	1.45	0.95
22	1	3.00	1.45	0.95	34	2	2.00	0.97	0.95
22	1	2.00	0.97	0.95	34	2	1.00	0.48	0.95
22	1	3.00	1.45	0.95	34	2	2.00	0.97	0.95
22	2	3.00	1.45	0.95	34	3	2.00	0.97	0.95
22	2	3.00	1.45	0.95	35	1	3.00	1.45	0.95
22	2	1.50	0.73	0.95	35	1	3.00	1.45	0.95
22	2	3.00	1.45	0.95	35	1	2.00	0.97	0.95
22	2	2.00	0.97	0.95	35	1	2.00	0.97	0.95
23	1	3.00	1.45	0.95	35	1	1.00	0.48	0.95
23	1	2.00	0.97	0.95	35	2	3.00	1.45	0.95
23	1	3.00	1.45	0.95	35	2	3.00	1.45	0.95
23	2	3.00	1.45	0.95	35	2	3.00	1.45	0.95
24	3	3.00	1.45	0.95	35	2	2.00	0.97	0.95
25	1	3.00	1.45	0.95	35	2	1.00	0.48	0.95
25	1	3.00	1.45	0.95	35	2	2.00	0.97	0.95
25	1	2.00	0.97	0.95	35	3	2.00	0.97	0.95
25	2	2.00	0.97	0.95	36	1	2.00	0.97	0.95
25	2	3.00	1.45	0.95	36	1	2.00	0.97	0.95
25	3	3.00	1.45	0.95	36	1	3.00	1.45	0.95
29	1	3.00	1.45	0.95	37	1	2.00	0.97	0.95
29	1	3.00	1.45	0.95	37	1	1.00	0.48	0.95
29	1	3.00	1.45	0.95	37	1	1.00	0.48	0.95
29	2	1.00	0.48	0.95	37	1	1.00	0.48	0.95
29	2	1.00	0.48	0.95	37	1	1.00	0.48	0.95
29	2	1.00	0.48	0.95	37	2	3.00	1.45	0.95
29	2	2.00	0.97	0.95	37	2	3.00	1.45	0.95
29	3	2.00	0.97	0.95	37	2	3.00	1.45	0.95
29	3	1.00	0.48	0.95	37	2	3.00	1.45	0.95
32	1	3.00	1.45	0.95	37	2	2.00	0.97	0.95
32	1	3.00	1.45	0.95	37	2	2.00	0.97	0.95
32	1	3.00	1.45	0.95	37	2	3.00	1.45	0.95

Appendix F

Low Voltage IT-111 Bus Distribution Network

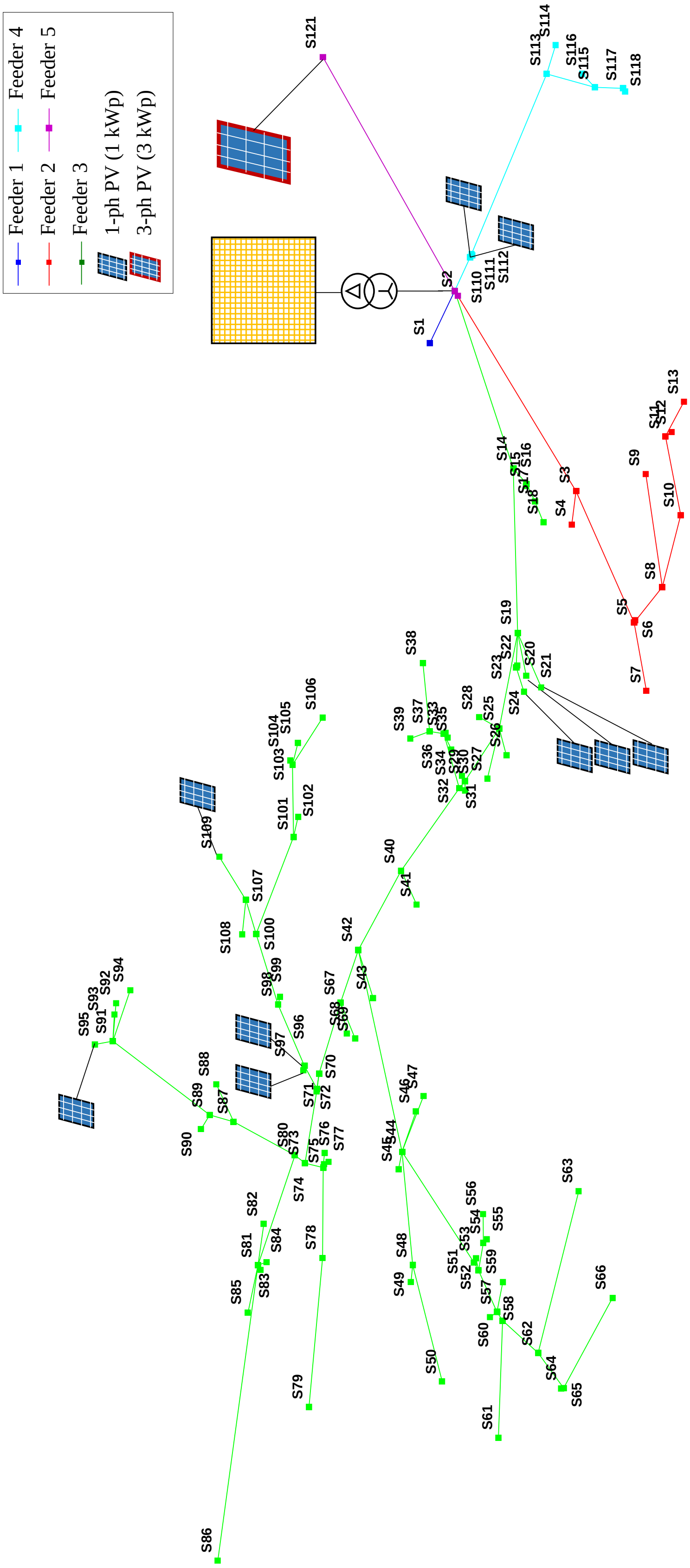

Figure F.1: Single line diagram of real low voltage IT-111 distribution network.

Table F.1: Wire data.

Wire Type	d [mm]	GMR [mm]	Rc [Ω]	g [S]	Imax [A]
1	0.003	0.7788	3.3	0	330
2	0.0052	0.7788	1.21	0	330
3	0.0063	0.7788	0.78	0	330
4	0.0094	0.7788	0.386	0	330
5	0.011	0.7788	0.272	0	330
6	0.0127	0.7788	0.206	0	330

Table F.2: Line configuration data.

Configuration	No. of Phases	PC Type	NC Type	Mutual Distance [m]		
				Type	x	y
1	3	1	1	UG	0.0030	0.0030
2	3	2	2	UG	0.0052	0.0052
3	3	3	3	UG	0.0063	0.0063
4	3	4	4	UG	0.0094	0.0094
5	3	4	3	UG	0.011	0.011
6	3	6	4	UG	0.0127	0.0127

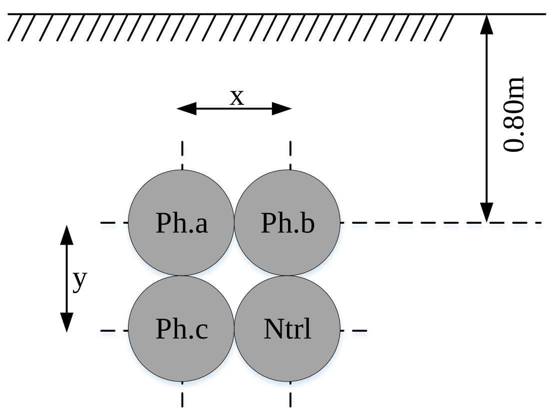

Figure F.2: Configuration of a 4-wire underground cable.

Table F.3: Branches connection data.

From Bus	To Bus	Line Type	Length [km]	From Bus	To Bus	Line Type	Length [km]
1	2	5	0.050	42	43	1	0.035
2	3	5	0.062	42	44	6	0.090
2	4	2	0.008	44	45	2	0.045
2	5	6	0.252	44	46	5	0.146
5	6	2	0.030	46	47	1	0.013
5	7	5	0.144	46	48	1	0.039
7	8	2	0.010	46	49	1	0.058
7	9	2	0.061	46	50	2	0.076
7	10	3	0.064	50	51	2	0.012
10	11	2	0.077	50	52	2	0.088
10	12	3	0.055	46	53	3	0.147
12	13	3	0.055	53	54	2	0.009
13	14	2	0.013	54	55	1	0.019
13	15	3	0.039	54	56	1	0.019
2	16	6	0.155	56	57	1	0.008
16	17	1	0.025	56	58	1	0.020
17	18	1	0.001	54	59	2	0.042
17	19	1	0.019	59	60	1	0.016
19	20	1	0.022	59	61	1	0.043
16	21	6	0.101	59	62	2	0.011
21	22	1	0.035	62	63	2	0.083
21	23	1	0.053	62	64	2	0.067
21	24	1	0.021	64	65	2	0.128
24	25	1	0.002	64	66	1	0.053
24	26	1	0.022	66	67	1	0.005
21	27	6	0.067	66	68	1	0.104
27	28	1	0.036	44	69	6	0.045
27	29	1	0.049	69	70	2	0.024
27	30	1	0.045	69	71	1	0.039
27	31	6	0.069	69	72	6	0.058
31	32	1	0.008	72	73	6	0.010
31	33	1	0.006	73	74	5	0.002
31	34	6	0.011	74	75	6	0.049
34	35	2	0.043	75	76	5	0.033
35	36	1	0.004	76	77	3	0.003
35	37	1	0.009	76	78	2	0.026
35	38	1	0.019	76	79	1	0.034
35	39	2	0.025	76	80	1	0.056
39	40	1	0.044	80	81	1	0.106
39	41	2	0.035	75	82	2	0.019
34	42	6	0.117	82	83	2	0.094

83	84	3	0.028	102	103	2	0.089
83	85	3	0.020	103	104	1	0.015
83	86	1	0.020	103	105	2	0.056
83	87	1	0.035	105	106	1	0.005
83	88	1	0.230	105	107	1	0.017
82	89	1	0.114	105	108	1	0.062
89	90	1	0.041	102	109	2	0.028
89	91	3	0.043	109	110	1	0.023
91	92	1	0.019	109	111	1	0.057
91	93	2	0.179	2	112	4	0.041
93	94	2	0.032	112	113	1	0.004
93	95	2	0.060	112	114	1	0.004
93	96	1	0.044	112	115	4	0.183
93	97	1	0.060	115	116	3	0.024
73	98	1	0.026	115	117	3	0.093
98	99	1	0.004	117	118	2	0.024
98	100	3	0.060	117	119	2	0.057
100	101	1	0.006	119	120	2	0.020
100	102	3	0.058	2	121	6	0.250

Table F.4: Installed load power data.

Bus	**Phase**	**P [kW]**	**Q [kVar]**	**p.f.**	**Bus**	**Phase**	**P [kW]**	**Q [kVAr]**	**p.f.**
3	1	0.33	0.16	0.90	20	3	1.00	0.48	0.90
3	2	0.33	0.16	0.90	20	2	1.00	0.48	0.90
3	3	0.33	0.16	0.90	22	1	1.00	0.48	0.90
4	1	0.67	0.32	0.90	23	1	1.00	0.48	0.90
4	2	0.67	0.32	0.90	23	3	1.00	0.48	0.90
4	3	0.67	0.32	0.90	25	2	1.00	0.48	0.90
6	1	1.00	0.48	0.90	25	3	1.00	0.48	0.90
6	2	1.00	0.48	0.90	26	2	1.00	0.48	0.90
6	3	1.00	0.48	0.90	28	2	2.00	0.97	0.90
8	1	1.00	0.48	0.90	29	3	1.00	0.48	0.90
9	2	1.00	0.48	0.90	30	1	1.00	0.48	0.90
9	3	1.00	0.48	0.90	33	2	1.00	0.48	0.90
11	3	1.00	0.48	0.90	36	3	1.00	0.48	0.90
14	1	0.33	0.16	0.90	37	2	1.00	0.48	0.90
14	2	0.33	0.16	0.90	38	1	1.00	0.48	0.90
14	3	0.33	0.16	0.90	40	2	1.00	0.48	0.90
15	1	0.33	0.16	0.90	40	3	1.00	0.48	0.90
15	2	0.33	0.16	0.90	41	1	1.00	0.48	0.90
15	3	0.33	0.16	0.90	43	3	1.00	0.48	0.90
18	3	1.00	0.48	0.90	45	1	1.00	0.48	0.90
20	1	1.00	0.48	0.90	47	3	1.00	0.48	0.90

47	2	1.00	0.48	0.90	90	2	1.00	0.48	0.90
48	1	1.00	0.48	0.90	92	1	1.00	0.48	0.90
49	1	1.00	0.48	0.90	94	1	1.00	0.48	0.90
51	1	1.00	0.48	0.90	95	1	1.00	0.48	0.90
52	2	1.00	0.48	0.90	96	1	1.00	0.48	0.90
55	2	1.00	0.48	0.90	97	3	1.00	0.48	0.90
57	3	1.00	0.48	0.90	99	3	1.00	0.48	0.90
58	1	1.00	0.48	0.90	101	2	1.00	0.48	0.90
60	1	1.00	0.48	0.90	104	1	1.00	0.48	0.90
61	1	1.00	0.48	0.90	106	3	1.00	0.48	0.90
63	1	1.00	0.48	0.90	107	2	1.00	0.48	0.90
65	1	1.00	0.48	0.90	108	3	1.00	0.48	0.90
67	3	1.00	0.48	0.90	110	3	1.00	0.48	0.90
68	2	1.00	0.48	0.90	111	1	0.33	0.16	0.90
70	2	1.00	0.48	0.90	111	2	0.33	0.16	0.90
77	1	1.00	0.48	0.90	111	3	0.33	0.16	0.90
78	3	1.00	0.48	0.90	113	1	1.00	0.48	0.90
79	3	1.00	0.48	0.90	114	1	1.00	0.48	0.90
81	1	1.00	0.48	0.90	116	1	0.33	0.16	0.90
84	3	1.00	0.48	0.90	116	2	0.33	0.16	0.90
85	3	2.00	0.97	0.90	116	3	0.33	0.16	0.90
86	1	1.00	0.48	0.90	120	1	0.33	0.16	0.90
87	3	1.00	0.48	0.90	120	2	0.33	0.16	0.90
88	2	1.00	0.48	0.90	120	3	0.33	0.16	0.90

Table F.5: Installed generator power data.

Bus	**Phase**	**P** [kW]	**Q** [kVAr]	**Bus**	**Phase**	**P** [kW]	**Q** [kVAr]
109	1	1.0	0	22	3	1.0	0
110	1	1.0	0	23	3	1.0	0
111	1	1.0	0	26	3	1.0	0
95	2	1.0	0	121	1	1.0	0
96	2	1.0	0	121	2	1.0	0
97	2	1.0	0	121	3	1.0	0

Appendix G

Real-Time Load and Generation Profiles

The various combinations of the below-mentioned profiles are used for all the loads connected in the above-mentioned distribution networks.

Table G.1: Weekly load and generation profiles coefficients [pu].

Day	COST	RES	IND	COM	PV
Mon	1	0.84645	0.870	0.693	0.636
Tue	1	0.8588	0.956	0.706	0.610
Wed	1	0.86355	0.989	0.731	0.631
Thu	1	0.86355	0.989	0.734	0.685
Fri	1	0.86165	0.972	0.719	0.716
Sat	1	0.83315	0.128	0.978	0.707
Sun	1	0.7619	0.111	0.361	0.637

Table G.2: Monthly load and generation profiles coefficients [pu].

Month	COST	RES	IND	COM	PV
Gen	1	0.633	0.559	0.968	0.124
Feb	1	0.629	0.589	0.993	0.359
Mar	1	0.548	0.792	0.695	0.495
Apr	1	0.539	0.696	0.585	0.484
May	1	0.513	0.651	0.547	0.670
Jun	1	0.508	0.68	0.546	1.000
Jul	1	0.504	0.683	0.54	0.717
Aug	1	0.501	0.661	0.525	0.629
Sep	1	0.52	0.675	0.565	0.607
Oct	1	0.588	0.768	0.65	0.354
Nov	1	0.627	0.579	1	0.119
Dec	1	0.633	0.553	0.952	0.123

Table G.3: Yearly load and generation profiles coefficients [pu].

Year	COST	RES	IND	COM	PV
2010	1	1.000	1.000	1.000	1.000
2011	1	1.020	1.010	1.030	1.000
2012	1	1.040	1.020	1.061	1.000
2013	1	1.061	1.030	1.093	1.000
2014	1	1.082	1.041	1.126	1.000
2015	1	1.104	1.051	1.159	1.000
2016	1	1.126	1.062	1.194	1.000
2017	1	1.149	1.072	1.230	1.000
2018	1	1.172	1.083	1.267	1.000
2019	1	1.195	1.094	1.305	1.000
2020	1	1.219	1.105	1.344	1.000
2021	1	1.243	1.116	1.384	1.000
2022	1	1.268	1.127	1.426	1.000
2023	1	1.294	1.138	1.469	1.000
2024	1	1.319	1.149	1.513	1.000
2025	1	1.346	1.161	1.558	1.000
2026	1	1.373	1.173	1.605	1.000
2027	1	1.400	1.184	1.653	1.000
2028	1	1.428	1.196	1.702	1.000
2029	1	1.457	1.208	1.754	1.000
2030	1	1.486	1.220	1.806	1.000

COST = Constant RES = Residential IND = Industrial COM =Commercial PV = Photo-Voltaic

Table G.4: Real load and generation profiles coefficients [pu].

Date	Time	Dom1	Dom2	Dom3	Dom4	Dom5	Dom6	NDom1	NDom2
1/1/2012	12:00:00 AM	0.924	0.245	0.297	0.608	0.617	0.595	0.202	0.354
1/1/2012	12:15:00 AM	0.924	0.245	0.297	0.608	0.617	0.595	0.202	0.354
1/1/2012	12:30:00 AM	0.892	0.324	0.375	0.620	0.637	0.441	0.176	0.354
1/1/2012	12:45:00 AM	0.937	0.417	0.417	0.619	0.780	0.289	0.189	0.353
1/1/2012	1:00:00 AM	0.807	0.563	0.425	0.597	0.913	0.117	0.191	0.354
1/1/2012	1:15:00 AM	0.288	0.552	0.376	0.551	0.917	0.492	0.177	0.353
1/1/2012	1:30:00 AM	0.737	0.439	0.391	0.579	0.869	0.547	0.178	0.353
1/1/2012	1:45:00 AM	0.713	0.552	0.403	0.520	0.919	0.479	0.175	0.353
1/1/2012	2:00:00 AM	0.415	0.577	0.407	0.523	0.941	0.537	0.213	0.353
1/1/2012	2:15:00 AM	0.287	0.532	0.436	0.525	0.900	0.119	0.208	0.353
1/1/2012	2:30:00 AM	0.279	0.360	0.417	0.581	0.607	0.545	0.188	0.353
1/1/2012	2:45:00 AM	0.445	0.368	0.413	0.508	0.565	0.331	0.215	0.353

1/1/2012	3:00:00 AM	0.320	0.195	0.347	0.495	0.448	0.371	0.155	0.354
1/1/2012	3:15:00 AM	0.271	0.320	0.273	0.479	0.645	0.367	0.203	0.353
1/1/2012	3:30:00 AM	0.293	0.065	0.271	0.476	0.477	0.647	0.187	0.353
1/1/2012	3:45:00 AM	0.269	0.015	0.284	0.473	0.473	0.765	0.191	0.354
1/1/2012	4:00:00 AM	0.543	0.245	0.293	0.472	0.484	0.355	0.187	0.353
1/1/2012	4:15:00 AM	0.281	0.053	0.303	0.485	0.471	0.516	0.186	0.354
1/1/2012	4:30:00 AM	0.271	0.017	0.317	0.480	0.455	0.375	0.202	0.353
1/1/2012	4:45:00 AM	0.303	0.195	0.349	0.480	0.560	0.333	0.160	0.353
1/1/2012	5:00:00 AM	0.271	0.015	0.329	0.505	0.728	0.341	0.203	0.353
1/1/2012	5:15:00 AM	0.349	0.013	0.269	0.563	0.716	0.472	0.189	0.353
1/1/2012	5:30:00 AM	0.541	0.145	0.272	0.576	0.601	0.339	0.185	0.353
1/1/2012	5:45:00 AM	0.265	0.127	0.265	0.572	0.397	0.315	0.182	0.353
1/1/2012	6:00:00 AM	0.283	0.020	0.297	0.569	0.392	0.404	0.203	0.353
1/1/2012	6:15:00 AM	0.291	0.015	0.319	0.263	0.352	0.437	0.216	0.353
1/1/2012	6:30:00 AM	0.269	0.207	0.339	0.179	0.547	0.403	0.216	0.353
1/1/2012	6:45:00 AM	0.284	0.013	0.336	0.171	0.389	0.361	0.229	0.353
1/1/2012	7:00:00 AM	0.295	0.047	0.287	0.160	0.380	0.461	0.201	0.353
1/1/2012	7:15:00 AM	0.477	0.053	0.259	0.105	0.408	0.337	0.185	0.353
1/1/2012	7:30:00 AM	0.287	0.188	0.253	0.103	0.387	0.327	0.177	0.353
1/1/2012	7:45:00 AM	0.272	0.015	0.231	0.105	0.360	0.477	0.190	0.353
1/1/2012	8:00:00 AM	0.533	0.015	0.233	0.101	0.380	0.333	0.203	0.354
1/1/2012	8:15:00 AM	0.739	0.015	0.240	0.103	0.388	0.347	0.170	0.353
1/1/2012	8:30:00 AM	0.651	0.237	0.299	0.160	0.363	0.603	0.199	0.353
1/1/2012	8:45:00 AM	0.275	0.064	0.260	0.104	0.407	0.819	0.170	0.353
1/1/2012	9:00:00 AM	0.047	0.041	0.231	0.101	0.573	0.639	0.187	0.353
1/1/2012	9:15:00 AM	0.205	0.025	0.253	0.115	0.181	0.368	0.203	0.353
1/1/2012	9:30:00 AM	0.520	0.027	0.333	0.144	0.025	0.451	0.179	0.353
1/1/2012	9:45:00 AM	0.513	0.301	0.343	0.105	0.047	0.325	0.181	0.353
1/1/2012	10:00:00 AM	0.512	0.188	0.317	0.369	0.181	0.332	0.178	0.353
1/1/2012	10:15:00 AM	0.544	0.549	0.328	0.136	0.037	0.352	0.210	0.354
1/1/2012	10:30:00 AM	0.368	0.508	0.425	0.285	0.148	0.440	0.177	0.353
1/1/2012	10:45:00 AM	0.067	0.467	0.563	0.163	0.507	0.349	0.219	0.353
1/1/2012	11:00:00 AM	0.068	0.472	0.549	0.156	0.425	0.331	0.187	0.353
1/1/2012	11:15:00 AM	0.052	0.568	0.648	0.164	0.737	0.368	0.191	0.353
1/1/2012	11:30:00 AM	0.103	0.572	0.704	0.661	0.048	0.613	0.186	0.353
1/1/2012	11:45:00 AM	0.620	0.596	0.608	0.989	0.327	0.628	0.447	0.353
1/1/2012	12:00:00 PM	0.745	0.960	0.691	0.592	0.727	0.971	0.586	0.353
1/1/2012	12:15:00 PM	0.527	0.829	0.792	0.792	0.431	0.907	0.534	0.353
1/1/2012	12:30:00 PM	0.283	0.724	0.755	0.764	0.439	0.855	0.957	0.353
1/1/2012	12:45:00 PM	0.289	0.653	0.740	0.605	0.412	0.863	0.754	0.353

1/1/2012	1:00:00 PM	0.273	0.731	0.700	0.743	0.639	0.761	0.585	0.353
1/1/2012	1:15:00 PM	0.297	0.701	0.621	0.956	0.792	0.485	0.675	0.353
1/1/2012	1:30:00 PM	0.275	0.551	0.491	0.905	0.481	0.371	0.599	0.353
1/1/2012	1:45:00 PM	0.300	0.524	0.551	0.712	0.481	0.480	0.537	0.353
1/1/2012	2:00:00 PM	0.316	0.172	0.519	0.712	0.521	0.385	0.734	0.353
1/1/2012	2:15:00 PM	0.299	0.207	0.872	0.308	0.516	0.496	0.699	0.353
1/1/2012	2:30:00 PM	0.303	0.224	0.968	0.295	0.508	0.437	0.755	0.353
1/1/2012	2:45:00 PM	0.276	0.212	0.764	0.604	0.496	0.496	0.647	0.353
1/1/2012	3:00:00 PM	0.275	0.212	0.433	0.489	0.496	0.128	0.558	0.353
1/1/2012	3:15:00 PM	0.297	0.219	0.451	0.664	0.852	0.501	0.621	0.353
1/1/2012	3:30:00 PM	0.275	0.635	0.421	0.587	0.541	0.567	0.620	0.354
1/1/2012	3:45:00 PM	0.283	0.625	0.409	0.533	0.580	0.563	0.464	0.353
1/1/2012	4:00:00 PM	0.279	0.633	0.459	0.601	0.377	0.559	0.480	0.353
1/1/2012	4:15:00 PM	0.264	0.660	0.459	0.511	0.359	0.576	0.372	0.353
1/1/2012	4:30:00 PM	0.303	0.624	0.405	0.541	0.333	0.609	0.390	0.353
1/1/2012	4:45:00 PM	0.315	0.592	0.408	0.553	0.348	0.640	0.395	0.353
1/1/2012	5:00:00 PM	0.315	0.631	0.469	0.521	0.396	0.555	0.369	0.353
1/1/2012	5:15:00 PM	0.333	0.644	0.456	0.608	0.488	0.680	0.422	0.353
1/1/2012	5:30:00 PM	0.304	0.671	0.457	0.647	0.384	0.521	0.365	0.353
1/1/2012	5:45:00 PM	0.336	0.649	0.495	0.632	0.460	0.440	0.388	0.353
1/1/2012	6:00:00 PM	0.341	0.708	0.519	0.681	0.417	0.603	0.428	0.353
1/1/2012	6:15:00 PM	0.567	0.731	0.488	0.668	0.405	0.444	0.409	0.353
1/1/2012	6:30:00 PM	0.773	0.603	0.496	0.577	0.431	0.417	0.385	0.353
1/1/2012	6:45:00 PM	0.728	0.583	0.532	0.580	0.457	0.644	0.379	0.353
1/1/2012	7:00:00 PM	0.775	0.588	0.561	0.440	0.543	0.719	0.448	0.353
1/1/2012	7:15:00 PM	0.747	0.604	0.565	0.117	0.496	0.472	0.551	0.353
1/1/2012	7:30:00 PM	0.716	0.629	0.579	0.113	0.501	0.835	0.617	0.353
1/1/2012	7:45:00 PM	0.735	0.312	0.572	0.113	0.461	0.624	0.487	0.353
1/1/2012	8:00:00 PM	0.636	0.225	0.553	0.112	0.475	0.527	0.693	0.353
1/1/2012	8:15:00 PM	0.509	0.672	0.517	0.509	0.477	0.561	0.530	0.353
1/1/2012	8:30:00 PM	0.512	0.671	0.493	0.576	0.472	0.417	0.603	0.353
1/1/2012	8:45:00 PM	0.487	0.668	0.648	0.205	0.471	0.183	0.666	0.353
1/1/2012	9:00:00 PM	0.523	0.248	0.687	0.177	0.652	0.316	0.515	0.353
1/1/2012	9:15:00 PM	0.495	0.587	0.660	0.416	0.755	0.425	0.612	0.353
1/1/2012	9:30:00 PM	0.512	0.592	0.720	0.356	0.557	0.632	0.598	0.353
1/1/2012	9:45:00 PM	0.495	0.635	0.824	0.307	0.820	0.631	0.564	0.353
1/1/2012	10:00:00 PM	0.488	0.604	0.633	0.328	0.564	0.180	0.543	0.353
1/1/2012	10:15:00 PM	0.307	0.772	0.452	0.316	0.691	0.525	0.596	0.354
1/1/2012	10:30:00 PM	0.032	0.592	0.421	0.272	0.705	0.335	0.585	0.353
1/1/2012	10:45:00 PM	0.035	0.301	0.408	0.263	0.643	0.247	0.431	0.354

1/1/2012	11:00:00 PM	0.269	0.576	0.371	0.248	0.461	0.139	0.441	0.354
1/1/2012	11:15:00 PM	0.273	0.496	0.972	0.224	0.403	0.140	0.392	0.353
1/1/2012	11:30:00 PM	0.427	0.479	0.512	0.184	0.412	0.284	0.408	0.354
1/1/2012	11:45:00 PM	0.721	0.487	0.388	0.164	0.424	0.687	0.221	0.354
2/1/2012	12:00:00 AM	0.269	0.272	0.337	0.160	0.421	0.916	0.180	0.354

Dom = Domestic NDom = Non-Domestic

Bibliography

[1] "Status of power system transformation: System integration and local grids", International Energy Agency, Tech. Report, 2017. [Online]. Available: `https://www.iea.org/publications/freepublications/publication/StatusofPowerSystem-Transformation2017.pdf`.

[2] I. E. Agency, "Re-powering markets: Market design and regulation during the transition to low-carbon power systems", 2016. [Online]. Available: `https://webstore.iea.org/re-powering-markets`.

[3] M. Shah, J. M. Valenzuela, H. A. B. Mora, K. Moller Porst, A. Hasselager, S. Friis-Jensen, M. Vingaard, F. Wigand, S. Tiedemann, L. Bird, *et al.*, "Clean restructuring: Design elements for low-carbon wholesale markets and beyond. a 21st century power partnership thought leadership report", National Renewable Energy Lab.(NREL), Golden, CO (United States), Tech. Rep., 2016.

[4] O. Zinaman, M. Miller, A. Adil, D. Arent, J. Cochran, R. Vora, S. Aggarwal, M. Bipath, C. Linvill, A. David, *et al.*, "Power systems of the future", *The Electricity Journal*, vol. 28, no. 2, pp. 113–126, 2015.

[5] "Getting wind and sun onto the grid: A manual for policy makers", International Energy Agency. [Online]. Available: `https://webstore.iea.org/insights-series-2017-getting-wind-and-solar-onto-the-grid`.

[6] "Public-private partnership stories: India: Gujarat solar", International Finance Corporation, Washington, DC, Tech. Report, [Online]. Available: `https://www.ifc.org/wps/wcm/connect/bd4127f7-9597-440d-ae46-c012e0009973/PPPStories_India_VadodaraSolar.pdf?MOD=AJPERES&CVID=lHIiD6z`.

[7] "Next generation wind and solar power", International Energy Agency. [Online]. Available: `https://webstore.iea.org/next-generation-wind-and-solar-power`.

[8] B. O.Neill and I. Chernyakhovskiy, "Designing wind and solar power purchase agreements to support grid integration", Jul. 2016. DOI: `10.2172/1262663`.

[9] I. E. Agency, *Development Prospects of the ASEAN Power Sector*. 2015, p. 80. DOI: `https://doi.org/10.1787/9789264247529-en`.

[10] N. Rai, T. Walters, S. Esterly, S. Cox, M. Muzammil, T. Mahmood, L. T. Nanki Kaur, S. Mamuye, J. Knuckles, E. Morris, *et al.*, "Policies to spur energy access: Volume 2: Case studies of public-private models to finance decentralized electricity access", *Golden, CO: National Renewable Energy Laboratory*, 2015.

[11] "Energy technology perspectives 2016 - towards sustainable urban energy systems", International Energy Agency, Tech. Report, [Online]. Available: `https://www.iea.org/etp2016/`.

[12] C. Ö. Bo Normark Power Circle and S. A. Susanne Ackeby, *Spotlight on smart and strong power and T&D infrastructure*.

[13] "Global ev outloo", International Energy Agency, Tech. Report, 2017. [Online]. Available: `https://webstore.iea.org/global-ev-outlook-2017`.

[14] I. Pvps, "Task 14: Transition from uni-directional to bi-directional distribution grids", International Energy Agency, Tech. Report, 2014. [Online]. Available: `http://www.iea-pvps.org/index.php?id=294`.

[15] "Tracking clean energy progress", International Energy Agency, Tech. Report, 2015. [Online]. Available: `https://www.iea.org/tcep/`.

[16] A. Gaul, S. Ubermasser, S. Rapoport, P. Almeida, C. Madina, C. Silvestri, G. Coppola, S. Bocker, R. Rodriguez, L. Silvestre, E. Zabala, S. Greve, S. Leyder, D. Feismann, and G. Odena, "Plangridev - distribution grid planning and operational principles for electric vehicle mass roll-out while enabling integration of renewable distributed energy resources", Feb. 2016. DOI: `10.13140/RG.2.1.4482.5365`.

[17] E. Carpaneto, G. Chicco, and J. S. Akilimali, "Loss partitioning and loss allocation in three-phase radial distribution systems with distributed generation", *IEEE Transactions on Power Systems*, vol. 23, no. 3, pp. 1039–1049, 2008.

[18] S. Mirhassani, H. C. Ong, W. T. Chong, and K. Y. Leong, "Advances and challenges in grid tied photovoltaic systems", *Renewable and Sustainable Energy Reviews*, vol. 49, pp. 121–131, 2015, ISSN: 18790690. DOI: `10.1016/j.rser.2015.04.064`.

[19] M. Karimi, H. Mokhlis, K. Naidu, S. Uddin, and A. H. A. Bakar, "Photovoltaic penetration issues and impacts in distribution network - A review", *Renewable and Sustainable Energy Reviews*, vol. 53, pp. 594–605, 2016, ISSN: 18790690. DOI: `10.1016/j.rser.2015.08.042`.

[20] M. M. Haque and P. Wolfs, "A review of high PV penetrations in LV distribution networks: Present status, impacts and mitigation measures", *Renewable and Sustainable Energy Reviews*, vol. 62, pp. 1195–1208, 2016, ISSN: 18790690. DOI: `10.1016/j.rser.2016.04.025`.

[21] W. H. Kersting, *Distribution System Modeling and Analysis*, 2nd. CRC Press, 2007, ISBN: 0849308127.

[22] D. J. Wilcox, "Theory of transformer modelling using modal analysis", *IEE Proceedings C - Generation, Transmission and Distribution*, vol. 138, no. 2, pp. 121–128, 1991, ISSN: 0143-7046. DOI: `10.1049/ip-c.1991.0015`.

[23] D. J. Wilcox, W. G. Hurley, T. P. McHale, and M. Conlon, "Application of modified modal theory in the modelling of practical transformers", *IEE Proceedings C - Generation, Transmission and Distribution*, vol. 139, no. 6, pp. 513–520, 1992, ISSN: 01437046. DOI: `10.1049/ip-c.1992.0071`.

[24] T. H. Chen, M. S. Chen, T. Inoue, P. Kotas, and E. A. Chebli, "Three-phase cogenerator and transformer models for distribution system analysis", *IEEE Transactions on Power Delivery*, vol. 6, no. 4, pp. 1671–1681, 1991, ISSN: 19374208. DOI: `10.1109/61.97706`.

[25] M. J. Gorman and J. J. Grainger, "Transformer modelling for distribution system studies–I: Linear modelling basics", *IEEE Transactions on Power Delivery*, vol. 7, no. 2, pp. 567–574, 1992. DOI: `10.1109/61.127050`.

[26] T.-H. Chen and J.-D. Chang, "Open wye-open delta and open delta-open delta transformer models for rigorous distribution system analysis", *IEE Proceedings C - Generation, Transmission and Distribution*, vol. 139, no. 3, pp. 227–234, 1992, ISSN: 01437046. DOI: `10.1049/ip-c.1992.0035`.

[27] M. Shin, C. Park, J. Jung, K. Kim, and S. So, "Nodal Admittance Modeling of Three-phase Step-Voltage Regulators and their Applications", in *International Conference on Electrical Machines and Systems (ICEMS)*, 2013, pp. 362–367, ISBN: 9781479914470. DOI: `10.1109/ICEMS.2013.6754440`.

[28] I. Kocar and J. S. Lacroix, "Implementation of a modified augmented nodal analysis based transformer model into the backward forward sweep solver", *IEEE Transactions on Power Systems*, vol. 27, no. 2, pp. 663–670, 2012, ISSN: 08858950. DOI: `10.1109/TPWRS.2011.2175256`.

[29] R. D. Youssef, "Phase-shifting transformers in load flow and short-circuit analysis: modelling and control", *IEE Proceedings C - Generation, Transmission and Distribution*, vol. 140, no. 4, pp. 331–336, 1993, ISSN: 0143-7046. DOI: 10.1049/ip-c.1993.0049.

[30] I. Dzafic, R. A. Jabr, and H. T. Neisius, "Transformer Modeling for Three-Phase Distribution Network Analysis", *IEEE Transactions on Power Systems*, vol. 30, no. 5, pp. 2604–2611, 2015, ISSN: 08858950. DOI: 10.1109/TPWRS.2014.2360812.

[31] M. Persson, W. Baig, and T. Thiringer, "Measurements and modelling of three- and five-limb transformer behaviour during large voltage and frequency disturbances", *IET Generation, Transmission & Distribution*, vol. 10, no. 2, pp. 334–340, 2016, ISSN: 1751-8687. DOI: 10.1049/iet-gtd.2015.0194.

[32] M. Coppo, F. Bignucolo, and R. Turri, "Generalised transformer modelling for power flow calculation in multi-phase unbalanced networks", *IET Generation, Transmission and Distribution*, vol. 11, no. 15, pp. 3843–3852, 2017, ISSN: 17518687. DOI: 10.1049/iet-gtd.2016.2080.

[33] J. G. Vlachogiannis, "An accurate autotransformer model for load flow studies effect on the steady-state analysis of the Hellenic transmission system", *Electric Power Systems Research*, vol. 50, no. 2, pp. 147–153, 1999, ISSN: 03787796. DOI: 10.1016/S0378-7796(99)00009-7.

[34] L. Gallego and A. Padilha-Feltrin, "Voltage regulator modeling for the three-phase power flow in distribution networks", in *Transmission and Distribution Conference and Exposition: Latin America (T&D-LA)*, 2008, pp. 1–6, ISBN: 978-1-4244-2217-3. DOI: 10.1109/TDC-LA.2008.4641843.

[35] D. Filipovic-Grcic, B. Filipovic-Grcic, and K. Capuder, "Modeling of three-phase autotransformer for short-circuit studies", *International Journal of Electrical Power and Energy Systems*, vol. 56, pp. 228–234, 2014, ISSN: 01420615. DOI: 10.1016/j.ijepes.2013.11.005.

[36] T. H. Chen and Y. L. Chang, "Integrated models of distribution transformers and their loads for three-phase power flow analyses", *IEEE Transactions on Power Delivery*, vol. 11, no. 1, pp. 507–513, 1996, ISSN: 08858977. DOI: 10.1109/61.484135.

[37] C. A. Ferreira and R. B. Prada, "Improved model for tap-changing transformer", *IET Generation, Transmission and Distribution*, vol. 7, no. 11, pp. 1289–1295, 2013, ISSN: 17518687. DOI: 10.1049/iet-gtd.2012.0466.

[38] N. D. Hatziargyriou, J. M. Prousalidis, and B. C. Papadias, "Generalised transformer model based on the analysis of its magnetic core circuit", *IEE Proceedings C - Generation, Transmission and Distribution*, vol. 140, no. 4, pp. 269–278, 1993, ISSN: 01437046. DOI: 10.1049/ip-c.1993.0040.

[39] M. Elleuch and M. Poloujadoff, "New transformer model including joint air gaps and lamination anisotropy", *IEEE Transactions on Magnetics*, vol. 34, no. 5, pp. 3701–3711, 1998, ISSN: 00189464. DOI: 10.1109/20.718532.

[40] W. Chandrasena, P. G. McLaren, U. D. Annakkage, and R. P. Jayasinghe, "An improved low-frequency transformer model for use in GIC studies", *IEEE Transactions on Power Delivery*, vol. 19, no. 2, pp. 643–651, 2004, ISSN: 08858977. DOI: 10.1109/TPWRD.2004.824429.

[41] M. Zou, W. Sima, M. Yang, L. Li, Q. Yang, and P. Sun, "Improved low-frequency transformer model based on Jiles–Atherton hysteresis theory", *IET Generation, Transmission & Distribution*, vol. 11, no. 4, pp. 915–923, 2017, ISSN: 1751-8687. DOI: 10.1049/iet-gtd.2016.0866.

[42] S. Liu, Z. Liu, and O. A. Mohammed, "FE-based modeling of single-phase distribution transformers with winding short circuit faults", *IEEE Transactions on Magnetics*, vol. 43, no. 4, pp. 1841–1844, 2007, ISSN: 00189464. DOI: 10.1109/TMAG.2006.892302.

[43] T. Noda, H. Nakamoto, and S. Yokoyama, "Accurate modeling of core-type distribution transformers for electromagnetic transient studies", *IEEE Transactions on Power Delivery*, vol. 17, no. 4, pp. 969–976, 2002, ISSN: 08858977. DOI: 10.1109/TPWRD.2002.803700.

[44] IEEE Task Force on Load Representation for Dynamic Performance, "Standard Load Models for Power Flow and Dynamic Performance Simulation", *IEEE Transactions on Power Systems*, vol. 10, no. 3, pp. 1302–1313, 1995, ISSN: 08858950. DOI: 10.1109/59.466523.

[45] ——, "Load representation for dynamic performance analysis (of power systems)", *IEEE Transactions on Power Systems*, vol. 8, no. 2, pp. 472–482, 1993, ISSN: 08858950. DOI: 10.1109/59.260837.

[46] ——, "Bibliography on Load Models for Power Flow and Dynamic Performance Simulation", *IEEE Transactions on Power Systems*, vol. 10, no. 1, pp. 523–538, 1995. DOI: 10.1109/59.373979.

[47] CIGRE WG C4.605, "Modelling and aggregation of loads in flexible power networks", Tech. Rep., 2013.

[48] K. Yamashita, S. Djokic, J. Matevosyan, F. O. Resende, L. M. Korunovic, Z. Y. Dong, and J. V. Milanovic, "Modelling and aggregation of loads in flexible power networks - Scope and status of the work of cigre WG C4.605", *IFAC Proceedings Volumes*, vol. 45, no. 21, pp. 405–410, 2012, ISSN: 14746670. DOI: 10.3182/20120902-4-FR-2032.00072.

[49] J. V. Milanovic, K. Yamashita, S. Martinez Villanueva, S. Ž. Djokic, and L. M. Korunovic, "International industry practice on power system load modeling", *IEEE Transactions on Power Systems*, vol. 28, no. 3, pp. 3038–3046, 2013, ISSN: 08858950. DOI: 10.1109/TPWRS.2012.2231969.

[50] J. V. Paatero and P. D. Lund, "A model for generating household electricity load profiles", *International Journal of Energy Research*, vol. 30, no. 5, pp. 273–290, 2006, ISSN: 0363907X. DOI: 10.1002/er.1136.

[51] J. Widen and E. Wäckelgaard, "A high-resolution stochastic model of domestic activity patterns and electricity demand", *Applied Energy*, vol. 87, no. 6, pp. 1880–1892, 2010, ISSN: 03062619. DOI: 10.1016/j.apenergy.2009.11.006.

[52] M. Muratori, M. C. Roberts, R. Sioshansi, V. Marano, and G. Rizzoni, "A highly resolved modeling technique to simulate residential power demand", *Applied Energy*, vol. 107, pp. 465–473, 2013, ISSN: 03062619. DOI: 10.1016/j.apenergy.2013.02.057.

[53] L. Rodriguez-Garcia, S. Perez-Londono, and J. Mora-Florez, "A methodology for composite load modeling in power systems considering distributed generation", in *6th IEEE/PES Transmission and Distribution Conference and Exposition: Latin America (T&D-LA)*, 2012, pp. 1–7, ISBN: 978-1-4673-2673-5. DOI: 10.1109/TDC-LA.2012.6319122.

[54] A. Savio, F. Bignucolo, R. Sgarbossa, P. Mattavelli, A. Cerretti, and R. Turri, "A novel measurement-based procedure for load dynamic equivalent identification", in *1st International Forum on Research and Technologies for Society and Industry (RTSI)*, 2015, pp. 274–279, ISBN: 9781467381666. DOI: 10.1109/RTSI.2015.7325110.

[55] J. V. Milanovic and S. Mat Zali, "Validation of equivalent dynamic model of active distribution network cell", *IEEE Transactions on Power Systems*, vol. 28, no. 3, pp. 2101–2110, 2013, ISSN: 08858950. DOI: 10.1109/TPWRS.2012.2227844.

[56] T. A. Papadopoulos, G. A. Barzegkar-Ntovom, V. C. Nikolaidis, P. N. Papadopoulos, and G. M. Burt, "Online parameter identification and generic modeling derivation of a dynamic load model in distribution grids", in *IEEE PowerTech, Manchester*, 2017, pp. 1–6. DOI: 10.1109/PTC.2017.7980994.

[57] D. Karlsson and D. J.Hill, "Modelling and identification of nonlinear dynamic loads in power systems", *IEEE Transactions on Power Systems*, vol. 9, no. 1, pp. 157–166, 1994, ISSN: 08858950. DOI: 10.1109/59.317546.

[58] E. O. Kontis, A. I. Chrysochos, G. K. Papagiannis, and T. A. Papadopoulos, "Development of measurement-based generic load models for dynamic simulations", in *IEEE PowerTech, Eindhoven*, 2015, pp. 1–6, ISBN: 9781479976935. DOI: 10.1109/PTC.2015.7232800.

[59] K. S. Metallinos, T. A. Papadopoulos, and C. A. Charalambous, "Derivation and evaluation of generic measurement-based dynamic load models", *Electric Power Systems Research*, vol. 140, pp. 193–200, 2016, ISSN: 03787796. DOI: 10.1016/j.epsr.2016.06.022.

[60] M. G. Jahromi, S. D. Mitchell, G. Mirzaeva, and D. Gay, "A new method for power system load modeling using a nonlinear system identification estimator", in *Industry Applications Society Annual Meeting*, 2015, pp. 1–8. DOI: 10.1109/IAS.2015.7356902.

[61] G. Giasemidis, S. Haben, T. Lee, C. Singleton, and P. Grindrod, "A genetic algorithm approach for modelling low voltage network demands", *Applied Energy*, vol. 203, pp. 463–473, 2017, ISSN: 03062619. DOI: 10.1016/j.apenergy.2017.06.057.

[62] Z. Fikri, "Statistical load analysis for distribution network planning", PhD thesis, Royal Institute Technology, Stockholm, Sweden, 1975.

[63] G. W. Irwin, W. Monteith, and W. C. Beattie, "Statistical electricity demand modelling from consumer billing data", *IEE Proceedings C - Generation, Transmission and Distribution*, vol. 133, no. 6, pp. 328–335, 1986, ISSN: 01437046. DOI: 10.1049/ip-c.1986.0048.

[64] S. W. Heunis and R. Herman, "A Probabilistic Model for Residential Consumer Loads", *IEEE Transactions on Power Systems*, vol. 17, no. 3, pp. 621–625, 2002. DOI: 10.1109/TPWRS.2002.800901.

[65] A. Seppaelae, "Statistical distribution of customer load profiles", in *International Conference on Energy Management and Power Delivery (EMPD)*, 1995, pp. 696–701, ISBN: 0-7803-2981-3. DOI: 10.1109/EMPD.1995.500813.

[66] R. Singh, B. C. Pal, and R. A. Jabr, "Statistical representation of distribution system loads using Gaussian mixture model", *IEEE Transactions on Power Systems*, vol. 25, no. 1, pp. 29–37, 2010, ISSN: 08858950. DOI: 10.1109/TPWRS.2009.2030271.

[67] T. Zhang, X. Song, X. Meng, J. Yu, and X. Chen, "A probabilistic load model based on chi-square method for distribution network", in *2nd IET Renewable Power Generation Conference (RPG)*, 2013, pp. 1–4, ISBN: 9781849197588. DOI: 10.1049/cp.2013.1738.

[68] M. S. ElNozahy, M. M. A. Salama, and R. Seethapathy, "A probabilistic load modelling approach using clustering algorithms", in *IEEE Power & Energy Society General Meeting*, 2013, pp. 1–5, ISBN: 978-1-4799-1303-9. DOI: 10.1109/PESMG.2013.6672073.

[69] J.-F. Toubeau, M. Hupez, V. Klonari, Z. D. Grève, and F. Vallee, "Statistical Load and Generation Modelling for Long Term Studies of Low Voltage Networks in Presence of Sparse Smart Metering Data", in *IEEE 42nd Annual Conference on Industrial Electronics Society*, 2016, pp. 3900–3905, ISBN: 9781509034741. DOI: 10.1109/IECON.2016.7793228.

[70] Y. M. Atwa, E. F. El-Saadany, M. M. A. Salama, and R. Seethapathy, "Optimal Renewable Resources Mix for Distribution System Energy Loss Minimization", *IEEE Transactions on Power Systems*, vol. 25, no. 1, pp. 360–370, 2010, ISSN: 08858950. DOI: 10.1109/TPWRS.2009.2030276.

[71] A. Soroudi, M. Aien, and M. Ehsan, "A probabilistic modeling of photo voltaic modules and wind power generation impact on distribution networks", *IEEE Systems Journal*, vol. 6, no. 2, pp. 254–259, 2012, ISSN: 19328184. DOI: 10.1109/JSYST.2011.2162994.

[72] W. Sheng, K. Liu, Y. Liu, X. Ye, and K. He, "Reactive power coordinated optimisation method with renewable distributed generation based on improved harmony search", *IET Generation, Transmission & Distribution*, vol. 10, no. 13, pp. 3152–3162, 2016, ISSN: 1751-8687. DOI: 10.1049/iet-gtd.2015.1051.

[73] A. Kusiak and Z. Zhang, "Short-horizon prediction of wind power: A data-driven approach", *IEEE Transactions on Energy Conversion*, vol. 25, no. 4, pp. 1112–1122, 2010, ISSN: 08858969. DOI: 10.1109/TEC.2010.2043436.

[74] A. Kusiak and W. Li, "Virtual models for prediction of wind turbine parameters", *IEEE Transactions on Energy Conversion*, vol. 25, no. 1, pp. 245–252, 2010, ISSN: 08858969. DOI: 10.1109/TEC.2009.2033042.

[75] ——, "Short-term prediction of wind power with a clustering approach", *Renewable Energy*, vol. 35, no. 10, pp. 2362–2369, 2010, ISSN: 09601481. DOI: 10.1016/j.renene.2010.03.027.

[76] A. A. Abdelsalam and E. F. El-Saadany, "Probabilistic approach for optimal planning of distributed generators with controlling harmonic distortions", *IET Generation, Transmission & Distribution*, vol. 7, no. 10, pp. 1105–1115, 2013, ISSN: 1751-8687. DOI: 10.1049/iet-gtd.2012.0769.

[77] S. Talari, M. Yazdaninejad, and M.-R. Haghifam, "Stochastic-based scheduling of the microgrid operation including wind turbines, photovoltaic cells, energy storages and responsive loads", *IET Generation, Transmission & Distribution*, vol. 9, no. 12, pp. 1498–1509, 2015, ISSN: 1751-8687. DOI: 10.1049/iet-gtd.2014.0040.

[78] S. Mohammadi, B. Mozafari, S. Solimani, and T. Niknam, "An Adaptive Modified Firefly Optimisation Algorithm based on Hong's Point Estimate Method to optimal operation management in a microgrid with consideration of uncertainties", *Energy*, vol. 51, pp. 339–348, 2013, ISSN: 03605442. DOI: 10.1016/j.energy.2012.12.013.

[79] R. Herman and C. T. Gaunt, "Probabilistic modelling of parameter variability for analysing grid-connected LV feeders with DG", in *48th International Universities Power Engineering Conference (UPEC)*, 2013, pp. 1–5, ISBN: 9781479932542. DOI: 10.1109/UPEC.2013.6714857.

[80] K. P. Kumar and B. Saravanan, "Recent techniques to model uncertainties in power generation from renewable energy sources and loads in microgrids – A review", *Renewable and Sustainable Energy Reviews*, vol. 71, pp. 348–358, 2017, ISSN: 18790690. DOI: 10.1016/j.rser.2016.12.063.

[81] K. Sunderland, M. Coppo, M. Conlon, and R. Turri, "A correction current injection method for power flow analysis of unbalanced multiple-grounded 4-wire distribution networks", *Electric Power Systems Research*, vol. 132, pp. 30–38, 2016.

[82] J. A. Martinez and J. Mahseredjian, "Load flow calculations in distribution systems with distributed resources. A review", in *IEEE Power and Energy Society General Meeting*, 2011, pp. 1–8, ISBN: 978-1-4577-1000-1. DOI: 10.1109/PES.2011.6039172.

[83] F. Bignucolo, R. Caldon, and V. Prandoni, "Radial MV networks voltage regulation with distribution management system coordinated controller", *Electric Power Systems Research*, vol. 78, no. 4, pp. 634–645, 2008, ISSN: 03787796. DOI: 10.1016/j.epsr.2007.05.007.

[84] F. Yang and Z. Li, "Improve Distribution System Energy Efficiency With Coordinated Reactive Power Control", *IEEE Transactions on Power Systems*, vol. 31, no. 4, pp. 2518–2525, 2016, ISSN: 0885-8950. DOI: 10.1109/TPWRS.2015.2477378.

[85] X. Liu, A. Aichhorn, L. Liu, and H. Li, "Coordinated control of distributed energy storage system with tap changer transformers for voltage rise mitigation under high photovoltaic penetration", *IEEE Transactions on Smart Grid*, vol. 3, no. 2, pp. 897–906, 2012, ISSN: 19493053. DOI: 10.1109/TSG.2011.2177501.

[86] K. M. Muttaqi, A. D. T. Le, M. Negnevitsky, and G. Ledwich, "A Coordinated Voltage Control Approach for Coordination of OLTC, Voltage Regulator, and DG to Regulate Voltage in a Distribution Feeder", *IEEE Transactions on Industry Applications*, vol. 51, no. 2, pp. 1239–1248, 2015, ISSN: 00939994. DOI: 10.1109/TIA.2014.2354738.

[87] A. Kulmala, S. Repo, and P. Jarventausta, "Coordinated voltage control in distribution networks including several distributed energy resources", *IEEE Transactions on Smart Grid*, vol. 5, no. 4, pp. 2010–2020, 2014, ISSN: 19493053. DOI: 10.1109/TSG.2014.2297971.

[88] R. Caldon, M. Coppo, and R. Turri, "Coordinated voltage control in MV and LV distribution networks with inverter-interfaced users", in *IEEE PowerTech, Grenoble*, 2013, pp. 1–5, ISBN: 9781467356695. DOI: 10.1109/PTC.2013.6652491.

[89] A. Bokhari, A. Raza, M. Diaz-Aguilo, F. De Leon, D. Czarkowski, R. E. Uosef, and D. Wang, "Combined Effect of CVR and DG Penetration in the Voltage Profile of Low-Voltage Secondary Distribution Networks", *IEEE Transactions on Power Delivery*, vol. 31, no. 1, pp. 286–293, 2016, ISSN: 08858977. DOI: 10.1109/TPWRD.2015.2422308.

[90] CENELEC, *Requirements for micro- generating plants to be connected in parallel with public low-voltage distribution networks*, 2015.

[91] I. Bielchev, M. Richter, M. Banka, P. Trojan, Z. A. Styczynski, A. Naumann, and P. Komarnicki, "Dynamic distribution grid management through the coordination of decentralized power units", in *IEEE Power & Energy Society General Meeting*, 2015, pp. 1–5, ISBN: 9781467380409. DOI: 10.1109/PESGM.2015.7286124.

[92] S. Ghosh, S. Rahman, and M. Pipattanasomporn, "Local distribution voltage control by reactive power injection from PV inverters enhanced with active power curtailment", in *2014 IEEE PES General Meeting | Conference & Exposition*, 2014, pp. 1–5, ISBN: 978-1-4799-6415-4. DOI: 10.1109/PESGM.2014.6939358.

[93] B. I. Craciun, D. Sera, E. A. Man, T. Kerekes, V. A. Muresan, and R. Teodorescu, "Improved voltage regulation strategies by PV inverters in LV rural networks", in *Proceedings - 2012 3rd IEEE International Symposium on Power Electronics for Distributed Generation Systems, PEDG 2012*, 2012, pp. 775–781, ISBN: 9781467320238. DOI: 10.1109/PEDG.2012.6254089.

[94] S. Weckx, C. Gonzalez, and J. Driesen, "Combined central and local active and reactive power control of PV inverters", *IEEE Transactions on Sustainable Energy*, vol. 5, no. 3, pp. 776–784, 2014, ISSN: 19493029. DOI: 10.1109/TSTE.2014.2300934.

[95] L. Collins and J. K. Ward, "Real and reactive power control of distributed PV inverters for overvoltage prevention and increased renewable generation hosting capacity", *Renewable Energy*, vol. 81, pp. 464–471, 2015, ISSN: 18790682. DOI: 10.1016/j.renene.2015.03.012.

[96] E. Demirok, P. C. Gonzalez, K. H. B. Frederiksen, D. Sera, P. Rodriguez, and R. Teodorescu, "Local reactive power control methods for overvoltage prevention of distributed solar inverters in low-voltage grids", *IEEE Journal of Photovoltaics*, vol. 1, no. 2, pp. 174–182, 2011, ISSN: 21563381. DOI: 10.1109/JPHOTOV.2011.2174821.

[97] A. Safayet, P. Fajri, and I. Husain, "Reactive power management for overvoltage prevention at high PV penetration in low voltage distribution system", in *2015 IEEE Energy Conversion Congress and Exposition (ECCE)*, IEEE, Sep. 2015, pp. 1988–1994, ISBN: 978-1-4673-7151-3. DOI: 10.1109/ECCE.2015.7309941.

[98] S. Pukhrem, M. Basu, M. Conlon, and K. Sunderland, "Enhanced network voltage management techniques under the proliferation of rooftop solar PV installation in low voltage distribution network", *IEEE Journal of Emerging and Selected Topics in Power Electronics*, pp. 1–15, 2016, ISSN: 2168-6777. DOI: 10.1109/JESTPE.2016.2614986.

[99] J. A. Taylor and F. S. Hover, "Convex models of distribution system reconfiguration", *IEEE Transactions on Power Systems*, vol. 27, no. 3, pp. 1407–1413, 2012.

[100] C. Lee, C. Liu, S. Mehrotra, and Z. Bie, "Robust distribution network reconfiguration", *IEEE Transactions on Smart Grid*, vol. 6, no. 2, pp. 836–842, 2014.

[101] Z. Tian, W. Wu, B. Zhang, and A. Bose, "Mixed-integer second-order cone programing model for var optimisation and network reconfiguration in active distribution networks", *IET Generation, Transmission & Distribution*, vol. 10, no. 8, pp. 1938–1946, 2016.

[102] A. Swarnkar, N. Gupta, and K. R. Niazi, "Adapted ant colony optimization for efficient reconfiguration of balanced and unbalanced distribution systems for loss minimization", *Swarm and Evolutionary Computation*, vol. 1, no. 3, pp. 129–137, 2011, ISSN: 22106502. DOI: 10.1016/j.swevo.2011.05.004.

[103] A. Y. Abdelaziz, F. M. Mohamed, S. F. Mekhamer, and M. A. L. Badr, "Distribution system reconfiguration using a modified Tabu Search algorithm", *Electric Power Systems Research*, vol. 80, no. 8, pp. 943–953, 2010, ISSN: 03787796. DOI: 10.1016/j.epsr.2010.01.001.

[104] A. Y. Abdelaziz, F. M. Mohammed, S. F. Mekhamer, and M. A.L. Badr, "Distribution Systems Reconfiguration using a modified particle swarm optimization algorithm", *Electric Power Systems Research*, vol. 79, no. 11, pp. 1521–1530, 2009, ISSN: 03787796. DOI: 10.1016/j.epsr.2009.05.004.

[105] N. Gupta, A. Swarnkar, K. R. Niazi, and R. C. Bansal, "Multi-objective reconfiguration of distribution systems using adaptive genetic algorithm in fuzzy framework", *IET Generation, Transmission & Distribution*, vol. 4, no. 12, pp. 1288–1298, 2010, ISSN: 17518687. DOI: 10.1049/iet-gtd.2010.0056.

[106] T. Niknam, "An efficient multi-objective HBMO algorithm for distribution feeder reconfiguration", *Expert Systems with Applications*, vol. 38, no. 3, pp. 2878–2887, 2011, ISSN: 09574174. DOI: 10.1016/j.eswa.2010.08.081.

[107] A. Saffar, R. Hooshmand, and A. Khodabakhshian, "A new fuzzy optimal reconfiguration of distribution systems for loss reduction and load balancing using ant colony search-based algorithm", *Applied Soft Computing Journal*, vol. 11, no. 5, pp. 4021–4028, 2011, ISSN: 15684946. DOI: 10.1016/j.asoc.2011.03.003.

[108] R. Srinivasa Rao, S. V. L. Narasimham, M. Ramalinga Raju, and A. Srinivasa Rao, "Optimal network reconfiguration of large-scale distribution system using harmony search algorithm", *IEEE Transactions on Power Systems*, vol. 26, no. 3, pp. 1080–1088, 2011, ISSN: 08858950. DOI: 10.1109/TPWRS.2010.2076839.

[109] A. Azizivahed, H. Narimani, E. Naderi, M. Fathi, and M. R. Narimani, "A hybrid evolutionary algorithm for secure multi-objective distribution feeder reconfiguration", *Energy*, vol. 138, pp. 355–373, 2017, ISSN: 03605442. DOI: 10.1016/j.energy.2017.07.102.

[110] T. T. Nguyen, T. T. Nguyen, A. V. Truong, Q. T. Nguyen, and T. A. Phung, "Multi-objective electric distribution network reconfiguration solution using runner-root algorithm", *Applied Soft Computing Journal*, vol. 52, pp. 93–108, 2017, ISSN: 15684946. DOI: 10.1016/j.asoc.2016.12.018.

[111] H. Wu and P. Dong, "PPSO method for distribution network reconfiguration considering the stochastic uncertainty of wind turbine, photovoltaic and load", *The Journal of Engineering*, vol. 2017, no. 13, pp. 2032–2036, 2017, ISSN: 2051-3305. DOI: 10.1049/joe.2017.0686.

[112] I. I. Atteya, H. Ashour, N. Fahmi, and D. Strickland, "Radial distribution network reconfiguration for power losses reduction using a modified particle swarm optimisation", *CIRED - Open Access Proceedings Journal*, vol. 2017, no. 1, pp. 2505–2508, 2017, ISSN: 2515-0855. DOI: 10.1049/oap-cired.2017.1286.

[113] A. Asrari, S. Lotfifard, and M. Payam, "Pareto Dominance-Based Multiobjective Optimization Method for Distribution Network Reconfiguration", *IEEE Transactions on Smart Grid*, vol. 7, no. 3, pp. 1401–1410, 2016. DOI: 10.1109/TSG.2015.2468683.

[114] S. R. Tuladhar, J. G. Singh, and W. Ongsakul, "Multi-objective approach for distribution network reconfiguration with optimal DG power factor using NSPSO", *IET Generation, Transmission & Distribution*, vol. 10, no. 12, pp. 2842–2851, 2016, ISSN: 1751-8687. DOI: 10.1049/iet-gtd.2015.0587.

[115] S. Ahmadi and S. Abdi, "Optimal reconfiguration of unbalanced distribution systems using a new hybrid Big Bang-Big Crunch algorithm for loss reduction", in *20th Electrical Power Distribution Networks Conference (EPDC)*, 2015, pp. 53–59, ISBN: 9781467366120. DOI: 10.1109/EPDC.2015.7330473.

[116] M. R. Dorostkar-Ghamsari, M. Fotuhi-Firuzabad, M. Lehtonen, and A. Safdarian, "Value of Distribution Network Reconfiguration in Presence of Renewable Energy Resources", *IEEE Transactions on Power Systems*, vol. 31, no. 3, pp. 1879–1888, 2015, ISSN: 0885-8950. DOI: 10.1109/TPWRS.2015.2457954.

[117] A. Bose, Z. Tian, W. Wu, and B. Zhang, "Mixed-integer second-order cone programing model for VAR optimisation and network reconfiguration in active distribution networks", *IET Generation, Transmission & Distribution*, vol. 10, no. 8, pp. 1938–1946, May 2016, ISSN: 1751-8687. DOI: `10.1049/iet-gtd.2015.1228`.

[118] N. C. Koutsoukis, D. O. Siagkas, P. S. Georgilakis, and N. D. Hatziargyriou, "Online Reconfiguration of Active Distribution Networks for Maximum Integration of Distributed Generation", *IEEE Transactions on Automation Science and Engineering*, vol. 14, no. 2, pp. 437–448, Apr. 2017, ISSN: 1545-5955. DOI: `10.1109/TASE.2016.2628091`.

[119] F. de Oliveira Saraiva and E. N. Asada, "Multi-agent systems applied to topological reconfiguration of smart power distribution systems", in *International Joint Conference on Neural Networks (IJCNN)*, 2014, pp. 2812–2819, ISBN: 978-1-4799-1484-5. DOI: `10.1109/IJCNN.2014.6889791`.

[120] D. Shu, Z. Huang, J. Li, and X. Zou, "Application of multi-agent particle swarm algorithm in distribution network reconfiguration", *Chinese Journal of Electronics*, vol. 25, no. 6, pp. 1179–1185, 2016, ISSN: 10224653. DOI: `10.1049/cje.2016.10.015`.

[121] S. M. Miri Larimi, M. R. Haghifam, and A. Moradkhani, "Risk-based reconfiguration of active electric distribution networks", *IET Generation, Transmission & Distribution*, vol. 10, no. 4, pp. 1006–1015, 2016, ISSN: 1751-8687. DOI: `10.1049/iet-gtd.2015.0777`.

[122] X. Bai, Y. Mavrocostanti, D. Strickland, and C. Harrap, "Distribution network reconfiguration validation with uncertain loads – network configuration determination and application", *IET Generation, Transmission & Distribution*, vol. 10, no. 12, pp. 2852–2860, 2016, ISSN: 1751-8687. DOI: `10.1049/iet-gtd.2015.0734`.

[123] F. Capitanescu, L. F. Ochoa, H. Margossian, and N. D. Hatziargyriou, "Assessing the potential of network reconfiguration to improve distributed generation hosting capacity in active distribution systems", *IEEE Transactions on Power Systems*, vol. 30, no. 1, pp. 346–356, 2015, ISSN: 08858950. DOI: `10.1109/TPWRS.2014.2320895`.

[124] J. Wen, Y. Tan, L. Jiang, and K. Lei, "Dynamic reconfiguration of distribution networks considering the real-time topology variation", *IET Generation, Transmission & Distribution*, vol. 12, no. 7, pp. 1509–1517, 2018, ISSN: 1751-8687. DOI: `10.1049/iet-gtd.2017.1304`.

[125] A. S. Bouhouras, G. T. Andreou, D. P. Labridis, and A. G. Bakirtzis, "Selective automation upgrade in distribution networks towards a smarter grid", *IEEE Transactions on Smart Grid*, vol. 1, no. 3, pp. 278–285, 2010, ISSN: 19493053. DOI: `10.1109/TSG.2010.2080294`.

[126] S. Koohi-Kamali, V. V. Tyagi, N. A. Rahim, N. L. Panwar, and H. Mokhlis, "Emergence of energy storage technologies as the solution for reliable operation of smart power systems: A review", *Renewable and Sustainable Energy Reviews*, vol. 25, pp. 135–165, 2013, ISSN: 13640321. DOI: `10.1016/j.rser.2013.03.056`.

[127] M. Yekini Suberu, M. Wazir Mustafa, and N. Bashir, "Energy storage systems for renewable energy power sector integration and mitigation of intermittency", *Renewable and Sustainable Energy Reviews*, vol. 35, pp. 499–514, 2014, ISSN: 13640321. DOI: `10.1016/j.rser.2014.04.009`.

[128] J. Kim, Y. Suharto, and T. U. Daim, "Evaluation of Electrical Energy Storage (EES) technologies for renewable energy: A case from the US Pacific Northwest", *Journal of Energy Storage*, vol. 11, pp. 25–54, 2017, ISSN: 2352152X. DOI: `10.1016/j.est.2017.01.003`.

[129] S. Wolfe and A. Mensah, "Overcoming Challenges to High Penetration of Solar PV: Using Optimized Energy Storage and Distribution Grid Controls", *The Electricity Journal*, vol. 25, no. 9, pp. 43–47, 2012, ISSN: 10406190. DOI: `10.1016/j.tej.2012.09.009`.

[130] D. Q. Hung and N. Mithulananthan, "Community Energy Storage and Capacitor Allocation in Distribution Systems", in *21st Australasian Universities Power Engineering Conference (AUPEC)*, 2011, pp. 1–6, ISBN: VO -.

[131] G. Mokhtari, A. Ghosh, G. Nourbakhsh, and G. Ledwich, "Smart robust resources control in lv network to deal with voltage rise issue", *IEEE Transactions on Sustainable Energy*, vol. 4, no. 4, pp. 1043–1050, 2013, ISSN: 19493029. DOI: 10.1109/TSTE.2013.2265100.

[132] M. J. E. Alam, K. M. Muttaqi, and D. Sutanto, "Mitigation of rooftop solar PV impacts and evening peak support by managing available capacity of distributed energy storage systems", *IEEE Transactions on Power Systems*, vol. 28, no. 4, pp. 3874–3884, 2013, ISSN: 08858950. DOI: 10.1109/TPWRS.2013.2259269.

[133] Y. Riffonneau, S. Bacha, F. Barruel, and A. Delaille, "Energy flow management in grid connected PV systems with storage - A deterministic approach", in *IEEE International Conference on Industrial Technology (ICIT)*, 2009, ISBN: 978-1-4244-3506-7. DOI: 10.1109/ICIT.2009.4939609.

[134] Y. Riffonneau, S. Bacha, F. Barruel, and S. Ploix, "Optimal Power Flow Management for Grid Connected PV Systems With Batteries", *IEEE Transactions on Sustainable Energy*, vol. 2, no. 3, pp. 309–320, 2011, ISSN: 1949-3029. DOI: 10.1109/TSTE.2011.2114901.

[135] Z. Wang, C. Gu, F. Li, S. Member, and P. Bale, "Active Demand Response Using Shared Energy Storage for Household Energy Management", *IEEE Transactions on Smart Grid*, vol. 4, no. 4, pp. 1888–1897, 2013. DOI: 10.1109/TSG.2013.2258046.

[136] S. Teleke, M. E. Baran, S. Bhattacharya, and A. Q. Huang, "Rule-based control of battery energy storage for dispatching intermittent renewable sources", *IEEE Transactions on Sustainable Energy*, vol. 1, no. 3, pp. 117–124, 2010, ISSN: 19493029. DOI: 10.1109/TSTE.2010.2061880.

[137] F. M. Camilo, R. Castro, M. E. Almeida, and V. F. Pires, "Self-consumption and storage as a way to facilitate the integration of renewable energy in low voltage distribution networks", *IET Generation, Transmission & Distribution*, vol. 10, no. 7, pp. 1741–1748, 2016, ISSN: 1751-8687. DOI: 10.1049/iet-gtd.2015.0431.

[138] S. X. Chen, H. B. Gooi, and M. Q. Wang, "Sizing of energy storage for microgrids", *IEEE Transactions on Smart Grid*, vol. 3, no. 1, pp. 142–151, 2012, ISSN: 19493053. DOI: 10.1109/TSG.2011.2160745.

[139] J. Tant, F. Geth, D. Six, P. Tant, and J. Driesen, "Multiobjective battery storage to improve PV integration in residential distribution grids", *IEEE Transactions on Sustainable Energy*, vol. 4, no. 1, pp. 182–191, 2013, ISSN: 19493029. DOI: 10.1109/TSTE.2012.2211387.

[140] N. Jayasekara, M. A. S. Masoum, and P. J. Wolfs, "Optimal operation of distributed energy storage systems to improve distribution network load and generation hosting capability", *IEEE Transactions on Sustainable Energy*, vol. 7, no. 1, pp. 250–261, 2016, ISSN: 19493029. DOI: 10.1109/TSTE.2015.2487360.

[141] D. Q. Hung, N. Mithulananthan, and R. C. Bansal, "Integration of PV and BES units in commercial distribution systems considering energy loss and voltage stability", *Applied Energy*, vol. 113, pp. 1162–1170, 2014, ISSN: 03062619. DOI: 10.1016/j.apenergy.2013.08.069.

[142] J. D. Watson, N. R. Watson, and I. Lestas, "Optimized dispatch of energy storage systems in unbalanced distribution networks", *IEEE Transactions on Sustainable Energy*, vol. 9, no. 2, pp. 639–650, 2017, ISSN: 19493029. DOI: 10.1109/TSTE.2017.2752964.

[143] T. Gozel, M. H. Hocaoglu, U. Eminoglu, and A. Balikci, "Optimal placement and sizing of distributed generation on radial feeder with different static load models", in *International Conference on Future Power Systems*, 2005, pp. 2–6, ISBN: 90-78205-02-4. DOI: 10.1109/FPS.2005.204319.

[144] N. Acharya, P. Mahat, and N. Mithulananthan, "An analytical approach for DG allocation in primary distribution network", *International Journal of Electrical Power and Energy Systems*, vol. 28, no. 10, pp. 669–678, 2006, ISSN: 01420615. DOI: 10.1016/j.ijepes.2006.02.013.

[145] A. L. Devi and B. Subramanyam, "Optimal DG unit placement for loss reduction in radial distribution system-A case study", *ARPN Journal of Engineering and Applied Sciences*, vol. 2, no. 6, pp. 57–61, 2007.

[146] T. Gozel and M. H. Hocaoglu, "An analytical method for the sizing and siting of distributed generators in radial systems", *Electric Power Systems Research*, vol. 79, no. 6, pp. 912–918, 2009, ISSN: 03787796. DOI: 10.1016/j.epsr.2008.12.007.

[147] H. Hamedi and M. Gandomkar, "A straightforward approach to minimizing unsupplied energy and power loss through DG placement and evaluating power quality in relation to load variations over time", *International Journal of Electrical Power and Energy Systems*, vol. 35, no. 1, pp. 93–96, 2012, ISSN: 01420615. DOI: 10.1016/j.ijepes.2011.10.001.

[148] M. Shahzad, I. Ullah, P. Palensky, and W. Gawlik, "Analytical approach for simultaneous optimal sizing and placement of multiple Distributed Generators in primary distribution networks", in *IEEE 23rd International Symposium on Industrial Electronics (ISIE)*, 2014, pp. 2554–2559, ISBN: 9781479923991. DOI: 10.1109/ISIE.2014.6865022.

[149] J. Lei and Q. Gong, "Operating strategy and optimal allocation of large-scale VRB energy storage system in active distribution networks for solar/wind power applications", *IET Generation, Transmission & Distribution*, vol. 11, no. 9, pp. 2403–2411, 2017, ISSN: 1751-8687. DOI: 10.1049/iet-gtd.2016.2076.

[150] D. Q. Hung and N. Mithulananthan, "Multiple Distributed Generator Placement in Primary Distribution Networks for Loss Reduction", *IEEE Transactions on Industrial Electronics*, vol. 60, no. 4, pp. 1700–1708, Apr. 2013, ISSN: 0278-0046. DOI: 10.1109/TIE.2011.2112316.

[151] K. Mahmoud, N. Yorino, and A. Ahmed, "Optimal Distributed Generation Allocation in Distribution Systems for Loss Minimization", *IEEE Transactions on Power Systems*, vol. 31, no. 2, pp. 960–969, 2015, ISSN: 08858950. DOI: 10.1109/TPWRS.2015.2418333.

[152] D. Q. Hung, N. Mithulananthan, and R. C. Bansal, "Analytical expressions for DG allocation in primary distribution networks", *IEEE Transactions on Energy Conversion*, vol. 25, no. 3, pp. 814–820, 2010, ISSN: 08858969. DOI: 10.1109/TEC.2010.2044414.

[153] L. F. Ochoa and G. P. Harrison, "Minimizing energy losses: Optimal accommodation and smart operation of renewable distributed generation", *IEEE Transactions on Power Systems*, vol. 26, no. 1, pp. 198–205, 2011, ISSN: 08858950. DOI: 10.1109/TPWRS.2010.2049036.

[154] S. Ganguly and D. Samajpati, "Distributed generation allocation on radial distribution networks under uncertainties of load and generation using genetic algorithm", *IEEE Transactions on Sustainable Energy*, vol. 6, no. 3, pp. 688–697, 2015, ISSN: 19493029. DOI: 10.1109/TSTE.2015.2406915.

[155] ——, "Distributed generation allocation with on-load tap changer on radial distribution networks using adaptive genetic algorithm", *Applied Soft Computing Journal*, vol. 59, pp. 45–67, 2017, ISSN: 15684946. DOI: 10.1016/j.asoc.2017.05.041.

[156] R. Sanjay, T. Jayabarathi, T. Raghunathan, V. Ramesh, and N. Mithulananthan, "Optimal Allocation of Distributed Generation Using Hybrid Grey Wolf Optimizer", *IEEE Access*, vol. 5, pp. 14 807–14 818, 2017. DOI: 10.1109/ACCESS.2017.2726586.

[157] K. Khalid Mehmood, S. U. Khan, S.-J. Lee, Z. M. Haider, M. K. Rafique, and C.-H. Kim, "Optimal sizing and allocation of battery energy storage systems with wind and solar power DGs in a distribution network for voltage regulation considering the lifespan of batteries", *IET Renewable Power Generation*, vol. 11, no. 10, pp. 1305–1315, 2017, ISSN: 1752-1416. DOI: 10.1049/iet-rpg.2016.0938.

[158] I. Kim, "Optimal distributed generation allocation for reactive power control", *IET Generation, Transmission & Distribution*, vol. 11, no. 6, pp. 1549–1556, 2017, ISSN: 1751-8687. DOI: 10.1049/iet-gtd.2016.1393.

[159] I. Hussain and A. K. Roy, "Optimal distributed generation allocation in distribution systems employing modified artificial bee colony algorithm to reduce losses and improve voltage profile", in *IEEE-International Conference On Advances In Engineering, Science And Management*, 2012, pp. 565–570, ISBN: 978-1-4673-0213-5.

[160] F. S. Abu-Mouti and M. E. El-Hawary, "Optimal Distributed Generation Allocation and Sizing in Distribution Systems via Artificial Bee Colony Algorithm", *IEEE Transactions on Power Delivery*, vol. 26, no. 4, pp. 2090–2101, 2011, ISSN: 0885-8977. DOI: 10.1109/TPWRD.2011.2158246.

[161] K. Nara, Y. Hayashi, K. Ikeda, and T. Ashizawa, "Application of tabu search to optimal placement of distributed generators", in *IEEE Power Engineering Society Winter Meeting*, 2001, pp. 918–923, ISBN: 0-7803-6672-7. DOI: 10.1109/PESW.2001.916995.

[162] M. E. H. Golshan and S. Ali Arefifar, "Optimal allocation of distributed generation and reactive sources considering tap positions of voltage regulators as control variables", *International Transactions on Electrical Energy Systems*, vol. 17, no. 3, pp. 219–239, 2007. DOI: 10.1002/etep.130.

[163] A. El-Zonkoly, "Optimal placement of multi-distributed generation units including different load models using particle swarm optimisation", *IET Generation, Transmission & Distribution*, vol. 5, no. 7, pp. 760–771, 2011, ISSN: 17518687. DOI: 10.1049/iet-gtd.2010.0676.

[164] H. Falaghi and M. R. Haghifam, "ACO based algorithm for distributed generation sources allocation and sizing in distribution systems", in *IEEE PowerTech, Lausanne*, 2007, pp. 555–560, ISBN: 9781424421909. DOI: 10.1109/PCT.2007.4538377.

[165] D. P. Reddy, V. Reddy, and G. Manohar, "(in press) Optimal renewable resources placement in distribution networks by combined power loss index and whale optimization algorithms", *Journal of Electrical Systems and Information Technology*, 2017, ISSN: 23147172. DOI: 10.1016/j.jesit.2017.05.006.

[166] P. R. Dinakara, V. Reddy, and G. Manohar, "(in press) Ant Lion optimization algorithm for optimal sizing of renewable energy resources for loss reduction in distribution systems", *Journal of Electrical Systems and Information Technology*, 2017, ISSN: 23147172. DOI: 10.1016/j.jesit.2017.06.001.

[167] M. Kumawat, N. Gupta, N. Jain, and R. C. Bansal, "Optimally Allocation of Distributed Generators in Three-Phase Unbalanced Distribution Network", *Energy Procedia*, vol. 142, pp. 749–754, 2017, ISSN: 18766102. DOI: 10.1016/j.egypro.2017.12.122.

[168] S. K. Injeti, "(in press) A Pareto optimal approach for allocation of distributed generators in radial distribution systems using improved differential search algorithm", *Journal of Electrical Systems and Information Technology*, 2017, ISSN: 23147172. DOI: 10.1016/j.jesit.2016.12.006.

[169] N. Kanwar, N. Gupta, K. R. Niazi, A. Swarnkar, and R. C. Bansal, "Simultaneous allocation of distributed energy resource using improved particle swarm optimization", *Applied Energy*, vol. 185, pp. 1684–1693, 2017, ISSN: 03062619. DOI: 10.1016/j.apenergy.2016.01.093.

[170] P. P. Biswas, R. Mallipeddi, P. N. Suganthan, and G. A. Amaratunga, "A multiobjective approach for optimal placement and sizing of distributed generators and capacitors in distribution network", *Applied Soft Computing Journal*, vol. 60, pp. 268–280, 2017, ISSN: 15684946. DOI: 10.1016/j.asoc.2017.07.004.

[171] S. M. Hosseini and F. Abbasi, "Optimal DG allocation and sizing in presence of storage systems considering network configuration effects in distribution systems", *IET Generation, Transmission & Distribution*, vol. 10, no. 3, pp. 617–624, 2016, ISSN: 1751-8687. DOI: 10.1049/iet-gtd.2015.0367.

[172] M.-A. Akbari, J. Aghaei, and M. Barani, "Convex probabilistic allocation of wind generation in smart distribution networks", *IET Renewable Power Generation*, vol. 11, no. 9, pp. 1211–1218, 2017, ISSN: 1752-1416. DOI: 10.1049/iet-rpg.2017.0100.

[173] X. Zhang, G. G. Karady, and S. T. Ariaratnam, "Optimal allocation of chp-based distributed generation on urban energy distribution networks", *IEEE Transactions on Sustainable Energy*, vol. 5, no. 1, pp. 246–253, 2014, ISSN: 19493029. DOI: 10.1109/TSTE.2013.2278693.

[174] M. Chen, G. Zou, X. Jin, Z. Yao, Y. Liu, and H. Yin, "Optimal Allocation method on Distributed Energy Storage System in Active Distribution Network", *Energy Procedia*, vol. 141, pp. 525–531, 2017, ISSN: 18766102. DOI: 10.1016/j.egypro.2017.11.070.

[175] Y. Zhao, Y. An, and Q. Ai, "Research on size and location of distributed generation with vulnerable node identification in the active distribution network", *IET Generation, Transmission & Distribution*, vol. 8, no. 11, pp. 1801–1809, 2014, ISSN: 1751-8687. DOI: 10.1049/iet-gtd.2013.0887.

[176] M. F. Shaaban, Y. M. Atwa, and E. F. El-Saadany, "DG allocation for benefit maximization in distribution networks", *IEEE Transactions on Power Systems*, vol. 28, no. 2, pp. 639–649, 2013, ISSN: 08858950. DOI: 10.1109/TPWRS.2012.2213309.

[177] M. Gandomkar, M. Vakilian, and M. Ehsan, "A genetic based Tabu search algorithm for optimal DG allocation in distribution networks", *Electric Power Components and Systems*, vol. 33, no. 12, pp. 1351–1362, 2005. DOI: 10.1080/15325000590964254.

[178] B. R. Pereira, G. R. M. da Costa, J. Contreras, and J. R. S. Mantovani, "Optimal Distributed Generation and Reactive Power Allocation in Electrical Distribution Systems", *IEEE Transactions on Sustainable Energy*, vol. 7, no. 3, pp. 975–984, 2016, ISSN: 19493029. DOI: 10.1109/TSTE.2015.2512819.

[179] M. Gomez-Gonzalez, F. J. Ruiz-Rodriguez, and F. Jurado, "Metaheuristic and probabilistic techniques for optimal allocation and size of biomass distributed generation in unbalanced radial systems", *IET Renewable Power Generation*, vol. 9, no. 6, pp. 653–659, 2015, ISSN: 1752-1416. DOI: 10.1049/iet-rpg.2014.0336.

[180] M. Vatani, D. Solati Alkaran, M. J. Sanjari, and G. B. Gharehpetian, "Multiple distributed generation units allocation in distribution network for loss reduction based on a combination of analytical and genetic algorithm methods", *IET Generation, Transmission & Distribution*, vol. 10, no. 1, pp. 66–72, 2016, ISSN: 1751-8687. DOI: 10.1049/iet-gtd.2015.0041.

[181] J. O. Kim, S. K. Park, K. W. Park, and C. Singh, "Dispersed Generation Planning Using Improved Hereford Ranch Algorithm", in *IEEE International Conference on Evolutionary Computation Proceedings*, 1998, pp. 678–683, ISBN: 0780348699. DOI: 10.1109/ICEC.1998.700121.

[182] P. Siano, G. P. Harrison, A. Piccolo, and A. R. Wallace, "Strategic placement of distributed generation capacity", in *19th Conference on Electricity Distribution, Austria*, 2007.

[183] H. Falaghi, C. Singh, M. R. Haghifam, and M. Ramezani, "DG integrated multistage distribution system expansion planning", *International Journal of Electrical Power and Energy Systems*, vol. 33, no. 8, pp. 1489–1497, 2011, ISSN: 01420615. DOI: 10.1016/j.ijepes.2011.06.031.

[184] K. H. Kim, Y. J. Lee, S. B. Rhee, S. K. Lee, and S. K. You, "Dispersed generator placement using fuzzy-GA in distribution systems", in *IEEE Power Engineering Society Summer Meeting*, 2002, pp. 1148–1153, ISBN: 0-7803-7518-1. DOI: 10.1109/PESS.2002.1043458.

[185] D. Singh, D. Singh, and K. S. Verma, "Multiobjective optimization for DG planning with load models", *IEEE Transactions on Power Systems*, vol. 24, no. 1, pp. 427–436, 2009, ISSN: 08858950. DOI: 10.1109/TPWRS.2008.2009483.

[186] O. A. Zongo and A. Oonsivilai, "Optimal placement of distributed generator for power loss minimization and voltage stability improvement", *Energy Procedia*, vol. 138, pp. 134–139, 2017, ISSN: 18766102. DOI: 10.1016/j.egypro.2017.10.080.

[187] J. Zhu, W. Gu, G. Lou, L. Wang, B. Xu, M. Wu, and W. Sheng, "Learning Automata-Based Methodology for Optimal Allocation of Renewable Distributed Generation Considering Network Reconfiguration", *IEEE Access*, vol. 5, pp. 14 275–14 288, 2017, ISSN: 21693536. DOI: 10.1109/ACCESS.2017.2730850.

[188] S. N. Salih and P. Chen, "On Coordinated Control of OLTC and Reactive Power Compensation for Voltage Regulation in Distribution Systems With Wind Power", *IEEE Transactions on Power Systems*, vol. 31, no. 5, pp. 4026–4035, 2016. DOI: 10.1109/TPWRS.2015.2501433.

[189] K. Tanaka, M. Oshiro, S. Toma, A. Yona, T. Senjyu, T. Funabashi, and C.-H. Kim, "Decentralised control of voltage in distribution systems by distributed generators", *IET Generation, Transmission & Distribution*, vol. 4, no. 11, pp. 1251–1260, 2010, ISSN: 17518687. DOI: 10.1049/iet-gtd.2010.0003.

[190] P. Tenti, A. Costabeber, P. Mattavelli, and D. Trombetti, "Distribution loss minimization by token ring control of power electronic interfaces in residential microgrids", *IEEE Transactions on Industrial Electronics*, vol. 59, no. 10, pp. 3817–3826, 2012, ISSN: 02780046. DOI: 10.1109/TIE.2011.2161653.

[191] R. Caldon, M. Coppo, and R. Turri, "Distributed voltage control strategy for LV networks with inverter-interfaced generators", *Electric Power Systems Research*, vol. 107, pp. 85–92, 2014, ISSN: 03787796. DOI: 10.1016/j.epsr.2013.09.009.

[192] A. J. Conejo, J. M. Arroyo, N. Alguacil, and A. L. Guijarro, "Transmission Loss Allocation: A Comparison of Different Practical Algorithms", *IEEE Transactions on Power Systems*, vol. 17, no. 3, pp. 571–576, 2002. DOI: 10.1109/TPWRS.2002.800894.

[193] J. Mutale, G. Strbac, S. Curcic, and N. Jenkins, "Allocation of losses in distribution systems with embedded generation", *IEE Proceedings - Generation, Transmission and Distribution*, vol. 147, no. 1, pp. 7–14, 2000. DOI: 10.1049/ip-gtd:20000003.

[194] A. J. Conejo, F. D. Galiana, and I. Kockar, "Z-bus loss allocation", *IEEE Transactions on Power Systems*, vol. 16, no. 1, pp. 105–110, 2001, ISSN: 08858950. DOI: 10.1109/59.910787.

[195] N. Zhao, Y. Song, Z. Bie, S. Takahashi, and Y. Sekine, "Improved Z-bus loss allocation method through redistribution", in *39th International Universities Power Engineering Conference*, 2004, pp. 1101–1105.

[196] J. Salehi and M. R. Haghifam, "Modified Z-bus loss allocation method for distribution network with distributed generation", in *20th International Conference and Exhibition on Electricity Distribution - Part 2, CIRED*, 2009. DOI: 10.1049/cp.2009.0654.

[197] W. L. Fang and H. W. Ngan, "Succinct method for allocation of network losses", *IEE Proceedings - Generation, Transmission and Distribution*, vol. 149, no. 2, pp. 171–174, 2002. DOI: 10.1049/ip-gtd:20020126.

[198] P. M. Costa and M. A. Matos, "Loss Allocation in Distribution Networks With Embedded Generation", *IEEE Transactions on Power Systems*, vol. 19, no. 1, pp. 384–389, 2004, ISSN: 08858950. DOI: 10.1109/TPWRS.2003.820698.

[199] S. S. Kashyap and M. De, "Loss allocation and loss minimisation for radial distribution system including DGs", *IET Renewable Power Generation*, vol. 11, no. 6, pp. 806–818, 2017, ISSN: 1752-1416. DOI: 10.1049/iet-rpg.2016.0506.

[200] E. Carpaneto, G. Chicco, and J. S. Akilimali, "Branch current decomposition method for loss allocation in radial distribution systems with distributed generation", *IEEE Transactions on Power Systems*, vol. 21, no. 3, pp. 1170–1179, 2006. DOI: 10.1109/TPWRS.2006.876684.

[201] E. Carpaneto, G. Chicco, and J. Sumaili Akilimali, "Characterization of the loss allocation techniques for radial systems with distributed generation", *Electric Power Systems Research*, vol. 78, no. 8, pp. 1396–1406, 2008, ISSN: 03787796. DOI: 10.1016/j.epsr.2008.01.001.

[202] J. S. Savier and D. Das, "Energy loss allocation in radial distribution systems: A comparison of practical algorithms", *IEEE Transactions on Power Delivery*, vol. 24, no. 1, pp. 260–267, 2009, ISSN: 08858977. DOI: 10.1109/TPWRD.2008.2007018.

[203] ——, "An exact method for loss allocation in radial distribution systems", *International Journal of Electrical Power and Energy Systems*, vol. 36, no. 1, pp. 100–106, 2012, ISSN: 01420615. DOI: 10.1016/j.ijepes.2011.10.030.

[204] K. M. Jagtap and D. K. Khatod, "Allocation of distribution network losses with different types of distributed generation", in *IEEE Annual India Conference (INDICON)*, 2015, pp. 1–6, ISBN: 9781467373999. DOI: 10.1109/INDICON.2015.7443156.

[205] M. Atanasovski and R. Taleski, "Power summation method for loss allocation in radial distribution networks with DG", *IEEE Transactions on Power Systems*, vol. 26, no. 4, pp. 2491–2499, 2011. DOI: 10.1109/TPWRS.2011.2182663.

[206] J. S. Savier and D. Das, "Loss allocation to consumers before and after reconfiguration of radial distribution networks", *International Journal of Electrical Power and Energy Systems*, vol. 33, no. 3, pp. 540–549, 2011, ISSN: 01420615. DOI: 10.1016/j.ijepes.2010.11.007.

[207] K. M. Jagtap and D. K. Khatod, "Loss allocation in radial distribution networks with different load models and distributed generations", *IET Generation, Transmission & Distribution*, vol. 9, no. 12, pp. 1275–1291, 2015, ISSN: 1751-8687. DOI: 10.1049/iet-gtd.2014.0884.

[208] K. M. Jagtap and D. K. Khatod, "Novel approach for loss allocation of distribution networks with DGs", *Electric Power Systems Research*, vol. 143, pp. 303–311, 2017, ISSN: 03787796. DOI: 10.1016/j.epsr.2016.10.032.

[209] ——, "Distribution loss allocation technique with distributed generations", in *National Power Systems Conference*, 2017, pp. 1–5, ISBN: 9781467399685. DOI: 10.1109/NPSC.2016.7858852.

[210] K. M. Jagtap and D. K. Khatod, "Loss allocation in distribution network with distributed generations", *IET Generation, Transmission & Distribution*, vol. 9, no. 13, pp. 1628–1641, 2015, ISSN: 1751-8687. DOI: 10.1049/iet-gtd.2014.0923.

[211] ——, "Loss allocation in radial distribution networks with various distributed generation and load models", *International Journal of Electrical Power and Energy Systems*, vol. 75, pp. 173–186, 2016, ISSN: 01420615. DOI: 10.1016/j.ijepes.2015.07.042.

[212] M. Atanasovski and R. Taleski, "Energy summation method for loss allocation in radial distribution networks with DG", *IEEE Transactions on Power Systems*, vol. 27, no. 3, pp. 1433–1440, 2012, ISSN: 08858950. DOI: 10.1109/TPWRS.2011.2182663.

[213] Z. Ghofrani-Jahromi, Z. Mahmoodzadeh, and M. Ehsan, "Distribution loss allocation for radial systems including DGs", *IEEE Transactions on Power Delivery*, vol. 29, no. 1, pp. 72–80, 2014, ISSN: 08858977. DOI: 10.1109/TPWRD.2013.2277717.

[214] S. Ghaemi and K. Zare, "Loss allocation in restructured radial distribution networks considering the contractual power", *IET Generation, Transmission & Distribution*, vol. 11, no. 6, pp. 1389–1397, 2017, ISSN: 1751-8687. DOI: 10.1049/iet-gtd.2016.0697.

[215] S. Sharma and A. R. Abhyankar, "Loss allocation of radial distribution system using Shapley value: A sequential approach", *International Journal of Electrical Power and Energy Systems*, vol. 88, pp. 33–41, 2017, ISSN: 01420615. DOI: 10.1016/j.ijepes.2016.11.015.

[216] M. E. Oliveira, L. F. Ochoa, A. Padilha-Feltrin, and J. R. S. Mantovani, "Network reconfiguration and loss allocation in a deregulated environment of distributed systems", in *18th International Conference on Electricity Distribution*, 2005, pp. 6–9.

[217] E. Carpaneto, G. Chicco, and J. Sumaili Akilimali, "Application of the circuit-based loss allocation techniques to radial distribution systems", in *VI World Energy System Conference*, 2006, pp. 127–132.

[218] L. F. Ochoa, M. E. Oliveira, and A. Padilha-Feltrin, "Minimal cross-subsidies approach for loss allocation in distribution networks with open access", in *IEEE Power Engineering Society General Meeting (PES)*, 2007, pp. 1–6, ISBN: 1424412986. DOI: 10.1109/PES.2007.385804.

[219] J. S. Daniel, R. S. Salgado, and M. R. Irving, "Transmission loss allocation through a modified Ybus", *IEE Proceedings - Generation, Transmission and Distribution*, vol. 152, no. 2, pp. 208–214, 2005. DOI: 10.1049/ip-gtd:20041192.

[220] W. Kersting, "The computation of neutral and dirt currents and power losses", in *Power Systems Conference and Exposition, 2004. IEEE PES*, IEEE, 2004, pp. 213–218.

[221] A. Barbato, A. Dede, D. Della Giustina, G. Massa, A. Angioni, G. Lipari, F. Ponci, and S. Repo, "Lessons learnt from real-time monitoring of the low voltage distribution network", *Sustainable Energy, Grids and Networks*, vol. 15, pp. 76–85, 2018.

[222] F. Shahnia, P. J. Wolfs, and A. Ghosh, "Voltage unbalance reduction in low voltage feeders by dynamic switching of residential customers among three phases", *IEEE Transactions on Smart Grid*, vol. 5, no. 3, pp. 1318–1327, 2014.

[223] J. A. Taylor, *Convex optimization of power systems*. Cambridge University Press, 2015.

[224] J. Carpentier, "Contribution to the economic dispatch problem", *Bulletin de la Societe Francoise des Electriciens*, vol. 3, no. 8, pp. 431–447, 1962.

[225] K. Lehmann, A. Grastien, and P. Van Hentenryck, "Ac-feasibility on tree networks is np-hard", *IEEE Transactions on Power Systems*, vol. 31, no. 1, pp. 798–801, 2015.

[226] H. W. Dommel and W. F. Tinney, "Optimal power flow solutions", *IEEE Transactions on power apparatus and systems*, no. 10, pp. 1866–1876, 1968.

[227] O. Alsac and B. Stott, "Optimal load flow with steady-state security", *IEEE transactions on power apparatus and systems*, no. 3, pp. 745–751, 1974.

[228] G. Contaxis, C. Delkis, and G. Korres, "Decoupled optimal load flow using linear or quadratic programming", *IEEE Transactions on Power systems*, vol. 1, no. 2, pp. 1–7, 1986.

[229] B. Ghaddar, J. Marecek, and M. Mevissen, "Optimal power flow as a polynomial optimization problem", *IEEE Transactions on Power Systems*, vol. 31, no. 1, pp. 539–546, 2015.

[230] I. M. Nejdawi, K. A. Clements, and P. W. Davis, "An efficient interior point method for sequential quadratic programming based optimal power flow", *IEEE Transactions on Power Systems*, vol. 15, no. 4, pp. 1179–1183, 2000.

[231] S. Frank, I. Steponavice, and S. Rebennack, "Optimal power flow: A bibliographic survey i", *Energy Systems*, vol. 3, no. 3, pp. 221–258, 2012.

[232] ——, "Optimal power flow: A bibliographic survey ii", *Energy Systems*, vol. 3, no. 3, pp. 259–289, 2012, ISSN: 1868-3975. DOI: 10.1007/s12667-012-0057-x.

[233] D. K. Molzahn, I. A. Hiskens, *et al.*, "A survey of relaxations and approximations of the power flow equations", *Foundations and Trends® in Electric Energy Systems*, vol. 4, no. 1-2, pp. 1–221, 2019.

[234] H. Saadat *et al.*, *Power system analysis*. 1999.

[235] M. E. Baran and F. F. Wu, "Optimal capacitor placement on radial distribution systems", *IEEE Transactions on Power Delivery*, vol. 4, no. 1, pp. 725–734, Jan. 1989. DOI: 10.1109/61.19265.

[236] B. Lesieutre and D. Wu, "An efficient method to locate all the load flow solutions-revisited", in *2015 53rd Annual Allerton Conference on Communication, Control, and Computing (Allerton)*, IEEE, 2015, pp. 381–388.

[237] Y. C. Chen and S. V. Dhople, "Power divider", *IEEE Transactions on Power Systems*, vol. 31, no. 6, pp. 5135–5143, Nov. 2016. DOI: 10.1109/TPWRS.2016.2519900.

[238] R. A. Jabr, "Radial distribution load flow using conic programming", *IEEE transactions on power systems*, vol. 21, no. 3, pp. 1458–1459, 2006.

[239] I. A. Hiskens and R. J. Davy, "Exploring the power flow solution space boundary", *IEEE transactions on power systems*, vol. 16, no. 3, pp. 389–395, 2001.

[240] D. K. Molzahn, S. S. Baghsorkhi, and I. A. Hiskens, "Semidefinite relaxations of equivalent optimal power flow problems: An illustrative example", in *2015 IEEE International Symposium on Circuits and Systems (ISCAS)*, IEEE, 2015, pp. 1887–1890.

[241] D. K. Molzahn and I. A. Hiskens, "Convex relaxations of optimal power flow problems: An illustrative example", *IEEE Transactions on Circuits and Systems I: Regular Papers*, vol. 63, no. 5, pp. 650–660, 2016.

[242] W. A. Bukhsh, A. Grothey, K. I. McKinnon, and P. A. Trodden, "Local solutions of the optimal power flow problem", *IEEE Transactions on Power Systems*, vol. 28, no. 4, pp. 4780–4788, 2013.

[243] D. K. Molzahn, "Computing the feasible spaces of optimal power flow problems", *IEEE Transactions on Power Systems*, vol. 32, no. 6, pp. 4752–4763, 2017.

[244] X. Bai, H. Wei, K. Fujisawa, and Y. Wang, "Semidefinite programming for optimal power flow problems", *International Journal of Electrical Power and Energy Systems*, vol. 30, no. 6-7, pp. 383–392, 2008, ISSN: 01420615. DOI: `10.1016/j.ijepes.2007.12.003`.

[245] J. Lavaei and S. H. Low, "Zero duality gap in optimal power flow problem", *IEEE Transactions on Power Systems*, vol. 27, no. 1, pp. 92–107, 2012, ISSN: 08858950. DOI: `10.1109/TPWRS.2011.2160974`.

[246] D. K. Molzahn, J. T. Holzer, B. C. Lesieutre, and C. L. DeMarco, "Implementation of a large-scale optimal power flow solver based on semidefinite programming", *IEEE Transactions on Power Systems*, vol. 28, no. 4, pp. 3987–3998, 2013.

[247] C. Josz and D. K. Molzahn, "Moment/sum-of-squares hierarchy for complex polynomial optimization", *arXiv preprint arXiv:1508.02068*, 2015.

[248] J. Lavaei, D. Tse, and B. Zhang, "Geometry of power flows and optimization in distribution networks", *IEEE Transactions on Power Systems*, vol. 29, no. 2, pp. 572–583, 2013.

[249] B. Zhang and D. Tse, "Geometry of injection regions of power networks", *IEEE Transactions on Power Systems*, vol. 28, no. 2, pp. 788–797, 2012.

[250] S. Sojoudi and J. Lavaei, "Physics of power networks makes hard optimization problems easy to solve", in *2012 IEEE Power and Energy Society General Meeting*, IEEE, 2012, pp. 1–8.

[251] S. Abdelouadoud, R. Girard, F.-P. Neirac, and T. Guiot, "Optimal power flow of a distribution system based on increasingly tight cutting planes added to a second order cone relaxation", *International Journal of Electrical Power & Energy Systems*, vol. 69, pp. 9–17, 2015.

[252] H. Gao, J. Liu, L. Wang, and Y. Liu, "Cutting planes based relaxed optimal power flow in active distribution systems", *Electric Power Systems Research*, vol. 143, pp. 272–280, 2017.

[253] B. C. Lesieutre, D. K. Molzahn, A. R. Borden, and C. L. DeMarco, "Examining the limits of the application of semidefinite programming to power flow problems", in *2011 49th Annual Allerton Conference on Communication, Control, and Computing (Allerton)*, Sep. 2011, pp. 1492–1499. DOI: `10.1109/Allerton.2011.6120344`.

[254] B. Kocuk, S. S. Dey, and X. A. Sun, "Inexactness of sdp relaxation and valid inequalities for optimal power flow", *IEEE Transactions on Power Systems*, vol. 31, no. 1, pp. 642–651, Jan. 2016. DOI: `10.1109/TPWRS.2015.2402640`.

[255] S. H. Low, "Convex Relaxation of Optimal Power Flow, Part II: Exactness", *IEEE Transactions on Control of Network Systems*, vol. 1, no. 2, pp. 177–189, 2014, ISSN: 2325-5870. DOI: `10.1109/TCNS.2014.2323634`. arXiv: `1405.0814`.

[256] R. A. Jabr, "Exploiting sparsity in SDP Relaxations of the OPF Problem", *IEEE Transactions on Power Systems*, vol. 27, no. 2, pp. 1138–1139, 2012, ISSN: 00255610. DOI: 10.1007/s10107-010-0402-6.

[257] L. Gan and S. H. Low, "Convex Relaxation and Linear Approximation for optimal power flow in multiphase radial networks", in *Power Systems Computation Conference (PSCC)*, 2014, pp. 1–9.

[258] C. Bingane, M. F. Anjos, and S. Le Digabel, "Tight-and-cheap conic relaxation for the ac optimal power flow problem", *IEEE Transactions on Power Systems*, vol. 33, no. 6, pp. 7181–7188, 2018.

[259] M. S. Andersen, A. Hansson, and L. Vandenberghe, "Reduced-Complexity Semidefinite Relaxations of Optimal Power Flow Problems", *IEEE Transactions on Power Systems*, vol. 29, pp. 1855–1863, 2014. arXiv: arXiv:1308.6718v2.

[260] A. Y. Lam, B. Zhang, and N. T. David, "Distributed algorithms for optimal power flow problem", in *2012 IEEE 51st IEEE Conference on Decision and Control (CDC)*, IEEE, 2012, pp. 430–437.

[261] B. Zhang, A. Y. Lam, A. D. Dominguez-Garcia, and D. Tse, "An optimal and distributed method for voltage regulation in power distribution systems", *IEEE Transactions on Power Systems*, vol. 30, no. 4, pp. 1714–1726, 2014.

[262] R. Madani, A. Kalbat, and J. Lavaei, "Admm for sparse semidefinite programming with applications to optimal power flow problem", in *2015 54th IEEE Conference on Decision and Control (CDC)*, IEEE, 2015, pp. 5932–5939.

[263] Q. Peng and S. H. Low, "Distributed Optimal Power Flow Algorithm for Radial Networks, I: Balanced Single Phase Case", *IEEE Transactions on Smart Grid*, vol. 9, no. 1, pp. 111–121, 2018. DOI: 10.1109/TSG.2016.2546305. arXiv: 1404.0700.

[264] E. DallAnese, Hao Zhu, and G. B. Giannakis, "Distributed Optimal Power Flow for Smart Microgrids", *IEEE Transactions on Smart Grid*, vol. 4, no. 3, pp. 1464–1475, 2013, ISSN: 1949-3053. DOI: 10.1109/TSG.2013.2248175. arXiv: 1211.5856.

[265] J. B. Lasserre, "Global optimization with polynomials and the problem of moments", *SIAM Journal on optimization*, vol. 11, no. 3, pp. 796–817, 2001.

[266] J.-B. Lasserre, *Moments, positive polynomials and their applications*. World Scientific, 2010, vol. 1.

[267] D. K. Molzahn, C. Josz, and I. A. Hiskens, "Moment relaxations of optimal power flow problems: Beyond the convex hull", in *2016 IEEE Global Conference on Signal and Information Processing (GlobalSIP)*, Dec. 2016, pp. 856–860.

[268] J. Tian and H. Wei, "Global optimization for the opf problem via two-degree sdp method", *IEEJ Transactions on Electrical and Electronic Engineering*, vol. 10, no. 1, pp. 109–111, 2015. DOI: 10.1002/tee.22068.

[269] B. Ghaddar, J. Marecek, and M. Mevissen, "Optimal power flow as a polynomial optimization problem", *IEEE Transactions on Power Systems*, vol. 31, no. 1, pp. 539–546, Jan. 2016.

[270] D. K. Molzahn and I. A. Hiskens, "Moment-based relaxation of the optimal power flow problem", in *2014 Power Systems Computation Conference*, IEEE, 2014, pp. 1–7.

[271] C. Josz, J. Maeght, P. Panciatici, and J. C. Gilbert, "Application of the moment-sos approach to global optimization of the opf problem", *IEEE Transactions on Power Systems*, vol. 30, no. 1, pp. 463–470, 2014.

[272] D. Molzahn, C. Josz, I. Hiskens, and P. Panciatici, "Solution of optimal power flow problems using moment relaxations augmented with objective function penalization", in *2015 54th IEEE Conference on Decision and Control (CDC)*, IEEE, 2015, pp. 31–38.

[273] D. K. Molzahn and I. A. Hiskens, "Sparsity-exploiting moment-based relaxations of the optimal power flow problem", *IEEE Transactions on Power Systems*, vol. 30, no. 6, pp. 3168–3180, 2015.

[274] M. Farivar and S. H. Low, "Branch flow model: Relaxations and convexification—part i", *IEEE Transactions on Power Systems*, vol. 28, no. 3, pp. 2554–2564, 2013.

[275] M. Farivar and S. H. Low, "Branch flow model: Relaxations and convexification—part ii", *IEEE Transactions on Power Systems*, vol. 28, no. 3, pp. 2565–2572, Aug. 2013. DOI: `10.1109/TPWRS.2013.2255318`.

[276] C. Coffrin, H. L. Hijazi, P. V. Hentenryck, and C. E. Feb, "The QC Relaxation : Theoretical and Computational Results on Optimal Power Flow", *IEEE Transactions on Power Systems*, vol. 31, no. 4, pp. 3008–3018, 2016, ISSN: 08858950. DOI: `10.1109/TPWRS.2015.2463111`. arXiv: `arXiv:1502.07847v1`.

[277] K. Bestuzheva, H. Hijazi, and C. Coffrin, "Convex relaxations for quadratic on/off constraints and applications to optimal transmission switching", *Preprint: http://www. optimization-online. org/DB FILE/2016/07/5565. pdf*, 2016.

[278] C. Coffrin, H. L. Hijazi, and P. Van Hentenryck, "Strengthening the sdp relaxation of ac power flows with convex envelopes, bound tightening, and valid inequalities", *IEEE Transactions on Power Systems*, vol. 32, no. 5, pp. 3549–3558, 2017.

[279] ——, "Strengthening convex relaxations with bound tightening for power network optimization", in *International Conference on Principles and Practice of Constraint Programming*, Springer, 2015, pp. 39–57.

[280] B. Kocuk, S. S. Dey, and X. A. Sun, "Strong socp relaxations for the optimal power flow problem", *Operations Research*, vol. 64, no. 6, pp. 1177–1196, 2016.

[281] ——, "Matrix minor reformulation and socp-based spatial branch-and-cut method for the ac optimal power flow problem", *Mathematical Programming Computation*, vol. 10, no. 4, pp. 557–596, 2018.

[282] D. Bienstock and G. Munoz, "On linear relaxations of opf problems", *arXiv preprint arXiv:1411.1120*, 2014.

[283] ——, "Approximate method for ac transmission switching based on a simple relaxation for acopf problems", in *2015 IEEE Power & Energy Society General Meeting*, IEEE, 2015, pp. 1–5.

[284] S. H. Low, "Convex Relaxation of Optimal Power Flow—Part I: Formulations and Equivalence", *IEEE Transactions on Control of Network Systems*, vol. 1, no. 1, pp. 15–27, 2014, ISSN: 2325-5870. DOI: `10.1109/TCNS.2014.2323634`. arXiv: `arXiv:1405.0766v1`.

[285] B. Subhonmesh, S. H. Low, and K. M. Chandy, "Equivalence of branch flow and bus injection models", in *2012 50th Annual Allerton Conference on Communication, Control, and Computing (Allerton)*, IEEE, 2012, pp. 1893–1899.

[286] S. Sojoudi and J. Lavaei, "Convexification of optimal power flow problem by means of phase shifters", in *2013 IEEE International Conference on Smart Grid Communications (SmartGridComm)*, IEEE, 2013, pp. 756–761.

[287] S. Huang, Q. Wu, J. Wang, and H. Zhao, "A sufficient condition on convex relaxation of ac optimal power flow in distribution networks", *IEEE Transactions on Power Systems*, vol. 32, no. 2, pp. 1359–1368, 2016.

[288] L. Gan and S. H. Low, "Optimal power flow in direct current networks", *IEEE Transactions on Power Systems*, vol. 29, no. 6, pp. 2892–2904, 2014.

[289] C. W. Tan, D. W. Cai, and X. Lou, "Resistive network optimal power flow: Uniqueness and algorithms", *IEEE Transactions on Power Systems*, vol. 30, no. 1, pp. 263–273, 2014.

[290] C. Coffrin, H. Hijazi, and P. Van Hentenryck, "Network flow and copper plate relaxations for ac transmission systems", in *2016 Power Systems Computation Conference (PSCC)*, IEEE, 2016, pp. 1–8.

[291] J. A. Taylor and F. S. Hover, "Linear relaxations for transmission system planning", *IEEE Transactions on Power Systems*, vol. 26, no. 4, pp. 2533–2538, 2011.

[292] G. P. McCormick, "Computability of global solutions to factorable nonconvex programs: Part i—convex underestimating problems", *Mathematical programming*, vol. 10, no. 1, pp. 147–175, 1976.

[293] Q. Gemine, D. Ernst, Q. Louveaux, and B. Cornelusse, "Relaxations for multi-period optimal power flow problems with discrete decision variables", in *2014 Power Systems Computation Conference*, IEEE, 2014, pp. 1–7.

[294] Z. Qin, Y. Hou, and Y. Chen, "Convex envelopes of optimal power flow with branch flow model in rectangular form", in *2015 IEEE Power & Energy Society General Meeting*, IEEE, 2015, pp. 1–5.

[295] D. Bienstock and G. Munoz, "Lp approximations to mixed-integer polynomial optimization problems", *arXiv preprint arXiv:1501.00288*, 2015.

[296] C. Chen, A. Atamtürk, and S. S. Oren, "Bound tightening for the alternating current optimal power flow problem", *IEEE Transactions on Power Systems*, vol. 31, no. 5, pp. 3729–3736, 2015.

[297] F. Geth, R. D'hulst, and D. Van Hertem, "Convex power flow models for scalable electricity market modelling", *CIRED-Open Access Proceedings Journal*, vol. 2017, no. 1, pp. 989–993, 2017.

[298] L. Gurobi Optimization, *Gurobi optimizer reference manual*, 2019. [Online]. Available: `http://www.gurobi.com`.

[299] M. ApS, *The mosek optimization toolbox for matlab manual. version 9.0.* 2019. [Online]. Available: `http://docs.mosek.com/9.0/toolbox/index.html`.

[300] M. Yamashita, K. Fujisawa, M. Fukuda, K. Nakata, and M. Nakata, "Algorithm 925: Parallel solver for semidefinite programming problem having sparse schur complement matrix", *ACM Transactions on Mathematical Software (TOMS)*, vol. 39, no. 1, p. 6, 2012.

[301] C. Zhao, E. Dall'Anese, and S. Low, "Convex relaxation of opf in multiphase radial networks with delta connection", in *Proceedings of the 10th Bulk Power Systems Dynamics and Control Symposium*, 2017.

[302] Y. Liu, J. Li, L. Wu, and T. Ortmeyer, "Chordal Relaxation Based ACOPF for Unbalanced Distribution Systems with DERs and Voltage Regulation Devices", *IEEE Transactions on Power Systems*, vol. 33, no. 1, pp. 970–984, 2017, ISSN: 0885-8950. DOI: `10.1109/TPWRS.2017.2707564`.

[303] W. Wang and N. Yu, "Chordal conversion based convex iteration algorithm for three-phase optimal power flow problems", *IEEE Transactions on Power Systems*, vol. 33, no. 2, pp. 1603–1613, 2017.

[304] D. K. Molzahn, B. C. Lesieutre, and C. L. DeMarco, "Approximate representation of zip loads in a semidefinite relaxation of the opf problem", *IEEE Transactions on Power Systems*, vol. 29, no. 4, pp. 1864–1865, 2014.

[305] R. Benato, A. Paolucci, and R. Turri, "Power flow solution by a complex admittance matrix method", *European transactions on electrical power*, vol. 11, no. 3, pp. 181–188, 2001.

[306] M. Coppo, F. Bignucolo, and R. Turri, "Generalised transformer modelling for power flow calculation in multi-phase unbalanced networks", *IET Generation, Transmission & Distribution*, vol. 11, no. 15, pp. 3843–3852, 2017.

[307] F. Bignucolo, A. Savio, R. Caldon, and A. Cerretti, "Effects of average power factor management in distribution systems with dispersed generation", in *2016 AEIT International Annual Conference (AEIT)*, IEEE, 2016, pp. 1–6.

[308] K. Yamashita, S. Djokic, J. Matevosyan, F. Resende, L. Korunovic, Z. Dong, and J. Milanovic, "Modelling and aggregation of loads in flexible power networks–scope and status of the work of cigre wg c4. 605", *IFAC Proceedings Volumes*, vol. 45, no. 21, pp. 405–410, 2012.

[309] J. Csatar and A. Dan, "Novel load flow method for networks with multipoint-grounded-neutral and phase-to-neutral connected equipment", *International Journal of Electrical Power & Energy Systems*, vol. 107, pp. 726–734, 2019.

[310] F. Bignucolo, R. Caldon, M. Coppo, and R. Turri, "Effects of distributed generation on power losses in unbalanced low voltage networks", in *2018 IEEE Power Energy Society General Meeting*, Aug. 2018, pp. 1–5.

[311] J. Löfberg, "Yalmip : A toolbox for modeling and optimization in matlab", in *In Proceedings of the CACSD Conference*, Taipei, Taiwan, 2004.

[312] S. Bose, S. H. Low, T. Teeraratkul, and B. Hassibi, "Equivalent relaxations of optimal power flow", *IEEE Transactions on Automatic Control*, vol. 60, no. 3, pp. 729–742, 2014.

[313] A. Venzke, S. Chatzivasileiadis, and D. K. Molzahn, "Inexact convex relaxations for ac optimal power flow: Towards ac feasibility", *arXiv preprint arXiv:1902.04815*, 2019.

[314] A. Wächter and L. T. Biegler, "On the implementation of an interior-point filter line-search algorithm for large-scale nonlinear programming", *Mathematical programming*, vol. 106, no. 1, pp. 25–57, 2006.

[315] J. Currie and D. I. Wilson, "OPTI: Lowering the Barrier Between Open Source Optimizers and the Industrial MATLAB User", in *Foundations of Computer-Aided Process Operations*, N. Sahinidis and J. Pinto, Eds., Savannah, Georgia, USA, Aug. 2012.

[316] P. E. Gill, W. Murray, and M. A. Saunders, "Snopt: An sqp algorithm for large-scale constrained optimization", *SIAM review*, vol. 47, no. 1, pp. 99–131, 2005.

[317] J. F. Sturm, "Using sedumi 1.02, a matlab toolbox for optimization over symmetric cones", *Optimization Methods and Software*, vol. 11, no. 1-4, pp. 625–653, 1999. DOI: 10.1080/10556789908805766.

[318] R. H. Tütüncü, K.-C. Toh, and M. J. Todd, "Solving semidefinite-quadratic-linear programs using sdpt3", *Mathematical programming*, vol. 95, no. 2, pp. 189–217, 2003.

[319] R. Louca, P. Seiler, and E. Bitar, "A rank minimization algorithm to enhance semidefinite relaxations of optimal power flow", in *2013 51st Annual Allerton Conference on Communication, Control, and Computing (Allerton)*, IEEE, 2013, pp. 1010–1020.

[320] R. Madani, S. Sojoudi, G. Fazelnia, and J. Lavaei, "Finding low-rank solutions of sparse linear matrix inequalities using convex optimization", *SIAM Journal on Optimization*, vol. 27, no. 2, pp. 725–758, 2017.

[321] J. Marecek and M. Takac, "A low-rank coordinate-descent algorithm for semidefinite programming relaxations of optimal power flow", *Optimization Methods and Software*, vol. 32, no. 4, pp. 849–871, 2017.

[322] J. Liu, A. C. Liddell, J. Marecek, and M. Takac, "Hybrid methods in solving alternating-current optimal power flows", *IEEE Transactions on Smart Grid*, vol. 8, no. 6, pp. 2988–2998, 2017.